

DOCUMENT NUMBER VOY-CO-FR
28 JULY 1967

VOLUME 2
RTG SPACECRAFT STUDY

PREPARED BY:
VOYAGER PROJECT
MISSILE & SPACE DIVISION
GENERAL ELECTRIC CO.

A. Kipich
COGNIZANT ENGINEER

APPROVED:

B. H. Caldwell
B.H. CALDWELL
VOYAGER PROJECT MANAGER

PREPARED FOR
CALIFORNIA INSTITUTE OF TECHNOLOGY
JET PROPULSION LABORATORY
4800 OAK GROVE DRIVE
PASADENA, CALIFORNIA
UNDER CONTRACT No. 951112

GENERAL  ELECTRIC

MISSILE AND SPACE DIVISION
Valley Forge Space Technology Center
P. O. Box 8555 • Philadelphia, Penna. 19101

TABLE OF CONTENTS

<u>Section</u>		<u>Page</u>
1	SUMMARY	1-1
2	INTRODUCTION	2-1
3	RTG SPACECRAFT DESIGN	3-1
3.1	Guidelines	3-1
3.1.1	RTG Guidelines	3-1
3.1.2	Spacecraft Design	3-2
3.2	Design Evolution	3-5
3.2.1	Preliminary RTG Sizing Model	3-5
3.2.2	Spacecraft Design Evolution	3-7
3.3	Selected RTG Spacecraft Design	3-10
3.3.1	Spacecraft Description	3-10
3.3.2	RTG Description	3-22
3.3.3	Structure	3-29
3.3.4	Weight and Mass Properties	3-46
3.3.5	Thermal Analysis	3-49
3.3.6	Radiation Mapping	3-65
3.4	Subsystem Design.	3-76
3.4.1	Power Subsystem	3-76
3.4.2	Guidance and Control	3-88
3.4.3	Telecommunications	3-93
3.4.4	Other Subsystems	3-98
3.5	Operational Support Equipment and Ground Operation	3-99
3.5.1	Basic Effects of RTG Use	3-99
3.5.2	Factory Operations	3-99
3.5.3	Launch Site Operations	3-102
3.5.4	Other LCE and AHSE	3-104
4	SOLAR/RTG INTERCHANGEABILITY	4-1
4.1	Guidelines	4-1
4.2	Design Evolution	4-1
4.3	Selected Solar Spacecraft Design	4-1
4.3.1	Description	4-1
4.3.2	Structure	4-4
4.3.3	Mass Properties	4-4
4.3.4	Thermal Analysis	4-13
4.4	Subsystem Design	4-16
4.4.1	Power Subsystem	4-16

TABLE OF CONTENTS (Cont'd)

<u>Section</u>	<u>Page</u>
4.5	Interchangeability Summary 4-26
4.5.1	Power 4-26
4.5.2	Guidance and Control 4-27
4.5.3	Computer and Sequencer 4-27
4.5.4	Communications. 4-28
4.5.5	Structure 4-28
4.5.6	Science. 4-28
4.5.7	Harness 4-28
5	SUPPORTING STUDIES 5-1
5.1	RTG Sizing Results 5-1
5.1.1	Beginning-of-Life (BOL) Characteristics 5-1
5.1.2	Margin Analysis. 5-9
5.1.3	Nominal RTG Specifications. 5-15
5.2	Radiation Sensitivity. 5-18
5.2.1	Radiation Effects on Spacecraft Bus Electronics and Materials 5-19
5.2.2	Radiation Effects on Science Instruments 5-25
5.2.3	Radiation Sensitivity Studies by Texas Instruments, Inc. 5-39
5.3	Safety. 5-48
5.3.1	Mission Abort Study 5-48
5.3.2	Launch Azimuth Considerations 5-49
6	COMPARISON OF RTG-POWERED AND SOLAR-POWERED SPACECRAFT 6-1
6.1	Spacecraft Growth Versions 6-1
6.2	Weight and Power Comparisons 6-5
6.3	Reliability 6-11
6.4	Mission Flexibility 6-13
6.5	Design Implementation 6-14
6.6	Program Implementation 6-20
7	CONCLUSIONS 7-1
7.1	Spacecraft Design Effects 7-1
7.2	RTG Power Relative to Solar Power 7-5
7.3	Recommendations 7-7

LIST OF ILLUSTRATIONS

Figure		Page
2-1	RTG Spacecraft Study — Work Flow Chart	2-3
3-1	Voyager Task B Spacecraft Design	3-3
3-2	SNAP-27 Generator	3-5
3-3	Preliminary RTG Sizing Model	3-6
3-4	RTG Spacecraft Configuration Evolution	3-8
3-5	Over-the-Nose Shroud Separation	3-8
3-6	RTG Spacecraft	3-11
3-7	RTG Spacecraft Model	3-12
3-8	General Arrangement of RTG Spacecraft	3-13
3-9	RTG Spacecraft Antenna and Sensor Locations	3-17
3-10	Operational Sequence of Sun-Biased System	3-19
3-11	Nominal RTG Configuration	3-23
3-12	Voyager Orbiter RTG	3-27
3-13	Variation of Shroud Separation Tip-Off Velocity Ratio with Initial Radial Clearance and Shroud Thickness	3-30
3-14	Schematic and Results of Dynamic Analysis	3-35
3-15	Schematic Representation of the Primary Structure	3-38
3-16	Equipment Arrangement	3-45
3-17	Thermal Analysis Model	3-50
3-18	Thermal Analysis Nodal Breakdown	3-50
3-19	Shroud Cooling Nomenclature	3-53
3-20	Air and Shroud Heat Load Variations	3-53
3-21	Shroud Heat Removal Effectiveness	3-54
3-22	Electronics Temperature Determination (Operational)	3-54
3-23	Electronics Temperature Determination (Non-Operational)	3-55
3-24	Air Heat Removal Effectiveness	3-55
3-25	Cooling Options for $T_E = 100^\circ F$	3-58
3-26	External Shroud Heat Source	3-61

LIST OF ILLUSTRATIONS (Continued)

Figure		Page
3-27	RTG Temperature History	3-61
3-28	Parking Orbit Maximum Temperatures	3-64
3-29	Spacecraft Temperature Distribution Without Shroud	3-64
3-30	Neutron Flux Energy Distribution (Normalized to Total Number of Neutrons)	3-66
3-31	Gamma Photon Energy Distribution Outside RTG	3-66
3-32	Voyager Spacecraft Bus Configuration	3-69
3-33	Vehicle Schematic for Voyager Bus Radiation Mapping (Pu-238 Fuel) . .	3-71
3-34	Isodose Contours	3-73
3-35	Voyager RTG Power Subsystem Functional Block Diagram	3-78
3-36	RTG Schematic	3-82
3-37	Partial Shunt Regulator	3-83
3-38	Earth Cone and Clock Angles for Several Launch Opportunities	3-89
3-39	Solar Aspect Sensor	3-92
3-40	Radio Subsystem	3-94
3-41	Performance Margin Versus Range	3-98
4-1	Solar-Powered Spacecraft	4-2
4-2	Solar Array Spacecraft -- General Arrangement	4-5
4-3	Antenna and Sensor Fields of View	4-7
4-4	Electronic Equipment Bay Arrangement	4-8
4-5	Solar Array Temperature Variation Versus Distance from Sun	4-14
4-6	Temperature Distribution Along Solar Array	4-14
4-7	Voyager Spacecraft Temperatures near Earth	4-15
4-8	Voyager Spacecraft Temperatures near Mars	4-15
4-9	Simplified Power Subsystem Schematic	4-17
4-10	Solar Array Output Versus Sun Distance	4-18
4-11	Solar Array Output Versus Mission Time	4-18

LIST OF ILLUSTRATIONS (Continued)

Figure		Page
4-12	Solar Array Voltage-Current Characteristics	4-19
4-13	Solar Array Power-Voltage Characteristics	4-19
4-14	Solar Panel Layouts	4-21
5-1	Weight, Power, Length and Diameter Relationships for Pb-Te Thermopile RTG's, 1100° F Hot Junction Temperature	5-2
5-2	Cold Junction Temperature vs RTG Diameter for Pb-Te Thermopile RTG's, 1100° F Hot Junction Temperature	5-2
5-3	Weight, Power, Length and Diameter Relationships for Pb-Te Thermopile RTG's, 1050° F Hot Junction Temperature	5-3
5-4	Cold Junction Temperature vs RTG Diameter for Pb-Te Thermopile RTG's, 1050° F Hot Junction Temperature	5-3
5-5	Efficiency vs Cold Junction Temperature for Pb-Te Thermopile RTG's, 1050° F Hot Junction Temperature.	5-3
5-6	Weight, Power, Length and Diameter Relationships for Si-Ge Thermopile RTG's, 1200° F Hot Junction Temperature	5-5
5-7	Cold Junction Temperature vs RTG Diameter for Si-Ge Thermopile RTG's, 1200° F Hot Junction Temperature	5-5
5-8	Weight, Power, Length and Diameter Relationships for Si-Ge Thermopile RTG's, 1400° F Hot Junction Temperature	5-6
5-9	Cold Junction Temperature vs RTG Diameter for Si-Ge Thermopile RTG's, 1400° F Hot Junction Temperature	5-6
5-10	Weight, Power, Length and Diameter Relationships for Si-Ge Thermopile RTG's, 1600° F Hot Junction Temperature	5-7
5-11	Cold Junction Temperature vs RTG Diameter for Si-Ge Thermopile RTG's, 1600° F Hot Junction Temperature	5-7
5-12	Efficiency vs Cold Junction Temperature for Si-Ge Thermopile RTG's	5-7
5-13	Weight Correction for Recessed RTG's	5-8
5-14	Diameter Correction for Recessed RTG's	5-8
5-15	RTG Temperature Rise vs Sink Temperature	5-8
5-16	RTG Re-entry Protection Weight	5-8

LIST OF ILLUSTRATIONS (Continued)

Figure		Page
5-17	Effect of Isotope Fuel	5-12
5-18	Lead-telluride Thermopile Degradation	5-12
5-19	Silicon-germanium Thermopile Degradation	5-13
5-20	RTG Reliability Margin	5-13
5-21	Lead-telluride RTG Combined Degradation	5-14
5-22	Silicon-germanium RTG Combined Degradation	5-14
5-23	Specific Weight vs Time for Lead-telluride RTG's	5-16
5-24	Specific Weight vs Time for Silicon-germanium RTG's	5-16
5-25	Neutron Effects Summary	5-20
5-26	Gamma Effects Summary	5-20
5-27	Number Transmission Coefficient Incident at 0° on Various Thicknesses of Aluminum	5-34
5-28	Schematic View of the Shadow Shield for the Gamma Ray Spectrometer	5-37
5-29	Shadow Shield Weight vs Boom Length	5-37
5-30	Total Weight of the Tip Shield, Boom and Deployment Mechanism vs Boom Length	5-38
5-31	Minimum Weight Shield Systems for the Gamma Ray Spectrometer	5-38
5-32	Damage Thresholds for Instruments	5-40
5-33	MOSFET Test Circuit	5-46
5-34	MOSFET Device Gate Threshold vs Radiation Exposure	5-47
5-35	MOSFET Device Transconductance vs Radiation Exposure	5-47
5-36	MOSFET Device Source Leakage vs Radiation Exposure	5-47
5-37	Saturn V--Voyager Vacuum Impact Critical Events	5-50

LIST OF ILLUSTRATIONS (Continued)

Figure		Page
6-1	RTG Spacecraft Growth Version	6-1
6-2	Solar Spacecraft Growth Version	6-4
6-3	Power After Encounter	6-6
6-4	Usable Array Power Versus Fractional Eclipse Time	6-6
6-5	RTG and PV/B Power Performance -- 1973 Mission	6-7
6-6	Conditional Power Versus Weight	6-10
6-7	Accumulated Energy Comparison	6-10
6-8	Lander Thermal Integration	6-15
6-9	Spacecraft Project Cycle	6-21
6-10	RTG Development Schedule and Hardware Requirements	6-25
6-11	Isotope Fuel Inventory Requirements	6-27

SECTION 1

SUMMARY

One of the studies conducted by GE^(page 4) as part of the Voyager Phase IA Task C activity has concerned the use of radioisotope thermoelectric (RTG's) for powering the spacecraft bus. The purpose of this study was to determine the feasibility of an RTG powered bus and to compare its merits with a solar powered bus.

As a starting point, the functional definition for the spacecraft was based on the design resulting from the Voyager Phase IA, Task B studies performed by GE. From this and from RTG design data (drawn largely from the SNAP-27 RTG program), a spacecraft design was evolved. The design, shown on the opposite page, largely duplicates the functional capability of the Task B design. However, there are several notable differences, including the ability to use a fixed high-gain antenna, at least for missions to the outer planets, and the independence of power generation with solar distance.

The spacecraft uses eight RTG's with each rated at 75 watts. This size is considered to be within the scope of available technology. Plutonium-238 fuel is used for the heat source and lead-telluride thermoelements are used for heat to electrical energy conversion. Development will be required to provide the RTG's with earth re-entry capability in the event of a mission abort. This is based on an assumed isotope fuel containment safety criterion.

Power growth may be accommodated by using initially larger RTG's or by mounting additional RTG's at available locations.

The principal RTG interactions with the spacecraft result from thermal and nuclear radiation. For each spacecraft the RTG's dissipate about 15 kilowatts of heat. During space-flight this does not cause a problem, but during prelaunch operation with the spacecraft enshrouded it is necessary to provide continuous cooling. Cooling is not required during the launch phase provided temperatures are sufficiently low at the start of launch.

The effect of nuclear radiation on the spacecraft subsystem, excluding the science payload, is minimal. For certain elements attention may have to be given to component and circuit de-rating but no significant damage is anticipated. Certain science instruments, mainly those devoted to radiation detection, would encounter problems of dynamic interference. The use of shielding, remote mounting, and possible instrument redesign might relieve some of these difficulties.

The possibility of designing the spacecraft to be adaptable to either solar or RTG power was examined and found to be practical.

A comparison of RTG and solar power was conducted as part of the study. Although the RTG's would appear to result in a more reliable spacecraft the principal motivation for their use lies in their application to missions beyond Mars.

The principal recommendations resulting from this study are enumerated below and pertain to considerations in early spacecraft design efforts to facilitate future RTG integration:

- Cooling capability should be considered in the design of the shroud.
- Spacecraft systems should be designed to operate in an RTG radiation environment.
- Convertibility to solar or RTG power should be considered in the spacecraft design.
- Early consideration should be given to the development of RTG re-entry capability.
- Effort should be devoted to science instrument compatibility with RTG's.

SECTION 2

INTRODUCTION

This volume of the Final Report of the GE Task C Voyager study discusses the application of radioisotope thermoelectric generators (RTG's) for electrically powering the Voyager spacecraft bus. The study objectives were to develop an RTG spacecraft design equaling or surpassing the functional capability of previous solar-powered designs. Both the pros and cons of RTG's were to be investigated. The power, weight, dimensions and thermal behavior were to be determined along with those principal environments likely to affect the design. Finally, the study was to compare solar-powered and RTG-powered spacecraft, based on weight, reliability, mission flexibility, design implementation, and schedule implications.

The consideration of RTG power is based on two principal limitations of photovoltaic power:

- a. The dependence of photovoltaic power sources on solar energy strongly influences both spacecraft design and mission flexibility. The length of time that spacecraft operations can proceed without solar input is limited by the stored energy capacity of on-board rechargeable batteries.
- b. Photovoltaic systems depend on solar power intensity. Except for some small compensating effects related to panel temperature, the electrical power output of photovoltaic systems, measured in watts per square foot, varies inversely as the square of the sun distance. Thus, at a mean Mars-Sun distance of 1.52 astronomical units (AU) the installed photovoltaic capacity must be about 2.3 times that required at Earth; at a mean Jupiter-Sun distance of 5.2 AU, 27 times the area is required.

Considering the objectives of future planetary missions, these limitations provide the impetus for considering alternative power sources.

Because an external energy source is not required, radioisotope thermoelectric generators (RTG's) potentially overcome the limitations of photovoltaic systems. Their underlying principles of operation are well understood and they have been proposed for many applications. Flight operation has been successfully demonstrated with the experimental SNAP 3 and SNAP 9A generators. Design concepts have evolved to the extent that operational RTG programs are underway. The SNAP-27 generator, with a power requirement of 56 watts, is being developed by GE. It will be used in the ALSEP program as a power source for lunar surface experiments. The SNAP-19 generator, with a power requirement of 50 watts, is under development by the Martin Company. It will complement the solar panel power for the Nimbus B spacecraft.

Recognition of the improvements in the RTG state of the art resulting from the programs cited above, along with the potential for spacecraft simplification and mission enhancement, provided the motivation for conducting this study of an RTG-powered Voyager spacecraft.

The principal elements of the study program are shown on the Work Flow Chart, Figure 2-1, which shows the chronological progression of activities from program initiation to completion. The program was organized into the 9 subtasks shown on the left hand side of the chart. The mainstream of activity has been that associated with Vehicle Integration, Subtask No. 6. As information from other subtasks became available, it was used to modify and update the vehicle integration studies. Table 2-1 lists the reports on the results of the various subtasks, and gives the authors of each report.

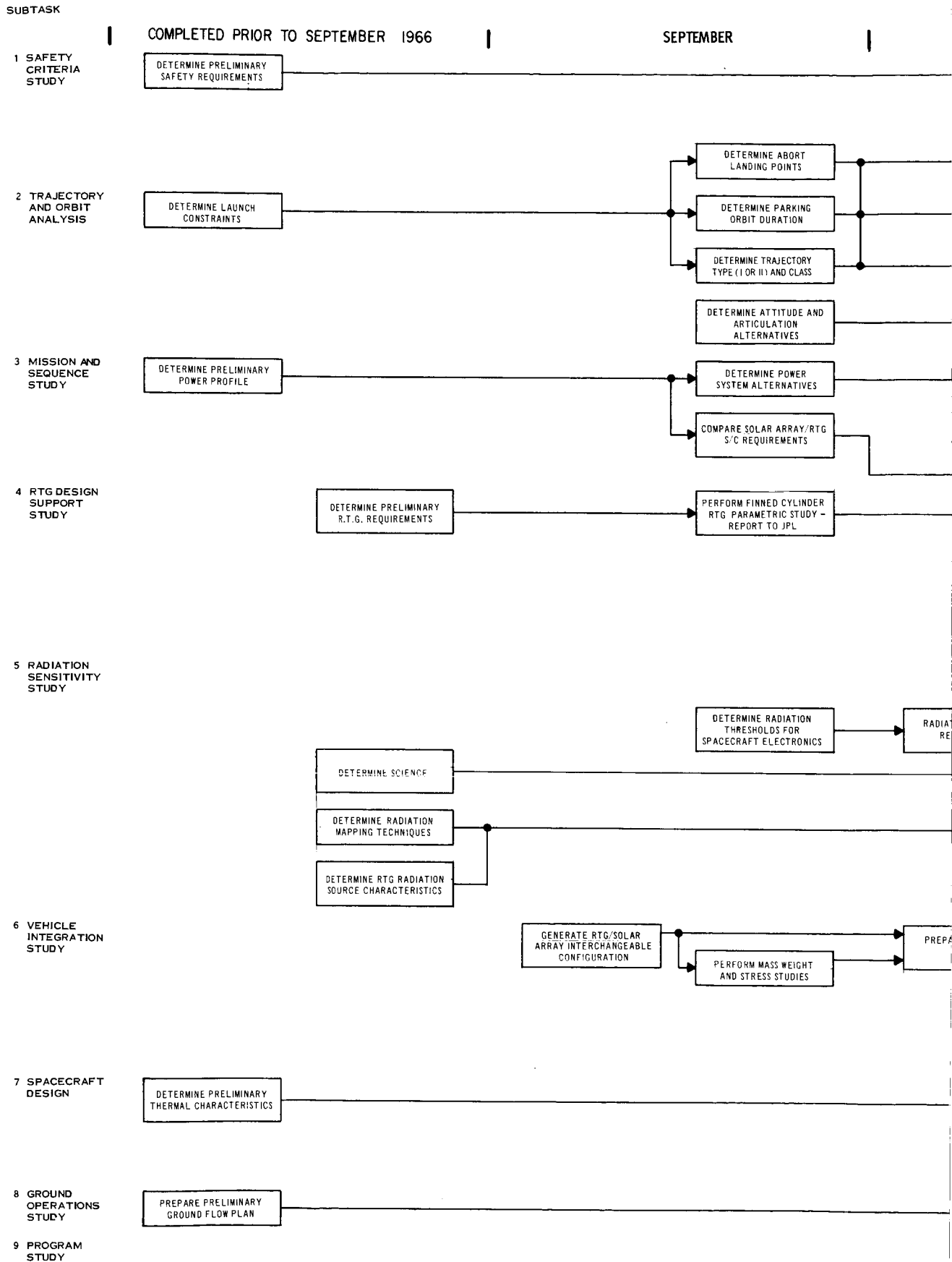
In this Final Report, the vehicle integration studies are used as the focal point for further detailed elaboration. Thus, Section 3 proceeds directly into the guidelines, design evolution, and description of the RTG spacecraft design. The results of related studies concerning RTG integration, thermal analysis, RTG radiation flux distribution, subsystem design and Operational Support Equipment (OSE) definition support the basic spacecraft description.

Section 4 describes the extent to which modifications are required to convert the spacecraft to a solar-powered version. This convertibility may be desirable, since it appears that either RTG or solar power may be used for Mars missions, whereas only RTG power appears feasible for the more remote outer planets. The solar-powered version developed as part of this interchangeability goal served as the basis for comparing RTG and solar power.

Section 5 describes the principal results of the major supporting studies: (1) sensitivity of spacecraft and science equipment to the RTG radiation, (2) RTG sizing study results, and (3) safety considerations.

Section 6 presents the principal comparison results of RTG and solar-powered Voyager spacecraft.

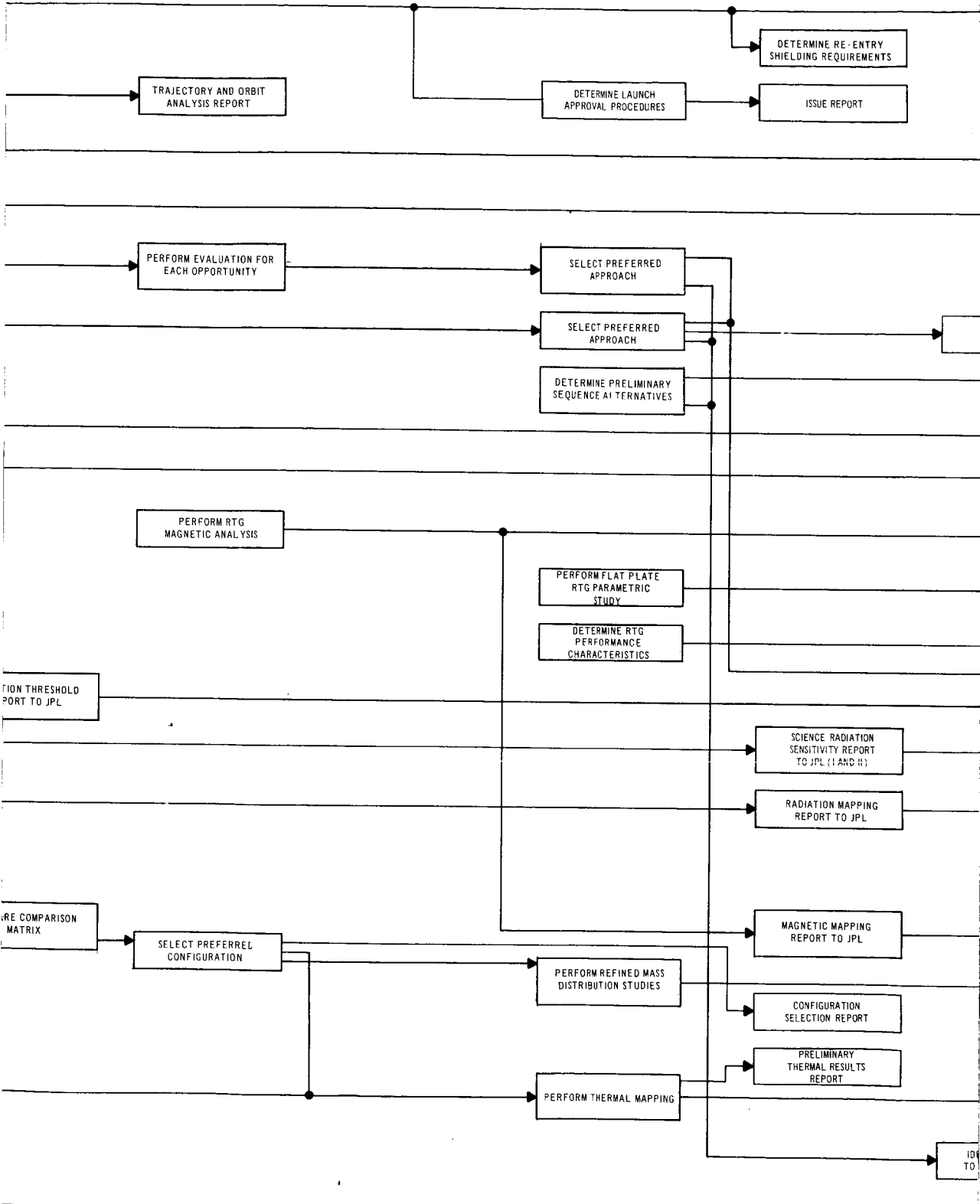
Section 7 presents the conclusions and recommended courses of action resulting from the overall study.



OCTOBER

NOVEMBER

DECEMBER

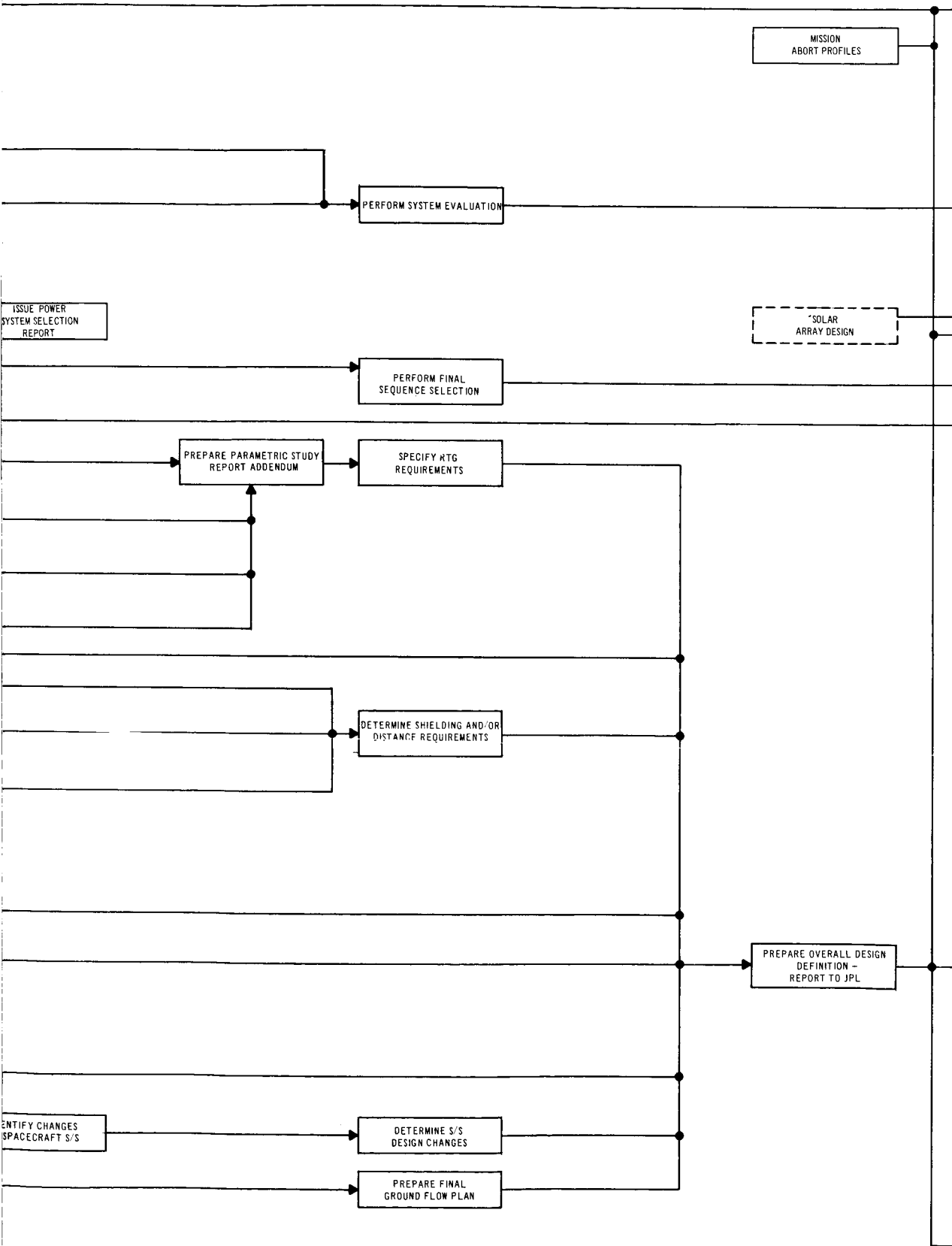


2-47

1967

JANUARY

FEBRUARY



2-4-2

MARCH

APRIL

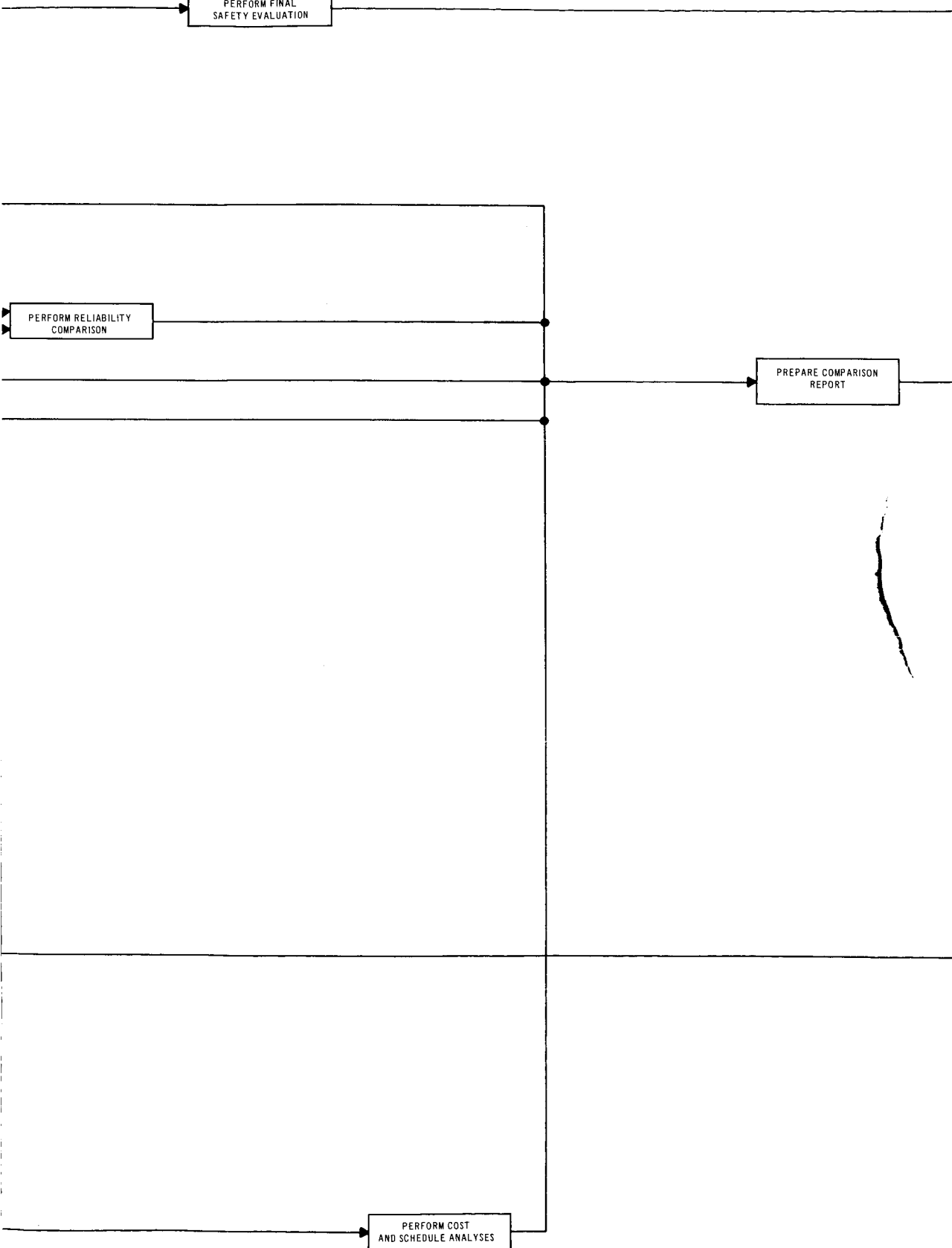
PERFORM FINAL
SAFETY EVALUATION

PERFORM RELIABILITY
COMPARISON

PREPARE COMPARISON
REPORT

PERFORM COST
AND SCHEDULE ANALYSES

2-4-3



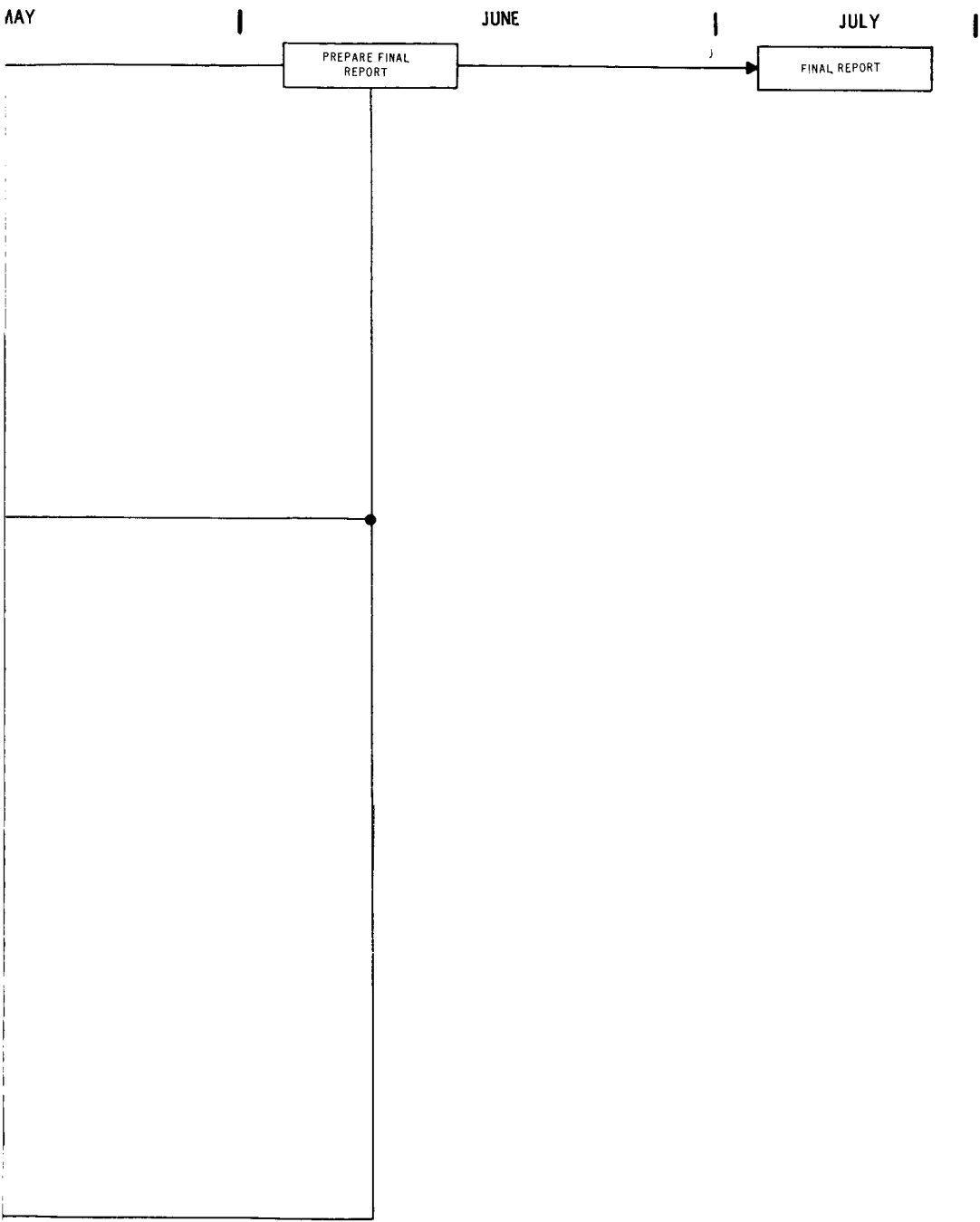


Figure 2-1. RTG Spacecraft Study --
Work Flow Chart

2-4-4

~~2-3-4~~

SECTION 3
RTG SPACECRAFT DESIGN

3.1 Guidelines

Throughout the Voyager program the design philosophy has been to use proven technologies wherever possible. Current Voyager concepts may be viewed as a recombination and synthesis of techniques developed on other programs. This general approach was adopted at the outset of the RTG spacecraft study. The RTG design guidelines adopted for the purpose of this study are summarized below in section 3.1.1. Spacecraft design guidelines are discussed in section 3.1.2.

3.1.1 RTG GUIDELINES

The basic elements of an RTG consist of an isotope fuel heat source, a thermoelectric converter (thermopile) which transforms about 4 to 5 percent of the thermal energy to electrical energy, and a radiator which rejects the unused thermal energy.*

At the outset of the study it was decided to limit the consideration of RTG concepts to those that are undergoing significant development and will find application in the near future. Also considered was the possible use of materials for which considerable test data is available. Summarized below are the basic guidelines pertaining to design concepts and materials that were adopted:

- a. Isotope fuel - Plutonium 238 (Curium 244, backup).
- b. Thermoelectric Materials - Lead telluride (3M Company). Silicon - germanium (RCA).
- c. Radiator - By passive means only.
- d. Isotope fuel containment for all credible abort environments.

In general the above guidelines reflect the use of technology developed on the SNAP-27 or SNAP-19 RTG's. Although the use of advanced concepts might provide advantages (e.g.,

*The operation of RTG's is described in Task C Document No. VOY-C1-TR15. References 3-1 to 3-2 provide general background information.

fluid heat exchanges for spacecraft thermal control) these concepts were not considered to be developed sufficiently for the purpose of this study.

3.1.2 SPACECRAFT DESIGN GUIDELINES

The spacecraft design which resulted from the GE contribution to the Voyager Phase 1A, Task B studies is shown in Figure 3-1. It provided a logical starting point for the RTG integration studies. Some of the principal characteristics of this design are listed below and were adopted as initial guidelines in developing the RTG-powered spacecraft:

- a. Two spacecraft and landers are launched on a single Saturn V launch vehicle. Each spacecraft/lander combination is contained in a separate shroud section. To assure cleanliness during field assembly to the launch vehicle, each shroud section with its spacecraft/lander combination is sealed off by end diaphragms. The encapsulated vehicles are interchangeable and are designed to permit replacement by a standby encapsulated vehicle in the event that last minute difficulties develop prior to launch. The field assembly procedure consists of stacking the 2 encapsulated vehicles along with an upper nose fairing assembly.
- b. The spacecraft fits within a cylindrical envelope 240 inches in diameter by 160 inches in height. Spacecraft structural support is provided by the shroud through an intermediate adaptor. Separation after the boost phase occurs at the spacecraft/adaptor interface. The separation sequence is briefly as follows: The nose fairing and an upper portion of the upper vehicle shroud are jettisoned subsequent to an intermediate boost phase. After injection into a Mars transfer orbit the upper vehicle is separated. Intermediate shroud sections are then removed and finally the lower vehicle is separated.
- c. At its upper end the spacecraft supports a 3000-to-5000 pound encapsulated lander on a 120-inch bolt circle. A shroud length of 104 inches is allocated to the lander. The spacecraft transports the lander to Mars. Except during midcourse correction maneuvers and the Mars orbit insertion operation the lander is transported on the shaded side of the spacecraft. Also, excluding the maneuver periods, the spacecraft continuously provides 200 watts of electrical power to the lander.
- d. A modified Minuteman solid propellant engine for insertion into Mars orbit occupies the central core of the spacecraft. A monopropellant midcourse propulsion system surrounds the nozzle end of the solid propellant orbit insertion engine.
- e. Spacecraft electronics are contained in 16 thermally controlled equipment bays with a volume of 44 cubic feet and a thermal radiation area of 68 square feet. These are arranged in a torus ring surrounding the orbit insertion engine. In normal cruise the central spacecraft axis points toward the sun and therefore the equipment bays are not affected by solar heating.

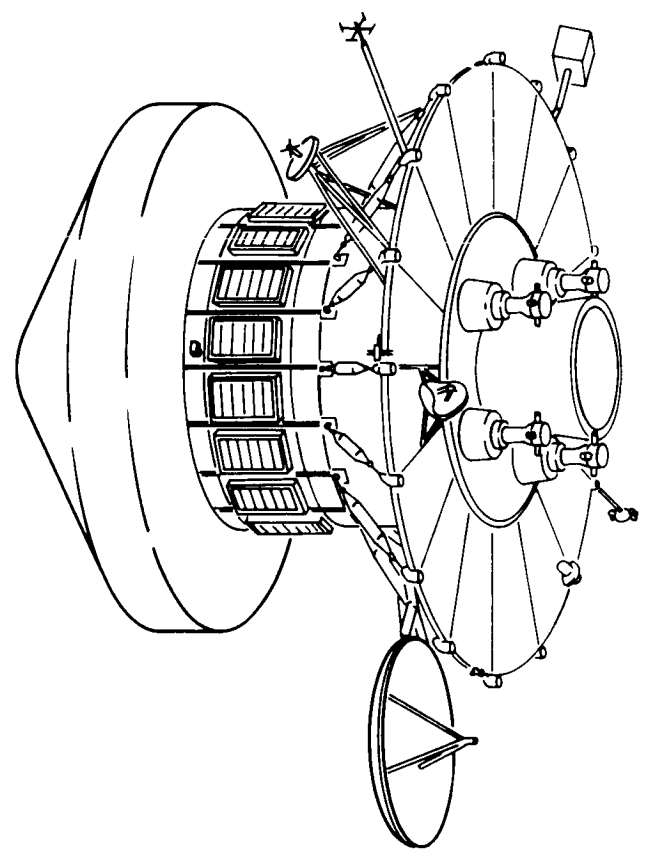
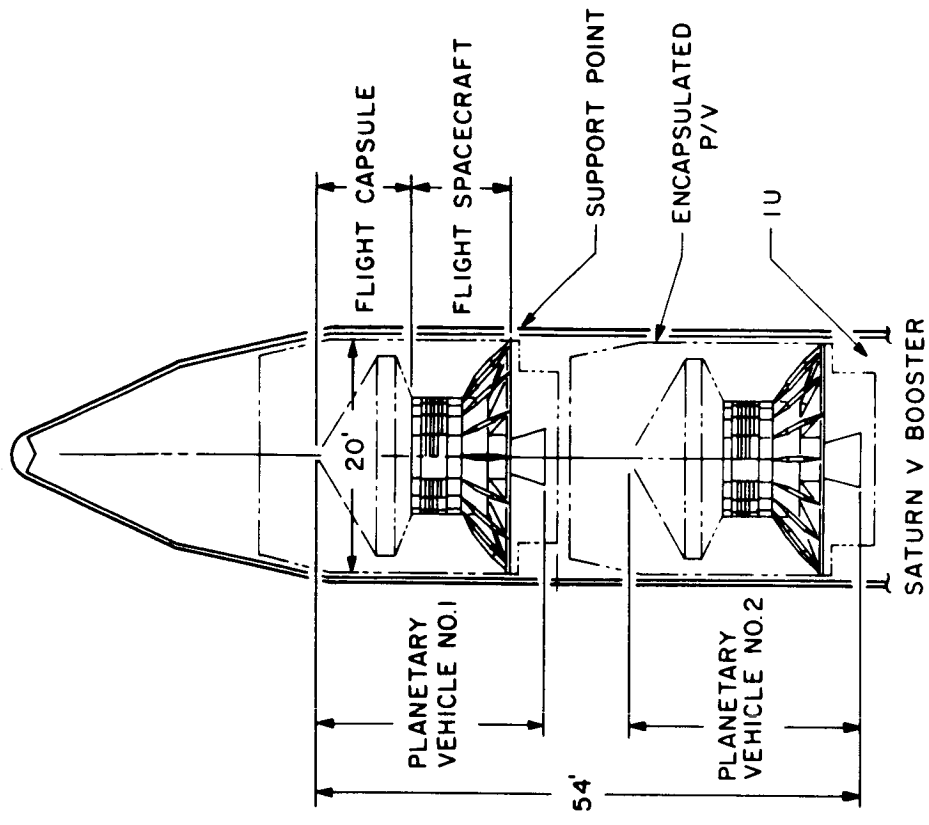


Figure 3-1. Voyage Task B Spacecraft Design

- f. A Sun-Canopus reference system is used for spacecraft 3-axis attitude control. As indicated above, the central or roll axis is sunpointing and accounts for 2 axes of control. Rotation about the roll axis to permit Canopus acquisition accounts for the third control axis. During maneuvers gyro inertial control is used.
- g. A 90-inch parabolic high-gain antenna gimbaled on two axes is used for high data rate communication to Earth. A backup medium gain antenna is also installed in the event of failure of the high-gain antenna. It is mounted to be Earth pointing at the time of Mars encounter. Low-gain antennas provide communication capability during both near-Earth and maneuver operations. A relay antenna is provided for communications with the lander.
- h. A Planet Scan Platform, gimbaled on 3 axes, is mounted near the periphery of the spacecraft for science viewing of the planet.
- i. The average power requirement before Mars encounter is about 600 watts, including 200 watts for the lander. Higher momentary power demands of low energy content occur throughout the mission, the highest being a 900-watt, 90-second requirement during Mars orbit insertion. Subsequent to lander separation (occurring possibly up to 30 days after orbit insertion), the power requirement is still on the order of 600 watts because of increased science power demands.

The above characteristics provided the groundrules for the examination of RTG integration. These groundrules were not inviolate. If RTG's offered significant simplification in certain areas these were critically examined to assure that other characteristics were not compromised. The RTG's themselves imposed conditions that had to be satisfied in one way or another. The more significant ones concerned: (1) the means for handling the RTG heat load of about 15 kilowatts per spacecraft during all mission phases; (2) the number of RTG's to be used in terms of weight optimization, reliability, growth, heat load distribution, and RTG sizes commensurate with present technology; and (3) RTG location on the spacecraft for ease of fuel loading and suitable accommodation of thermal, nuclear radiation, structural, center of gravity and safety considerations.

Several additional goals were set for the integration study. First, the feasibility of designing a solar-powered spacecraft that could be converted to an RTG-powered spacecraft, without severe compromises, was to be determined. This feature provides overall mission flexibility. For missions out to several AU, either version might be acceptable; beyond that range only RTG power is practical. A second additional goal was to develop the design to be adaptable to either clamshell or over-the-nose shroud designs.

3.2 DESIGN EVOLUTION

3.2.1 PRELIMINARY RTG SIZING MODEL

To aid in the spacecraft design process it was first necessary to prepare preliminary RTG design data that would permit rapid size and weight estimates for alternative numbers and locations of RTG's. The SNAP-27 generator shown in Figure 3-2 provides a basis for determining these preliminary estimate characteristics. Its gross properties are summarized below:

- a. Power: 65 watts at end-of-life (8800 hours)
- b. Weight (without re-entry protection): 38.5 lb
- c. Weight (estimated - with re-entry protection): 58.5 lb
- d. Length: 18.1 inches
- e. Diameter: 15.7 inches
- f. Heat rejection: To space above mounting plane of the RTG.

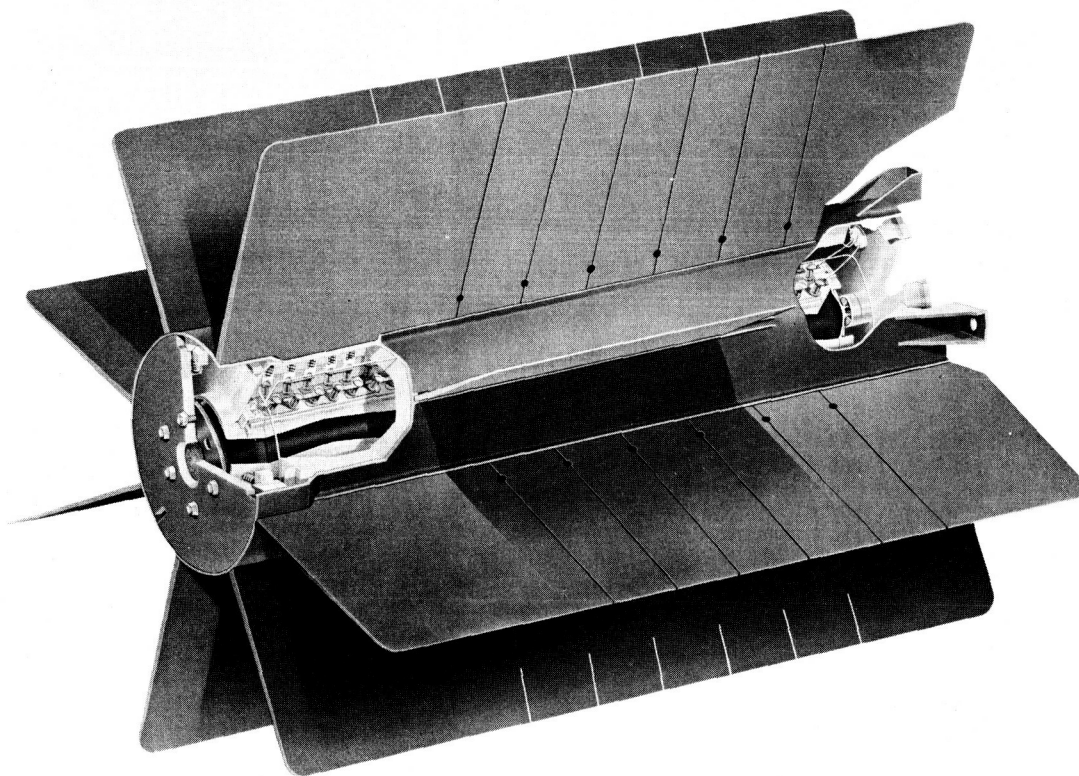


Figure 3-2. SNAP-27 Generator

The heat rejection area of an RTG may be characterized by that surface area which surrounds the extremities of the heat rejection fins. Assuming a constant heat rejection temperature, it is this area which is proportional to RTG power. For the SNAP-27 generator this area is about 1000 square inches, taking into account the outer cylindrical area and 85 percent of the area of one end. (The other 15 percent is not considered to provide to the effective radiating area since it is insulated to prevent fuel capsule heat leaks; the opposite end is ignored completely because of blockage of the mounting plane.) Thus, the effective radiating area required is about 16.7 square inches per watt (e). For the same factors of cylindrical and end area utilization, Figure 3-3 shows the corresponding dependence of RTG length on power for various RTG diameters. The case for extended SNAP-27 configuration is identified. For all of these cases an overall specific weight of 0.9 watt per pound provides a reasonable first approximation, though it should be realized that this is based on the specific design conditions of the SNAP-27 generator.

Design optimization for specific applications will in general result in some deviation from the nominal characteristics described here. Section 5.1 provides a more definitive evaluation of RTG sizing.

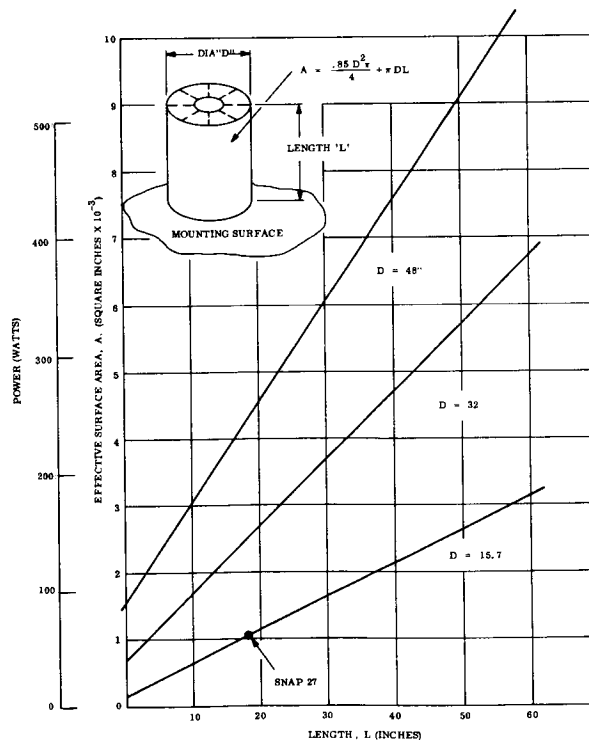


Figure 3-3. Preliminary RTG Sizing Model

3.2.2 SPACECRAFT DESIGN EVOLUTION

An examination of the location requirements of some of the major elements of spacecraft equipment reveals that the RTG's are best mounted near the periphery of the spacecraft. Because the propulsion units must occupy the central core of the spacecraft, the available RTG mounting locations are in the annular zone between this core and the shroud. The spacecraft electronic equipment is conveniently arranged in the form of a torus surrounding the propulsion unit. Together with the structural elements required to provide load paths of the propulsion units, electronic torus ring and lander to the supporting shroud, the annular space available for RTG mounting is about 5 feet thick, not counting clearance allowance required during shroud separation. The use of at least 2 RTG's would be required for balance purposes. With each rated at 300 watts, their diameter would be on the order of 26 inches as shown in Figure 3-3. Although 2 units of this size could conceivably be integrated into the design, this does not appear desirable because of the high concentration of rejected heat onto a limited zone of the shroud. For this reason an arrangement using 4 or more units was considered in the initial phases of the study. The reasons for the final selection of an arrangement using 8 RTG's are given in Section 3.3.

With this basic guideline in mind, a number of spacecraft designs were considered. A matrix with appropriate weighting factors was used to assist in the selection process and is described in Task C Document No. VOY-C1-TR9. The principal results of the selection process are summarized below.

Figure 3-4 shows a progression of the three principal configurations considered. This figure lists numerous design criteria considered to be of importance in the development of the spacecraft design. The relative heights of the cross-hatching indicate the relative ability of each candidate configuration to meet the particular criterion.

Configuration A is an RTG adaptation of the Task B design with the RTG's mounted around the central cylinder. As indicated on the criteria comparison chart, the principal shortcomings relate to shroud separation and gimbaling. The shroud problem concerns the compatibility with an over-the-nose shroud as illustrated on Figure 3-5. The vehicle on the left, representative of Configuration A, has two large diameters separated by an appreciable

CONFIGURATION	CRITERIA	EXPLANATION	MEASURE OF CRITERIA		
			A	B	C
	AIR CONDITIONING	PREVENTION OF RTG OVERHEATING DURING ON-PAD OPERATION	[Bar chart showing high performance for A, B, and C]		
	THERMAL INTERACTION	PREVENTION OF SPACECRAFT EQUIPMENT ON-PAD OVERHEATING DUE TO RTG'S	[Bar chart showing high performance for A, B, and C]		
	RTG EJECTABILITY	PERMIT RTG EJECTION IN CASE OF MISSION ABORT	[Bar chart showing high performance for A, B, and C]		
	RADIATION INTERACTION	SUITABLE EQUIPMENT LOCATION TO MINIMIZE RTG RADIATION EFFECTS	[Bar chart showing high performance for A, B, and C]		
	OVER THE NOSE SHROUD	ADAPTABILITY TO EITHER OVER-THE-NOSE OR CLAMSHELL SHROUD	[Bar chart showing high performance for A, B, and C]		
	NUMBER OF RTG'S	INFLUENCE OF MOUNTING SPACE, WEIGHT DISTRIBUTION, HEAT REJECTION CAPABILITY, RELIABILITY IN DETERMINING MULTIPLICITY OF UNITS	[Bar chart showing high performance for A, B, and C]		
	INTERCHANGEABILITY	ADAPTABILITY AS A SOLAR ARRAY DESIGN. MAY USE SOLAR POWER IN EARLY MISSION AND RTG'S IN LATER MISSIONS	[Bar chart showing high performance for A, B, and C]		
	SERVICEABILITY	EASE OF TEST, REPAIR, MANUFACTURE, ETC.	[Bar chart showing high performance for A, B, and C]		
	VIEW REQUIREMENTS	MINIMIZE DEPLOYABLE BOOMS, ETC. FOR CRITICAL SENSORS	[Bar chart showing high performance for A, B, and C]		
	EFFECT ON PAYLOAD WEIGHT	MINIMIZE STRUCTURAL WEIGHT TO INCREASE PAYLOAD CAPACITY	[Bar chart showing high performance for A, B, and C]		
	MINIMIZE GIMBALLING COMPLEXITY	MINIMIZE MOVING PARTS	[Bar chart showing high performance for A, B, and C]		

Figure 3-4. RTG Spacecraft Configuration Evolution

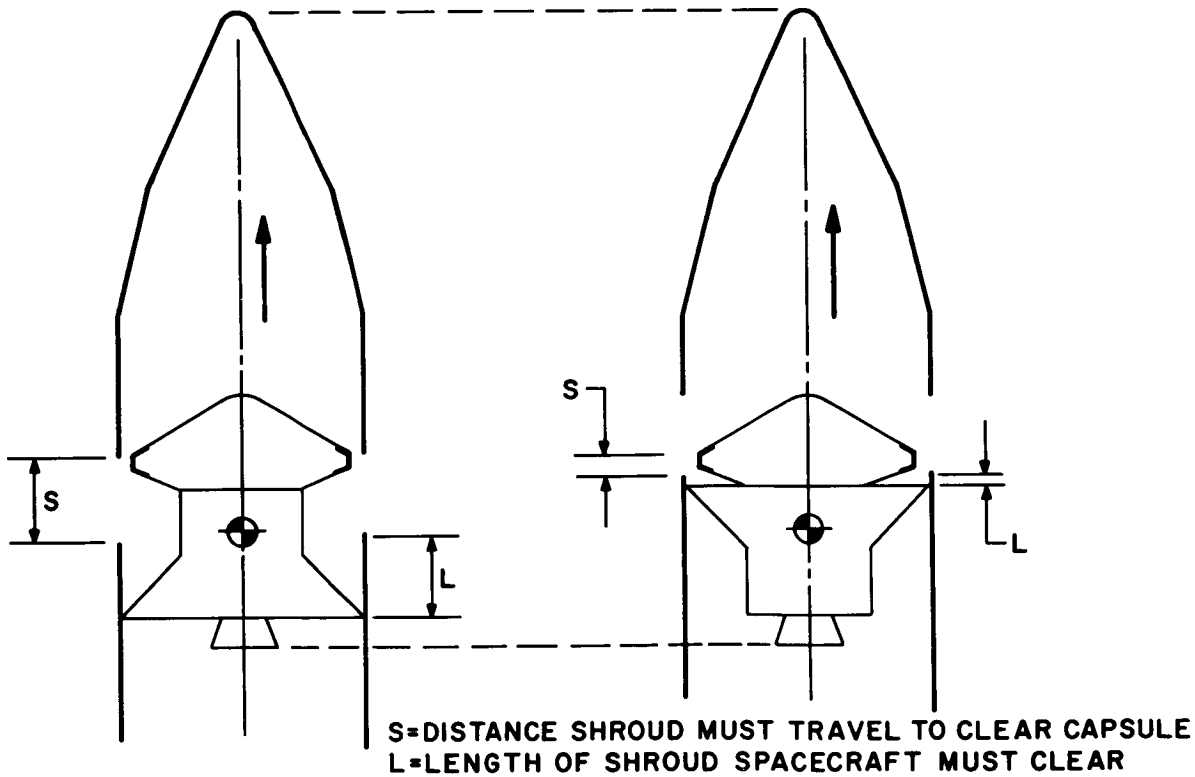


Figure 3-5. Over-the-Nose Shroud Separation

distance. Depending on the location of the shroud separation joint, either the shroud or spacecraft requires low tipoff rates during separation to prevent collision. The vehicle on the right relieves this significantly by decreasing the distance between the large diameters. The gimbaling problem relates to the fact that a fixed high-gain antenna cannot be utilized since deployment is necessary.

Configuration B is representative of the next class of configurations examined. The spacecraft is supported by a cone adapter attached to the shroud. As noted on the criteria comparison chart (Figure 3-4), the principal objection involved interchangeability with a solar array version and convenience of sensor location. No convenient location for a solar array appeared available without requiring panel deployment. Similarly, sensors required to view past the Flight Capsule would require mounting on deployable booms. Also, attitude control jets could not be located to provide maximum moment arm capability.

Configuration C appeared to solve the shortcomings of A and B by use of a high-truss structural support. This also resulted in an excellent mounting location for the Planet Scan Package by providing an extended field of view. Objections were associated with the proximity of the RTG's to the Flight Capsule and support structure, creating potential thermal problems. This configuration served as the basis for the selected RTG spacecraft design described in Section 3.3. The potential thermal problems were avoided by selecting an RTG design with appropriate thermal insulation near its mounting region and by mounting the RTG's on the outermost structural elements.

3.3 SELECTED RTG SPACECRAFT DESIGN

3.3.1 SPACECRAFT DESCRIPTION

An isometric view of the RTG spacecraft and a model photograph are shown in Figures 3-6 and 3-7 respectively, together with the Flight Capsule. The combination forms a Planetary Vehicle, two of which are launched from a single Saturn V Launch Vehicle. They are attached to the shroud fairing as shown in Figure 3-6.

The general arrangement of the Flight Spacecraft is shown in Figure 3-8, and spacecraft antenna and sensor locations with fields of view are shown in Figure 3-9. The spacecraft comprises the following principal elements:

- a. The selected Task B solid propellant orbit insertion engine occupies the central region of the spacecraft.
- b. Surrounding the nozzle of the orbit insertion engine are the tanks and four engines comprising the Midcourse and Orbit Adjust (MC&OA) system, also defined by the Task B design. These are contained in the lower cylindrical housing.
- c. Above the MC&OA system are located 12 electronic equipment bays in the form of a torus ring surrounding the orbit insertion engine. Environmental control is provided by radiator plates and thermally-controlled louvers. Just below the equipment bays, a shelf extends circumferentially around the body to prevent direct solar input into the equipment bays during long periods of operation when the vehicle roll axis is misaligned with the solar vector.
- d. Above the equipment bay torus ring a 12-sided truss structure with trapezoidal shear panels extends upward and outward to join the shroud at 12 separation and support points. An inner structural cone transfers the orbit insertion engine loads to the truss structure. A similar cone and upper truss structure transfers the Flight Capsule loads to the shroud support points.
- e. Eight RTG's are mounted to eight of the trapezoidal shear panels. Each RTG is nominally rated at 75 electrical watts. The RTG's are described further in Section 3.3.2.
- f. A 90-inch high-gain parabolic antenna is rigidly attached to the spacecraft with its axis lying in the X-Z plane and subtending an angle of about 40 degrees with the Z axis. Low-gain, medium-gain, and Flight Capsule relay antennas are also provided to accommodate various mission communication requirements.
- g. A Planet Scan Package (PSP) is mounted near the periphery of the truss support. In a stowed position during heliocentric transfer, it rests against one of the trapezoidal shear panels. Once deployed, the PSP will track the planet utilizing two periodically stepped gimbals and a servo-driven third gimbal. With the Flight Capsule attached the PSP has an unobstructed view of the planet for orbits inclined up to about 40 degrees from the plane of the ecliptic.

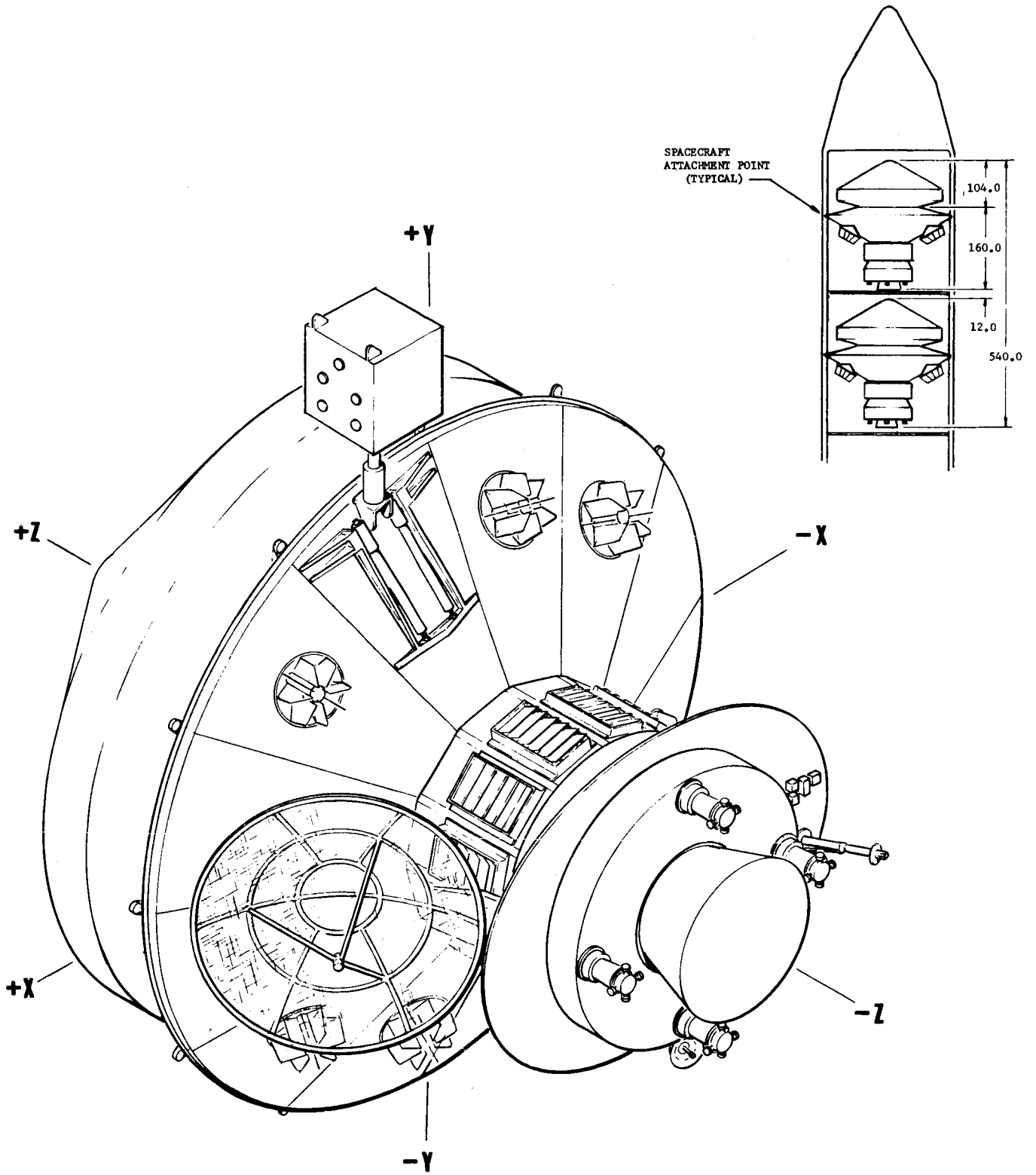


Figure 3-6. RTG Spacecraft

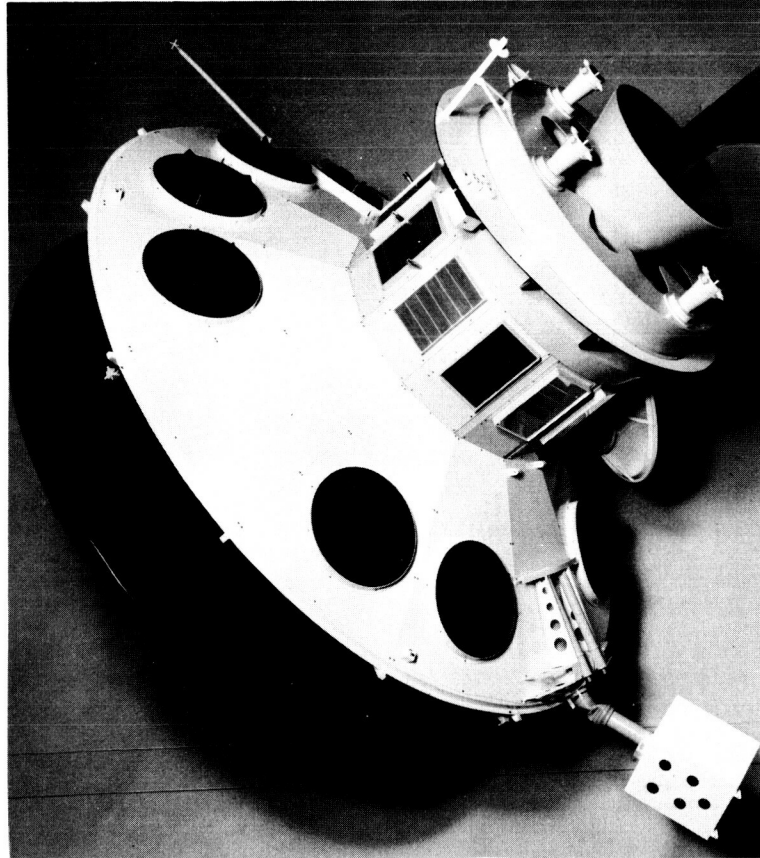
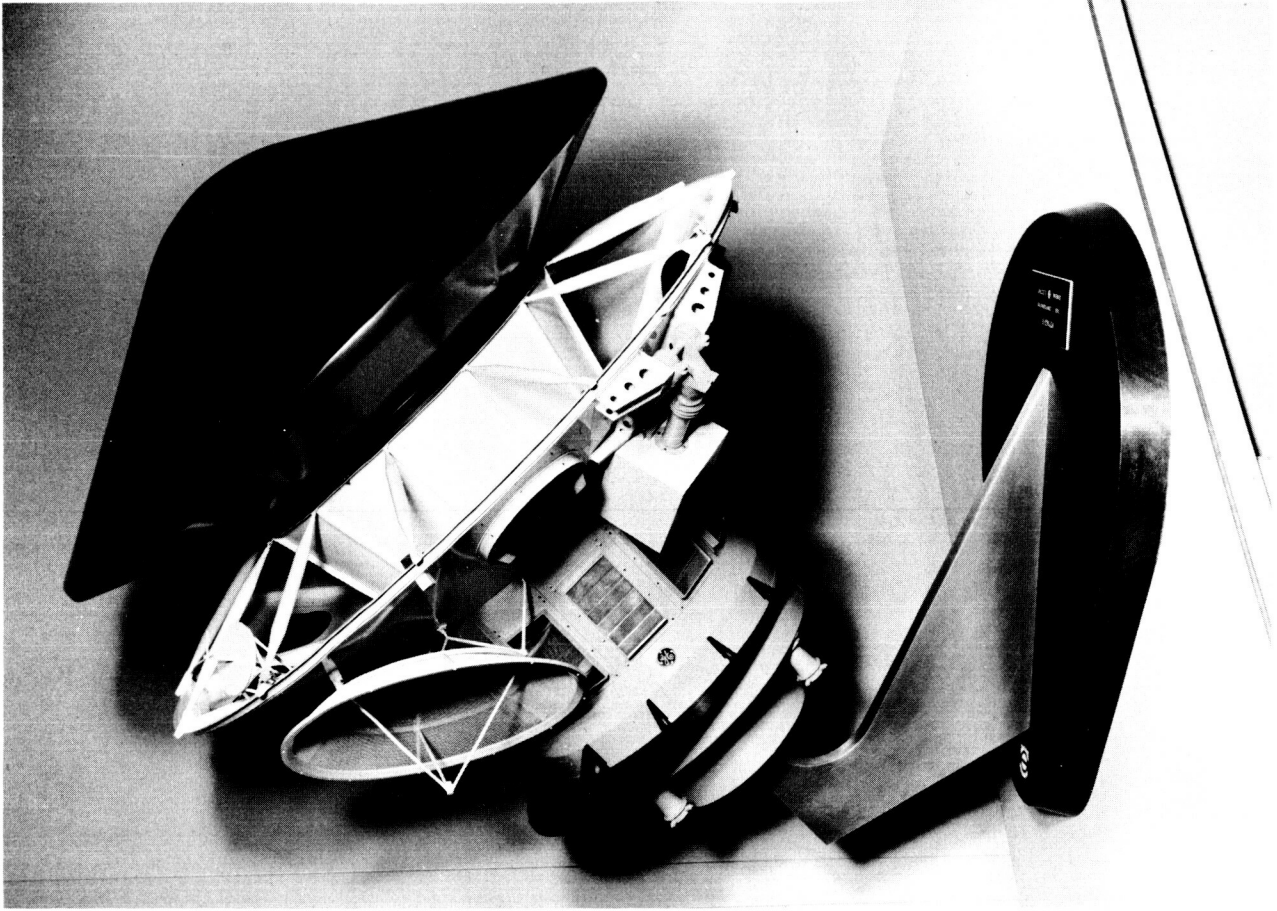
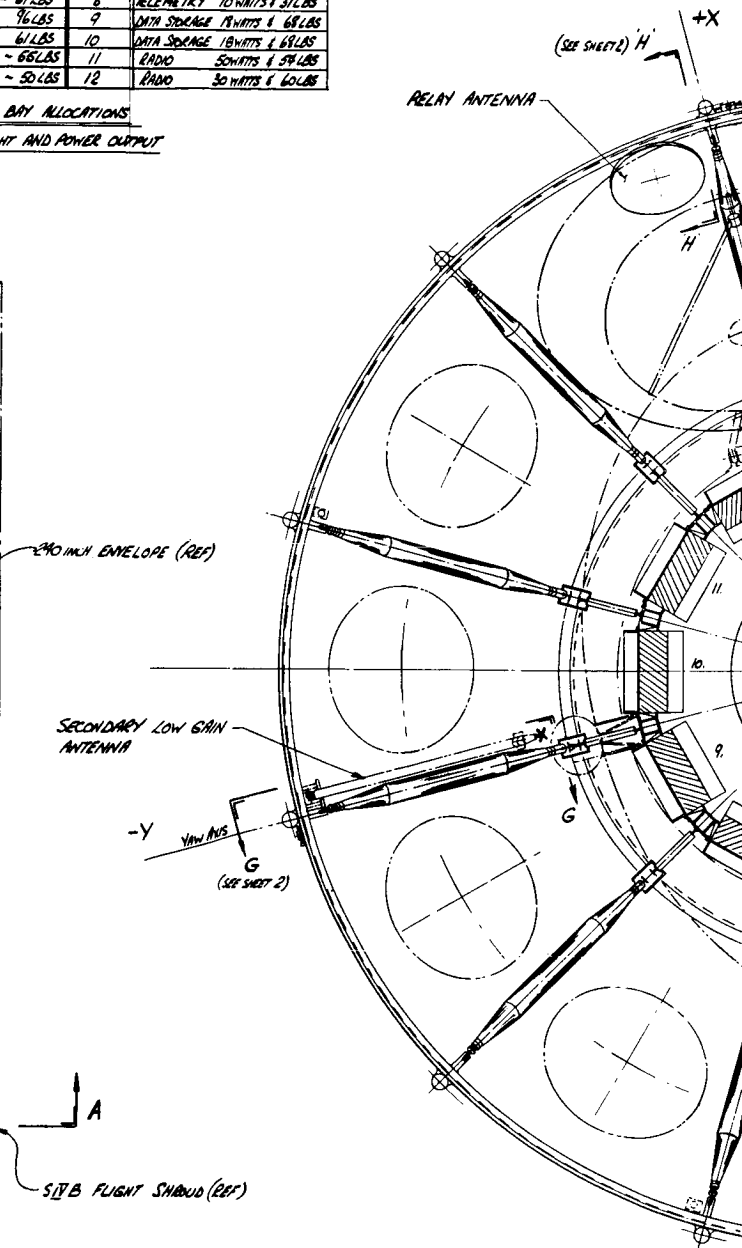
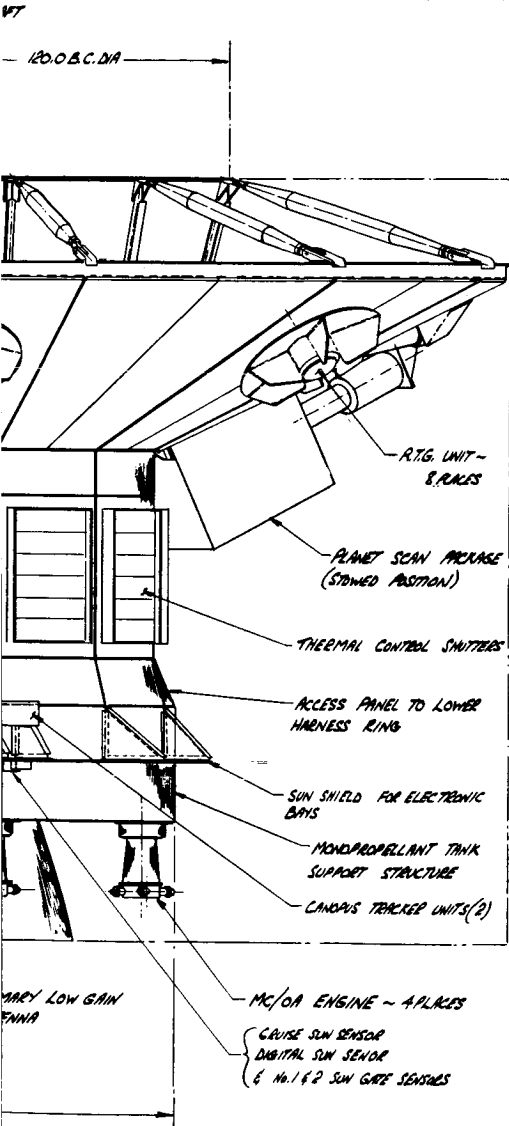


Figure 3-7. RTG Spacecraft Model

BAY No.	SUBSYSTEM	BAY No.	SUBSYSTEM
1	POWER 53 WATTS - 68 LBS	7	COMMAND 20 WATTS & 39 LBS
2	POWER 66 WATTS - 67 LBS	8	TELEMETRY 10 WATTS & 31 LBS
3	SCIENCE ~ 96 LBS	9	DATA STORAGE 18 WATTS & 68 LBS
4	SCIENCE ~ 67 LBS	10	DATA STORAGE 18 WATTS & 68 LBS
5	G & C 35 WATTS - 66 LBS	11	RADIO 50 WATTS & 59 LBS
6	C & S 50 WATTS - 50 LBS	12	RADIO 30 WATTS & 60 LBS

TABLE SHOWING BAY ALLOCATIONS
WITH APPROX WEIGHT AND POWER OUTPUT



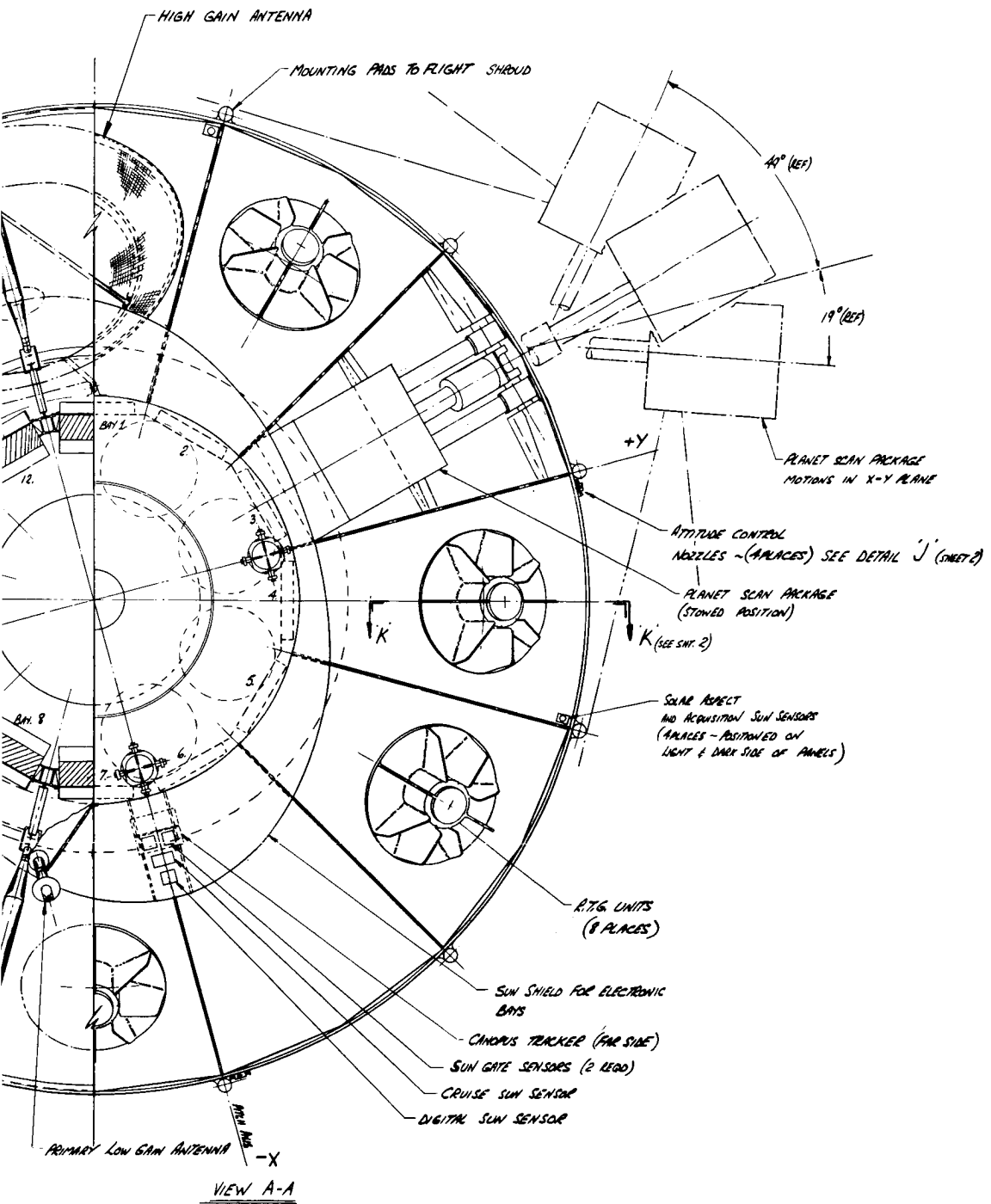
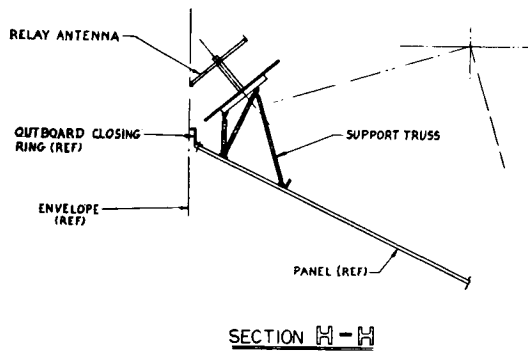
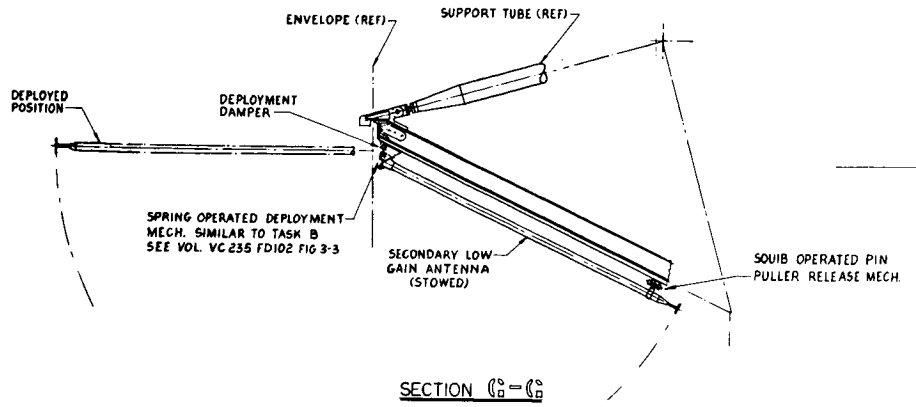
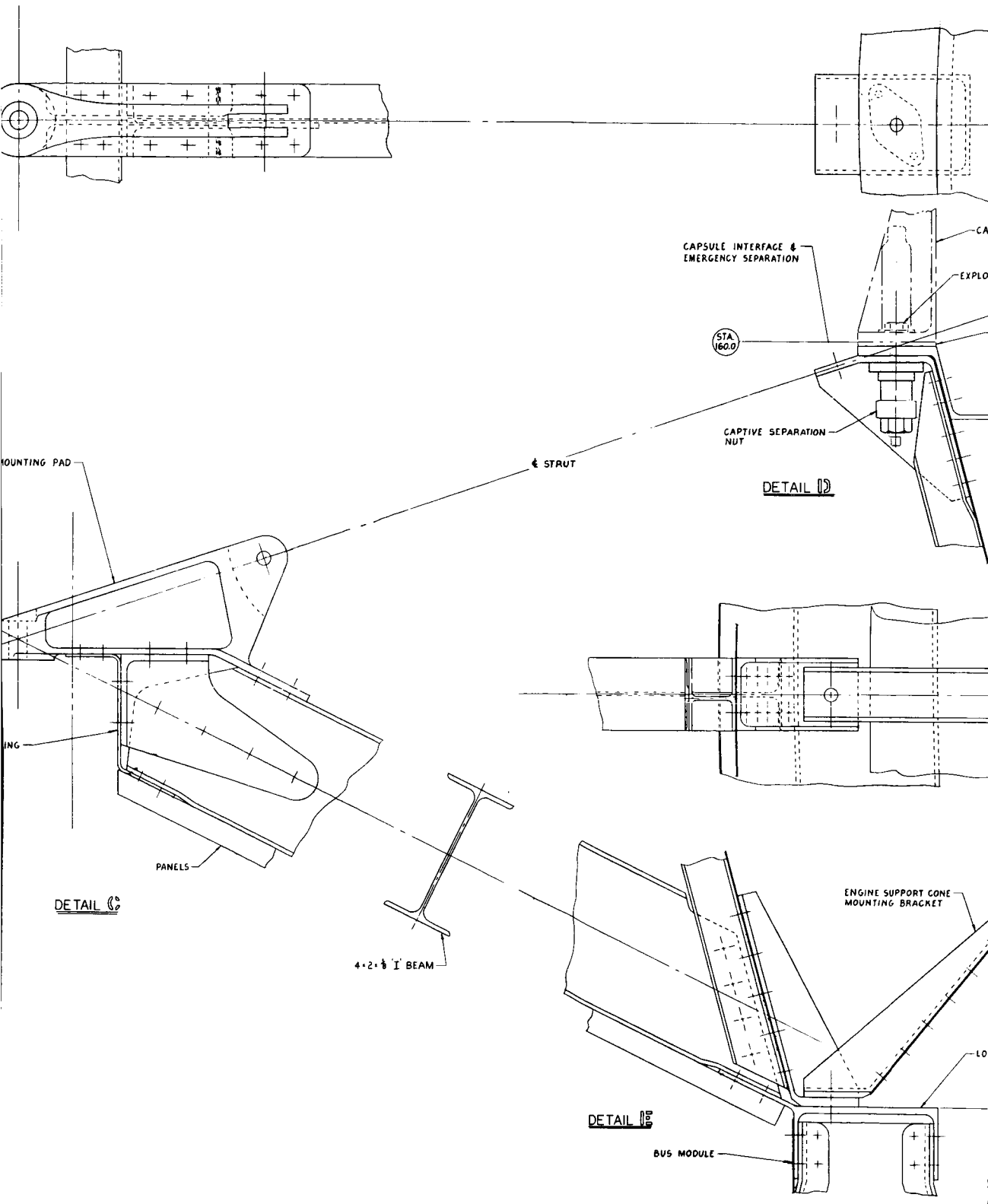


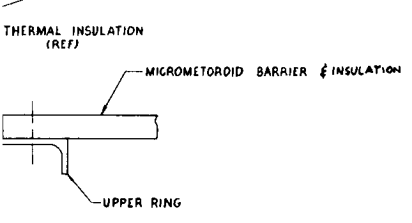
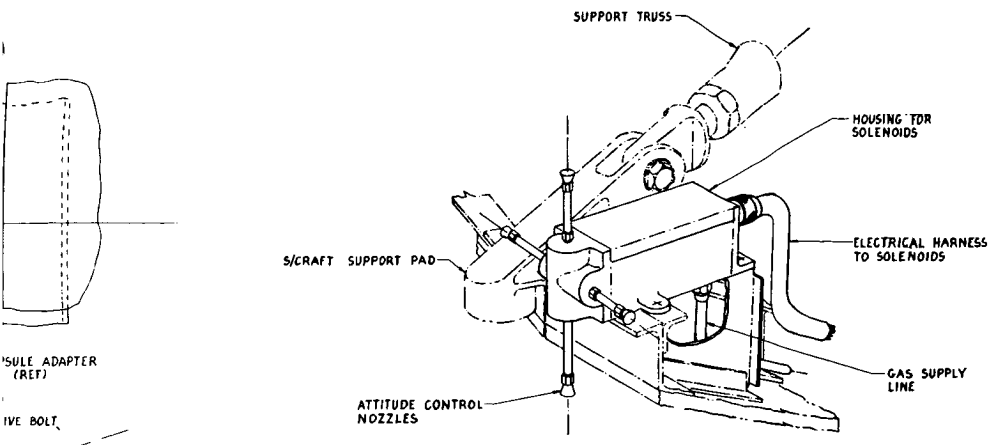
Figure 3-8. General Arrangement of RTG Spacecraft (Sheet 1 of 2)



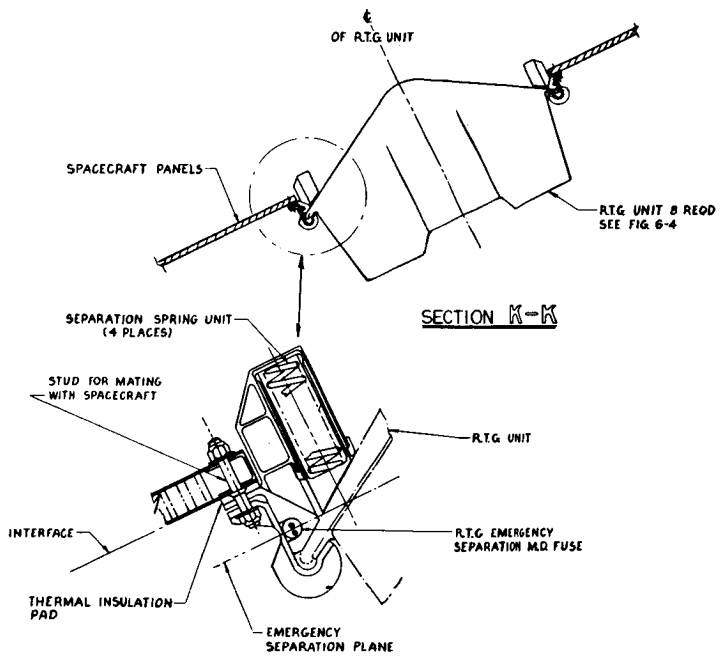
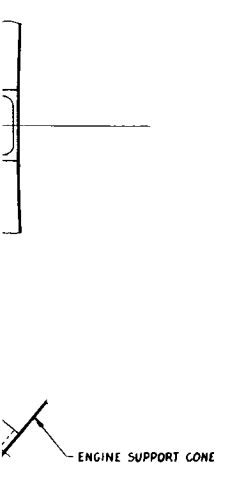
ENCLOSURE 1

3-15





DETAIL J



ENLARGED VIEW OF RTG EMERGENCY SEPARATION

Figure 3-8. General Arrangement of RTG Spacecraft (Sheet 2 of 2)

STA 103.0

3-16-2

8-167-16

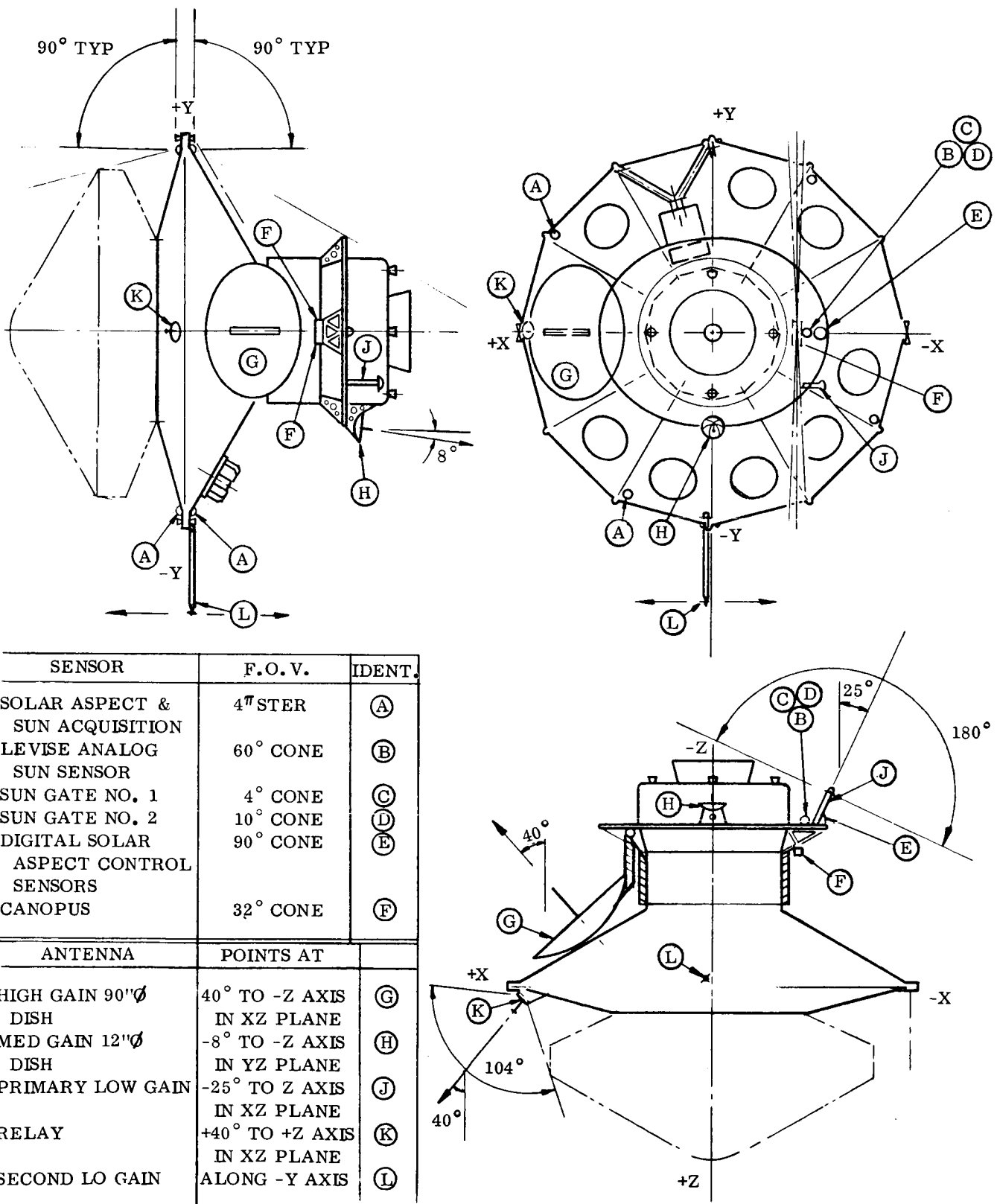


Figure 3-9. RTG Spacecraft Antenna and Sensor Locations

- h. A cold gas system for attitude control, identical to the Task B design, is located in the upper structure. Yaw, pitch and roll control jets are located at the periphery of the truss support to provide maximum fixed moment arm capability. Tankage and piping are nested in the upper structure.
- i. The principal solar and Canopus sensors are mounted on a bracket near the Guidance and Control electronic equipment. Additional acquisition Sun sensors are located on the high truss structure.
- j. The Flight Capsule is joined to the Flight Spacecraft by means of mating flanges identical to those in the Task B design.

Operation of the spacecraft during various mission phases is quite similar to that of the Task B design. The principal differences are associated with prelaunch procedures for handling the RTG's and changes in the attitude reference system required to accommodate Earth-pointing of the fixed high-gain antenna. The following summary phase descriptions are generalized to highlight significant changes from the Task B design.

3.3.1.1 Prelaunch Phase

Principal differences in operational procedures during this phase will follow from the time that live fuel capsules are first inserted into the RTG's. This will be accomplished in the Explosive Safe Area prior to shroud encapsulation of the Planetary Vehicle. From this point on specific measures will be necessary to ensure personnel safety regarding RTG nuclear radiation. After shroud encapsulation, continuous cooling will be required to remove the RTG heat up to the time of liftoff. These aspects are described in greater detail in Section 3.5 concerning OSE and Section 3.3.5 concerning thermal analysis.

3.3.1.2 Launch To Injection Phase

No significant changes in operation are anticipated for this phase. Electrical loads are kept to a minimum to maintain acceptable temperature levels during the time that the spacecraft are enshrouded by the nose fairing. Separation sequences will vary somewhat, depending on whether clamshell or over-the-nose shroud separation methods are used. Injection into the heliocentric transfer orbit proceeds as described in the Task B design.

3.3.1.3 Acquisition Phase

Solar and Canopus attitude references are acquired by the methods utilized in the Task B design.

3.3.1.4 Early Cruise Phase

Reference is made to Figure 3-10 in describing operation at this and subsequent phases. The orbits and relative positioning of Mars, Earth and the spacecraft are shown and all lie approximately within the plane of the ecliptic. This is represented by the plane of the figure itself. Position A is a representative location during the early cruise phase. Operation proceeds as in the Task B design with the Sun and Canopus as primary references. The spacecraft Z axis is Sun-pointing with the Flight Capsule on the shaded end. The high-gain antenna axis is nonaligned with the direction to Earth and communications depend initially on the low-gain antenna and later, as communication distance increases, on the medium-gain antenna. Short of executing a special maneuver, the high-gain antenna is not available as a means for verifying Canopus acquisition.

3.3.1.5 Midcourse Corrections

These are executed in a manner similar to the Task B approach. Maneuver attitude verification is by means of digital sun sensor information relayed either through the primary or

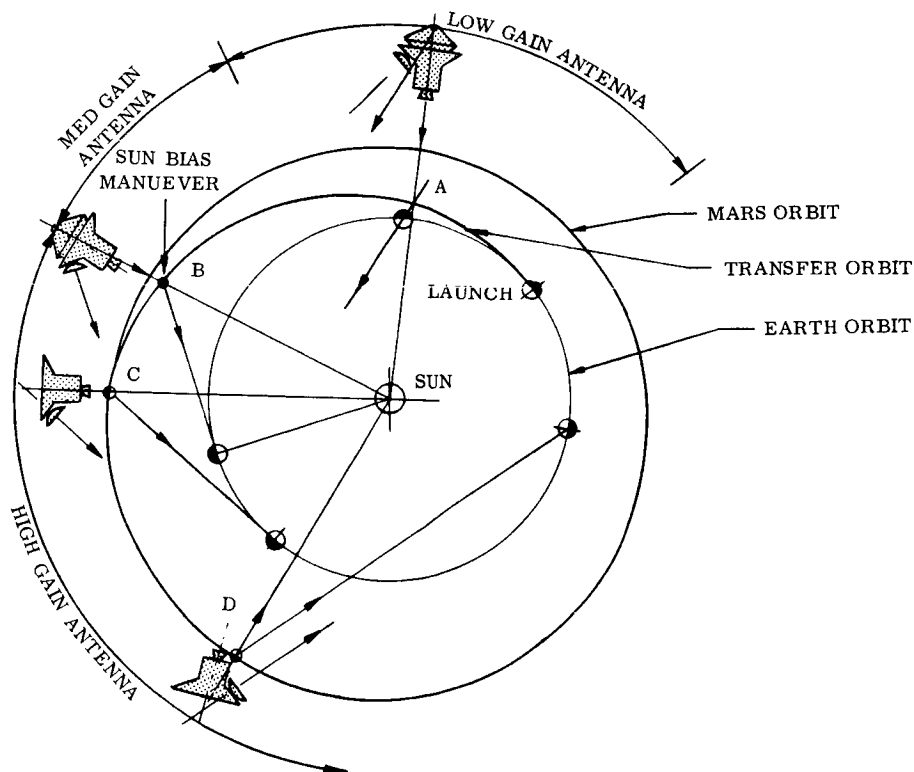


Figure 3-10. Operational Sequence of Sun-Biased System

secondary low-gain antennas, depending on attitude. The RTG's permit longer time periods for correction because they do not depend on battery energy. An upper limit on this time depends on the allowable amount of direct solar heat input to the Flight Capsule and equipment bays.

3.3.1.6 Late Cruise Phase

At a certain time in the heliocentric transfer orbit, the performance of the medium-gain antenna becomes marginal, and it is necessary to use the high-gain antenna (HGA) for communications. The spacecraft Z axis must be biased from the solar direction in order to Earth-point the HGA. This is shown at position B in Figure 3-10. The degree of solar bias in both X and Y spacecraft directions is predetermined as a function of time, and depends on the heliocentric transfer orbit characteristics and the orientation of the fixed high-gain antenna axis with respect to the vehicle axes. This information is stored in the Computer and Sequencer (C&S) Subsystem. At the time that bias operation must commence the C&S provides the proper X and Y bias values. These are combined with the output of X and Y digital Sun sensors to operate the attitude control system in a normal null seeking mode. As shown at position B, the vehicle Z axis is biased in the X direction. Bias occurs in the Y direction as well, since the Mars, Earth and transfer orbits are not perfectly coplanar. The bias maneuver is not a maneuver in the same sense as those required for midcourse correction. Rather, a step change in the apparent location of the sun is introduced and the attitude control cold gas system reacts to compensate for this. As the mission proceeds, the C&S periodically provides updated bias information, gradually redirecting the spacecraft orientation. With bias operation, a continuous means of Canopus verification becomes available through the use of the high-gain antenna.

3.3.1.7 Orbit Insertion

Orbit insertion is similar to that in the Task B design. Here, too, the RTG's permit additional time to verify and conduct this critical maneuver because there is no battery energy constraint.

3.3.1.8 Planetary Encounter

Just after orbit insertion the spacecraft attitude is as shown at position C in Figure 3-10. The orientation of the high-gain antenna axis with the spacecraft axes has been so selected to result in direct Sun-pointing of the spacecraft Z axis. In the event of failure of the digital Sun sensor(s), this permits use of a backup null Sun sensor of the type used in the Task B design. In this backup mode of operation, no sacrifice is made in mission capability until several weeks after encounter when the high-gain antenna axis diverges excessively from the Earth-pointing direction.

3.3.1.9 Flight Capsule Separation and Orbit Adjust

These are similar to the Task B approach. The RTG's permit greater latitude in parameter selection because of removal of the battery energy constraint.

3.3.1.10 Planetary Orbit Phase

Position D on Figure 3-10 is typical of this phase. Updated values of X and Y bias from the C&S gradually displace the Z axis to an angle of about 30 degrees with the solar vector after six months in orbit. Solar, Earth and Canopus occultations are handled similarly to those in the Task B design. Terminator and limb crossings are detected in the Task B design by properly combining planetary disk measurements taken by the PSP with the PSP gimbal angular position. The method depends on the Sun orientation of the spacecraft Z axis. With the Sun-biased attitude reference system, the X and Y bias values from the C&S are combined with the gimbal angular measurements to compensate for the nonalignment to the Sun. Beyond this, operation is identical to that of the Task B approach.

3.3.2 RTG DESCRIPTION

3.3.2.1 RTG Integration

Eight RTG's are mounted on 8 of the 12 shear panels which form part of the truss support structure (Figure 3-8). This location was favored for several reasons. First, since the RTG's are above the more temperature sensitive spacecraft equipment, namely the electronic bays and propulsion units, there is a reduced tendency to transport RTG waste heat by convective means during prelaunch operation. Second, since the RTG's are located near the largest periphery of the spacecraft, more mounting space is available, permitting the required capacity to be easily installed. It is estimated that a 50 percent growth is possible by using larger RTG's on the same mounting location. This is discussed further in Section 7 concerning overall growth implications. Third, with the RTG's canted as shown, the high location avoids concentrated heating of the Saturn V Instrument Unit which is located near the 20-foot diameter base of the lower spacecraft shroud. At the same time, because the RTG's are canted they reject their waste heat over a broad region of the internal shroud wall, thus resulting in more gradual temperature gradients. Since the 8 RTG's are distributed more or less uniformly around the spacecraft, the temperature distribution on the shroud wall is somewhat axisymmetric, favoring a reduction in shroud thermal stress conditions.

The nominal configuration of the RTG is shown in Figure 3-11. In this figure the RTG is shown mounted to the shear panels at the periphery of the heat rejection fins, though a variety of other mounting methods are available. A headlight shaped thermal barrier prevents heat transport toward the inboard side of the mounting panels; thus, heat rejection is predominantly in the outward axial direction. The basic RTG design and its mounting arrangement will not be greatly affected by whether overall cladding techniques or aerodynamic re-entry shields are used for re-entry protection. In the latter case, the headlight thermal barrier would be replaced by a similarly shaped re-entry shield, thereby serving two functions. Separation is a complicating requirement for this approach; if used, the mounting location permits a clear ejection path.

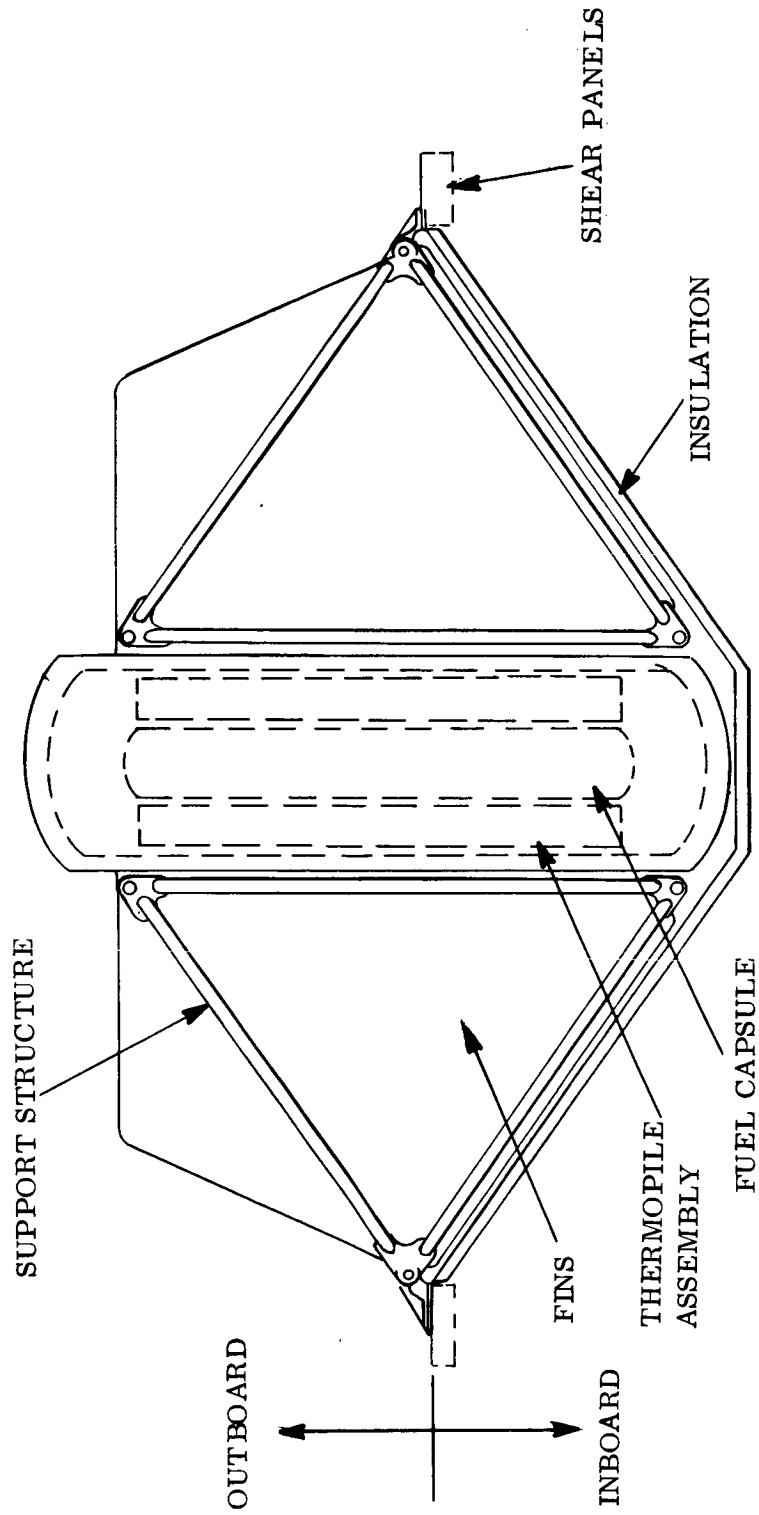


Figure 3-11. Nominal RTG Configuration

The selection of 8 RTG's was simply based on the fact that this number of panels was conveniently available for RTG mounting. As it turned out, a broad minimum in weight exists between 4 to 12 RTG's, so that the selection was not critical in terms of weight. The 75-watt size resulting from the selection of 8 RTG's is close to the capability of the SNAP-27 RTG and therefore advantage can be taken of the technology developed on that program.

The RTG's are intended to be fueled prior to enclosure by the shroud. This operation takes place in an explosive safe facility before transport of the encapsulated spacecraft/lander for assembly to the launch vehicle. The orientation of the RTG's on the spacecraft permits easy accomplishment of this operation. The fuel capsules are inserted along the RTG axis and locked in place. After placement of the shroud and end seal diaphragms, some form of internal and shroud wall cooling is required to remove the RTG waste heat. This must continue, with the possibility of short interruption, until liftoff. Although the orientation of the RTG's does permit the option of on-pad fuel loading through appropriately placed ports on the shroud, it is not favored because of violation of the internal cleanliness requirement during the loading operation. Also, some fairly complicated loading equipment could be involved. In any case, subsequent cooling would be required since it is not likely that liftoff would occur sufficiently soon after fuel loading, and the possibility of an extended hold would have to be considered.

The need for cooling is associated with the electronic and propulsion equipment rather, than with the RTG's. It was estimated that in a worst case, without cooling, the RTG operating temperatures would rise no higher than 30° F. This is considered to be within their design margin. The electronic equipment temperatures, however, could rise to excessive levels for the case of no cooling on a hot day. With internal cooling air some relief is provided. Increased flow lowers the temperature but at a diminishing rate. This results from the poor convective heat transfer coefficient of air unless at prohibitively high velocities. A more effective means of relief is obtained by cooling of the shroud walls, as discussed more thoroughly in Section 3.3.5, Thermal Analysis.

3.3.2.2 RTG Design

Both integral and separable re-entry protection techniques for assuring isotope fuel containment in the event of a mission abort were considered. The relative merit of these techniques are discussed further in Section 5.3. In summary, the separable approach uses a directional heat shield which is aerodynamically stabilized during re-entry. Its successful operation requires RTG separation from the spacecraft prior to re-entry heating. The integral approach uses cladding which surrounds the vulnerable portions of the RTG. No specific re-entry orientation is required and therefore the need for separation is avoided, at least insofar as such separation is required to permit proper re-entry orientations.

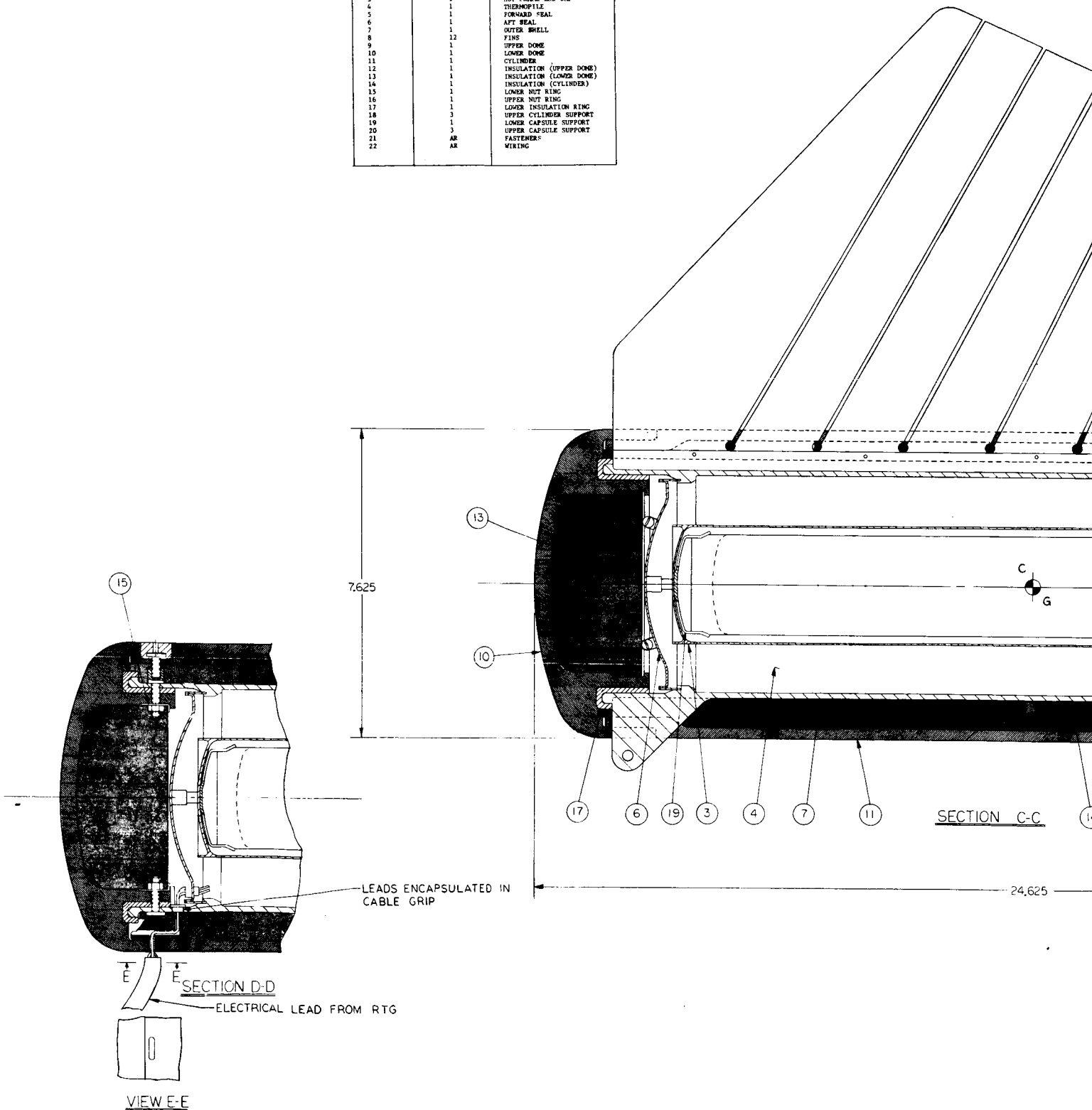
The separable approach was initially considered since the weight uncertainty of the integral approach appeared larger. An examination of the RTG separation requirement has revealed that the separable approach is applicable to a limited class of abort situations in which sufficient structural integrity of the spacecraft is maintained to permit successful RTG separation. For this reason greater emphasis was subsequently placed on the integral approach. In connection with other RTG programs particular cladding concepts have evolved and have been studied in considerable depth. Section 2.5 of Document No. VOY-C1-TR15 describes some of this analysis in greater detail. Calculations of re-entry protection weight using graphitic material cladding indicated values (and uncertainties) comparable with those of the separable approach. These results have led to preference for the integral approach.

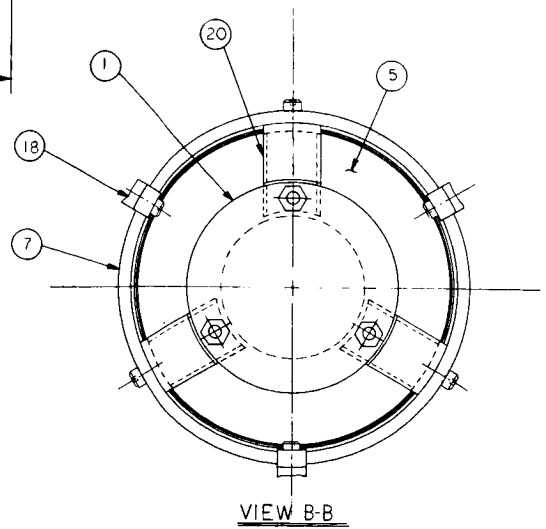
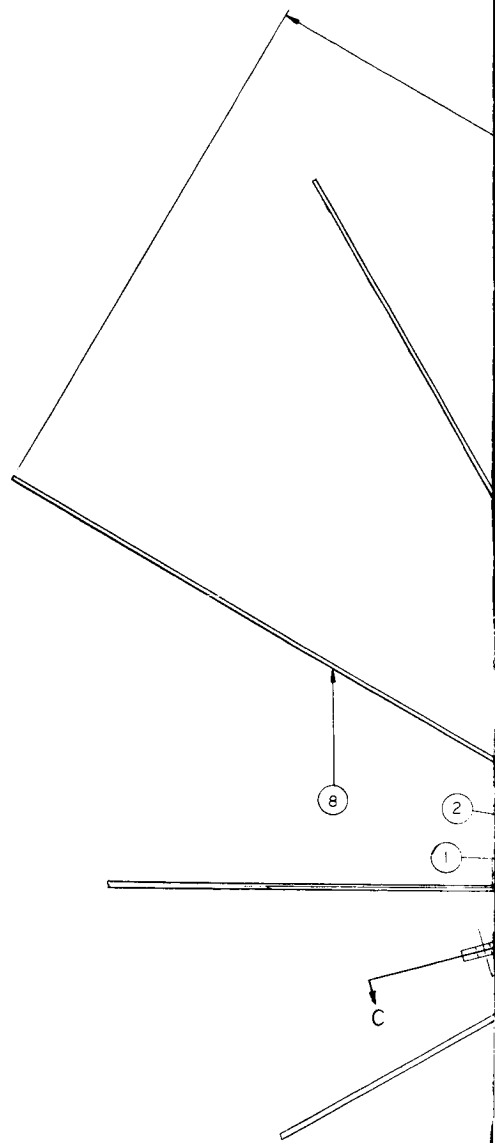
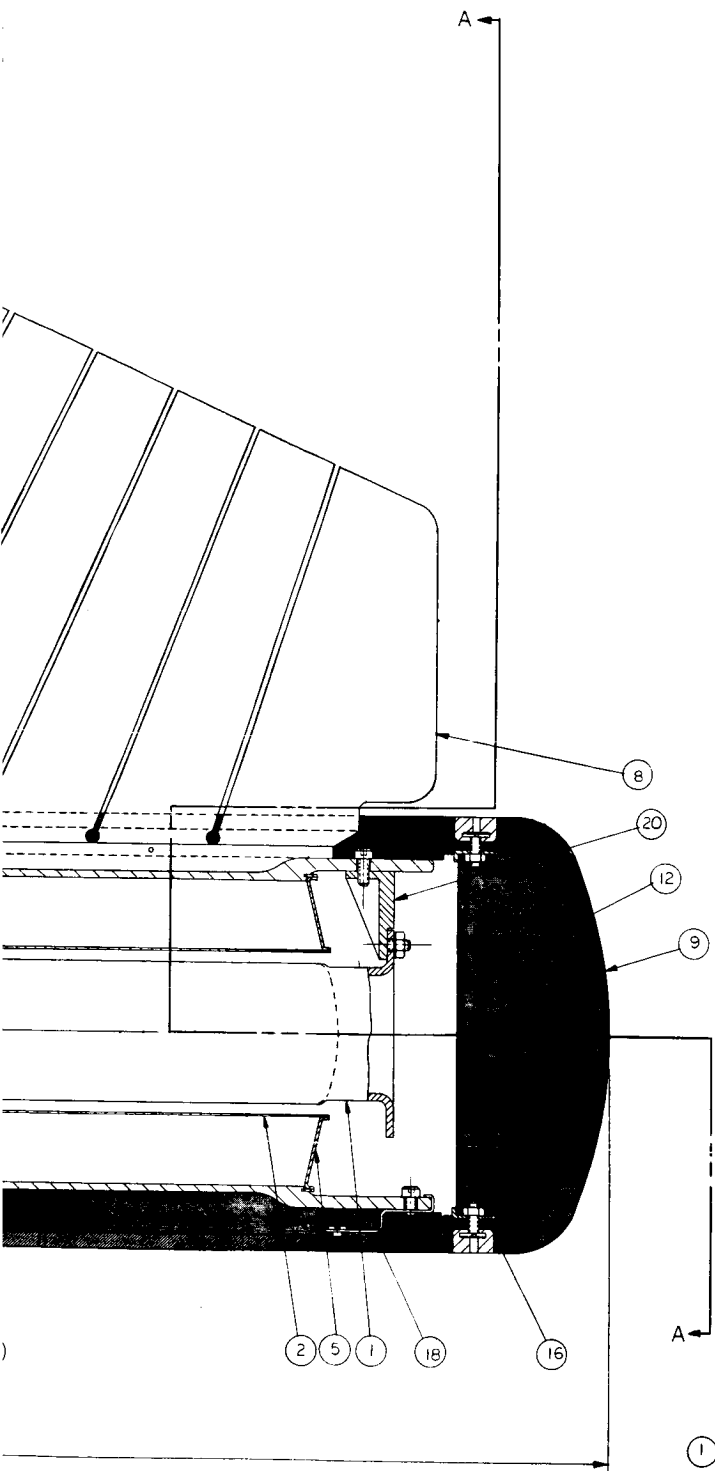
A preliminary layout of the RTG based on integral re-entry is shown in Figure 3-12. From the beginning-of-life (BOL) sizing analysis described in Section 5.1 the nominal characteristics of the RTG are summarized as follows:

<u>Parameter</u>	<u>Value</u>
Life	17 months*
EOL Power	75 watts
Fuel	Pu-238
Thermopile	Lead telluride
Length	25 inches
BOL Power	84 watts
Hot Junction Temperature	1050° F
RTG Weight	49.2 pounds
Re-entry Protection Weight	17 to 21 pounds
Diameter	28.4 inches
Cold Junction Temperature	500° F
BOL Thermal Power	1810 watts
EOL Thermal Power	1790 watts
Thermal Power at Capsule Assembly	1830 watts

*The mission time from liftoff is approximately 14 months. A three-month period is added to take account of prelaunch test time.

PART NO.	NO. REQUIRED	DESCRIPTION
1	1	FUEL CAPSULE ASSEMBLY
2	1	HOT FRAME
3	1	HOT FRAME END CAP
4	1	THERMOPILE
5	1	FORWARD SEAL
6	1	AFT SEAL
7	1	OUTER SHELL
8	12	FINS
9	1	UPPER DOME
10	1	LOWER DOME
11	1	CYLINDER
12	1	INSULATION (UPPER DOME)
13	1	INSULATION (LOWER DOME)
14	1	INSULATION (CYLINDER)
15	1	LOWER NUT RING
16	1	UPPER NUT RING
17	1	LOWER INSULATION RING
18	3	UPPER CYLINDER SUPPORT
19	1	LOWER CAPSULE SUPPORT
20	3	UPPER CAPSULE SUPPORT
21	AK	FASTENERS
22	AK	WIRING





3-28-7

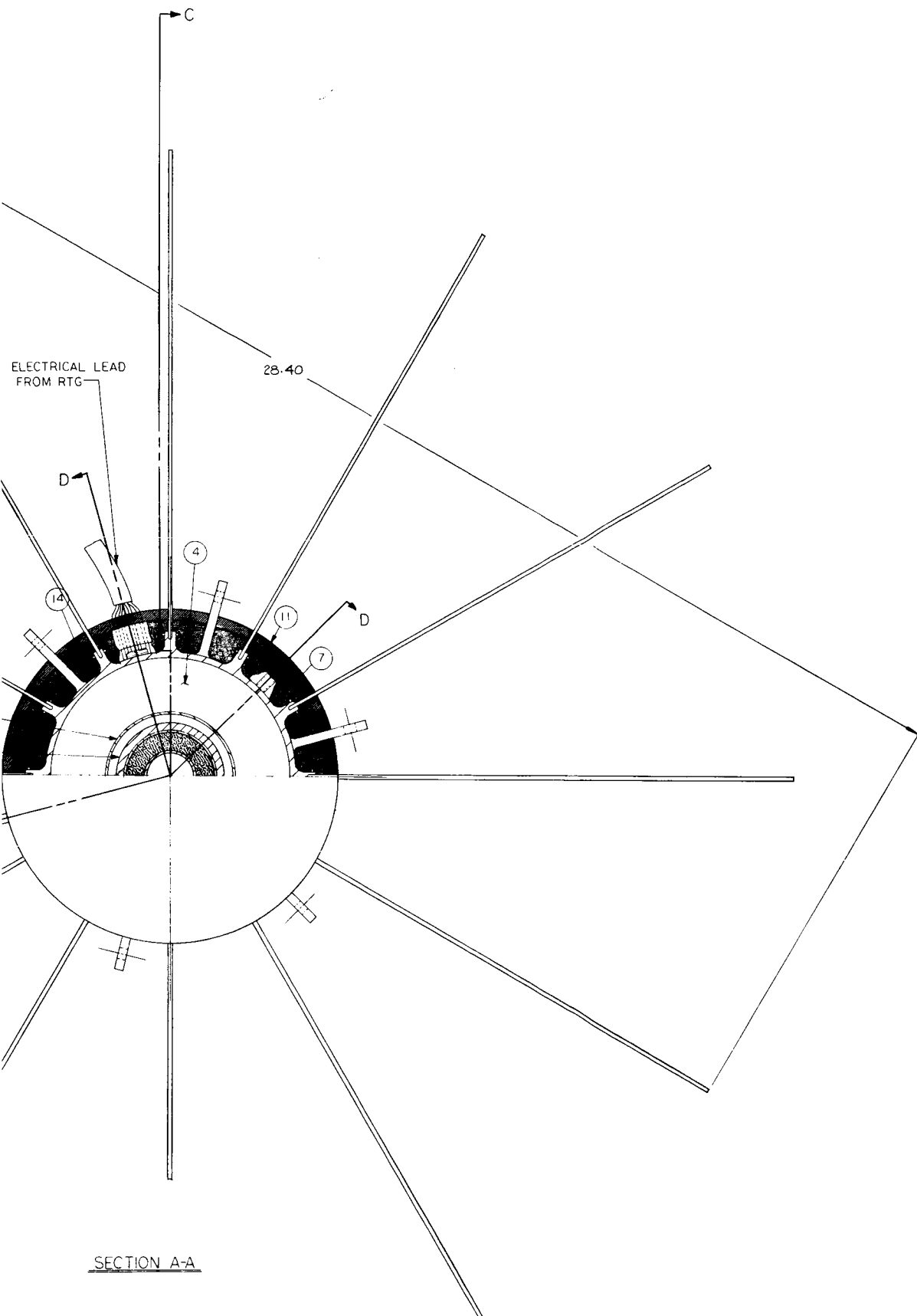


Figure 3-12. Voyager Orbiter RTG

3-24-2

3-27-28

3.3.3 STRUCTURE

The selected structural concept is shown on the general arrangement drawing, Figure 3-8. The reasons leading to this selection with supporting analyses are presented in the following sections.

3.3.3.1 Selection of Structural Concept

The structural subsystem for the Planetary Vehicle utilizing RTG power sources was selected on the basis of strength and rigidity requirements, and on RTG and mission criteria. The latter requirements were: (1) compatibility with an over-the-nose shroud separation concept, (2) RTG thermal considerations, (3) use of solid retro engine, and (4) a structure as similar as possible to the Task B GE-preferred Voyager design.

3.3.3.1.1 Influence of Shroud Separation Concept

Contemplation of an over-the-nose shroud separation concept for Voyager led to consideration of spacecraft-shroud clearances during shroud ejection. Assuming shroud separation just after second stage burnout, equations describing shroud translational and rotational motion relative to the spacecraft and launch vehicle were derived. These expressions established shroud geometry, separation velocity and tip-off (pitching) velocity criteria necessary to preclude the shroud from striking the spacecraft. The parameter curves of Figure 3-13 were established from these equations, employing estimated shroud geometries and the GE-preferred Voyager design. It was shown that shroud forward separation concept could be employed only if: (1) extremely close tolerances and balancing requirements were imposed on the shroud, (2) the spacecraft envelope forward of the separation plane were reduced from the JPL-specified nominal diameter to the actual capsule diameter, (3) the capsule diameter were reduced, (4) a close-tolerance separation system were designed to impart the shroud with a separation velocity to tip-off rate ratio nearly an order of magnitude greater than that of the spacecraft, (5) guide rails were used for the shroud, or (6) locating the Planetary Vehicle and shroud separation planes further forward on the Planetary Vehicle. To minimize any potential difficulties with an over-the-nose shroud separation concept, the Planetary Vehicle separation plane was removed to a location 19 inches below the bus-capsule interface; i. e., item (6) above was incorporated into the design.

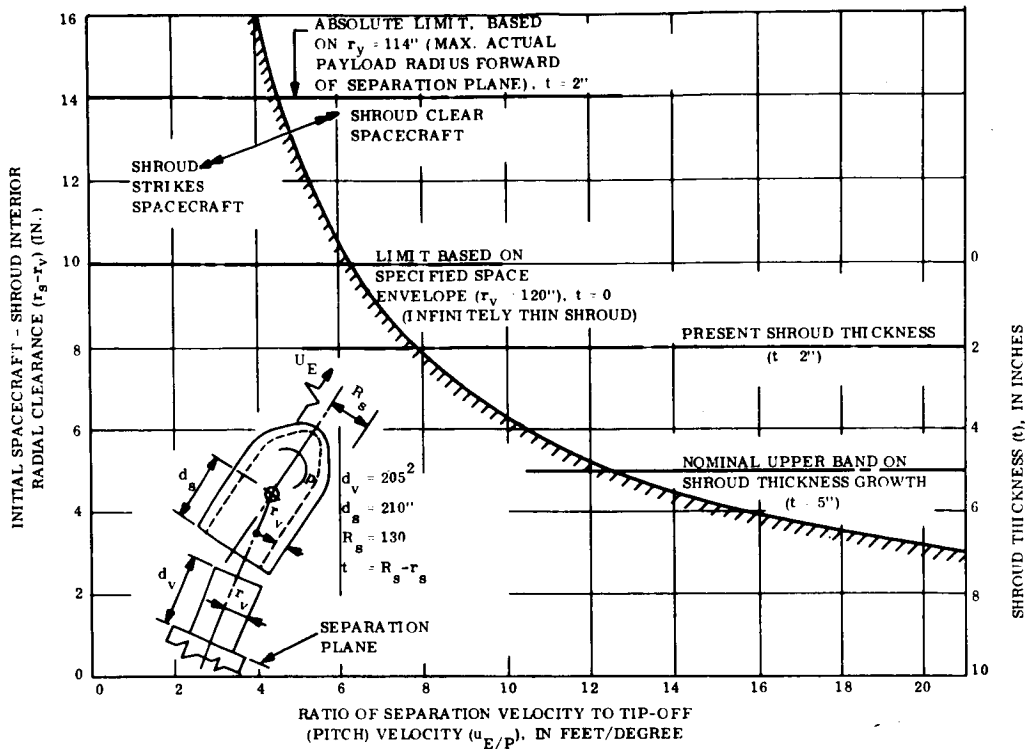


Figure 3-13. Variation of Shroud Separation — Tip-Off Velocity Ratio with Initial Radial Clearance and Shroud Thickness

3.3.3.1.2 RTG-Support Structure

The temperature generated by the RTG's required their placement in a location where they can be provided with a clear field of view to radiate heat into space. Thermal considerations also require that the RTG's be located as far away as possible from the electronic bays. To meet these objectives, the RTG's were located on the semi-monocoque conical frustrum that also serves as part of the Planetary Vehicle/shroud interface structure. This is a structural element similar to that employed for the solar cell support structure in the Task B design.

This RTG support structure is of aluminum honeycomb construction and serves as a primary load path between the shroud and the Planetary Vehicle. It must be capable of sustaining large shear stresses induced by transverse and torsional engine and capsule loads. Other types of construction (e.g., corrugated or beaded sheet metal) would require more structural weight.

3.3.3.1.3 Bus-Shroud Interstage Structure

The bus-shroud interstage structure is that element of the Planetary Vehicle structure that transmits loads directly to the shroud. Since space allocations for equipment and subsystems necessitates the use of an RTG-support structure with a shallow cone angle, additional provision must be made to provide a path for longitudinal loads and part of the transverse loads due to the capsule. This is achieved by the addition of a conical frustrum-shaped structural element to form the interstage.

Before selecting the form of construction for this element, consideration was given to providing additional flexibility to the Planetary Vehicle design. While GE selected a solid propellant retro engine for Task B, the possible future use of a liquid engine was considered. Provision was made for the placement of liquid propellant tanks resulting in the selection of a conical space truss.

3.3.3.1.4 Resulting Structural Concept

The selected structural concept is very similar to the GE-preferred Task B design. The shroud-bus adapter structure has been moved forward, so that the Planetary Vehicle separation plane lies 19 inches below of the bus-capable interface plane. This adapter structure consists of a semi-monocoque conical frustrum and a 12-star conical space truss. The RTG's are attached to the semi-monocoque structure, a radial rib-stiffened aluminum honeycomb element. The shroud separation plane is located to provide non-interference during spacecraft and shroud separation.

3.3.3.2 Analysis of Selected Configuration

Boost flight environments are presented in Table 3-1. Of the seven loading conditions, specified there, cases (1), (3) and (7) were taken as the most severe environments and were those for which structural response loads were determined.

Environments other than those listed in Table 3-1 (e.g., random vibration acoustic noise, system shock, etc.) are considered to be negligible in sizing the structure.

TABLE 3-1. BOOST FLIGHT ACCELERATIONS

Condition	Static		Longitudinal		Lateral		Torsional	
	Long (g)	Lateral (g)	(g) (O-P)	Frequency Range (cps)	(g) (O-P)	Frequency Range (cps)	(g) (O-P) Radians ₂ per sec	Frequency Range (cps)
1. Launcher Release*	1.25	1.0	2.1	4-45	0.35	3-6	-	-
2. SIC Stage	3.0	1.0	1	-	0.1	1-5	-	-
3. SIC Shutdown*	4.75	1.0	1.25	6-70	-	-	-	-
4. SII Stage-B Shutdown	2.9	1.0	Undefined. Assumed less severe than for					
5. SIV Stage-B Shutdown	4.2	1.0	conditions (1) and (3)					
6.	-1.0	-	-	-	-	-	-	-
7. *	-	-	-	-	-	-	10	8-50

* Selected for Design Load Consideration

Notes

1. These accelerations are assumed to occur at the Planetary Vehicle adapter/ shroud interfaces.
2. Vibratory accelerations are described as decaying sinusoids of 20 cycles duration.
3. For each condition, all static and vibratory accelerations are assumed to occur simultaneously.
4. Conditions (6) and (7) do not represent any specific flight condition but are included to ensure that reasonable load carrying capability is provided for tension and torsion.
5. All load factors are for limit loads.

Component vibration levels are determined in a gross sense in this system mode. A more detailed dynamic model is required to prescribe levels for such equipment as the scanner package, array mounted antennas, etc.

A minimum allowable value for fundamental spacecraft resonances must be established to avoid deleterious dynamical interaction between the spacecraft and the launch vehicle. Adherence to this criteria is necessary for two reasons: (1) to eliminate coupling between the launch vehicle control system and the spacecraft resonances which would deteriorate control system operation, and (2) to prevent the spacecraft from acting as an energy absorber on the launch vehicle in the principal resonances of the latter. As a preliminary design criteria, therefore, the minimum allowable Planetary Vehicle resonance was assumed to be 10 cps. This value, employed in the absence of more definitive data, is felt to be slightly conservative, based on approximate frequency scaling.

3.3.3.2.1 Structural Dynamics

The design responses listed in Figure 3-14 are determined for the decaying sinusoid environment acting upon the spacecraft in a fixed-free configuration. The shroud attachment locations are considered as the foundation connections to which the environment is applied as base excitations. The resulting responses provide external loads for determining the preliminary sizing of elements of the primary structure. The launcher release and booster engine shutdown conditions develop the largest dynamic responses, and these flight conditions are used to evaluate the dynamic responses. The severest load condition is evaluated after combining these dynamic responses with the static accelerations at the respective flight conditions.

To determine the dynamic response and modal frequencies of this configuration, a mathematical system model is developed, using representative elastic elements for the primary structural members. A schematic of this model, together with the lower frequencies and respective mode shapes, is presented in Figure 3-14. The model consists of 6 mass stations and 20 associated degrees of freedom. Of these 20 degrees of freedom, 6 describe lateral translation, 5 present pitching rotation, 4 coordinates reflect axial motion, and 5 portray torsional rotation. Modeling techniques and coordinates are chosen to most accurately depict the dynamical behavior of the system in its principal resonances.

Three of the elastic elements used in the model are cylindrical shell elements which connect interfaces two, four, five and six together. Interface three is connected to interface two with a conical shell element and laterally supported also at interface five. Conical shell elements connect interface two with the shroud supports and interface one. A truss network of twelve tubular members supports interface one on the shroud supports.

Additional frequency data, listed in Table 3-2, contains modal frequency values for the RTG-powered configuration housing a 5000-pound capsule/lander. This frequency data is included to permit comparisons with a 3000-pound capsule.

The two flight conditions of launcher release and booster engine shutdown are investigated for their respective dynamic response levels. The static accelerations associated with

TABLE 3-2. MODAL FREQUENCIES WITH A 5000-POUND LANDER

Mode	Lateral Frequency (cps)	Longitudinal Frequency (cps)	Torsional Frequency (cps)
1	15.6	16.8	15.3
2	26.9	17.8	40.7
3	40.3	69.8	74.1
4	60.3	-	-

these two flight conditions are considerably different, and as such the design condition is evaluated after a detailed load analysis of the structure is performed, using both the static and dynamic levels.

The structural design loads used are the algebraic sum of the rigid body static and dynamic loads. Table 3-1 lists the limit static accelerations while Figure 3-14 lists the limit dynamic accelerations of the major mass items of the Planetary Vehicle for each of the critical loading conditions. Lateral and longitudinal loads were applied simultaneously since dynamic loads may be applied in either direction; two sets of loads were established for each flight condition. Table 3-3 summarizes the combination of accelerations given in Table 3-2 and Figure 3-14 and reflects the external loading conditions used to verify structural integrity. Major mass items described therein are:

- a. Flight capsule
- b. Retro engine
- c. MC&OA Subsystem

3.3.3.2.2 Stress Analysis

Figure 3-15 presents a schematical cross section of the RTG support structure, adapter truss element, and that portion of the bus structure to which both are attached. Looking down from the top, this structural segment may be considered as comprising 12 identical segments. Accordingly, the internal loads analysis can be concentrated on just one of these

Modal Frequency	Lateral Mode Shapes			
	15.7 cps	29.4 cps	44.9 cps	66.2 cps
X ₁	3,1508172 / -2	1,4131923 / -1	2,0185340 / -1	-6,0617359 / -2
θ _{y1}	1,1002653 / -3	2,3723659 / -3	3,2698215 / -3	1,1387690 / -3
X ₂	-2,6295954 / -2	7,5444619 / -2	-7,6479219 / -2	-8,2341947 / -2
θ _{y2}	1,4834629 / -3	3,1882666 / -3	-6,7603520 / -4	2,1398603 / -4
X ₃	-1,1638923 / -1	1,2269018 / -1	-6,7172283 / -2	-2,3944763 / -2
θ _{y3}	2,8059447 / -3	2,5352462 / -3	-2,2438713 / -3	-4,5254502 / -3
X ₄	-1,3548061 / -1	5,9710488 / -2	-4,1746255 / -2	1,0064149 / -1
θ _{y4}	1,9966361 / -3	3,3293683 / -3	-1,9125939 / -3	3,7537443 / -3
θ _{y5}	2,1474653 / -3	3,4990374 / -3	-2,5472903 / -3	5,9653116 / -3
X ₆	-2,6130247 / -1	-2,6067015 / -2	1,1971968 / -1	4,6813465 / -4
θ _{y6}	2,2111155 / -3	3,7136864 / -3	-3,0456263 / -3	8,2671144 / -3

Modal Frequency	Longitudinal Mode Shapes			Dynamic Response	
	17.5 cps	45.5 cps	70.3 cps	Normalized Response In g/g	Response At Launcher Release
Z ₁	1,2896339 / -1	3,0756327 / -1	-7,4413382 / -2	4.08	8.59
Z ₂	1,3756790 / -1	9,7606942 / -3	1,2343746 / -1	4.18	8.76
Z ₃	1,6478090 / -1	-8,7816179 / -2	-7,4523848 / -2	4.92	10.3
Z ₅	1,4297584 / -1	1,3092661 / -2	3,1520880 / -1	4.30	9.04

Modal Frequency	Torsional Mode Shapes			Dynamic Response	
	18.1	43.7	74.7	Normalized Response $\frac{\text{Rad/Sec}^2}{\text{Rad/Sec}^2}$	Response 10 Rad
θ _{z1}	4,1521480 / -3	-3,1371881 / -3	-1,1629771 / -3	5.0	
θ _{z2}	3,1369461 / -3	1,3179860 / -3	3,6751651 / -3	3.8	
θ _{z3}	3,2517468 / -3	1,6579609 / -3	9,2039666 / -3	4.0	
θ _{z3}	3,5137093 / -3	4,8748078 / -3	-1,0257596 / -3	4.2	
θ _{z5}	3,6676691 / -3	6,4465851 / -3	-3,5895946 / -3	4.4	

Dynamic Response	
Normalized Response In g/g or Rad/Sec ² /g	Peak Response At Launcher Release In g or Rad/Sec ²
2.04	.72
.040	.014
1.68	.59
.051	.018
1.94	.68
.055	.019
2.32	.81
.058	.020
.067	.020
2.80	.98
.065	.023

In g	Response At Booster Shutdown In g
	5.10
	5.20
	6.15
	5.38

Response At Sec ² Input
0.
8.
0.
2.
4.

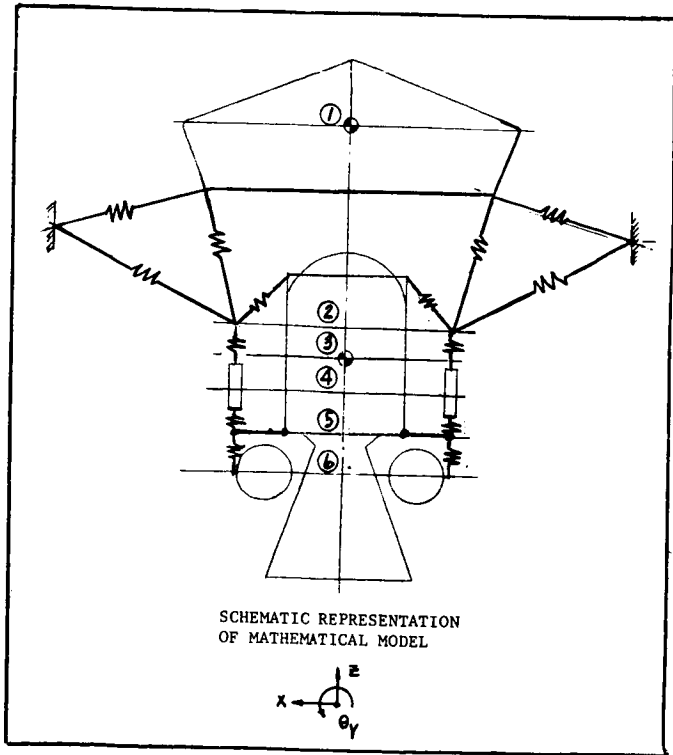


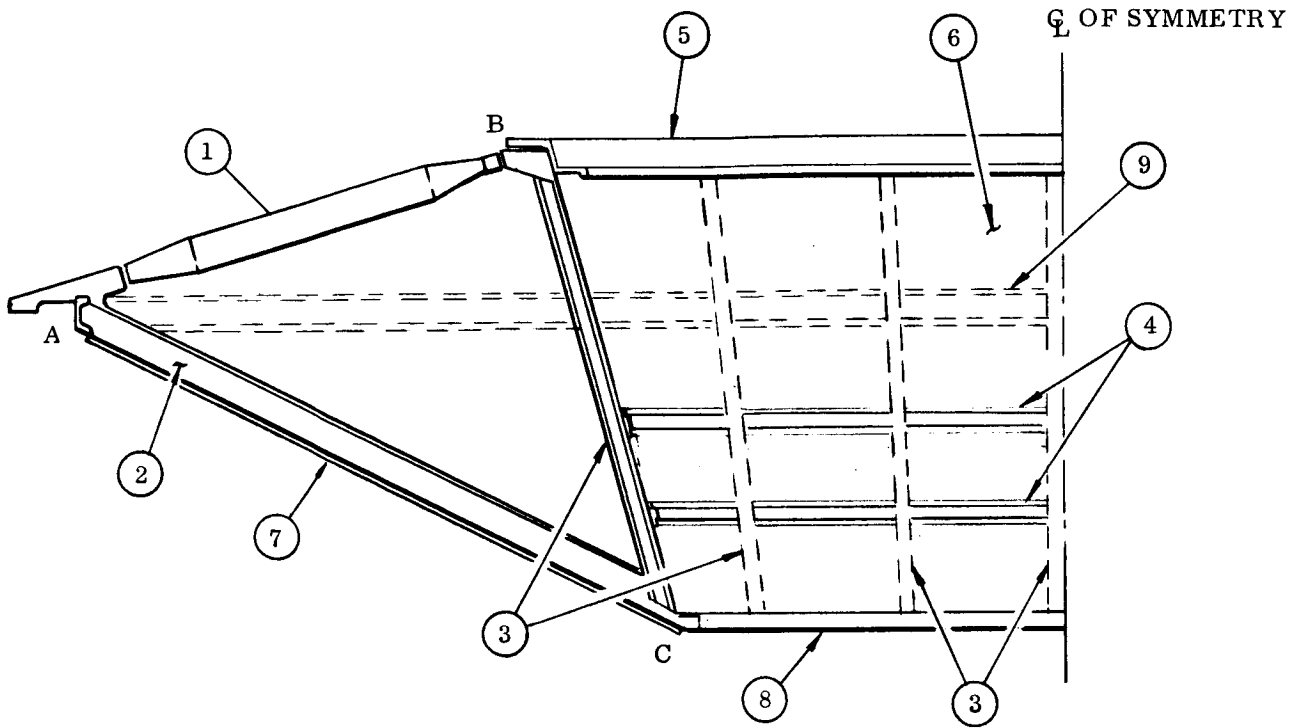
Figure 3-14. Schematic and Results of Dynamic Analysis

TABLE 3-3. ACCELERATION COMBINATIONS

Condition	Structural Element	Weight (lb)	Static Loads		Dynamic Loads			Combined Loads			
			Lateral (g)	Axial (g)	Lateral (g)	Axial (g)	Torsional $\frac{\text{rad}}{\text{sec}^2}$ g	Static-Dynamic		Static-Dynamic	
								Axial (g)	Lateral (g)	Axial (g)	Lateral (g)
Launcher Release	1	3000	1.00	1.25	.857	8.59	-	9.84	1.857	-7.34	.143
	2	9513	1.00	1.25	1.181	10.30	-	11.55	2.181	-9.05	-.181
	3	2187	1.00	1.25	2.133	8.97	-	10.22	3.133	-7.72	-1.133
Booster Shutdown	1	3000	1.00	4.75	-	5.10	-	9.85	1.00	-.35	1.00
	2	9513	1.00	4.75	-	6.15	-	10.90	1.00	-1.40	1.00
	3	2187	1.00	4.75	-	5.35	-	10.10	1.00	-.60	1.00
Torsional	1	3000	-	-	-	-	50.1	-	-	-	-
	2	9513	-	-	-	-	41.9	-	-	-	-
	3	2187	-	-	-	-	46.7	-	-	-	-

segments, which are statically indeterminate to the first degree. A computer program, especially formulated for investigating this segment, is used to establish the internal loads distribution within this segment.

Within the segment described in Figure 3-15, member AB is a pin-ended tube carrying axial load only. Member BC is a longitudinally and circumferentially stiffened conical shell. The longerons of hat-shaped cross section are located at the intersection of the truss plane and the conical shell, thus distributing axial load to the longerons and the shear load to the shell. Member CA, to which the RTG panels are attached, has an I-shaped cross section. This member allows axial load to be transmitted while the shear load is distributed to the panels. An analysis of this statically indeterminate assembly shows that the vertical load from the lander, combined with the "kick" load from the flight capsule interface ring, is transmitted to the shroud support by an axial load in member AB. The vertical loads from the midcourse correction engine and the MC&OA subsystem, combined with the kick load from the engine attachment ring, are transmitted to the shroud support by an axial load in member AC. Only a small axial load is applied to member BC. Shear due to lateral or torsional acceleration of the flight capsule cg is transmitted to the engine attachment ring by the semi-monocoque conical shell (BC). Shear from the flight capsule, retro-engine, and MC&OA subsystem is transmitted to the shroud by the RTG panels.



NO.	ELEMENT	QUANTITY
1	TRUSS TUBE	12
2	I-SECTION MEMBER	12
3	LONGERON	12
4	RING STIFFENER	2
5	LANDER INTERFACE RING	1
6	SEMIMONOCOQUE CONICAL SHELL	1
7	RTG PANELS	12
8	ENGINE INTERFACE RING	1
9	SHROUD RING	

Figure 3-15. Schematic Representation of the Primary Structure

Longitudinal loads are applied equally to the 12 load points; e.g., the longitudinal load at each of the 12 capsule support points is the total vertical load divided by twelve. Therefore

$$V = \frac{\sum_{i=1}^j W_i n_i}{12} \quad (1)$$

where:

V = Vertical load at each of the 12 load points due to the vertical load factors.

W_i = Weight of the i th element attached to the load point

n_i = Vertical acceleration of the cg of the i th mass element

j = Number of masses attached to each of the 12 load points

$$\left(\begin{array}{l} j = 1 \text{ for the 12 load points at B} \\ j = 2 \text{ for the 12 load points at C} \end{array} \right)$$

Lateral load factors at the cg of the elements create lateral loads and moments at the load points. Lateral loads are applied radially to the truss element at the 12 points, with a circumferential sinusoidal distribution. Bending moments are converted into a distribution of equivalent longitudinal loads, having a sinusoidal distribution about the circumference of the element.

The radial load at each of the 12 load points is given by

$$H = H_{\max} \cos \theta \quad (2)$$

where

θ = angular location of the load point measured from the j lateral load

$$H_{\max} = \frac{\sum_{i=1}^j W_i n_i}{12 \sum_{k=1}^j \cos^2 \theta_k}$$

Similarly, the vertical load at the load point, due to moment, is

$$P = P_{\max} \cos \theta \quad (3)$$

where

$$P_{\max} = \frac{\sum_{i=1}^j W_i n_i a_i}{12 r \sum_{k=1}^r \cos^2 \theta_k}$$

a_i = distance from plane of load points to cg of ith mass

Table 3-4 presents a tabulation of the maximum loads applied at the load points. Equations 1, 2, and 3 are used to calculate the maximum loads applied to the structure. Since the orientation of the spacecraft with respect to lateral load factors is arbitrary, all members must be designed for maximum loads (i.e., maximum axial loads plus or minus maximum lateral loads).

The aforementioned computer program yields the internal loads created by the external loads of Table 3-4. Internal loads in each structural member are summarized in Table 3-5.

TABLE 3-4. COMPUTED INTERNAL LOADS

Condition	Element	Weight	M_v		M_h		Arm	Load Point	V		H_{\max}		P	
			S+D	S-D	S+D	S-D			S+D	S-D	S+D	S-D		
Launcher Release	1	3000	9.84	-7.34	1.857	0.143	27.5	B	2460	-1835	932	89	424	32
	2	9513	11.55	-9.05	2.181	-0.181	12	C	9170	-7180	3480	-288	925	-77
	3	2187	10.22	-7.72	3.133	-1.133	46	C	1870	-1410	1144	415	1550	-561
Booster Shutdown	1	3000	9.85	-0.35	1.0	1.0	27.5	B	2460	87	500	500	230	230
	2	9513	10.90	-1.40	1.0	1.0	12	C	8650	-1140	1585	1585	425	425
	3	2187	10.10	-0.60	1.0	1.0	46	C	1840	-109	365	365	496	496

Note: S = Static Load
D = Dynamic Load

TABLE 3-5. INTERNAL LOAD SUMMARY

Condition	Member	Vertical		Lateral		Total (Ult)	
		S+D (lb)	S-D (lb)	S+D (lb)	S-D (lb)	S+D (lb)	S-D (lb)
Launcher Release	Bar AB	-18870	+14564	+2740	+830	-27000	+19200
	Bar BC	+2491	-1988	+1180	+255	+4600	-2810
	Bar CA	+20454	-15800	+3410	+930	+29800	-20900
	Ring A	-311	+251	+199	+39	*	*
	Ring B	-18877	+14590	+3900	+940	*	*
	Ring C	+19188	-14838	+1440	+1605	*	*
Booster Shutdown	Bar AB	-18113	+1590	+1148	+1148	-24050	+2738
	Bar BC	+2288	-514	+605	+605	+3610	-1400
	Bar CA	+19614	-1782	+1341	+1341	+26200	-3900
	Ring A	-281	-79	+131	+131	*	*
	Ring B	-18093	-1669	+2370	+2370	*	*
	Ring C	+18373	+1748	+1330	+1330	*	*
* Rings are treated separately and then superimposed.							
Note: S = Static Load D = Dynamic Load							

Ring loads are applied at twelve discrete points. The magnitude of the uniform loads for the vertical case and the magnitude of the sinusoidally distributed loads for the lateral and moment cases are presented in Table 3-5.

The loads produced by the torsion condition are shear loads in the semi-monocoque conical shell and in the RTG panels. These shear loads are less than those produced by the launch release and booster shutdown loading conditions.

The following examples illustrate the stress analysis performed on each structural element.

BAR AB

$$P = -27,000$$

$$L = 62.5 \text{ in.}$$

$$E = 10.5 \times 10^6$$

$$A = 1.88 \text{ in.}^2$$

$$I = 1.04 \text{ in.}^4$$

$$\sigma = \frac{27,000}{1.88} = 14,380$$

$$PCR = 27,900 \text{ lb}$$

$$\text{M.S.} = \frac{27,900}{27,000} - 1 = 0.03$$

RING B

$$P_{\text{uniform}} = -18,877 \text{ (LIM)}$$

$$P_{\text{sin}} = \pm 3900 \text{ (LIM)}$$

$$r = 60 \text{ in.}$$

$$E = 10.5 \times 10^6 \text{ psi}$$

$$A = 2.35 \text{ in.}^2$$

$$I = 9.16 \text{ in.}^4$$

From symmetry

$$P = 88,000 \text{ lb}$$

From GE Structures Manual

$$M_{\text{max}} = 76,500 \text{ in.} \cdot \text{lb}$$

$$\sigma = \frac{88,000}{2.35} + \frac{76,500 \times 3.15}{9.16} = 63,800 \text{ psi}$$

$$\sigma_{\text{all}} = 66,000 \text{ psi (7075-T16 MIL Handbook 5)}$$

$$MS = \frac{66,000}{63,800} - 1 = 0.035$$

SEMI-MONOCOQUE CONICAL SHELL

$$q_{\text{max}} = 206 \text{ lb/in.}$$

Beaded Curved Panel

$$18.6 \times 23.6 \text{ in.}$$

$$q_{\text{all}} = 235 \text{ lb/in.}$$

$$M.S. = \frac{235}{206} - 1 = 0.14$$

A summary of the stress analysis for Task C RTG Study is presented in Table 3-6. Ring loads are given as symmetrical and anti-symmetrical loads.

TABLE 3-6. SUMMARY OF STRESS ANALYSIS

Reference Figure 3-15	Member	Member Size (in.)	Critical Condition	Failure Mode	Critical Load (lb) (lb/in)	M. S.
AB	Truss Tube	4 OD x 0.065	Booster Shutdown	Comp	27,000	0.11
BC	Longeron	1 x 1 x 0.028 Hat	Launcher Release	Comp	2113	0.175
	Conical Shell (Shear Panel)	0.032	Booster Shutdown	Shear	206	0.14
CA	Longeron	4 x 2 x 0.125 I-Section	Launcher Release	Comp	20,900	High
	Panels (Sandwich)	0.010 Aluminum Face Sheets	Booster Shutdown	Shear	283	0.34
A	Shroud Attachment Ring	Modified Z-Section	Launcher Release	Tens	389/249	High
B	Capsule Interface Ring	Modified Z-Section	Launcher Release	Comp	23,600/3900	0.035
C	Engine Interface Ring	Modified Channel	Launcher Release	Tens	24,000/1790	0.035

3.3.3.3 Equipment Bays

The spacecraft electronic equipment is functionally grouped by subsystem and packaged in modular assemblies of standard size and shape in 12 bays of the Spacecraft. The arrangement of these equipment bays is shown in Figure 3-16. This arrangement is the result of the following considerations:

- a. Spacecraft mass balance
- b. Equipment bay thermal balance
- c. Radio subsystem located next to high gain antenna
- d. Science electronics located near the planet scan platform
- e. Proximity of C&S and G&C to sensors and science

The selection of 12 bays resulted from studies of 12 to 16 bay arrangements (16 bays similar to Task "B" Design). During these studies it was found that the overall across flat dimension of the electronic equipment bay arrangement was limited to less than 100 inches to accommodate conversion from an RTG power system to a maximum area fixed solar array power system. The 100-inch dimension is the minimum diameter in which the monopropellant tanks of the MC/OA System can be packaged (Station 25 to 49 of Figure 3-8). The resultant dimension of 90 inches across bay flats dictated bay widths of 24 inches for 12 bays and 17.9 inches for 16 bays. The number of single row maximum diameter (51 pin) connectors across the top or bottom of an equipment bay is limited to 16 for 12 bays and 8 for 16 bays. Double rows of connectors would be required for five of the 16 bays, creating a large, undesirable overhang and hindering access during installation and maintainance. Also the required total number of connectors is less for 12 bays because the larger bay packing volume results in less bay to bay connections. This fact, combined with the larger width per bay, allows single rows of connectors to be used at the top and bottom of all bays, thus providing good cable and connector access. Task B module concepts can be used in the 12-bay arrangement. The larger area per bay of the 12 bay arrangement can more adequately handle high thermal dissipation loads such as the radio subsystem transmitter.

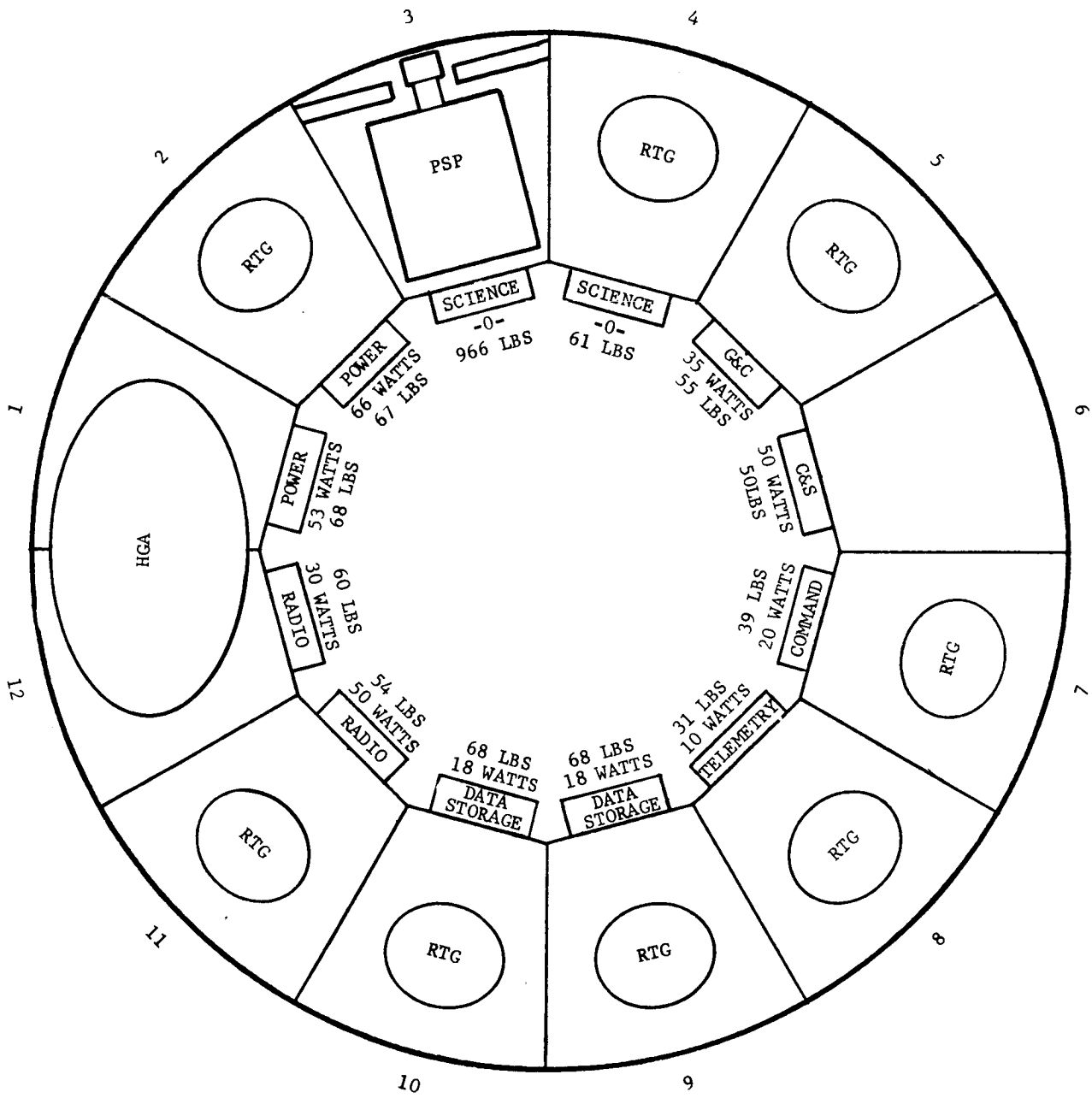


Figure 3-16. Equipment Arrangement

The equipment bays are assembled into a unifying structure to provide load and thermal paths which are integrated with the vehicle structure. Each bay is 24.0 inches wide, 34 inches high, and 10 inches deep. This is compatible with standard electronic packages measuring 17.30 inches x 24 inches x 8.5 inches. Thermal louvers for active temperature control are attached to the exterior face of each bay except bay 11, the radio bay, which must dissipate maximum heat and has no low temperature problem. The louvered bays have horizontal louvers which are pointed toward the Sun in the closed position for maximum direct view to space as they open. The honeycomb panels carrying the RTG units block most of the view to space away from the Sun. Also, radiation from the panels and RTG units precludes the use of vertical louvers and louvers opening away from the Sun.

The elliptical Sun shade shelf at Station 37 was added to shield the electronic equipment bays from direct sunlight during spacecraft biasing for HGA alignment. The shelf is designed to shield the equipment bays up to 30 degrees off the Sun line in the Z-X plane, and up to 10° off the Sun line in the Z-Y plane.

3.3.4 WEIGHT AND MASS PROPERTIES

A weight summary of the Planetary Vehicle is presented in Table 3-7. The weight breakdown is by vehicle function with subtotals shown for the Bus, the Propulsion System, the Capsule, the separated overall Vehicle, and the Planetary Vehicle.

Weight, center of gravity, moments and products of inertia are presented in summary form in Table 3-8 for specific times during the mission. Longitudinal centers of gravity are referenced to Station 0 (as shown in Figure 3-8) with positive distances in the direction of +Z. Lateral cg locations are referenced to the roll axis in compliance with the sign convention in Figure 3-6. Each inertia is about the center of gravity. A detailed weight statement is shown in Table 3-9.

TABLE 3-7. WEIGHT SUMMARY

Description	Weight (lb)
Bay No. 1 Power System	53.8
Bay No. 2 Power System	52.8
Bay No. 3 Science Electronics	96.0
Bay No. 4 Science Dae	61.0
Bay No. 5 Guidance and Control	55.5
Bay No. 6 Computer and Sequencer	50.1
Bay No. 7 Command System	38.9
Bay No. 8 Telemetry System	31.2
Bay No. 9 Data Storage	68.4
Bay No. 10 Data Storage	68.4
Bay No. 11 Radio System	54.0
Bay No. 12 Radio System	60.4
Primary Structure	395.6
Scan Platform	150.0
RTG System	628.4
A.C. Gas System	247.0
A.C. Independently Mtd. Sensors	16.6
Science Sensors	105.4
Antenna Assemblies	92.1
Thermal Control	151.4
Pyrotechnic	4.4
Harness	51.5
Total No. 1 Subtotal Bus Weight	2532.9
Retro Propulsion	9659.5
Mid-Course Propulsion	2202.8
Meteoroid Protection	71.1
Total No. 2 Subtotal Propulsion Weight	11933.4
Capsule (Includes Biobarrier)	3000.0
Total No. 3 Subtotal Capsule Weight	3000.0
Total No. 1 No. 2 No. 3 Separated Overall Planetary Vehicle	17466.3
Adapter	113.3
Planetary Vehicle	17579.6

TABLE 3-8. MASS PROPERTY SUMMARY

Flight Sequence Description	Case No.	Weight (lbs.)	\bar{Z} (in.)	\bar{X} (in.)	\bar{Y} (in.)	I_{zx} (slug ft ²)	I_{zy} (slug ft ²)	I_{xz} (slug ft ²)	I_{oz} (slug ft ²)	I_{ox} (slug ft ²)	I_{oy} (slug ft ²)
Launch Cond. (On PAD)	1	17579.3	114.4	.11	.18	-90.6	-65.8	-18.9	817*	22305	22014
Transit	2	17465.9	114.2	.07	.20	-92.9	-64.6	-38.5	796*	22165	21912
After Mid Course Correction	3	16049.9	120.9	.07	.22	-94.5	-69.7	-38.5	7553	19962	19709
After Retro Burn (Orbiting)	4	7538.9	151.6	.15	.46	-102.2	-92.6	-38.5	6973	16017	15764
P. S. P. Deployed	5	7338.9	152.2	.61	2.11	-102.4	-89.6	115.4	75*0	16511	15735
After Capsule Separation	6	5038.9	91.8	.92	3.16	-42.2	118.1	114.4	4044	3395	2622
After Orbit Adjust. Ant. Depld.	7	4732.9	94.4	1.25	3.36	-146.5	109.2	113.2	4016	3245	2521

Notes. 1. NOM C. G. ON 3000 pound capsule

TABLE 3-9. DETAILED WEIGHT STATEMENT

Item	Weight (lb)	Item	Weight (lb)	Item	Weight (lb)
BAY 12		RADIO SUBSYS	13.30	ANT ASSEMBLIES	
		TRANSPOUNDER	13.30	RELAY ANTENNA	2.00
		RELAY RADIO	25.00	ASSOCIATED ST	2.00
		EQUIPMENT CHS	5.47	HI GAIN ANT S	46.50
		BAY TEMP SEN	.10	ACTU + STR	33.50
		SHUTT ANG DET	.40	LO GAIN ANT P	.80
				LO GAIN ANT S	.80
				MEDIUM GAIN	4.40
				MITG STR	2.00
				TEMP SENSORS	.10
				THERMAL CONTL	10.80
				SHUTTER FACE	10.80
				SHUTTER FACE	10.80
				SHUTTER FACE	10.80
				INSUL + FACE	10.80
				SHUTTER FACE	10.80
				SHUTTER FACE	10.80
				SHUTTER FACE	10.80
				SHUTTER FACE	10.80
				INSUL + FACE	10.80
				INSUL AC SYS	2.50
				PAINT	4.00
				INSUL ORBITER	15.20
				PYROTECHNIC	2.20
				PIN PULLERS	2.20
				SQUIBS	
				HARNES	35.00
				MAIN HAR RING	1.00
				RELAY CABLE	4.00
				HI GAIN CABLE	5.00
				LO GAIN CABLE	2.00
				MEDIUM G CABLE	4.50
				UMBILICAL	
				RETRO PROPULS	9566.00
				RETRO ENGINE	60.80
				TAPERED STRUT	12.50
				KICK RING	16.40
				TUBLAR STRUT	3.80
				KICK RING	
				MID COURSE	532.75
				MONO ENGINE	12.95
				TANK SUPPORT	532.75
				MONO ENGINE	12.95
				TANK SUPPORT	532.75
				MONO ENGINE	12.95
				TANK SUPPORT	532.75
				MONO ENGINE	12.95
				TANK SUPPORT	20.00
				FRAMES	
				AC IND MTG S	2.60
				SUN SENSORS	6.30
				CANOPUS TRACK	6.30
				MISC MTG STR	1.20
				TEMP SENSORS	.20
				SCIENCE SENOR	95.00
				MISC SCIENCE	10.00
				MAGNETOMETER	.40
				TEMP SENSORS	

Item	Weight (lb)	Item	Weight (lb)
BAY 1		BAY 7	
POWER SUBSYT	14.00	COMMAND SSY	4.20
BATTERY	5.00	COMM DET P C	4.20
DIS BOOST	1.50	COMM DET P C	4.20
CHARGE REG	3.50	COMM DECODER	5.60
3 PHSE INVERT	4.50	COMM DECODER	5.60
2.4 KC INVERT	1.50	DEC ACES SWIT	3.00
1 PHSE INVERT	5.50	POWER SUPPLY	3.10
PWR SW + LOGC	4.00	BAY NO. 7 WIRE	3.00
SHUNTS	1.50	EQUIPMENT CHS	5.47
PAR SHUNT	6.70	BAY TEMP SEN	.10
BAY NO 1 WIRE	5.47	SHUTT ANG DET	.40
EQUIPMENT CHS	0.10		
BAY TEMP SEN	0.10	BAY 8	
BAY TEMP SEN	0.10	TELEMETRY SSY	7.50
SHUTT ANG DET	0.40	PYRO CONTROLLER	16.60
		TELEMETRY ELE	1.10
		BAY NO. 8 WIRE	5.47
		EQUIPMENT CHS	5.47
		BAY TEMP SEN	.10
		SHUTT ANG DET	.40
		BAY 9	
		DATA STORAGE	18.00
		TAPE RECORDER	18.00
		TAPE RECORDER	18.00
		TAPE RECORDER	18.00
		CONTROL LOGIC	.40
		CONTROL LOGIC	.40
		CONTROL LOGIC	.40
		PLAYBACK SEQ	.60
		POWER SUPPLY	2.00
		BAY NO 9 WIRE	4.60
		EQUIPMENT CHS	5.47
		BAY TEMP SEN	.10
		SHUTT ANG DET	.40
		BAY 10	
		DATA STORAGE	18.00
		TAPE RECORDER	18.00
		TAPE RECORDER	18.00
		CONTROL LOGIC	.40
		CONTROL LOGIC	.40
		CONTROL LOGIC	.40
		PLAYBACK SEQ	.60
		POWER SUPPLY	2.00
		BAY NO 10 WIRE	4.60
		EQUIPMENT CHS	5.47
		BAY TEMP SEN	.10
		SHUTT ANG DET	.40
		BAY 11	
		RADIO SUBSYTM	7.50
		PWR AMP TWT	7.50
		PWR AMP TWT	7.50
		POWER AMP TWT	3.00
		TRANSPOUNDER	13.30
		DIPLEX + SW	13.40
		BAY NO 11 WIRE	3.70
		EQUIPMENT CHS	5.47
		BAY TEMP SEN	.10
		BAY 12	
		COMP + SEQCR	35.00
		COMPUTING + SEQ	5.00
		SOLAR ASPECT	2.00
		EARTH NULLS	2.10
		BAY NO. 6 WIRE	5.47
		EQUIPMENT CHS	5.47
		BAY TEMP SEN	.10
		SHUTT ANG DET	.40

3.3.5 THERMAL ANALYSIS

RTG's introduce thermal loads which must be properly managed to prevent overheating of the RTG's themselves, other spacecraft equipment and the shroud. As noted in Section 3.3.2.2 the beginning-of-life (BOL) thermal power is 14480 watts (8 X 1810 watts per RTG) for each Planetary Vehicle. This amount of power must be thermally dissipated whether it appears as RTG rejected heat or as thermal dissipation of the spacecraft electrical loads.

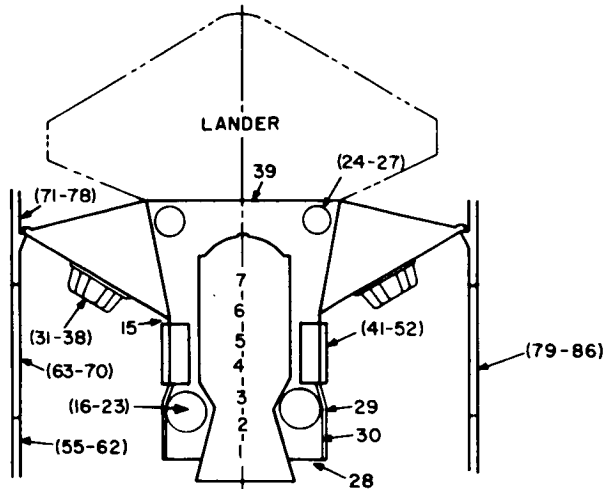
Adequate dissipation will be most difficult during the time period when the shroud encapsulates the spacecraft and prevents direct RTG radiation to space. For this reason, emphasis has been placed on the prelaunch and parking orbit phases of the Voyager mission.

A detailed thermal model of the Spacecraft, RTG's, and shroud was developed for computer analysis. Figures 3-17 and 3-18 illustrate the nodal geometry used to describe the RTG Spacecraft design. The following are the major assumptions and guidelines used in developing the multinodal thermal model and are valid for both the prelaunch and parking orbit analyses:

- a. RTG's designed to operate at 400° F during space flight
- b. Eight 75-watt RTG's with a Bol thermal power of 1810 watts each.
- c. RTG heat dissipation by radiation only with none rearward from the RTG mounting plane
- d. RTG physical characteristics:
 1. Emissivity = 0.85
 2. Effective radiating area = 8.7 ft²
 3. Heat Capacity = 15 Btu/°F
- e. Electronic bay thermal dissipation -- values are shown on Table 3-10.

3.3.5.1 Prelaunch Without Shroud

This phase relates to conditions before the Planetary Vehicle is encapsulated by the shroud and end seal diaphragms. The RTG's are fueled and it is assumed that steady-state temperature conditions are reached before the shroud encapsulation. With an assumed ambient



- | | |
|---------------------------|---------------------------|
| (1-7) TANK | (31-38) RTGs |
| (8-14) FUEL | (39) SUPER INSUL. LANDER |
| (15) STRUCTURE | (40) AIR |
| (16-23) M/O TANKS | (41-52) ELECTRONICS |
| (24-27) SPHERICAL TANKS | (53) SPACE |
| (28) BASE | (55-78) INSIDE OF SHROUD |
| (29) SUPER INSUL. OUTSIDE | (79-86) OUTSIDE OF SHROUD |
| (30) SUPER INSUL. INSIDE | |

Figure 3-17. Thermal Analysis Model

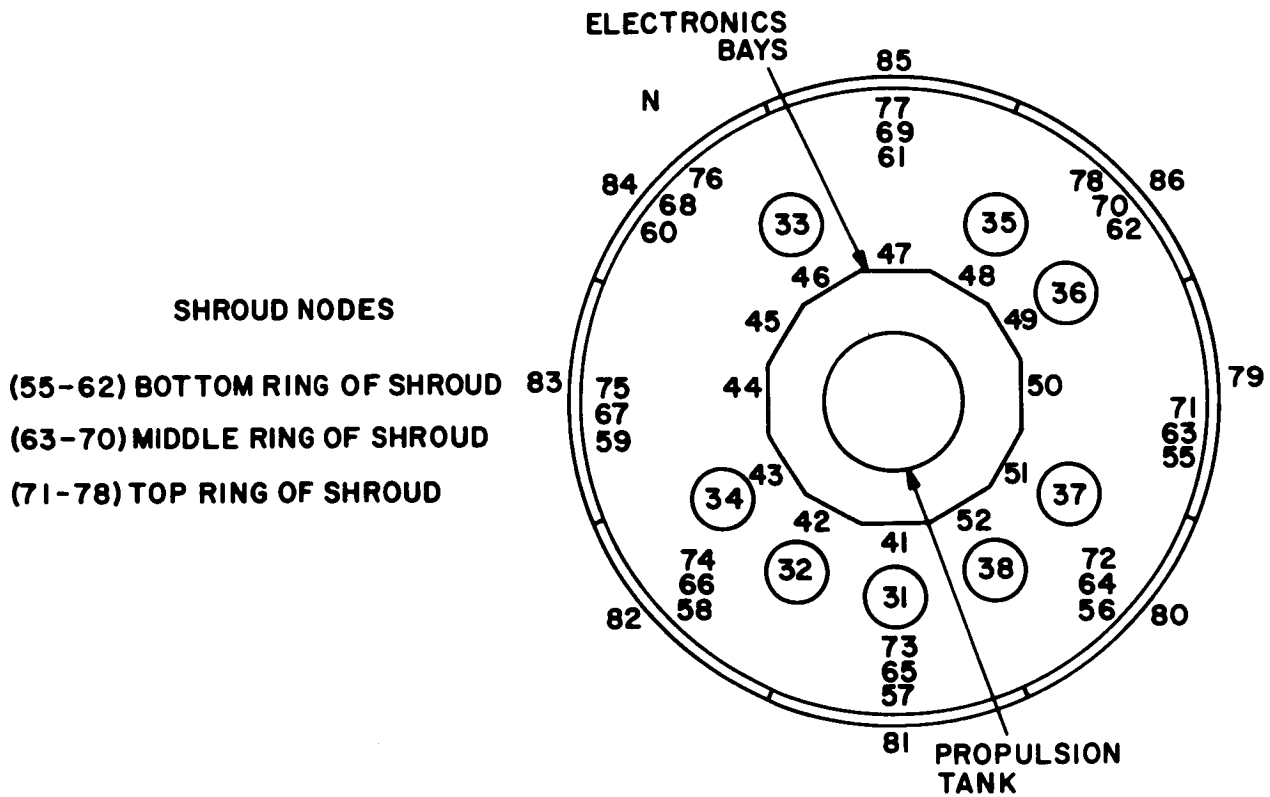


Figure 3-18. Thermal Analysis Nodal Breakdown

TABLE 3-10. ESTIMATED ELECTRONIC BAY THERMAL DISSIPATION, WATTS

Bay No.	Non-operational	Operational Pre-Shroud Separation	Operational Post-Shroud Separation
1	35*	53	53
2	35*	66	66
3	0	0	65
4	0	0	65
5	0	35	35
6	0	50	50
7	0	20	20
8	0	10	10
9	0	18	18
10	0	18	18
11	0	50	150
12	0	30	30

*RTG partial shunt regulator dissipation at no-load condition.

air temperature of 90° F and the occurrence of natural convective cooling, the average electronics temperature is predicted to be approximately 95° F. This result is based on the operational pre-shroud separation loads shown on Table 3-10. It is judged that the higher post-shroud separation loads could also be accommodated for checkout purposes. Limited periods of such operation or the use of localized forced convective cooling for the higher temperature bays might be necessary. If the spacecraft equipment must be designed to withstand higher temperatures in connection with ethylene oxide (ETO) decontamination (discussed in more detail later) then the problem of checkout with full operational loads before shroud encapsulation is eased significantly.

3.3.5.2 Prelaunch With Shroud Encapsulation

From the time of shroud encapsulation some form of active cooling will be required. Several possibilities are discussed below. First, the major assumptions regarding the shroud are:

- a. Shroud structured from 4 inch core aluminum honeycomb with 0.06 inch face-sheets and a transverse thermal conductance of $1.0 \text{ Btu/hr-ft}^2 - ^\circ \text{F}$.
- b. Shroud area taken as two-thirds its actual value since this is more indicative of the area seen by the spacecraft and RTG's.
- c. Shroud coatings, inside $\epsilon = 0.90$, outside $\alpha_s = 0.3$ and $\epsilon = 0.80$. A high emissivity inside shroud coating was selected to minimize the reflection of RTG thermal radiation from the shroud to the spacecraft electronic bays. A low α_s/ϵ outside shroud coating was selected to minimize the effect of solar heating on the spacecraft.
- d. Externally, shroud subjected to solar, albedo, and Earth fluxes using a solar flux at Earth of $320 \text{ Btu/ft}^2\text{-hr}$. This value is typical of solar flux at the Earth's surface after being attenuated by the Earth's atmosphere.
- e. Windage assumed to be sufficient to produce a convection heat transfer coefficient of $2 \text{ Btu/ft}^2\text{-hr-}^\circ \text{F}$ on the outside of the shroud. The value of the convection coefficient is based on Nimbus shroud test data which indicated a range of $1.0 - 4.0 \text{ Btu/ft}^2 - \text{hr} - ^\circ \text{F}$ for this coefficient depending on wind conditions.
- f. Ambient air external to the shroud assumed to be at 90°F .

Cooling methods considered include the use of internal air circulation and the reduction of shroud wall temperatures to increase radiative heat transfer capability. With the average temperature of the electronic bays taken as the criterion of cooling effectiveness, Figures 3-19 to 3-24 develop the options for providing this cooling. Figure 3-19 identifies nomenclature.

Figure 3-20 simply shows the variations of heat removal by air circulation with heat removal through the shroud walls for different system heat loads. The system heat load is equivalent to the installed RTG thermal power.

Figure 3-21 shows the result of an analysis for determining the average temperature of the inner shroud wall, \bar{T}_w , as a function of the shroud heat load, Q_{SH} , and shroud coolant heat removal, Q_C . The difference, $Q_{SH} - Q_C$, is the ambient heat load Q_R , which is transferred

NOMENCLATURE:

- \bar{T}_E = AVERAGE ELECTRONICS TEMPERATURE
- \bar{T}_W = AVERAGE INSIDE WALL TEMPERATURE
- Q_S = SYSTEM HEAT LOAD
- Q_{SH} = HEAT LOAD TO SHROUD AND DIAPHRAGM WALLS
- Q_A = AIR HEAT REMOVAL
- Q_R = AMBIENT HEAT REJECTION
- Q_C = SHROUD WALL COOLANT HEAT REMOVAL

RELATIONSHIPS:

$$Q_S = Q_{SH} + Q_A$$

$$Q_{SH} = Q_C + Q_R$$

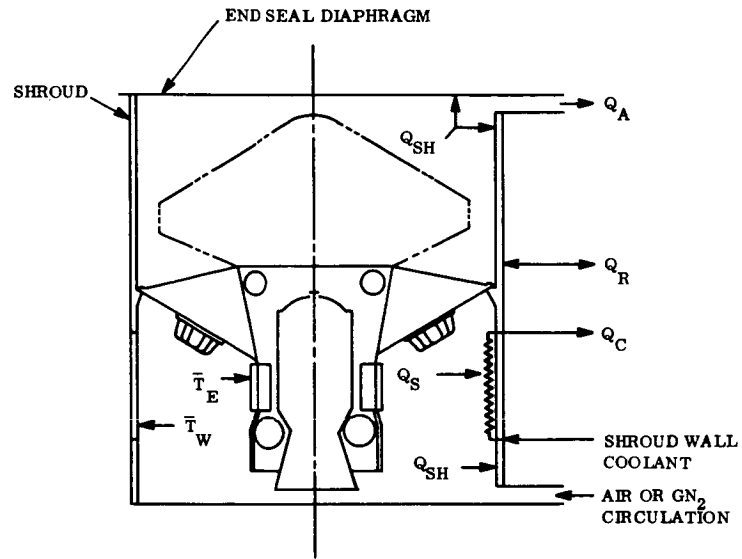


Figure 3-19. Shroud Cooling Nomenclature

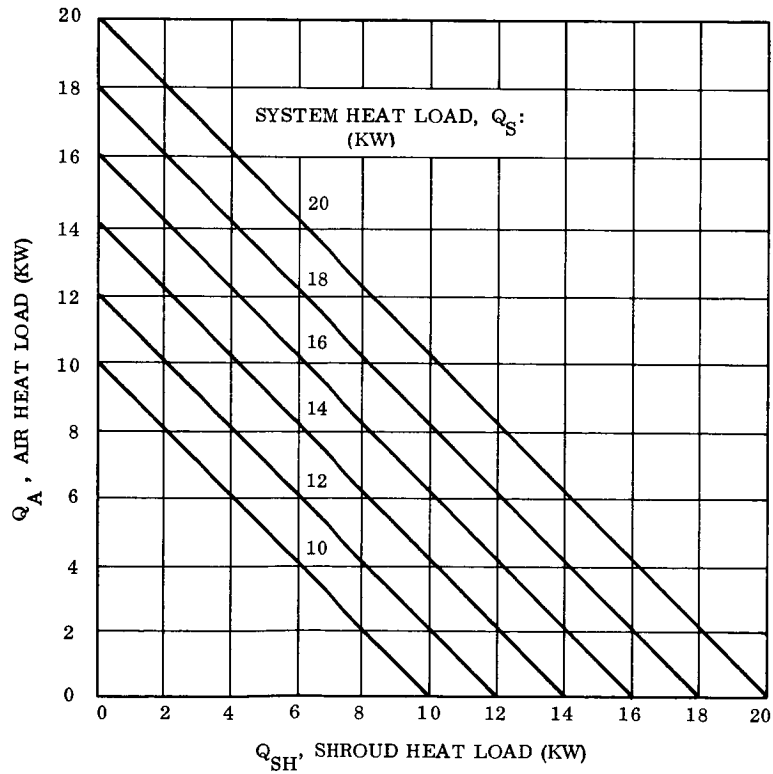


Figure 3-20. Air and Shroud Heat Load Variations

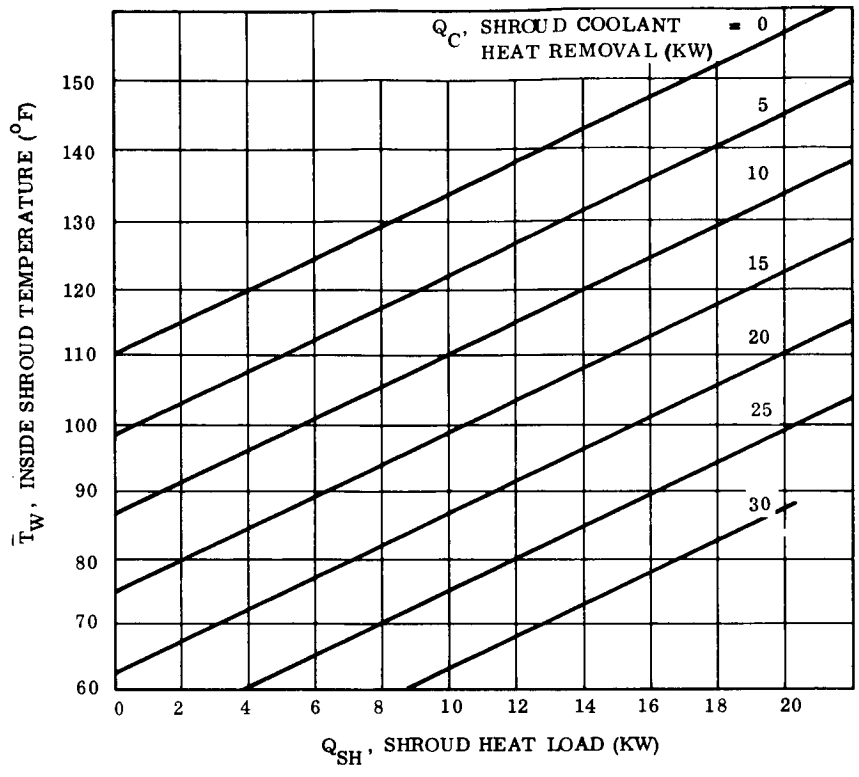


Figure 3-21. Shroud Heat Removal Effectiveness

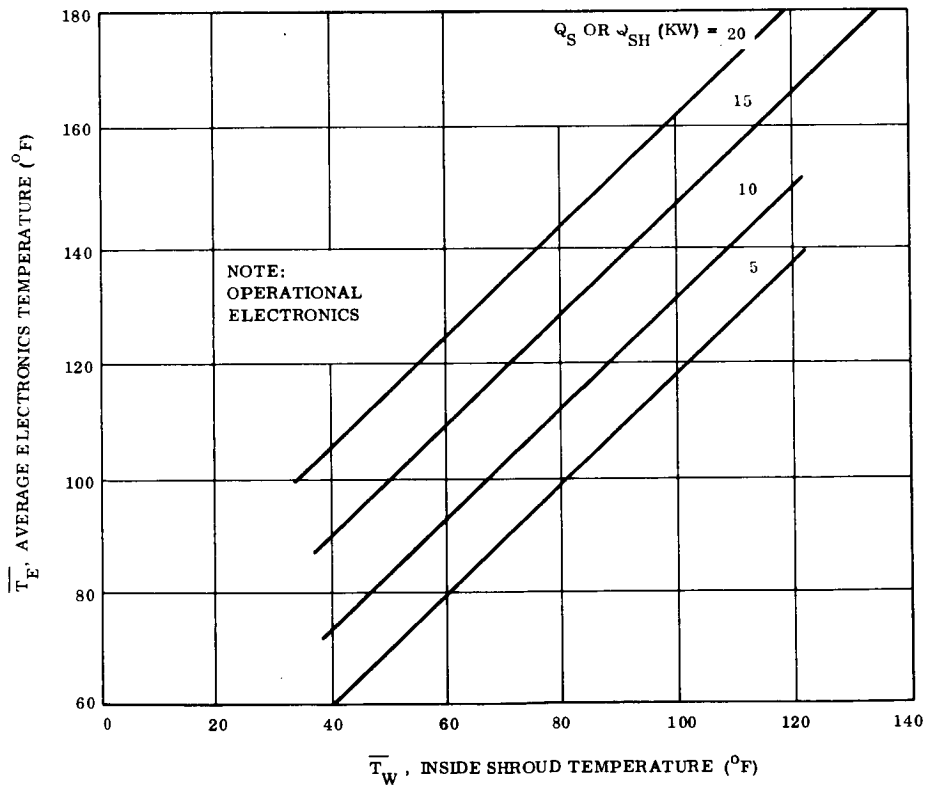


Figure 3-22. Electronics Temperature Determination (Operational)

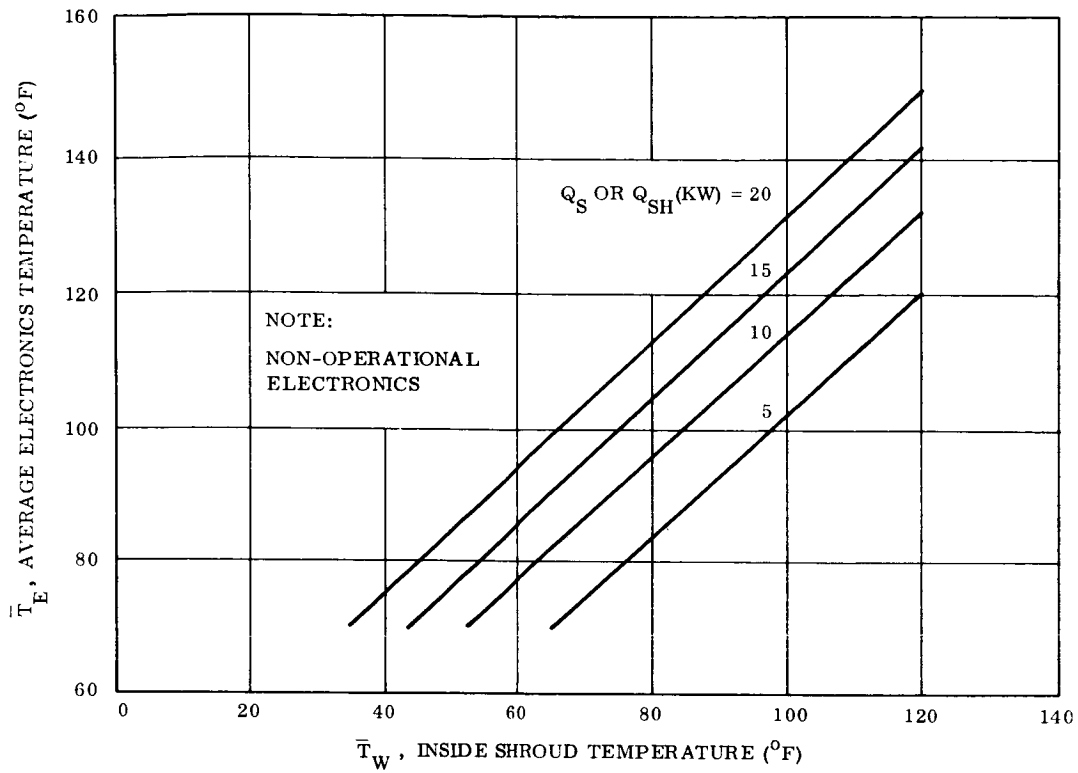


Figure 3-23. Electronics Temperature Determination (Non-Operational)

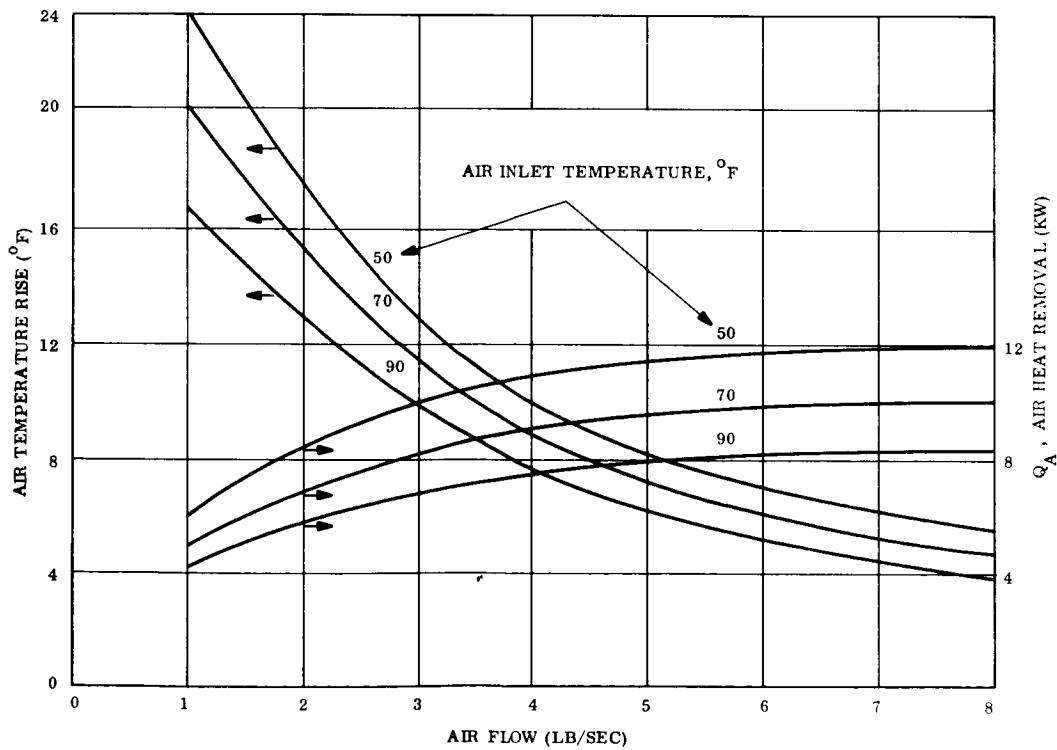


Figure 3-24. Air Heat Removal Effectiveness

by radiation to the ambient heat sink or by convection of external windage. Shroud coolant heat removal, Q_C , refers to such possibilities of including cooling coil heat exchangers in the shroud wall itself to achieve desired wall temperatures. The results of this figure are based on the shroud and ambient characteristics assumed earlier in this section. For negative values of $Q_{SH} - Q_C$, ambient heat is being transferred inward. Thus, at Q_{SH} equal to 16 kw and Q_C equal to 20 kw, 4 kw of ambient heat are transferred inward to maintain an inside wall temperature at 100° F.

Figure 3-22 shows the effect of the inside shroud wall temperature, \bar{T}_W , on the average electronics temperature, \bar{T}_E , for different values of shroud or system heat loads. This result is based on radiant heat transfer and conduction through the enclosed air (zero flow rate) and considers operational electronic loads as defined in Table 3-10.

Figure 3-23 shows a similar plot for non-operational conditions. The interpretation of whether the parametric values refer to system or shroud heat loads is simply a matter of how the air heat removal load, Q_A , is accounted for. If the system load is 20 kw and Q_A equals zero, then Q_S equals Q_{SH} and the 20 kw line defines the temperature conditions. If Q_A equals 5 kw then Q_{SH} equals 15 kw and temperature conditions are defined by the 15 kw line.

Figure 3-24 shows estimates of air heat removal effectiveness and are based on the assumption that air cooling occurs by free convection. This is considered conservative, since the existence of some degree of forced convection would in fact result in improved heat transfer.

To interpret these curves several cooling options are determined below. Assume a 15 kw system heat load with operational electronic loads. First, if there is no cooling by air circulation ($Q_A = 0$) or shroud coolant ($Q_C = 0$), then $Q_S = Q_{SH} = 15$ kw. Entering into Figure 3-21 for $Q_C = 0$, the inner wall temperature is 145° F. For this shroud wall temperature, Figure 3-22 indicates an average electronics temperature of 190° F for the case $Q_A = 0$.

As a second case, consider that it is desired to limit the electronics temperature to 100° F. With 50° F cooling air (Figure 3-24) this may be accomplished for different flow rates and corresponding values of Q_A . Suppose a flow rate of 1 lb/sec is used, resulting in Q_A equal

to 6 kw. Referring to Figure 3-22, $Q_{SH} = 15-6 = 9$ kw, resulting in an inside shroud temperature of about 70° F. Entering into Figure 3-21 with $Q_{SH} = 9$ and $\bar{T}_W = 68$ results in a value of $Q_C \approx 27$ kw. By repeating this process for different flow rates the locus of appropriate values of Q_C can be determined as a function of \bar{T}_W and is shown on Figure 3-25. The plot summarizes the cooling options for maintaining the electronics at 100° F.

If it is assumed that 50° F air is the lowest practical air temperature that could be considered, the results of Figure 3-25 suggest that sufficient cooling cannot be accomplished by air circulation alone. In fact, for the highest possible value of air circulation cooling, about 11 kw, shroud wall cooling is also about 11 kw. In general, the results indicate that refrigeration loads would be reduced with higher values of air cooling circulation. This results from higher inside wall temperatures which reduce the inflow of external ambient heat.

The above analysis only provides a preliminary basis for estimating cooling requirements. In particular, improved values of convective heat transfer coefficients may significantly alter the results shown in Figure 3-24 and this in turn will affect overall results. Also, the assumed ambient condition may be overly pessimistic, resulting in the rather high values of shroud wall cooling. Nevertheless, it does point out that extensive consideration should be given to means for reducing this heat load.

Nominally it appears that both air circulation and shroud wall cooling should be employed. Besides serving as backups to one another, they would also permit flexibility during certain operational procedures.

Tracing through some of the anticipated procedures, the significant thermal conditions likely to be encountered are as follows:

- a. Prior to Shroud Encapsulation - This was discussed earlier in Section 3.3.5.1. No significant problems are foreseen.
- b. Shroud Assembly - During the assembly process of the shroud and end seal diaphragm, continuous cooling appears mandatory. Whether assembly procedures and cleanliness requirements will permit the simultaneous use of air circulation cooling has not been ascertained. If the time from encapsulation to the time of startup of air circulation is sufficiently short, no additional cooling methods may be required. However, this

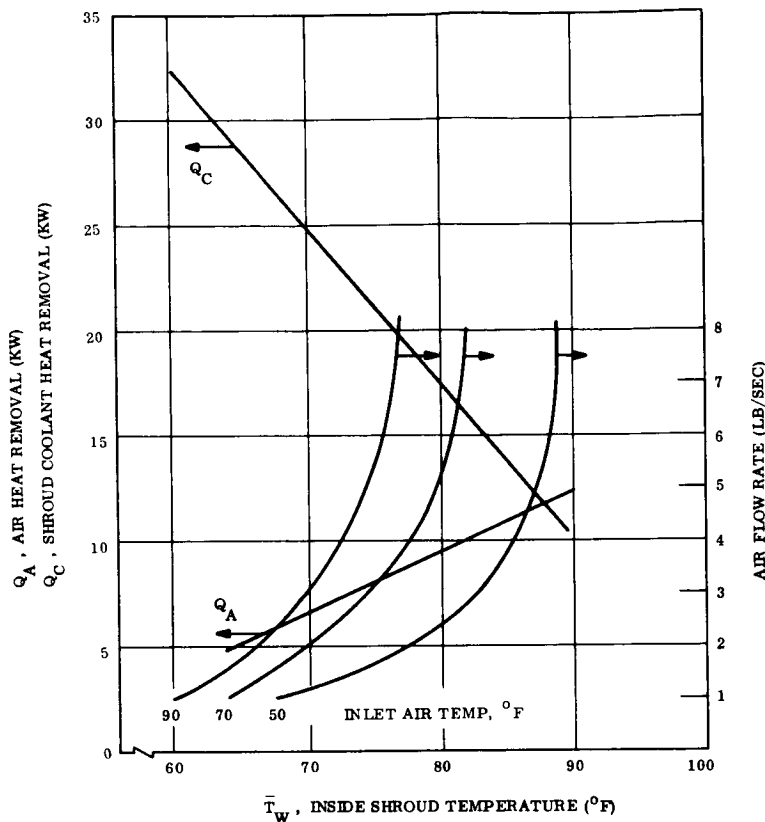


Figure 3-25. Cooling Options for $T_E = 100^\circ F$

possibility is doubtful for reasons of contingency and additional cooling means should be considered. Active shroud wall cooling cited earlier is one possibility. Another is to direct external cooling to the shroud to achieve a desired inner wall temperature. As noted on Figure 3-23 the inner wall temperature should be about $75^\circ F$ for non-operational electronics at $100^\circ F$ with zero air flow for a 15 kw system heat load.

- c. Post Shroud Assembly - Reference 3-3 indicates the possibility of pressurization cycles and shroud cavity purging with ethylene-oxide (ETO). Both relate to decontamination with respect to the planetary quarantine constraint. Pressurization of the shroud cavity pertains to the test of the integrity of various seals and flanges. Presumably one of the test procedures might be to seal off all ports, pressurize the cavity, and detect the rate of pressure decay resulting from leaks. As noted earlier, under this condition with zero flow rate the electronics could rise to $190^\circ F$ for the operational case, or about $165^\circ F$ for the non-operational case. Whether alternative pressurization test techniques, under conditions of flow for cooling purposes, can be employed, has not been determined. Again, the use of shroud wall cooling would tend to relieve this situation and reduce test complexities.

It has been suggested that if ETO decontamination of the Planetary Vehicle surfaces is used it would be carried out with the ETO mixture (12% ETO, 88% Freon-12) at a temperature of 40° C and a relative humidity of 35^{+15}_{-5} percent. The procedure for decontamination would be conducted as a phase of on-pad operations and would consist of: (1) removal of the normal cooling medium (air or gaseous nitrogen, GN₂) by ETO purging; (2) extended exposure to the ETO environment of the required temperature and humidity conditions; and (3) removal of the ETO by GN₂ (or air) purging. It is presumed that for ETO effectiveness all surfaces, including the inside shroud walls, must be no lower than 40° C. Assuming that no cooling is provided by the ETO mixture ($Q_A = 0$), Figure 3-23 indicates a non-operational electronics temperature of 127° F for a shroud wall temperature of 104° F (40° C) for a 15 kw system heat load. Therefore, from Figure 3-21, $Q_C = 18$ kw corresponding to a wall temperature of 104° F, indicating again the desirability of an independent means of shroud wall cooling.

3.3.5.3 Launch to Parking Orbit

This phase of the mission is critical from a thermal standpoint because the shroud encapsulates the lower Voyager spacecraft and RTG's up to possibly 90-minutes at a time when air conditioning cannot be provided. Areas of concern include:

- a. Overheating of the RTG's
- b. Local shroud hot spots causing severe thermal stresses in the shroud
- c. Possible overheating of electronic bays.

Overheating of the RTG's is not a problem through the pre-launch phase of the mission, primarily because air is available to convectively cool the RTG's. This air cooling more than compensates for the fact that the RTG's do not radiate to deep space. However, except for the first few minutes of launch, the spacecraft and RTG's will be subjected to vacuum conditions so that the cooling effect by the air will not exist. Therefore, it is conceivable that the RTG's could overheat during the time period from launch to shroud ejection and there was some concern that on-the-pad precooling of the RTG's would be necessary.

Since it is possible to produce a shroud failure by excessive local thermal stresses, mounting of the RTG's is quite important. For example, it is possible to mount the RTG's such that their view of the electronics bays is negligible. However, for this condition, the thermal radiation from the RTG's to the shroud would cause high local shroud temperatures and temperature gradients, resulting in excessive thermal stresses in the shroud. Conversely, the RTG's cannot be mounted in such a manner that their view of the electronics bays is significant enough to cause excessive electronics temperatures. Therefore, for the particular mounting geometry selected, it is necessary to evaluate both local shroud temperature distribution and electronics bay temperature rise. If overheating problems do arise, it is conceivable that a change in mounting geometry could alleviate them.

For the launch to shroud separation analysis, the nodal geometry and assumptions are the same as those used in the prelaunch analysis, with the following exceptions:

- a. External shroud heat sources as shown in Figure 3-26.
- b. Transient thermal analysis to be used with an average electronics temperature of approximately 80° F at the time of launch.
- c. Ninety-minute orbit with 45-minute shadow time. First 45 minutes in Sun with Sun normal to node 81 (i. e., parallel to the spacecraft Y axis) at 22.5 minutes.
- d. Solar absorptivity of outside shroud coating assumed to be 0.6 during parking orbit. This assumes degradation of 100% over the value used for the prelaunch analysis. Test data has shown that no appreciable degradation will occur at temperatures below 200° F. However, for purposes of conservatism, an $\alpha_S = 0.6$ was selected.

The results of the parking orbit analysis are as follows:

- a. The RTG average fin rejection temperature will rise about 30° F during parking orbit. This temperature overshoot is not considered significant enough to cause any detrimental effect to the RTG's, and therefore on-the-pad precooling of the RTG's is not required.

Furthermore, analysis has shown that due to the low heat capacity of an RTG and its high heat dissipation, precooling of the RTG's would be ineffective. Figure 3-27 shows the temperature history of an RTG designed to operate at an average fin temperature of 400° F. Inspection of this figure indicates that whether the RTG was pre-cooled to 150, 200, or 250° F, the temperature of the RTG would be essentially the same (430° F) after 90 minutes. In this analysis, a shroud heat sink temperature of 95° F was assumed.

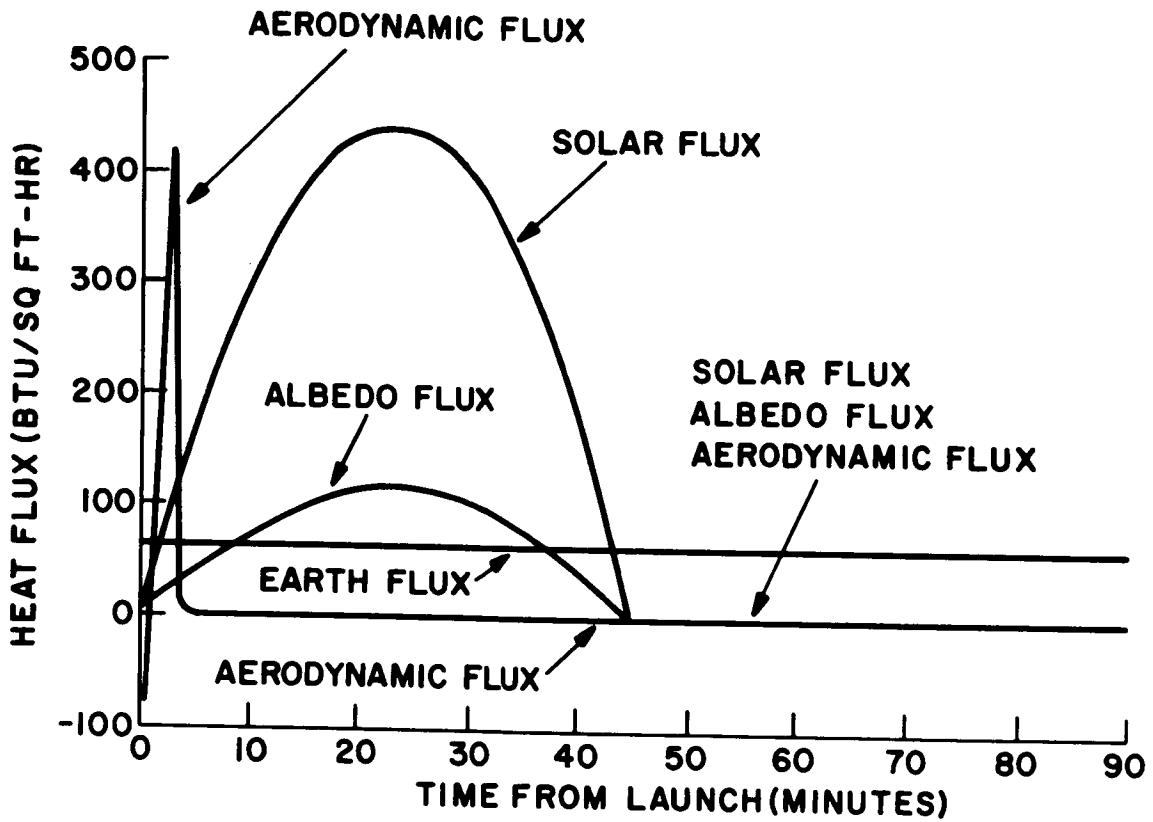


Figure 3-26. External Shroud Heat Source

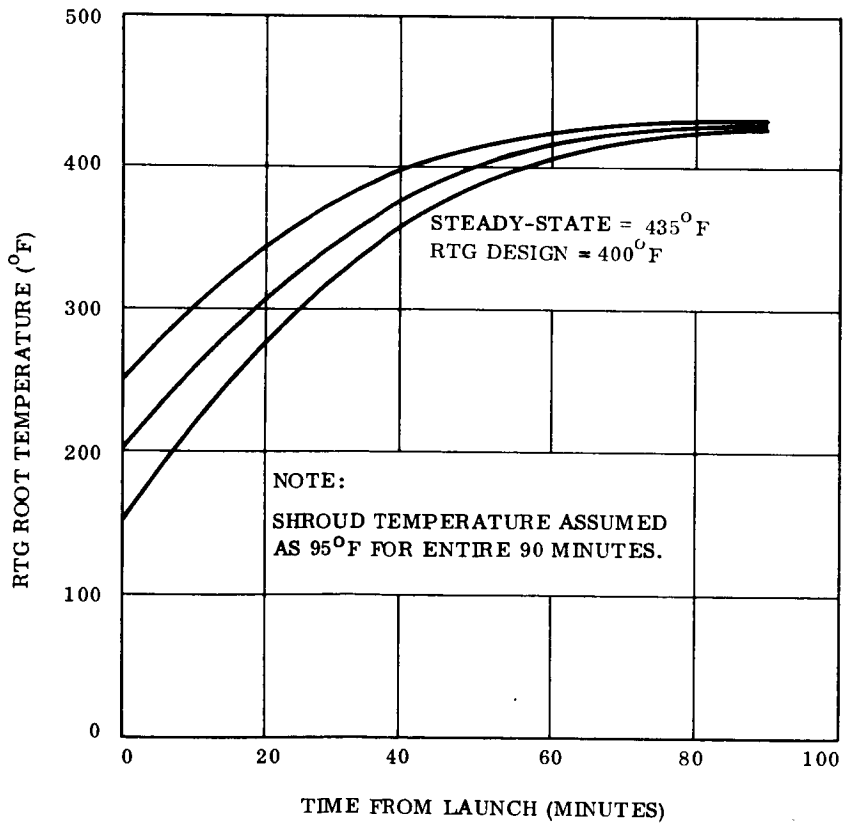


Figure 3-27. RTG Temperature History

- b. The average electronics temperature, initially at 80° F at launch, will increase 12° during parking orbit. Table 3-11 lists the initial temperatures of each electronics bay resulting from on-the-pad temperature control and the maximum temperature of each bay during parking orbit. The operational loads listed in Table 3-10 were used in this analysis.
- c. The maximum local shroud temperature during parking orbit is 165° F, and the maximum temperature drop through any portion of the shroud is 52° F. Table 3-12 shows the maximum temperatures of a section of the inside of the shroud during parking orbit. Neither the temperature level nor the temperature gradient appear severe enough to cause any significant thermal stress problems in the shroud.

Figure 3-28 summarizes the maximum temperature of the spacecraft, shroud, and RTG's during parking orbit.

3.3.5.4 Spaceflight

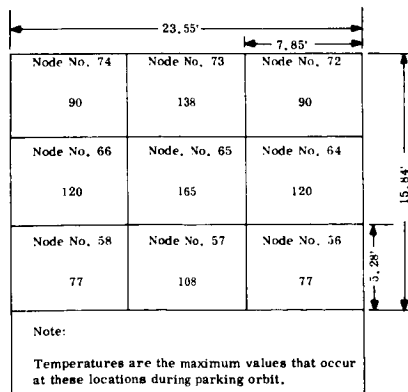
At the completion of parking orbit, the shroud encapsulating the lower Voyager spacecraft is ejected. Ejection of the shroud alleviates thermal problems since both the RTG's and electronics bays can now radiate to space. Figure 3-29 shows a typical, near-Earth, steady-state spacecraft temperature distribution after shroud ejection. For the remainder of the Martian mission, the effect of the RTG's on the spacecraft will be minimal and the thermal response of the spacecraft will be quite similar to that given in the analysis performed for the Task B design.

TABLE 3-11. ELECTRONICS BAY TEMPERATURES DURING PARKING ORBIT

Bay Function	Node No. (Bay No.)	Heat Dissipated (Watts)	Weight (lb)	*Initial Bay Temperature (° F)	Maximum Bay Temperature (° F)
Data Storage	41(9)	18	68	75	87
Data Storage	42(10)	18	68	76	88
Radio	43(11)	50	54	85	102
Radio	44(12)	30	60	80	92
Power	45(1)	53	68	90	103
Power	46(2)	66	67	94	109
Science	47(3)	0	96	67	74
Science	48(4)	0	61	67	76
G&C	49(5)	35	55	82	95
C&S	50(6)	50	50	88	104
Command	51(7)	20	39	76	92
Telemetry	52(8)	10	31	72	88
Average	-	29	60	80	92

*Initial temperatures based on ground cooling analysis with inside shroud temperature maintained at 80° F and with air conditioning.

TABLE 3-12. INSIDE SHROUD TEMPERATURE DISTRIBUTION DURING PARKING ORBIT



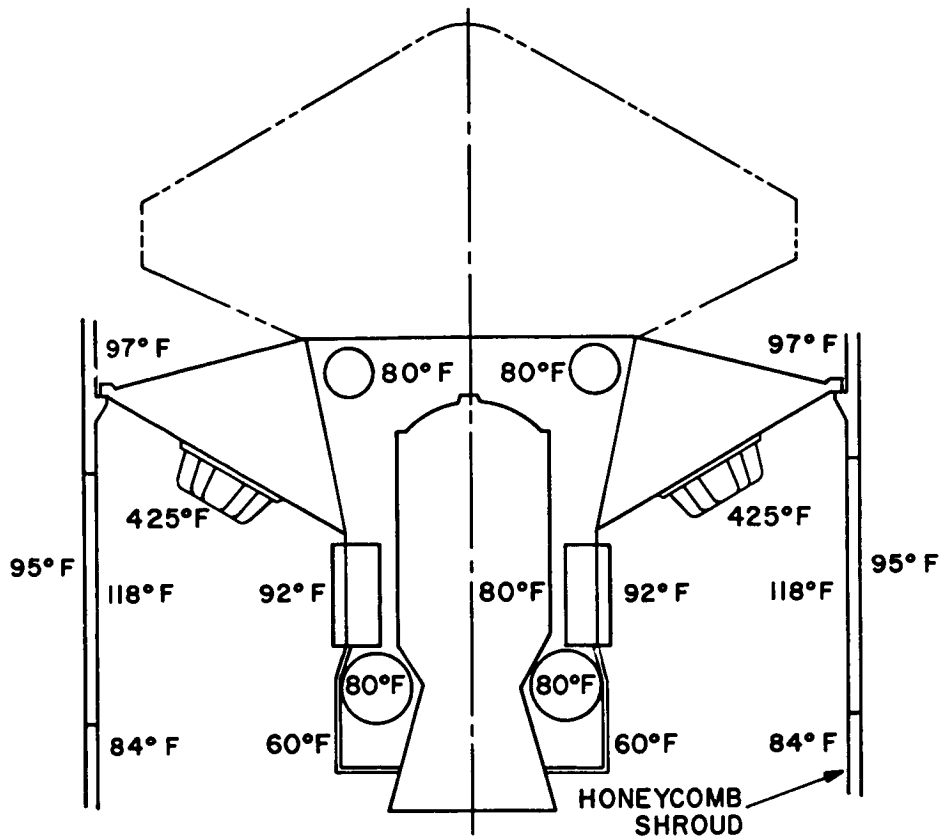


Figure 3-28. Parking Orbit Maximum Temperatures

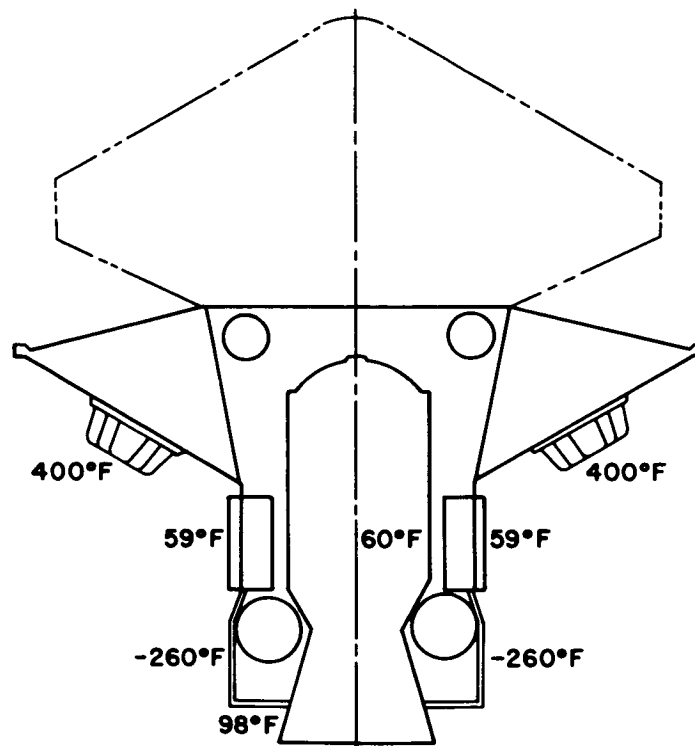


Figure 3-29. Spacecraft Temperature Distribution Without Shroud

3.3.6 RADIATION MAPPING

A fundamental concern in this study has been the effect which the nuclear radiation from the RTG's might have on the performance of spacecraft components and on prelaunch ground handling activities. A detailed knowledge of the radiation field was therefore required.

The radiation sensitivity thresholds for the Voyager Bus science payload and for support subsystems and their components was established independent of the radiation environment at the component location (see Section 5.2). Following this, preliminary estimates of the radiation field from plutonium-238 and from curium-244 fueled RTG's showed that the latter would only be usable in conjunction with rather massive neutron shields. For this reason, curium-244 has not been investigated further in this study.

3.3.6.1 Primary Radiation

Plutonium-238 decays by two modes: by emitting an alpha particle and certain characteristic gamma photons, and by spontaneous fissioning. The alpha particles may interact with the nuclei of light elements and in the process release a neutron. Because Pu-238 is fissionable by fast neutrons, the neutrons released during spontaneous fissions and from alpha reactions can induce further fissions in the fuel. On the other hand, some of the neutrons will be absorbed within the RTG by any of the materials present. The energy distribution of the net population of neutrons outside the RTG's is shown in Figure 3-30; the energy of the fission neutrons is not only lower than that of the (α , n) neutrons, but there are also considerably fewer of them.

The characteristic decay gammas have energies of 0.043, 0.099, 0.15, 0.716, and 0.81 Mev; there are also higher energy gamma photons, mostly from the decay of fission product nuclei and from the fission process itself. Some gammas result from certain neutron reactions. The dominant yield is for the 0.043 Mev gamma; however, essentially all of these are absorbed within the RTG itself. The distribution of gamma photons outside the RTG's is shown in Figure 3-31.

The valleys in the curve are only estimated because they represent gamma photons which were born with higher energy and lost some of it in one of a number of gamma interactions, most

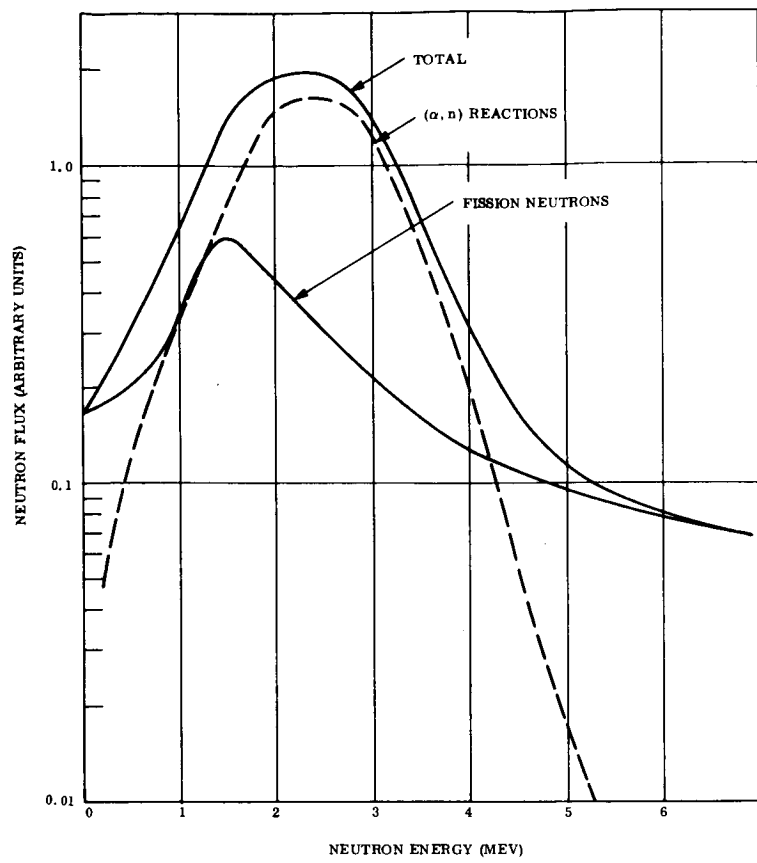


Figure 3-30. Neutron Flux Energy Distribution (Normalized to Total Number of Neutrons)

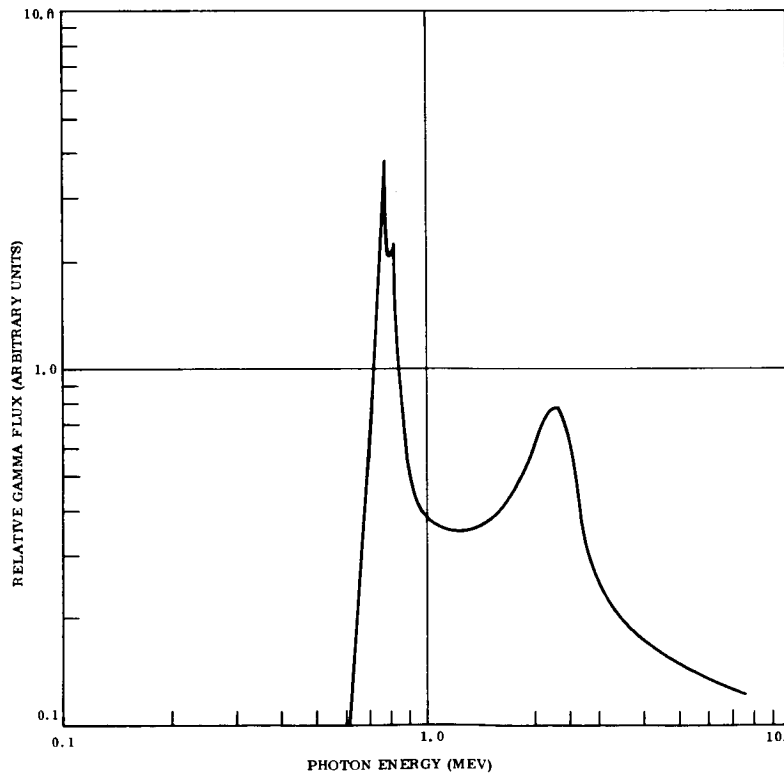


Figure 3-31. Gamma Photon Energy Distribution Outside RTG

probably a Compton scattering reaction, and these reaction rates depend strongly on the materials present.

The above does not consider the change in the gamma population with time. Plutonium-236, an isotopic contaminant of the fuel, may be present in small quantities (about one ppm in fuel originating at the Savannah River plant of the USAEC). One of the products of plutonium-236 decay is thallium-208. In the course of the thallium-208 decay to lead-208, a 2.614 Mev gamma photon is emitted. This is of concern because it is difficult to shield against such energetic gammas. Fortunately, the half-lives of the nuclides in the plutonium-236 decay chain are so ordered that the thallium-208 activity increases with time to a maximum about 17 years after fuel processing. At this maximum level the photon yield from thallium-208 is about the same order as from the plutonium-238 decay gamma radiation; however, during the first two years after fuel processing, it does not exceed 15 percent of this value. In this study the effect of fuel aging was therefore assumed as not decisive and was not included.

3.3.6.2 Radiation Analysis Method

The calculation of the radiation field was performed by the "point kernel" method. In this method the source region is subdivided into sufficiently small volumes so that only a slight error is introduced by assuming each such volume to act like an isotropically emitting point source of particles. The attenuation of a narrow beam of particles from each point source to a given receiver point is computed and then summed over all point sources to give the total number of particles (or dose rate) seen by the receiver point. Scattering of gammas into the beam is allowed for by using simple energy-dependent buildup factors for one representative material. For the neutron calculation the Albert-Welton kernel was used; here a complex exponential function is used to fit the measured attenuation of neutrons, through a slab of the given material in an "infinite" water medium, by means of an overall neutron "removal" cross section.

The calculation was performed with a version of QAD, a Los Alamos Scientific Laboratory originated shielding program. The gamma attenuation cross sections were obtained from Reference 3-4, the gamma build-up factors from Reference 3-5, and the neutron removal cross sections from Reference 3-6.

QAD performs an essentially three-dimensional analysis in cylindrical geometry. A sectional view of the configuration of the Spacecraft Bus used in this study is shown in Figure 3-32 as an overlay to the schematic model used in the actual computations, Figure 3-33. It is seen that the retropropulsion engine, equipment bay, harnessing, and the other more massive sections, along with the RTG's, are reasonably well represented because these components exercise a relatively strong influence on the radiation field. By the same token the light structures, such as the high-gain antenna and support struts, have very little effect on the radiation field, and have therefore been neglected.

The essential results of the mapping calculations are shown in Tables 3-13 and 3-14. The first shows the dose rate for gammas and the neutron flux at various selected points in and around the Spacecraft Bus. The location of these receiver points is shown graphically in Figure 3-33 and as (r, z) coordinates in the two tables. Table 3-14 shows the total time-integrated neutron flux and gamma carbon dose over a one-year time period at these same receiver points.

In addition to the selected receiver points listed in Tables 3-13 and 3-14, the dose rate and flux at many other receiver points was determined in order to construct a more general map of isodose contours around the schematically annular region containing the homogeneously distributed RTG sources. These contours are shown in Figure 3-34. The isodose lines are not extended into the vehicle structure, where they tend to take on rather complex shapes.

3.3.6.3 Accuracy of Radiation Map

It is difficult to assess the accuracy of these calculations without direct experimental verification. However, some degree of confidence in the analytical techniques and nuclear cross section data utilized in the calculations can be obtained from previous experience gained with the use of these same calculational techniques on other programs where experimental results were available, such as the SNAP-19 and SNAP-27 programs. Here the agreement between measurements and calculations similar to those developed above was about 5 percent. While this fine agreement is no doubt somewhat fortuitous, it does lend confidence to the results. Generally, the accuracy may be expected to be more like 25 percent.

Further discussion concerning secondary particle radiation and instrument shielding is contained in Section 5.2.

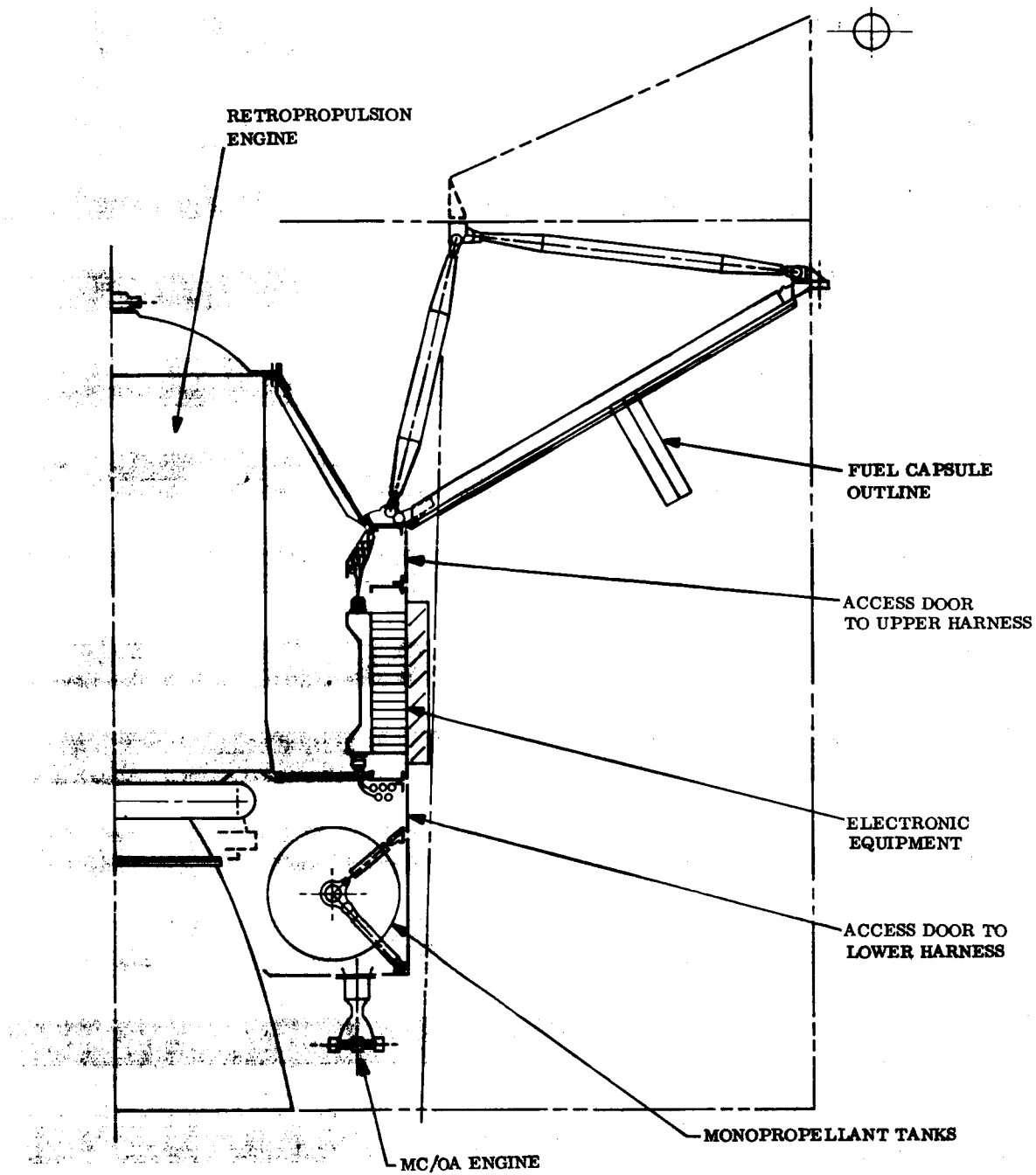


Figure 3-32. Voyager Spacecraft Bus Configuration

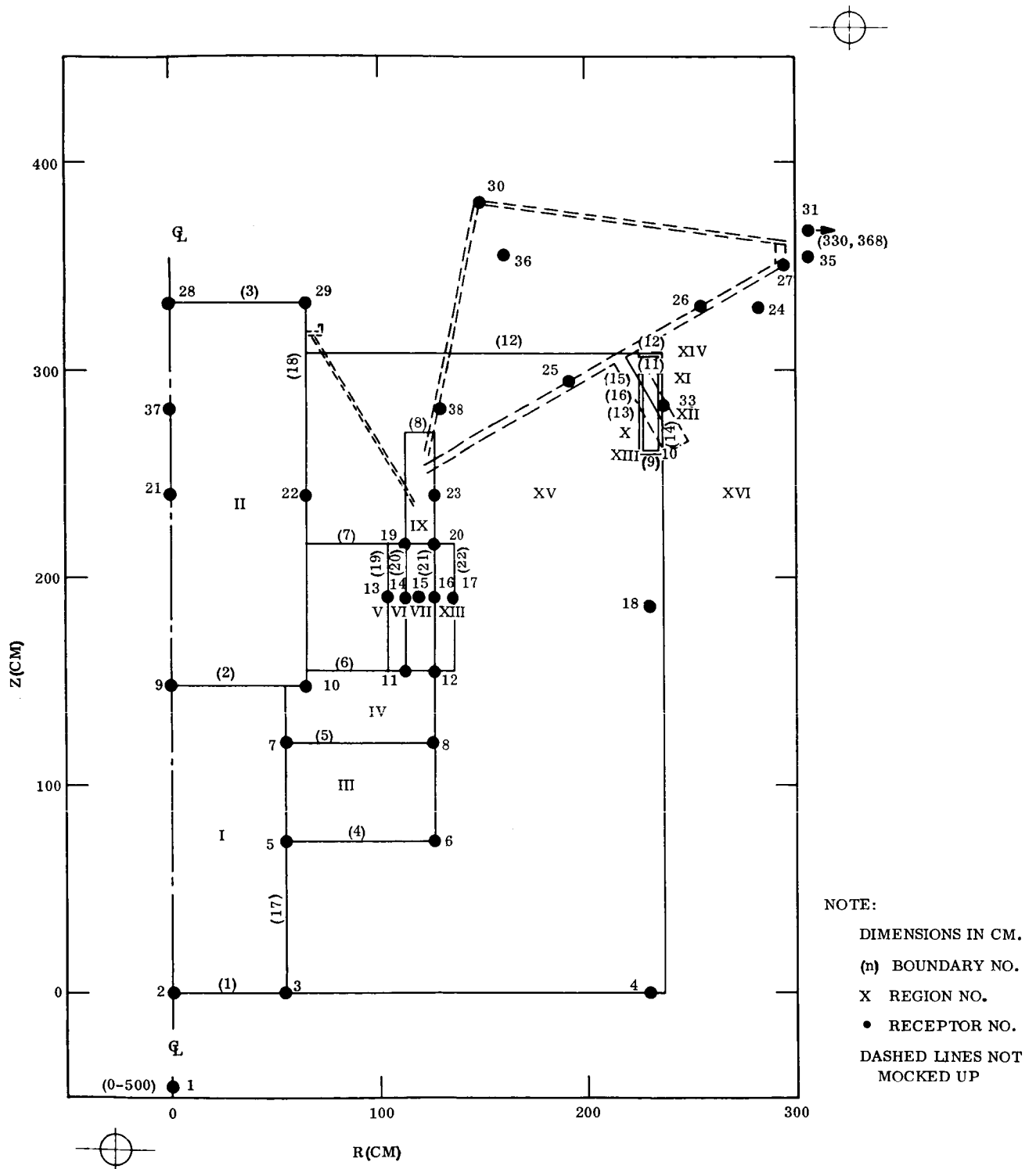


Figure 3-33. Vehicle Schematic for Voyager Bus Radiation Mapping (Pu-238 Fuel)

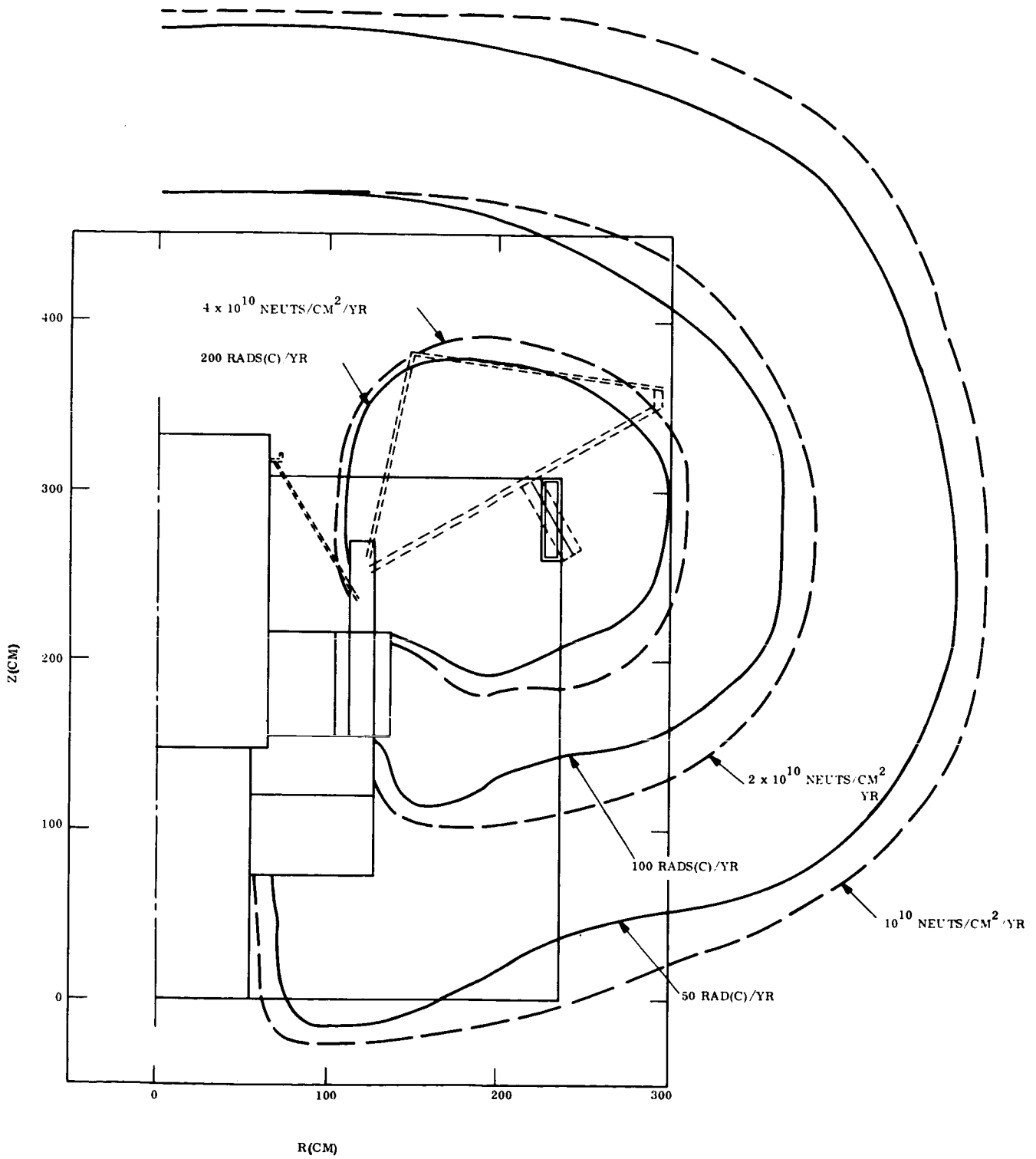


Figure 3-34. Isodose Contours

TABLE 3-13. FLUX AND DOSE RATE VALUES FOR VOYAGER BUS,
Pu-238 RTG RADIATION MAP

Receiver			Dose Rate	Flux	Receiver			Dose Rate	Flux
No.	Coordinates		γ Rad hr	n neutrons cm ² ·sec	No.	Coordinates		γ Rad hr	n neutrons cm ² ·sec
	R (cm)	Z (cm)				R (cm)	Z (cm)		
1	0	-500	1.4×10^{-3}	9.3×10^1	22	65	240	1.87×10^{-2}	9.65×10^2
2	0	0	2.72 ↓	5.75 ↓	23	126	253	2.91 ↓	1.54×10^3
3	55	0	4.87 ↓	2.75×10^2	24	330	282	2.28 ↓	1.59 ↓
4	230	0	5.15 ↓	3.46×10^2	25	192	295	5.84 ↓	3.32 ↓
5	55	73	5.39 ↓	3.12 ↓	26	255	330	3.03 ↓	2.17 ↓
6	126	73	8.31 ↓	5.15 ↓	27	295	350	1.81 ↓	1.2 ↓
7	55	121	5.79 ↓	3.54 ↓	28	0	333	2.2×10^{-4}	1.8 ↓
8	126	121	1.06×10^{-2}	6.30 ↓	29	65	333	1.47×10^{-2}	7.4×10^2
9	0	147	6.0×10^{-5}	5.30×10^{-1}	30	150	380	2.19 ↓	1.2×10^3
10	65	147	6.82×10^{-3}	4.05×10^2	31	330	368	1.22 ↓	7.85×10^2
11	111	155	8.73×10^{-3}	5.50 ↓	32	0	500	1.15 ↓	6.45×10^2
12	126	155	1.17×10^{-2}	6.85 ↓	33	237.6	282	4.58 ↓	4.5×10^3
13	104	185.5	1.30 ↓	7.80 ↓	34	305	212	1.66 ↓	1.08 ↓
14	111	185.5	1.25 ↓	7.70 ↓	35	305	355	1.61 ↓	1.05 ↓
15	118.5	185.5	1.31 ↓	8.05 ↓	36	162	355	2.68 ↓	1.53 ↓
16	126	185.5	1.59 ↓	9.20 ↓	37	0	282	2.7×10^{-4}	2.23 ↓
17	136	185.5	1.86 ↓	1.06×10^3	38	130	282	3.09×10^{-2}	1.62×10^3
18	230	185.5	1.91 ↓	1.32 ↓	39	330	282	1.65×10^{-2}	1.04×10^3
19	111	216	2.2 ↓	1.22 ↓	40	430	282	6.83×10^{-3}	4.48×10^2
20	126	216	2.4 ↓	1.32 ↓	41	1000	282	8.8×10^{-4}	6×10^1
21	0	240	2.25×10^{-4}	2.9×10^{-3}	42	230	1282	8.2×10^{-4}	5.6×10^1

TABLE 3-14. TOTAL YEARLY INTEGRATED FLUX AND DOSE VALUES FOR VOYAGER BUS Pu-238 RTG RADIATION MAP

Receiver			Total Yearly Dose	Integrated Flux	Receiver			Total Yearly Dose	Integrated Flux
No	Coordinates		γ Rad	n neutrons cm^2	No.	Coordinates		γ Rad	n neutrons cm^2
	R (cm)	Z (cm)				R (cm)	Z (cm)		
1	0	-500	1.2×10^1	2.92×10^9	22	65	240	1.65×10^2	3.03×10^{10}
2	0	0	2.39	1.8×10^9	23	126	253	2.56	4.84
3	55	0	4.27	8.65×10^9	24	330	282	2.0	5.0
4	230	0	4.52	1.09×10^{10}	25	192	295	5.13	1.04×10^{11}
5	55	73	4.73	9.80×10^9	26	255	330	2.67	6.8×10^{10}
6	126	73	7.30	1.62×10^{10}	27	295	350	1.59	3.76×10^{10}
7	55	121	5.08	1.11	28	0	333	1.9	5.65×10^7
8	126	121	9.3	1.98	29	65	333	1.29×10^2	2.32×10^{10}
9	0	147	5.3×10^{-1}	1.67×10^7	30	150	380	1.93	3.77
10	65	147	6.0×10^1	1.27×10^{10}	31	330	368	1.07	2.46
11	111	155	7.7×10^1	1.73	32	0	500	1.01	2.02
12	126	155	1.03×10^2	2.15	33	237.6	282	4.02	1.41×10^{11}
13	104	185.5	1.15	2.45	34	305	212	1.46	3.4×10^{10}
14	111	185.5	1.10	2.42	35	305	355	1.42	3.3
15	118.5	185.5	1.15	2.53	36	162	355	2.36	4.8
16	126	185.5	1.40	2.89	37	0	282	2.38	7.0×10^7
17	136	185.5	1.64	3.33	38	130	282	2.72×10^2	5.1×10^{10}
18	230	185.5	1.68	4.15	39	330	282	1.45×10^2	3.26
19	111	216	1.94	3.83	40	430	282	6×10^1	1.4
20	126	216	2.11	4.15	41	1000	282	7.75	1.88×10^9
21	0	240	2.0×10^1	5.9×10^7	42	230	1282	7.20	1.75×10^9

3.4 SUBSYSTEM DESIGN

This section describes the major effects of RTG's on the various spacecraft subsystems. With respect to the Task B solar powered design described in Section 3.1.2, the RTG's impose changes in power conditioning equipment since their source characteristics differ sufficiently from solar arrays. Also, of course, the amount of battery capacity is greatly reduced since the RTG's operate independently of solar occultation. Concerning other subsystems, the principal effects are those related to the ability to fix the high-gain antenna since direct Sun pointing is not required with RTG's. However, the Sun is used for attitude reference purposes and therefore some modification to the guidance control subsystem becomes necessary. Related changes are also required for the radio subsystem.

3.4.1 POWER SUBSYSTEM

The relatively constant output of RTG's over the mission time, along with substantial reduction in battery capacity, generally results in reduced power conditioning complexity. It is not as necessary to accommodate the wide voltage variations inherent in photovoltaic/battery systems.

The selection of a partial shunt regulating system for the RTG's has been adequately described in Task C Document No. VOY-C1-TR12. The overall power system was described in VOY-C1-TR16. The description below summarizes these results and updates some of the features, based on later considerations, particularly those concerning convertibility from solar to RTG power or vice versa. The design draws heavily from the features of the Task B design; these will be pointed out where appropriate.

3.4.1.1 Functional Description

The power subsystem supplies electrical power to the flight spacecraft from launch through all mission phases. It also supplies power to the flight capsule until capsule separation, except for limited periods when the full spacecraft science package is operated. Load requirements for each mission phase are presented in the Energy Balance Table, Table 3-15.

The power subsystem functional block diagram is shown in Figure 3-35. Primary power is derived from 8 RTG's whose sizing characteristics are defined in Section 3.3.2.2. The nominal total RTG power is 600 watts delivered at 20 volts dc. Each RTG is equipped with its own

TABLE 3-15. ENERGY BALANCE TABLE

POWER IN WATTS FOR →	Launch To Acquisition (Typical)	Cruise	Mars Orbit Insertion (Typical)	Orbit With Capsule		Orbit Without Capsule and Science
				Full Science	Other Times	
Boost Regulator Output						
Efficiency						
Thermal Loss	4.0	4.0	4.0	4.0	4.0	4.0
Boost Regulator Input	4.0	4.0	4.0	4.0	4.0	4.0
Direct Battery Loads:						
Failure Detectors	2.0	2.0	2.0	2.0	2.0	2.0
Thrust Vector Control			(875.0)			
Direct Battery Load Subtotal						
Harness Loss	0.1	0.1	0.1	0.1	0.1	0.1
Thermal Loss	0.1	0.1	0.1	0.1	0.1	0.1
Direct Battery Load	2.2	2.2	2.2	2.2	2.2	2.2
Battery Power Output	6.2	6.2	6.2	6.2	6.2	6.2
Battery Thermal Loss						
Battery Power Input	6.2	6.2	6.2	6.2	6.2	6.2
Battery Charger Output Efficiency						
Thermal Loss	2.0	2.0	2.0	2.0	2.0	2.0
Battery Charger Input	8.2	8.2	8.2	8.2	8.2	8.2
2400 Hz Inverter Loads:						
Battery Charger Input	8.2	8.2	8.2	8.2	8.2	8.2
Radio	30.0	30.0	30.0	30.0	30.0	30.0
Telemetry	8.0	8.0	8.0	8.0	8.0	8.0
Command	20.0	20.0	20.0	20.0	20.0	20.0
Data Storage	36.0	3.0	9.0	25.0	9.0	9.0
Guidance and Control	20.0	12.0	40.0	21.0	21.0	21.0
Pyrotechnic	2.0	2.0	2.0	2.0	2.0	2.0
Computer and Sequencer	50.0	50.0	50.0	50.0	50.0	50.0
Science		29.0	29.0	125.0	11.0	40.0
Clock and Synchronizer	9.0	9.0	9.0	9.0	9.0	9.0
Inverter Load Subtotal	183.2	171.2	205.2	298.2	168.2	197.2
Harness Loss	1.9	1.7	2.1	3.0	1.7	2.0
Total Inverter Output	185.1	172.9	207.3	301.2	169.9	199.2
2400 Hz Inverter Efficiency	0.86	0.86	0.88	0.90	0.86	0.88
Thermal Loss	27.0	26.3	28.3	33.5	26.2	27.8
Total 2400-Hz Inverter Input	212.1	199.2	235.6	334.7	196.1	227.0
400 Hz; 3/8 Inverter Loads:						
Guidance and Control (PF=0.35)	9.0		18.0	9.0	9.0	9.0
Inverter Load Subtotal	9.0		18.0	9.0	9.0	9.0
Harness Loss	0.1		0.2	0.1	0.1	0.1
Total Inverter Output	9.1		18.2	9.1	9.1	9.1
400 Hz 30 Inverter Efficiency	0.56		0.56	0.56	0.56	0.56
Thermal Loss	7.0		14.0	7.0	7.0	7.0
Total 400 Hz. 1/8 Inverter Input	16.1		32.2	16.1	16.1	16.1
400 Hz; 10 Inverter Loads:						
Science				10.0	5.0	5.0
Inverter Load Subtotal				10.0	5.0	5.0
Harness Loss				0.1	0.1	0.1
Total Inverter Output				10.1	5.1	5.1
400 Hz 10 Inverter Efficiency				0.80	0.73	0.73
Thermal Loss				2.5	1.9	1.9
Total 400 Hz, 1/8 Inverter input				12.6	7.0	7.0
DC Loads:						
Capsule		200			200	
Radio	147	147	147	147	147	147
Gyro Heaters	6		6	6	6	6
DC Load Subtotal	153	347	153	153	353	153
Harness Loss	1.5	3.5	1.5	1.5	3.6	1.5
Total DC Load	154.5	350.5	154.5	154.5	356.6	154.5
DC Bus Power	382.7	549.7	422.3	517.9	575.3	404.6
Thermal Loss	7.8	11.2	8.6	10.6	11.7	8.3
Main Regulator Output	390.5	560.9	430.9	528.5	587.5	412.9
Main Regulator Efficiency					0.99	
Thermal Loss	6.0	6.0	6.0	6.0	6.0	6.0
Main Regulator Input	396.5	566.9	436.9	534.5	593.5	418.9
Harness Loss	4.0	5.7	4.4	5.4	6.0	4.2
RTG Power Required (Watts)	400.5	572.6	441.3	539.9	599.5	423.1

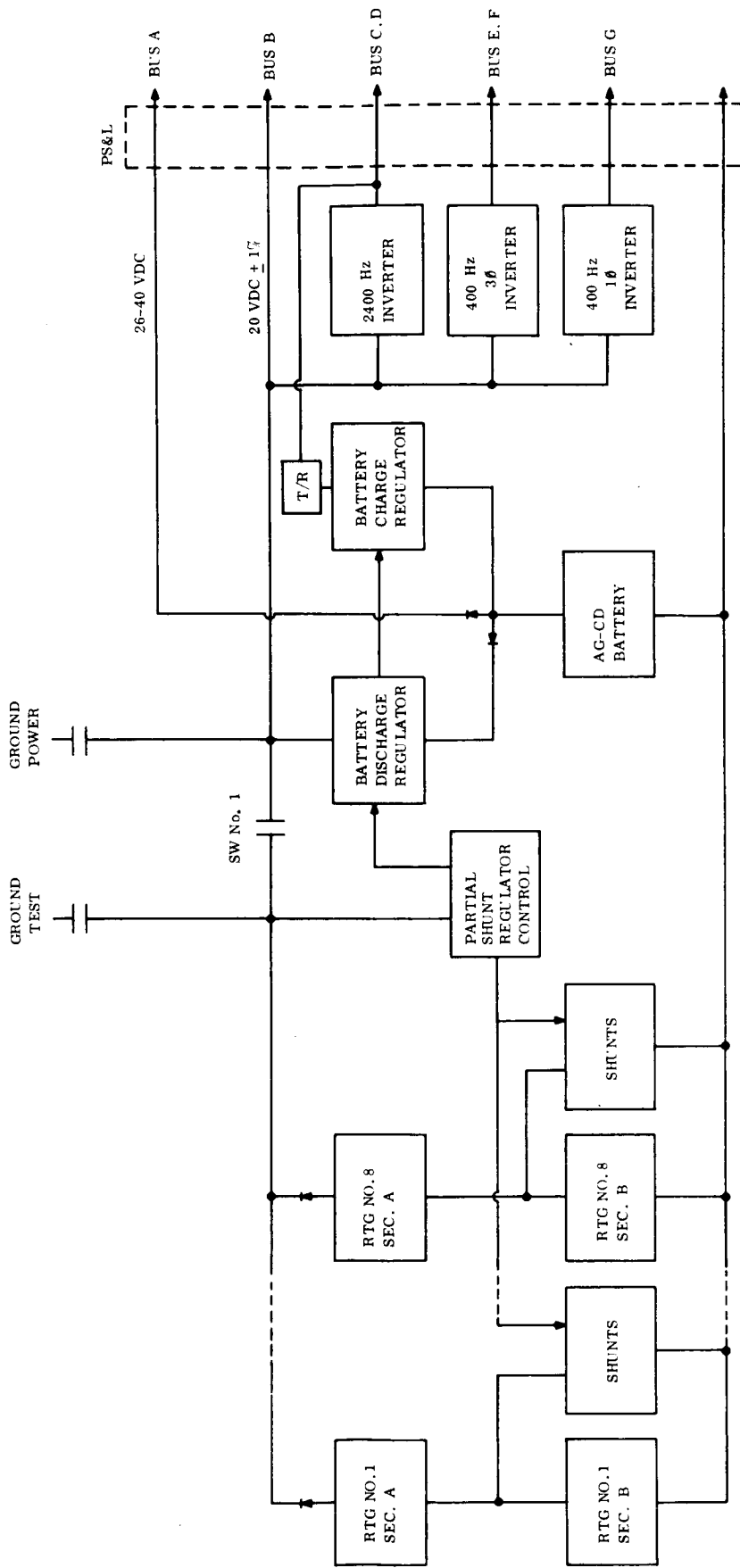


Figure 3-35. Voyager RTG Power Subsystem Functional Block Diagram

partial shunt regulator to provide a source of regulated dc power. All of the shunts operate in unison from a single shunt regulator control. The RTG's are diode-isolated from the regulated bus.

Auxiliary batter power is provided by 2 silver-cadmium batteries, each rated at a capacity of 290 watt-hours. The batteries are principally used for high-peak momentary loads but may also be used on a duty-cycle basis in the event of failure of one or more RTG's. Appropriate charge and discharge regulators are included in the subsystem.

DC to ac inverters are shown and reflect the principal use of ac distribution. Details concerning these elements and the inclusion of the clock and synchronizer were included in the Task B report.

Power is distributed to the loads through the following seven busses:

- a. Bus A: Supplies raw battery power at approximately 26 to 40 vdc, corresponding to the extremes of battery charge and discharge voltage, for momentary peak loads. DC power, instead of ac power, is distributed to these loads, since their associated peak power levels would require unnecessarily high ratings for the ac inverters. The loads are identified as solenoid valves, stepper motors, and the thrust vector control. The two silver-cadmium batteries supply this bus.
- b. Bus B: Supplies regulated power to the inverters and to the radio subsystem and the flight capsule at 20 vdc \pm 1 percent. The radio subsystem and the capsule receive regulated dc only incidentally, since the output voltage of the RTG is shunt-regulated.
- c. Busses C and D: Same as Task B. 2.4-kHz, single-phase, square wave at 50 v rms.
- d. Busses E and F: Same as Task B. 400-Hz, three-phase, stepped square wave at 26 v rms.
- e. Bus G: Same as Task B. 400-Hz, single-phase, square wave at 28 v rms.

The battery charge regulators are the current-limiting, voltage-limiting, series-dissipative type, identical to the BCR's for the Ag-Cd batteries of the PV/Battery power subsystem (see Section 4) with the exception of a lower current limit setting. Thus it should be possible to use the same qualified battery charger hardware for both types of power subsystem. The battery charger obtains its power through an external 43-volt transformer/rectifier from the 2400 Hz

ac bus. It is feasible to use this relatively less efficient source of conditioned power for battery charging since the total battery charge energy requirements are low.

There are two charge voltage settings (A and B) obtainable by ground command, and two associated float voltage settings (A' and B') obtained automatically when the charge current falls near the end of the charging period:

Setting A : 40.5 v (charge at 1.5 v/cell, 27 cells)

Setting A': 38.34 v (float at 1.42 v/cell, 27 cells)

Setting B : 39.0 v (charge at 1.5 v/cell, 26 cells)

Setting B': 36.92 v (float at 1.42 v/cell, 26 cells)

The lower, float voltage setting minimizes gas evolution in the batteries during the long inactive period before the Mars orbit insertion maneuver.

Normally, there will be no load sharing between the RTG's and the battery, since the RTG's produce enough power to supply all the needs of the spacecraft. The only power taken from the battery will be drawn directly from the separate battery bus for the thrust vector control, and for small loads such as solenoids and heaters. The battery discharge regulator will be used for high power, low duty cycle science loads, if such are installed, or in the event of failure of one or more RTG's.

The voltage reference of the battery discharge regulator is set slightly below the main bus. Thus, inability of the RTG's to supply the load will cause a small drop in the main bus voltage, allowing the battery to discharge onto the main bus through the regulator. Load management must be such as to limit the battery depth of discharge to about 50 percent and to permit periodic recharge.

3.4.1.2 Operational Modes

The principal modes of the power subsystem are as follows:

- a. Pre-Fueling — For system checkout, the RTG's are heated electrically. Test connections permit the checkout of the RTG's and their associated shunt regulators, before power is applied to the spacecraft. After the RTG's are operating, SW 1 is closed, the spacecraft is powered, and normal checkout of the power subsystem may proceed.

- b. Post-Fueling, Prelaunch — After the RTG's are fueled, they are producing power at all times. This power is controlled and dissipated by the partial shunt regulators. Under no-load conditions the elements of partial shunt regulators contained in the equipment bays will dissipate about 70 watts. Subsequent to on-pad mating, the spacecraft may be powered at any time by closing SW 1, restricted only by spacecraft electronic bay cooling requirements.
- c. All Post-Launch Phases Except Mars Orbit Insertion — All continuous power is supplied by the RTG's, voltage-controlled by the partial shunt regulators. The batteries are trickle-charged to maintain their capacity. Small pulses are taken from the battery, replenished by the battery charger.
- d. Mars Orbit Insertion Maneuver — During the maneuver, a large pulse of power, approximately 875 watts for 90 seconds, is required for the thrust vector control. This is taken directly from the batteries without any conditioning. After this point the batteries are no longer required for normal operation except for small pulse loads. The battery chargers will continue to trickle charge the batteries.
- e. RTG Failure — In the event one or two RTG's should fail, the spacecraft can continue to be operated by turning the science loads and the transmitter on for periods of 1 to 2 hours two to three times a day, permitting the batteries to recharge in the intervening times.

3.4.1.3 Component Descriptions

3.4.1.3.1 RTG's

A description of the nominal RTG design is given in Section 3.3.2. The circuit arrangement of the RTG along with the physical arrangement of the thermoelement strings is shown in Figure 3-36. By alternating strings of the upper and lower thermopile sections, relatively constant temperature conditions are maintained for minimal load conditions. This, together with low thermal dissipation in the electronic bays, is the principal advantage of the partial shunt regulator described below. (See also VOY-C1-TR12.)

3.4.1.3.2 Partial Shunt Regulator

Because of the desirability of maintaining constant RTG hot junction temperature, some form of shunt regulator is required for RTG voltage regulation. Types considered were the full shunt, partial shunt, and switching shunt regulators. A variation of the full and partial shunts is a sequential concept in which the shunt sections are turned on sequentially, resulting in reduced transistor power dissipation.

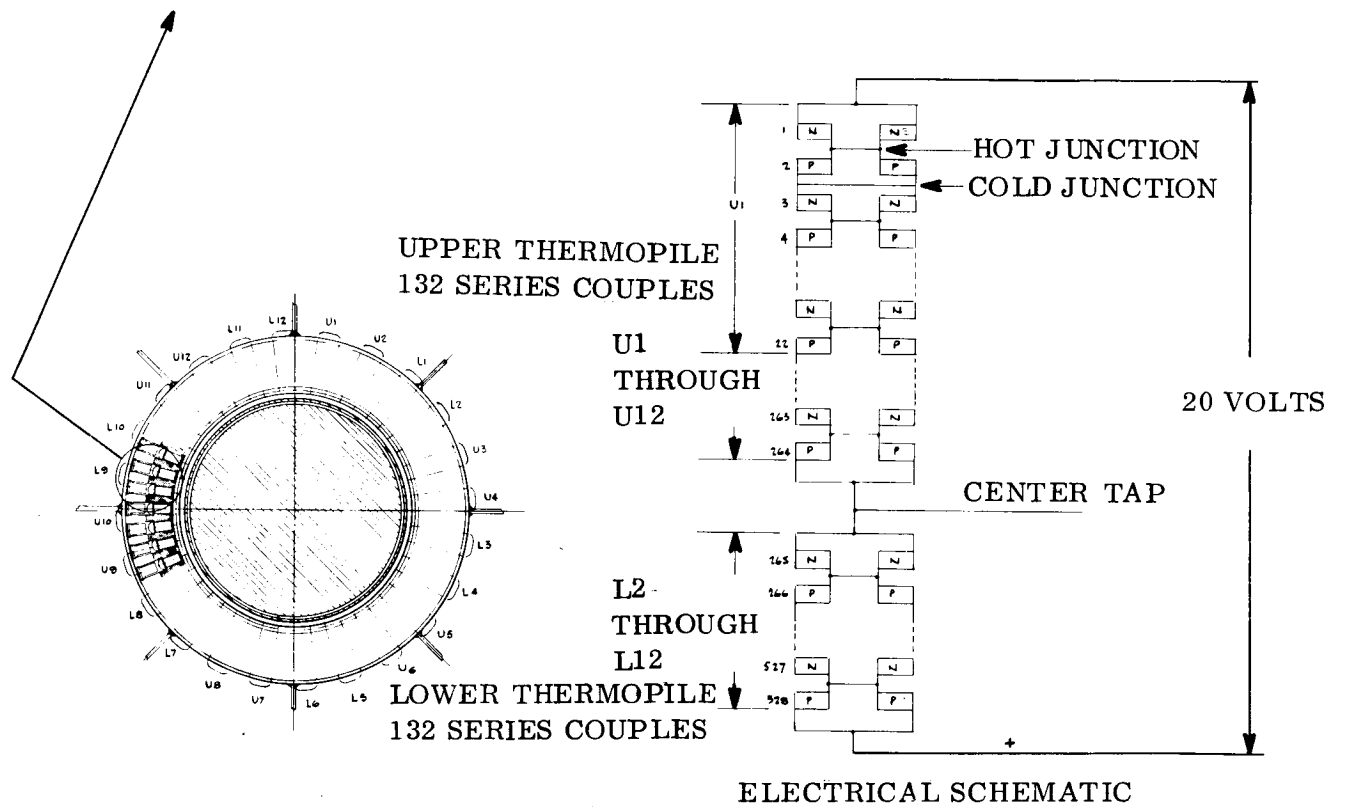
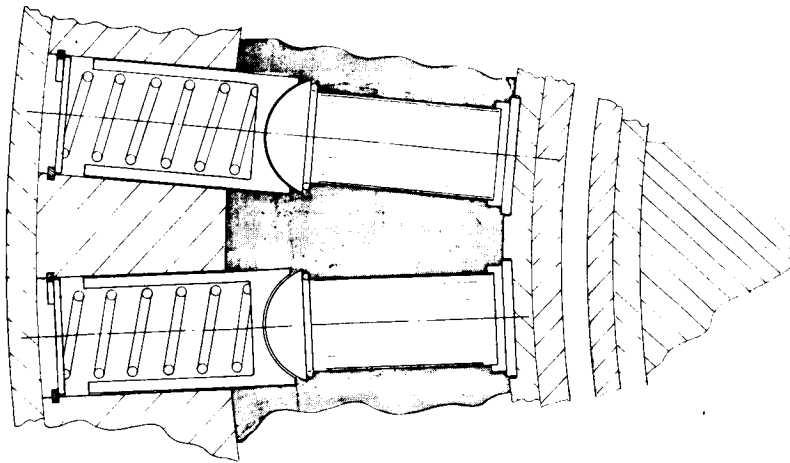


Figure 3-36. RTG Schematic

The partial shunt regulator was selected for the RTG power subsystem because of its reduced thermal dissipation (one fourth that of a full shunt), relative simplicity, and low weight. The sequential shunts were rejected because of the complexity involved in ensuring sequenced operation and obtaining redundancy. The switching shunt regulator was rejected because it is less efficient, is heavier, and all of its failure modes result in critical load effects.

The main regulator (partial shunt regulator) controls the bus voltage to 20 volts \pm 0.5 percent, and maintains nearly constant hot-junction temperatures in the RTG's. The schematic of the regulator is shown in Figure 3-37.

There is one central reference and control amplifier, and separate shunt elements are provided for each RTG. One special element in the reference and control amplifier is Q7, which is a pnp transistor connected to provide one stage of gain without phase inversion.

The shunt sections are diode-isolated from the reference and control amplifier to permit redundant shunt elements to be easily switched. The shunt section is a voltage sequenced

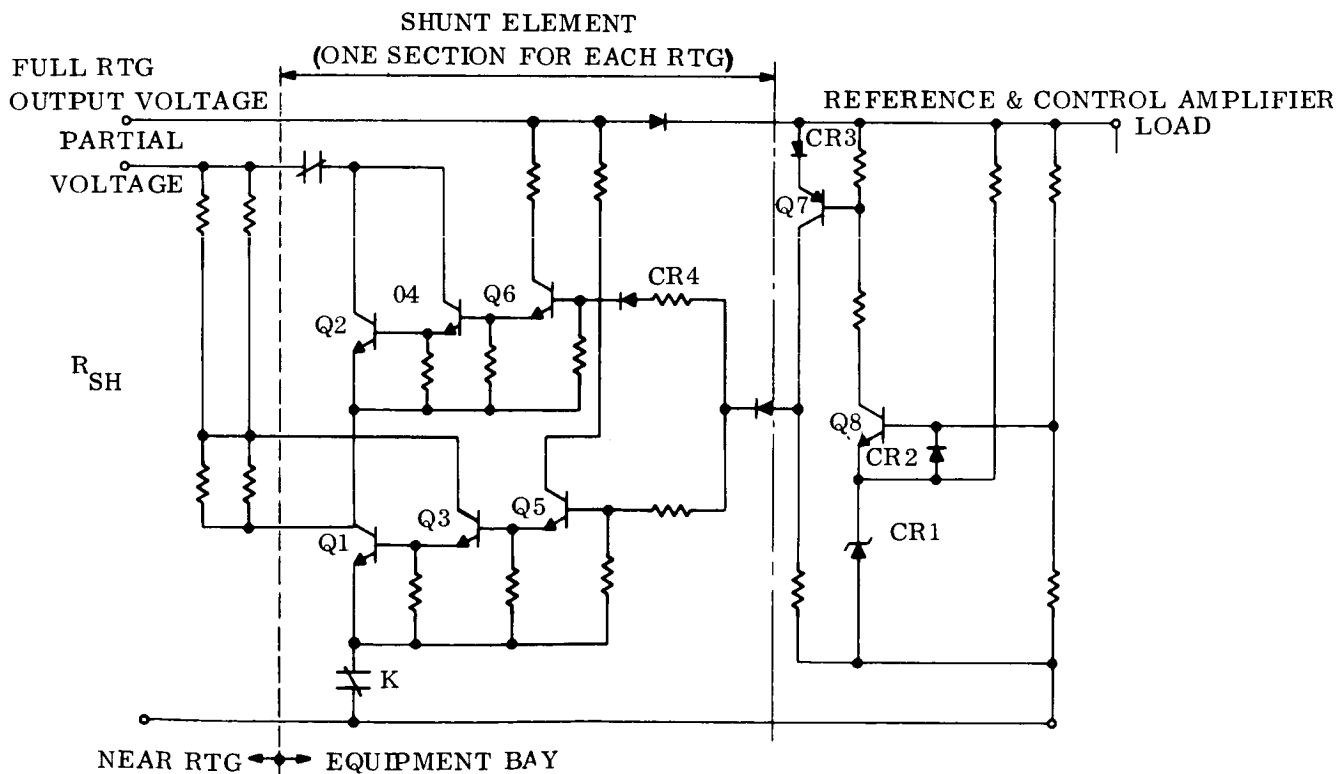


Figure 3-37. Partial Shunt Regulator

partial shunt element, consisting of a pair of three-transistor Darlington circuits, biased by the diode, CR4, so that Q1 and Q2 are never in their active regions simultaneously. Transistor Q1 begins to conduct first, causing power to be dissipated in R_{sh} . As Q1 saturates, Q2 begins to conduct. Thus, CR4 provides the sequencing which serves to reduce the thermal dissipation in the transistors, and permits a large portion of the heating to occur in R_{sh} , which may be mounted near the RTG.

3.4.1.3.3 Batteries

Two separate silver-cadmium batteries are used, discharged in parallel, and charged independently. Each battery is rated at 145 watt-hours and consists of 27 cells in series of 5 ampere-hour capacity. The battery weighs about 14 pounds, and has a volume of about 0.12 cubic feet. The cells are hermetically sealed in stainless steel cases, each with a positive terminal isolated from the case by a ceramic bushing. The case of the cell is the negative terminal. The battery case is of aluminum.

The nominal battery discharge voltage is 29 volts; maximum charge voltage is 40.5 volts. The batteries are sized to provide (with 100 percent redundancy) sufficient stored energy to operate the science package for up to two hours at a time in the event of an RTG failure.

3.4.1.3.4 Battery Charge Regulator

The battery charge regulator (BCR) derives power from the 2400 Hz ac bus through a separate transformer/rectifier. It will be a current-limit, voltage-limit, series-dissipative regulator, similar to the BCR of the Task B design, capable of providing four charge voltage limits to the battery. Two of these voltage limits can be set by command, and correspond to a charge voltage of 1.5 volts/cell, for 27 or 26 cells. The other two are float voltage settings of 1.42 volts/cell, and are switched in automatically when the batteries are fully charged.

The 26-cell voltage settings permit continued battery operation in the event of a short circuit failure of a single cell.

There is an interlock between the BCR and the battery discharge regulator (BDR) so that when the battery discharges through the BDR, the BCR is turned off, thus preventing the inefficient circulation of power through the BDR, the 2400-Hz inverter, the T/R, and the BCR.

3.4.1.3.5 Battery Discharge Regulator

The battery discharge regulator is a pulse-width modulated, series - switching regulator which reduces the battery discharge voltage down to the main regulated dc bus voltage.

To prevent battery discharge when the RTG's are fully capable of providing the required power, an interlock is incorporated in the BDR. The Main (partial shunt) Regulator and the BDR are operated from the same reference supply, a small differential being subtracted from the Main Regulator reference to obtain the BDR reference. When the main dc bus voltage is above the BDR reference, the BDR will supply no power to the main bus. The main regulator must go slightly out of regulation before the BDR permits the battery to discharge onto the main bus.

Since the BDR is intended to be a backup device itself, no redundant unit is used.

3.4.1.3.6 DC to AC Inverters

These units are basically similar to the inverters in the Task B photo-voltaic/battery power subsystem design.

In the RTG power subsystem, the voltage of the regulated bus which supplies the inverters is 20 vdc, instead of the 30 vdc of the Task B design. If the transformers alone were to be changed to accommodate this reduced input voltage, this would result in a decrease in inverter efficiency due to the relatively constant switching transistor series voltage drop. However, because the input voltage is low, germanium switching transistors can be used instead of the silicon switching transistors proposed for the Task B inverters. The lower series voltage drop in the germanium switching transistors should result in approximately the same inverter efficiency as estimated for the inverters in the Task B power subsystem design. Only the output switching transistors need be changed, since the silicon transistors in the remainder of the circuit have little effect on the inverter efficiency.

3.4.1.3.7 Fault Sensors

- a. Partial Shunt Regulator Fault Sensor — This regulator is subject to failure in four major modes: (1) short in shunt section, (2) open in shunt section, (3) failure in reference and control amplifier resulting in high voltage, and (4) failure in reference and control amplifier resulting in low voltage. These failures, and the corrective action tentatively selected are outlined in Table 3-16.
- b. Inverter Fault Sensors — This is the same as that shown in the Task B design.

3.4.1.3.8 Miscellaneous Elements

The Clock and Synchronizer, Power Switching and Logic Unit, and others are essentially identical to those of the Task B design.

3.4.1.4 Performance Parameters

The RTG requirements are determined with the aid of the Energy Balance Table, Table 3-15, where the electrical loads are summarized. The accounting of the loads includes the various Power Subsystem losses and is extended to determine the load directly at the RTG's.

TABLE 3-16. FAILURES AND CORRECTIVE ACTION

Bus Voltage	Current in Shunt Section	Battery Current	Total Bus Current	Probable Cause	Corrective Action
Normal	No	Yes	Normal		Normal
Normal	Yes	Yes	Normal	Short shunt	A
High	Yes		Normal	High Ref.	B
High	No	No	Low	Open shunt	A
Low	Yes		Normal	Low Ref.	B
Low	No	Yes	High	Overload	None

A - Replace shunt element
 B - Replace reference and control element

The loss factors used in the load analysis were the same as those used in Task B, with the following exceptions:

- a. Main (Partial Shunt) Regulator — Fixed loss of 6 watts
- b. Battery Diodes — The battery discharge diode loss of 0.35 volt results in an efficiency of 98 percent.
- c. Battery Charger — Constant loss of 1 watt each
- d. Battery Discharge Regulator — Constant non-operating loss of 4 watts
- e. RTG Isolation Diodes — Efficiency of 98 percent (germanium diode-connected transistor)

Estimates of voltage source regulation are given in Table 3-17.

3.4.1.5 Physical Characteristics

Power subsystem equipment, other than the RTG's, is mounted in the spacecraft electronics bays. The weight and volume characteristics of this equipment are listed in Table 3-18.

TABLE 3-17. ESTIMATE OF POWER SYSTEM CAPABILITY

Bus	Voltage	Frequency*	Regulation %		Max. Peak Power (watt)	Max. Avg. Power (watt)	Users	Notes
			Steady-State	Transient				
A	26-40	DC	-	-	2000	6	Misc. low-duty cycle loads	Capsule receives limited power during launch, maneuvers, and "Full Science"
B	20	DC	+0.5	±2	675	350	Radio, capsule	
C	50 rms	2.4 kHz 1 φ square wave	±2	±5	450	300	All other spacecraft loads	
D	50 rms	2.4 kHz 1 φ square wave	±2	±5	C&D combined	C&D combined		
E	26 rms	400 Hz, 3 φ stepped square wave	±5	±10	45	30	Gyros	
F	26 rms	400 Hz, 3 φ stepped square wave	±5	±10	45	30	Gyros	
G	28 rms	400 Hz, 1 φ square wave	±5	±10	15	10	Science	

*Frequency regulation of ac: Normal: ±0.01 percent
 Backup Oscillator: ±1 percent
 Free-running: -4 to -6 percent

TABLE 3-18. POWER SUBSYSTEM ELECTRONICS EQUIPMENT CHARACTERISTICS

Unit	Weight (lb)	Volume (cu ft)	Number
Battery (Ag-Cd)	14	0.12	2
Charge Regulator	1.5	0.03	2
Discharge Regulator	5	0.08	1
Partial Shunt Regulator			
Reference and Control	1.5	0.03	1*
Shunt Elements	1.0	0.05 (0.6 ft ²)	8*
Inverter, 2400-Hz	4.5	0.08	2
Inverter, 400-Hz, 3 ϕ	3.5	0.06	2
Inverter, 400-Hz, 1 ϕ	1.5	0.03	2
Master Clock and Synchronizer	6.0	0.11	1
Power Switching and Logic Unit	5.5	0.10	1

*Incorporates redundant unit in design

3.4.2 GUIDANCE AND CONTROL

With the application of an RTG power source, the planetary vehicle need not be sun-oriented and it becomes possible to use a body-fixed high-gain antenna (HGA). Earth pointing of the HGA is achieved by biasing the spacecraft axis from a purely Sun-pointing direction using attitude reference signals from digital solar aspect sensors and a Canopus sensor. In effect, a programmed two-axis "electronic gimbaling" is substituted for the two-axis gimbal of the HGA.

This section describes how the Guidance and Control subsystem will accommodate this option. In general this approach appears suitable for missions to the outer planets since bias angles are sufficiently small and would not seriously perturb the thermal balance of the Planetary Vehicle. For missions inbound toward The sun the bias approach is not as appropriate because of relatively large bias angles and higher solar flux intensities.

3.4.2.1 Operational Considerations

Figure 3-38 shows Earth cone and clock angle histories for the 1973 to 1979 Mars opportunities. The origin of this plot represents the location of the Sun and the curves represent the Earth's path as viewed from the spacecraft. The zero value of clock angle is established by the location of the star Canopus.

As noted, encounter occurs at a cone angle of about 40 degrees for all missions. By positioning the HGA axis at the proper cone and clock angles for a particular mission corresponding to encounter (Example: For 1973, cone angle = 39°, clock angle = 278°), the spacecraft will be directly Sun-pointing at the time of encounter. About six months after encounter the cone angle decreases to 10 degrees and therefore, with the HGA earth-pointing, the main vehicle axis is biased about 30 degrees from the sun direction. A similar bias occurs prior to encounter as shown on the plot. Considering that a 30 degree bias is the maximum allowable value in terms of thermal perturbation, it becomes necessary to use other means of communication earlier in the mission. Low-gain and medium gain antennae (LGA and MGA) are used for this purpose as shown on the plot. Their ability to provide adequate information rates is discussed in Section 3.4.3.

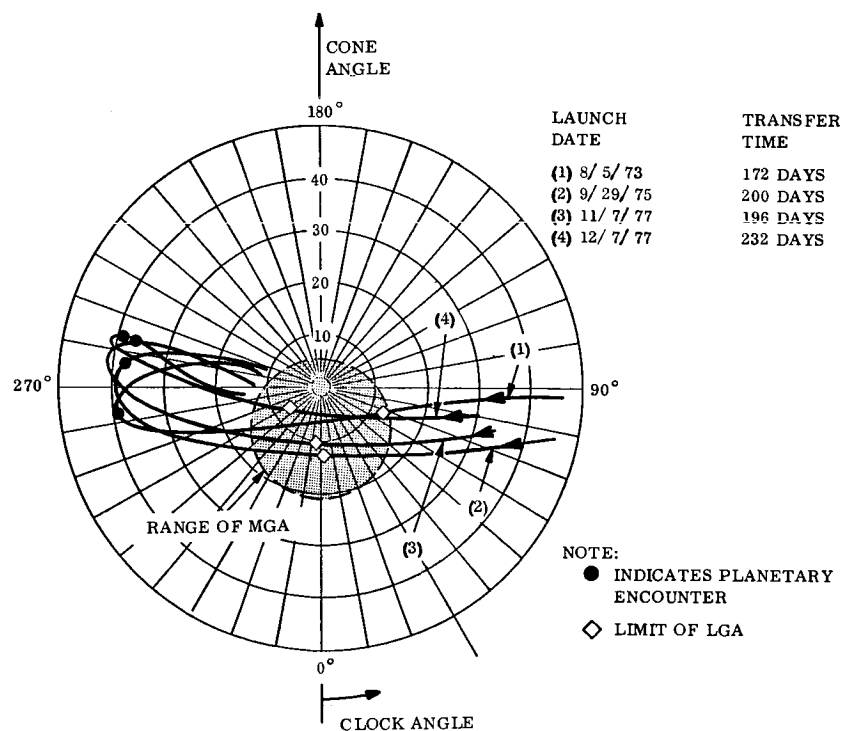


Figure 3-38. Earth Cone and Clock Angles for Several Launch Opportunities

With these considerations in mind the angular range of solar aspect sensors to provide the necessary bias is about 30 by 25 degrees.

In weighing the merits of a fixed high-gain antenna operating in conjunction with a Sun-bias attitude reference system, the possibility of PSP viewing blockage was considered. Since the problem is intimately related to orbit selection, which is beyond the scope of this study, no recommended means for avoiding this blockage is provided. However, several solution alternatives exist. First, it is felt that the possibility of PSP viewing blockage is minimized by the excellent mounting location of the PSP and that no special maneuver would be required for the class of planetary orbits inclined up to about 40 degrees from the plane of the ecliptic. For orbits of higher inclination, several alternatives are available. In one approach, a single-antenna deployment is executed at the time that PSP viewing blockage commences and the vehicle rolls 180 degrees about its Z axis to reacquire the Earth pointing of the high-gain antenna. The thermal shelf discussed in Section 3.3.1 was designed to provide shade for Sun angles of 30° in the +X and 30° in the -X directions as would be required for this flip maneuver. An additional solar aspect sensor would also be needed. Without the need for a flip maneuver the shelf would be required in the +X direction only. Another solution to the blockage problem is to simply accept viewing blockage for a brief period of each planetary orbit.

3.4.2.2 Functional Descriptions

The attitude control system is similar to that used in the Task B design. The major change involved in the RTG vehicle is the operational substitution of the digital solar aspect sensors for the null-type solar sensor during part of the cruise mode.

From a mechanization point of view the same solar acquisition sensors and null sensors are incorporated into the control system of the RTG vehicle as were used for the Task B solar-powered configuration. The acquisition sensors perform the same function as previously. The null solar sensors provide the primary pitch and yaw signals until the Sun-biased mode of operation is initiated during the later part of the cruise phase.

At the time of transfer to the Sun-bias mode of operation the null Sun sensors are switched out of the control loop and the digital solar aspect sensors and the associated bias program are

switched into the loop. From this point on, the bias program will be only a very slowly varying one, to accommodate the slowly changing Earth cone and clock angles. The bias program will be stored in the C&S subsystem. The continuous 7-bit bias signal will be provided in a parallel form.

The digital solar aspect sensors which are recommended for the RTG vehicle are of the type produced by the Adcole Corporation. Sensors of this type have been used in passive instrumentation loops to provide telemetered attitude information for numerous satellites and sounding rockets. These sensors are passive in operation, and are mechanically simple, lightweight and require low power (typically 1 watt).

In the basic Adcole sensor, shown in Figure 3-39, sunlight passes through a narrow entrance slit to the interior of a quartz reticle block, and falls on a Gray-coded digital mask on the bottom of the block. Below the mask, designed to preclude ambiguous signals, is mounted a bank of seven photocells. Individual photocells receive sunlight in accordance with the angular aspect of the Sun to the plane of the reticle. The Gray Code is utilized because one and only one bit (i.e., photocell ON or OFF) is changed between any two adjacent numbers. This precludes catastrophic errors in angle determination, possible with conventional binary coding, where several bits must change sign simultaneously, requiring almost perfect synchronization. Binary signals are made available to the spacecraft attitude control system by means of a Gray Code to binary converter.

Two orthogonal slits are mounted on each of two sensor heads to define the solar angle along two axes. Most of the existing Adcole sensors have a view-angle of 128 degrees. A seven-bit Gray Code mask operating with this field of view provides a discrete digital signal for each increment of one degree; an eight-bit sensor configuration could improve the resolution by a factor of two.

For the present application, a 7-bit digital solar aspect sensor having a 30 by 25-degree field of view is recommended. This would correspond to a sensor resolution of less than 0.25 degree, which is adequate for the attitude control requirement.

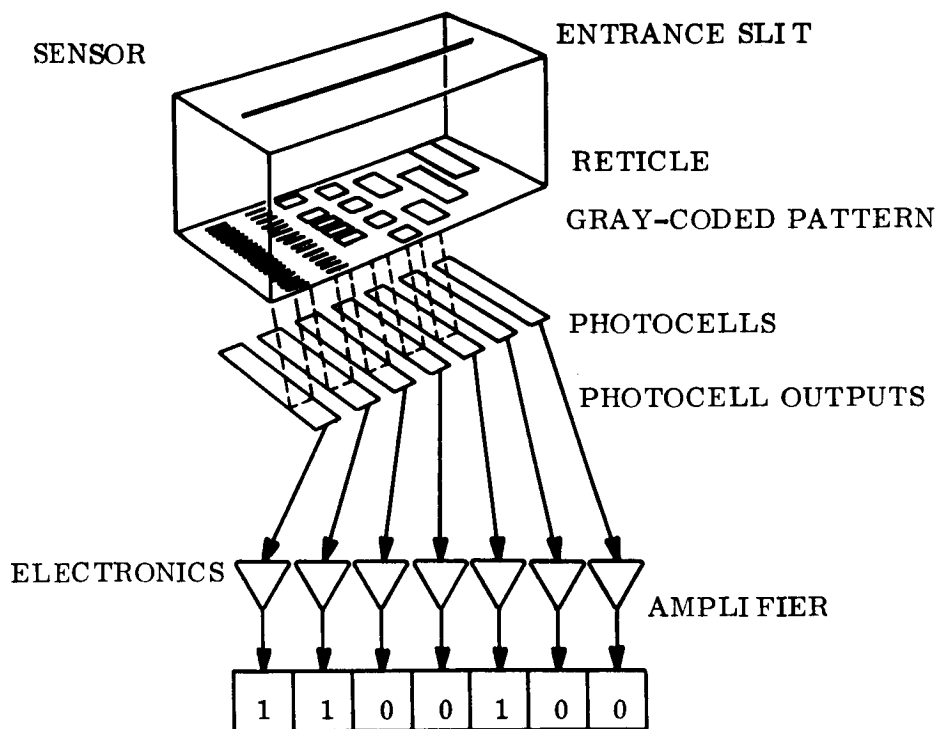


Figure 3-39. Solar Aspect Sensor

In addition to the normal photocell outputs and the associated Gray-coded reticle as shown in Figure 3-39, it is planned that the solar aspect sensor, designed for the present application, will include a separate "acquisition channel." This will provide a signal for the logic control unit of the attitude control system whenever the Sun is in the field of view of the solar aspect sensor.

The control logic for reacquisition of Canopus remains unchanged from that described in the Task B study. Upon loss of a Canopus acquisition gate signal the roll rate gyro will be activated preparatory to initiating the roll search operation.

Operation during Sun or Canopus occultation is similar to that described in the Task B study. The pitch and yaw controls are switched to the inertial mode when the output of the solar aspect sensor indicates a loss of solar radiation. The solar aspect sensor design is modified to incorporate its own acquisition sensing "channel." An additional reticle slit is provided

which provides a signal whenever the Sun is in the field of view of the solar aspect sensor. This signal when amplified is fed to the logic control unit to provide verification of solar acquisition.

Because of the possibility of delays in launch, some consideration must be given to allowance in variations in the Earth cone and clock angle profiles. The variations in Earth cone angle history within a given opportunity may typically be limited to a few degrees, whereas the variation in Earth clock angle may be a fraction of a degree.

With respect to the null type Sun sensor operation, there would be no need for making any adjustments were its use not desirable in a backup mode at Mars encounter as previously discussed. Because of this backup function, there will be a requirement for making some updating adjustments (on the launch pad) of the relative angular orientation of the high-gain antenna and the null Sun sensor. This can be done by a two degree of freedom adjustment of either the high-gain antenna or the Sun sensor. Alternatively the Sun sensor alignment can, in effect, be modified by adding calibrated analog bias signals to its output and would eliminate a requirement for a mechanical adjustment on the pad.

3.4.2.3 Physical Characteristics

Since the guidance and control mechanization is only slightly modified from the Task B design, the physical characteristics are not greatly changed. It is expected that the additional weight of the digital solar aspect sensors, and associated electronics plus the additions to the C&S specified here, will be from 1 to 2 pounds. Likewise, the additional power required will not exceed 1 to 2 watts.

3.4.3 TELECOMMUNICATIONS

Following is a description of the differences in design and performance of the RTG Spacecraft telecommunication subsystem relative to that defined in the GE Task B Final Report for a solar-powered spacecraft. Except for minor changes required in the placement of components, the latter design could have been retained. However, removal of the vehicle Sun-pointing constraint allowed the use of a fixed high-gain antenna, eliminating the need for the two-axis

antenna gimbal. Changes described below, therefore, result from the basic change and its implications.

3.4.3.1 Functional Description

The command, telemetry, and data storage subsystems defined for the Task B spacecraft design are unchanged in the RTG spacecraft. The radio subsystem definition remains the same except for the antenna changes noted below:

- a. The 7.5-foot diameter steerable dish is replaced by a 7.5-foot diameter fixed dish
- b. The fixed Mariner C high-gain antenna, used as a medium gain backup to the steerable dish, is replaced by a one-foot fixed dish

These changes are noted in Figure 3-40, the block diagram of the radio subsystem; this figure replaces Figure 3-2 of Section VC 233 FD 101 in the Task B report.

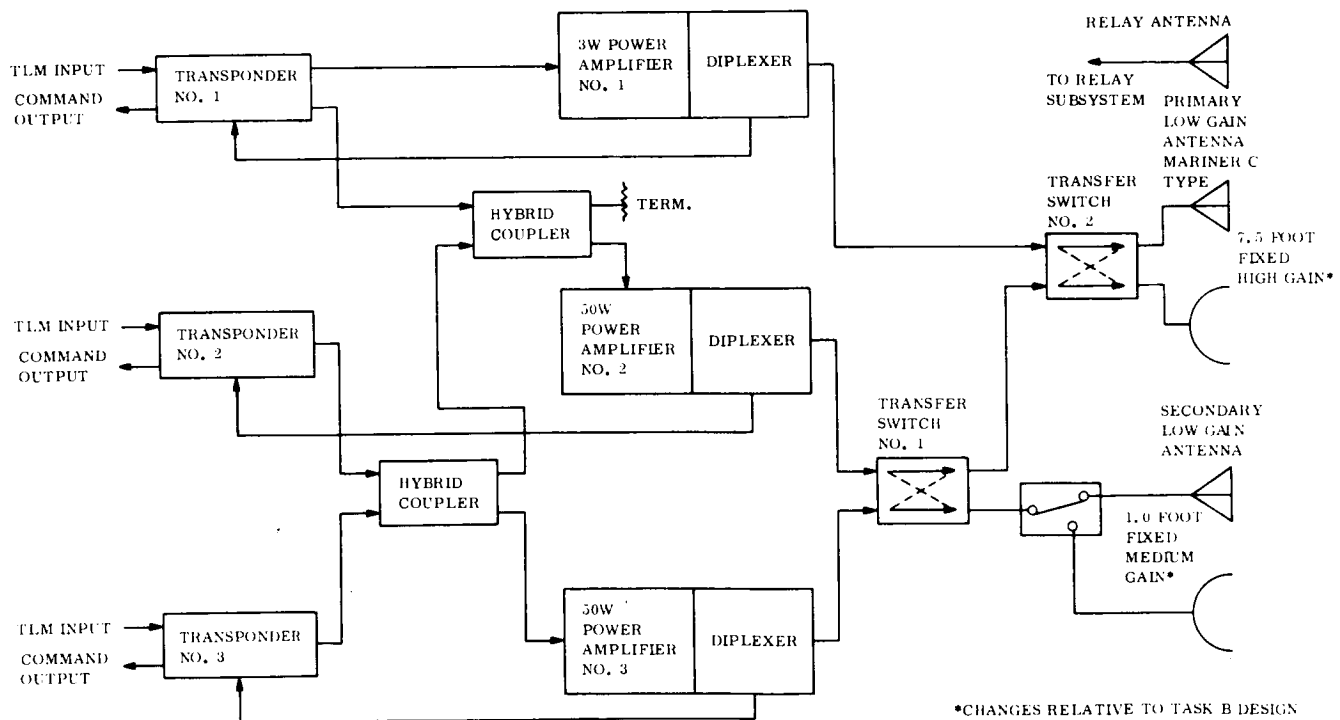


Figure 3-40. Radio Subsystem

Minor changes in the primary and secondary low-gain antennas are also incorporated:

- a. The circular waveguide of the primary low-gain antenna is extended to 28 inches to account for a change in the available mounting point.
- b. The secondary low-gain antenna position is shifted from the vehicle +X axis to the -Y axis.

Performance of the primary low-gain antenna is unchanged. Performance of the secondary antenna is changed only in that the toroid pattern now lies in the plane of the ecliptic. This change was allowed in the new vehicle configuration and was made intentionally to provide better backup to the primary low-gain antenna over a greater percentage of the mission.

Changes in modes of operation and in performance resulting from the high-gain and medium-gain antennas are described in the following section.

3.4.3.2 Performance

The high-gain antenna is pointed to Earth during the normal cruise and orbit phases by biasing the entire vehicle off the Sun line. However, during the early part of the cruise phase Earth pointing is undesirable because it requires the vehicle to take on attitudes with respect to the Sun which are not compatible with vehicle and capsule thermal control requirements. This leads to the constraint that Earth pointing not be provided, except for short periods of time, until the required pointing direction is within about 25 degrees of the pointing direction at encounter (at encounter the antenna points at Earth, which is about 40 degrees off the Sun line, when the vehicle is Sun-Camopus oriented). Therefore, all communications up to this point during normal cruise must be provided by other antennas. The primary low-gain antenna can maintain the 117 bps telemetry link to about 20×10^6 kilometers (which is in the order of 30 to 50 days before the high-gain antenna is available) with the 85-foot dish receiving system. Command and tracking can be maintained until the high-gain antenna is available (ranging has been excluded from the requirements on the RTG spacecraft); thus, only the telemetry link presents a problem during normal cruise.

The 210-foot dish receiving systems can be used during the intermediate phase to maintain telemetry, but this approach is assumed to be undesirable. It is therefore necessary to provide an additional antenna on the spacecraft.

A one-foot-diameter dish has been found to satisfy the telemetry requirements for typical trajectories assumed for the mission opportunities from 1973 to 1979. No attempt has been made to optimize this selection; however, it appears that an antenna with lower gain, and therefore larger beamwidth, would be adequate and perhaps more desirable.

The design control table for the new antenna and the 117 bps telemetry link is given in Table 3-19. Performance is referenced to 10^6 kilometers with no pointing loss. Actual performance, including pointing loss, is shown in Figure 3-41, versus range for a typical 1973 mission trajectory. Performance curves taken from the Task B report for the primary low-gain and the high-gain antennas are shown in the same figure. Switchover from one antenna to the next is shown to occur slightly before grayout. This selection was arbitrary since switching could have occurred several days in advance in each case. For this particular trajectory the high-gain antenna is available about 85 days after launch at a range of 40×10^6 kilometers.

A second mode of operation in which performance must be considered is that of high rate data readout from the recorders after a solar flare or a maneuver. In the Task B design the high-gain antenna and the 3733/117 bps transmission mode were used for this purpose. The 3733/117 bps mode (3733 bps of stored data and 117 bps of real-time data) requires about 13 db more link capability than the 117 bps mode described above; it can be noted from Figure 3-41 that the defined link capability during normal cruise is inadequate for high-rate data readout during portions of the cruise phase. In these isolated cases it seems reasonable to attain the additional capability either by orienting the high-gain antenna to Earth for the short period of time required for the data readout or by using the 210-foot receiving stations. The latter adds about 10 db to the link capability. This gain, in addition to the minimum available margin of about 4 db in the 117 bps mode, gives the 13-db gain required. For other trajectories the available margin might be less, resulting in the grayout periods of a few days.

TABLE 3-19. DESIGN CONTROL TABLE

Transmission Mode: 50 W; Med-Gain
 Channel : 117 bps
 Reception Mode : 85-Foot Dish

No.	Parameter	Value	Tolerance	No.	Parameter	Value	Tolerance
1	Total Transmitter Power	47.0	+1.0 -1.0				
2	Transmitting Circuit Loss	- 1.6	+0.4 -0.4				
3	Transmitting Antenna Gain	14.6	+0.3 -0.5				
4	Transmitting Antenna Pointing Loss	0.0*	+0 -0				
5	Space Loss (2295 mc, R = 10 ⁶ km)	-219.7	-				
6	Polarization Loss	0.0	+0 -0.1				
7	Receiving Antenna Gain	53.3	+1.0 -1.0				
8	Receiving Antenna Pointing Loss	- 0.1	+0.1 -0.0				
9	Receiving Circuit Loss	0.0	-0 +0				
10	Net Circuit Loss	-153.5	+1.8 -2.0				
11	Total Received Power	-106.5	+2.8 -3.0				
12	Receiver Noise Spectral Density (N/B)	-181.2	+0 -1.0				
13	Carrier Modulation Loss	- 6.0	+1.4 -1.8				
14	Received Carrier Power	-112.5	+4.2 -4.8				
15	Carrier APC Noise BW (2B _{LO} = 48 CFS)	10.8	+0 -0.5				
	CARRIER PERFORMANCE - TRACKING (ONE-WAY)						
16	Threshold SNR in 2B _{LO}	0.0	+0 -0				
17	Threshold Carrier Power	-170.4	+0 -1.5				
18	Performance Margin	57.9	+5.7 -4.8				
	CARRIER PERFORMANCE - TRACKING (TWO-WAY)						
19	Threshold SHR in 2B _{LO}	2.0	+0 -0				
20	Threshold Carrier Power	-168.4	+0 -1.5				
21	Performance Margin	55.9	+5.7 -4.8				
	CARRIER PERFORMANCE - TELEMETRY						
22	Threshold SNR in 2B _{LO}	10.0	+0 -0				
23	Threshold Carrier Power	-160.4	+0 -1.5				
24	Performance Margin	47.9	+5.2 -4.8				
	CHANNEL A						
	Channel A not included in this mode			25-36			
	SUBCARRIER PERFORMANCE						
37	Modulation Loss	- 1.3	+0.4 -0.6				
38	Received Subcarrier Power	-107.8	+3.2 -3.6				
39	Subcarrier APC Noise B (2B _{LO} = 1 cps)	0.0	+0 -0.5				
40	Threshold SHR in 2B _{LO}	26.2	+0 -0				
41	Threshold Subcarrier Power	-155.0	+0 -1.5				
42	Performance Margin	47.2	+4.7 -3.6				
	DATA CHANNEL B						
43	Modulation Loss	- 1.3	+0.4 -0.6				
44	Received Data Subcarrier Power	-107.8	+3.2 -3.6				
45	Bit Rate (1/T)	20.7	+0 -0				
46	Required (ST/N/B)	8.0	+0.5 -0.5				
47	Threshold Subcarrier Power	-152.5	+0.5 -1.5				
48	Performance Margin	44.7	+4.7 -4.1				
	SYNC CHANNEL B						
49	Modulation Loss	- 1.3	+0.4 -0.6				
50	Received SYNC Subcarrier Power	-107.8	+3.2 -3.6				
51	SYNC APC Noise BW (2B _{LO} = 1 cps)	0.0	+0.4 -0.4				
52	Threshold SNR in 2B _{LO}	21.6	+0 -0				
53	Threshold Subcarrier Power	-159.6	+0.4 -1.4				
54	Performance Margin	51.8	+4.6 -4.0				
	*No pointing error assumed for reference						

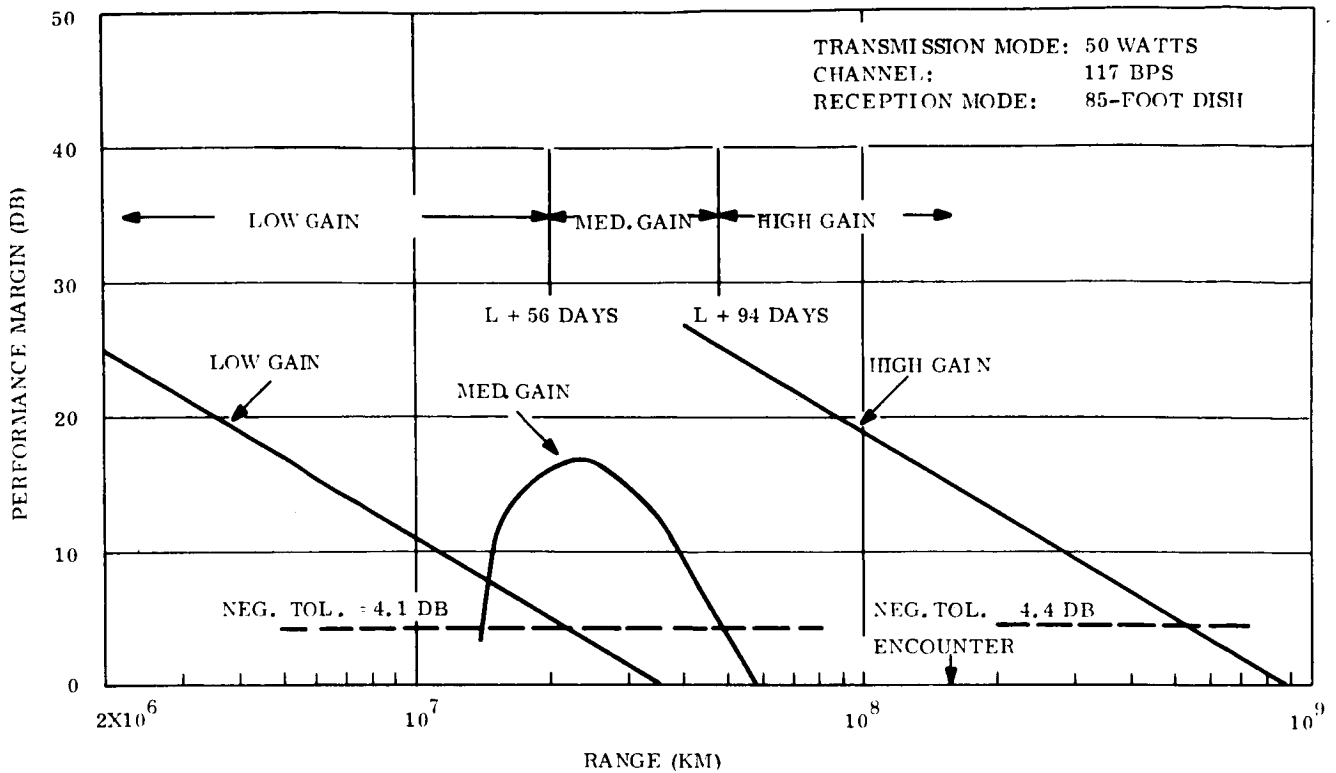


Figure 3-41. Performance Margin Versus Range

3.4.4 OTHER SUBSYSTEMS

Changes in other subsystems (C&S, Pyro, Data Storage, etc.) of the Task B design generally involve minor modifications in logic and sequence. Basic subsystem implementation remains the same.

3.5 OPERATIONAL SUPPORT EQUIPMENT AND GROUND OPERATIONS

OSE characteristics for an RTG-powered spacecraft have been described in detail in Task C Document No. VOY-C1-TR16. Presented below are the principal results in terms of basic RTG effects, factory operations and launch site operations.

3.5.1 BASIC EFFECTS OF RTG USE

The use of RTG's instead of solar cell arrays for power has little effect on the ground operations of the spacecraft, or on the OSE required by these operations. Factory assembly and test sequences, as well as launch area sequences, are functionally analagous to the case of the solar cell powered spacecraft. There are essentially two characteristics of RTG's which impose significant differences on ground handling procedures and equipment. The first of these is the thermal radiation, which requires that cooling equipment be provided during ground and test operations. Second, there is the neutron and gamma radiation of the RTG fuel capsules which imposes requirements for special handling equipment and procedures, monitoring and safety equipment, and shipping or storage containers.

3.5.2 FACTORY OPERATIONS

Insofar as the assembly and testing of the spacecraft's structure and electronics are concerned, there is no significant difference imposed by the choice of RTG or solar power. The sequence of operations, the number (and purpose) of test and flight models, and the OSE requirements are substantially the same. Equipment and procedures associated directly with the RTG's and with fuel capsules are different, however.

It is assumed that factory use of a complete complement of live fuel capsules for each test and flight spacecraft, throughout the factory cycle, is not economically or operationally practicable nor desirable. In lieu of actual live fuel capsules, the use of electrically controlled thermal simulators should be integrated with power subsystem OSE insofar as operating controls and displays are concerned.

Performance testing of an RTG, or the complete string of RTG's or of the overall power subsystem (conversion, distribution and battery) can be accomplished using these thermal

simulators. Current experience of other RTG programs indicates that this simulation can be achieved within 2 percent accuracy, compared to the use of live fuel. Complete dependence upon thermal simulators for the entire factory development, assembly and test cycle is not recommended. Live fuel capsule use for several of the RTG's in a spacecraft is desirable because:

- a. Radiation mapping and confirmation of predicted interactions with spacecraft electronics and instruments can be accomplished with greater accuracy and confidence. Radiation mapping using small gamma and neutron sources, and then scaling up, is not a high confidence procedure.
- b. An opportunity is provided to prove the design and function of handling equipment for the fuel capsules, and procedures for installation, removal, storage, etc., as well as the radiation safety program.
- c. The rigors of the Voyager mission and the inflexibility of the launch window suggest that every attempt be made to discover interactions and problems early in the development cycle, by realistic test and demonstration programs.

3.5.2.1 OSE For Factory Support

The system test complex, and the subsystem OSE incorporated within it, require no substantial changes in order to support the factory development, assembly and test program. There will be some minor changes, such as in the number and allocation of engineering telemetry channels, but these are regarded as minor in impact. The following summarizes these changes in requirements:

- a. Power Subsystem OSE:
 1. Electrically operated thermal simulators of fuel capsules.
 2. Thermal sensors, and gamma/neutron sensors, incorporated either in the Power Subsystem proper, or in the OSE.
 3. Load banks for RTG V-I mapping
 4. Elimination of support equipment unique to testing of solar cell arrays, such as stimulators.
 5. Emergency resistive loading, and suitable alarming, so that RTG's can be loaded in the event of opening of the spacecraft load.

b. Assembly, Handling and Shipping Equipment:

1. Cooling Equipment (air conditioning, with directive, flexible ductwork)
2. Dummy fuel capsules (equivalent in weight, balance and dimensions to live capsules) for checking fit, proving installation procedures and equipment, and for training of personnel
3. Changed configuration of assembly stand, etc., to accommodate the structural configuration of the RTG-powered spacecraft
4. Handling and assembly equipment for the RTG's, and for fuel capsules. The most significant item of this class is the fuel capsule handling installation tool. This must provide safe and positive capability for installing active fuel capsules into the RTG's already assembled into the spacecraft.
5. Fuel capsule shipping/storage containers. These containers are required to provide mechanical protection for the capsules, controlled thermal environment, and radiation protection. With adequate dimensions and design, active cooling will not be required.
6. Safety equipment, including shielding, for assembly and test operations on the spacecraft involving live fuel capsules.

3.5.2.2 Radiation and Personnel Safety

The use of live fuel capsules will require the institution of a radiation protection and health physics program during factory development, assembly and test operations.

The calculated isodose contours indicate that a man working at an electronic bay, after live fuel capsules have been installed, would be in a radiation field of approximately 180 mrem/hr. The maximum permitted dose over a 3 month period is 3 rems and therefore the number of hours that a technician could work in this radiation field is about 17 hours during the three month period. While this level is not unmanageable if properly designed protective shielding is used, a rigorous program of controls and health physics is required.

The safety and protective equipment requirements will be dictated by established AEC guidelines and statute requirements. This would include equipment and facilities for inspection and monitoring fuel capsules, storage areas including thermal and radiation monitoring capability, and the fuel capsule containers and handling tools already mentioned.

In addition to the tangible aspects mentioned above, a training program and personnel availability management program are required. The objective would be the assured availability of trained personnel, who have not exceeded permitted exposure, to the end that program schedules, especially the launch window, are not jeopardized.

3.5.3 LAUNCH SITE OPERATIONS

The sequence of assembly, test and launch preparation events for the RTG-powered spacecraft is analagous to the sequence required for the solar-cell-powered version. A dual test and service cycle, involving a preliminary "walk through" of all the facilities, and a second cycle for launch preparation and launch is recommended. The preliminary cycle may involve both of the flight models of the spacecraft bus.

The paramount ground operation and OSE problem unique to launch preparation of an RTG spacecraft is cooling. Temperature control of the spacecraft is required at all times that either live fuel capsules or thermal fuel capsule simulators are used to power the spacecraft. This is not anticipated to be a difficult problem, prior to shroud installation, as fuel capsules or simulators can be removed in the event of thermal control or air conditioning problems. In addition, thermal effect damage to the spacecraft is unlikely since heat will be radiated away from the spacecraft. However, once the Planetary Vehicle with actual live fuel capsules has been placed within the shroud, spacecraft performance capability and hence mission success are dependent directly upon uninterrupted cooling until launch. The shroud prevents heat from the RTG from being radiated away, and acts to contain this heat.

3.5.3.1 Launch Complex Equipment

The primary feature of the monitoring, control and launch conditioning equipment required at the ESA or at the Mobile Launcher, and that is unique to RTG use, is that supply and control of ground power to the spacecraft is not required. Control of the power subsystem, for electrically loading the RTG's is a requirement which should be implemented via the umbilical. External electrical load banks may also be required as part of the LCE.

Thermal monitoring of the spacecraft inside the shroud is of considerably greater significance in the case of the LCE for the RTG spacecraft. A processed display of temperature information derived from telemetry ground equipment in the STC, and presented on a printer or

other display, will probably be required. This contrasts with the solar-powered spacecraft's LCE which required as a minimum only a display of raw telemetry video. Temperature sensors mounted external to the spacecraft, within or on the shroud, would probably be hard-wired to direct displays in the LCE in the Mobile Launcher and relayed to the Launch Control Center.

3.5.3.2 LCE Cooling Requirements

As indicated in the foregoing discussion, highly reliable cooling of the enshrouded spacecraft in a continuous and critical requirement from shroud emplacement through liftoff. This requirement applies while the Planetary Vehicle is at the Explosive Safe Area, in transit from the ESA to the Launch Vehicle, during hoist and mating to the Launch Vehicle, and while awaiting launch at the launch pad.

Two candidate approaches to LCE cooling equipment have been considered (1) cooling with dry gas flow through the shroud, and (2) cooling with a liquid flow through a heat exchanger integral with the shroud. The latter method is considered preferable, although the capability of incorporating the heat exchanger within the shroud is not well understood at this time.

One reason for this preference is that the RTG installation design radiates heat outward to the shroud, making a heat exchanger in the shroud more attractive (from the point of view of efficiency) than gas circulation through the shroud. An additional reason is concern for the hazards of particulate contamination of the spacecraft and other potential effects of circulating approximately 500 lb/min through the shroud. Finally, it is considered very difficult and awkward to maintain this level of gas flow to the Planetary Vehicle while it is being transferred from a ground transporter to its position atop the launch vehicle, hundreds of feet in height. Once mated, the spacecraft's cooling gas requirements do appear to be within the supply capabilities of the gas distribution system at the LC 39 launch pad facilities.

Because of the time which would be required for removal of fuel capsules, a 100 percent backup capability appears warranted in the cooling system, regardless of the design ultimately chosen. The best time estimates available, which are based upon operations planning for the Apollo Spacecraft, indicate that in the event of a cooling failure the permissible time without cooling would be exceeded, with consequent thermal damage to the Planetary Vehicle.

Stated another way, the time to remove the fuel capsule will probably significantly exceed the time between liftoff and shroud separation (during which temperature is allowed to rise), if a cooling failure occurs at the pad after mating.

In the event that a program decision is made to have thermal, on-pad, ETO/Freon 12 sterilization of the Planetary Vehicle, the shroud heat exchanger appears to be better able to provide thermal control during sterilization.

3.5.4 OTHER LCE AND AHSE

The safety equipment, radiation monitoring equipment and RTG unique assembly, handling and shipping equipment used in prior ground operations appears to be all that is additionally required by RTG spacecraft launch operations.

Some consideration has been given to the requirements for collection and salvage of fuel capsules in the event of an on-pad or early launch phase catastrophic failure. The basic requirement is to find, safe and collect the fuel capsules.

For detection, either the radioactive or thermal properties, or both, may be utilized. In the event that the capsules end up in a significant depth of water, there does not appear to be a good detection mechanism and location will depend upon tracking and careful bottom search. For dry land, airborne search using infrared search equipment operating in the lead sulphide region of the spectrum will probably locate the landing site. For close in detection after the site has been determined, radiation detectors should also be used, as they will provide needed safety information. These kinds of equipment should not be considered as OSE peculiar to the RTG however. The cognizant agencies (DOD, AEC) involved in the detection-salvage operation will probably utilize their own equipment for these purposes.

The handling sequence for capsules that have been located will probably be as follows:

- a. Determine, by radiation sensing, if the capsule integrity has been maintained. If not, institute decontamination procedures.

- b. If the capsule has been separated from the RTG, utilize the same AHSE as before to handle, install, remove, etc. the capsule. This would require the handling tool and shielding. In the event that the capsule is within a damaged RTG, the RTG would subsequently have to be destroyed to provide access to the capsule.
- c. Install the capsule in the shipping-storage container, an AHSE item required in the nominal ground operation. Intact capsules placed in these containers may be handled by any convenient vehicle, as the dimensions, thermal characteristics, and shielding of these containers will permit such handling. In the event that a capsule has a small leak but is substantially intact, extra sealed containers will be required for their transport to an AEC processing laboratory.

It is recognized that the propellants and oxydizers which the spacecraft's propulsion would use are highly corrosive. The effect upon the integrity of the fuel capsule will probably be tolerable, however, as the capsule temperature will be well above the flash point of the fuels. The actual limiting design requirement on the fuel capsule is its ability to withstand the fire inside the RTG, rather than its corrosion resistance. This must be considered by the AEC in establishing the design of the capsule and RTG.

REFERENCES

- 3-1. Sutton, G. W., Direct Energy Conversion, McGraw-Hill, 1966
- 3-2. Heikes, R. R. and R. W. Ure, Thermoelectricity: Science and Engineering, Interscience Publishers, N. Y., 1961.
- 3-3. Schneider, H. W., "Considerations Regarding the Pneumatic Treatment of Voyager Shroud Structures," TM 33-295, Jet Propulsion Laboratory, April 15, 1967.
- 3-4. Capo, M. A. "Gamma Ray Absorption Coefficients for Elements and Mixtures," USAEC Report XDC59-10-19, General Electric Co., ANP Dept., Cincinnati, Ohio, 28 Sept. 59
- 3-5. Trubey, D. K., "A Survey of Empirical Functions Used to Fit Gamma-Ray Buildup Factors," USAEC Report ORNL-RSIC-10, Oak Ridge National Lab., Oak Ridge, Tenn., February 66
- 3-6. Edwards, W. E., et al., "Gas-Cooled High-Temperature Nuclear Reactor Design Technology, 7. Shield Design," USAEC Report APEX-800 Part E, General Electric Co., N. M. & P. O., Cincinnati, Ohio, 30 June 62

SECTION 4

SOLAR/RTG INTERCHANGEABILITY

This section considers the spacecraft design as a solar-powered version. The purpose of this consideration is twofold. First, the solar-powered version serves as the model against which the RTG spacecraft is compared on an overall basis. Second, it serves as the basis for determining the degree to which the design is convertible from a solar-powered to an RTG-powered spacecraft. This latter subject is treated in Section 4.5.

The solar-powered version described herein is for the most part functionally identical to the Task B design (Ref. GE Document No. DIN 65SD4514). Differences are principally confined to the arrangement of spacecraft equipment resulting from the objective of attaining an interchangeable design.

4.1 GUIDELINES

The guidelines used for the solar-powered spacecraft are identical to those for the RTG powered spacecraft. Array power requirements were assumed to be those developed for the Task B design with its associated mission profile.

4.2 DESIGN EVOLUTION

Design evolution proceeded simultaneously with that of the RTG spacecraft as discussed in Section 3.2.

4.3 SELECTED SOLAR SPACECRAFT DESIGN

4.3.1 DESCRIPTION

An isometric view of the solar-powered spacecraft together with the flight capsule is shown in Figure 4-1.

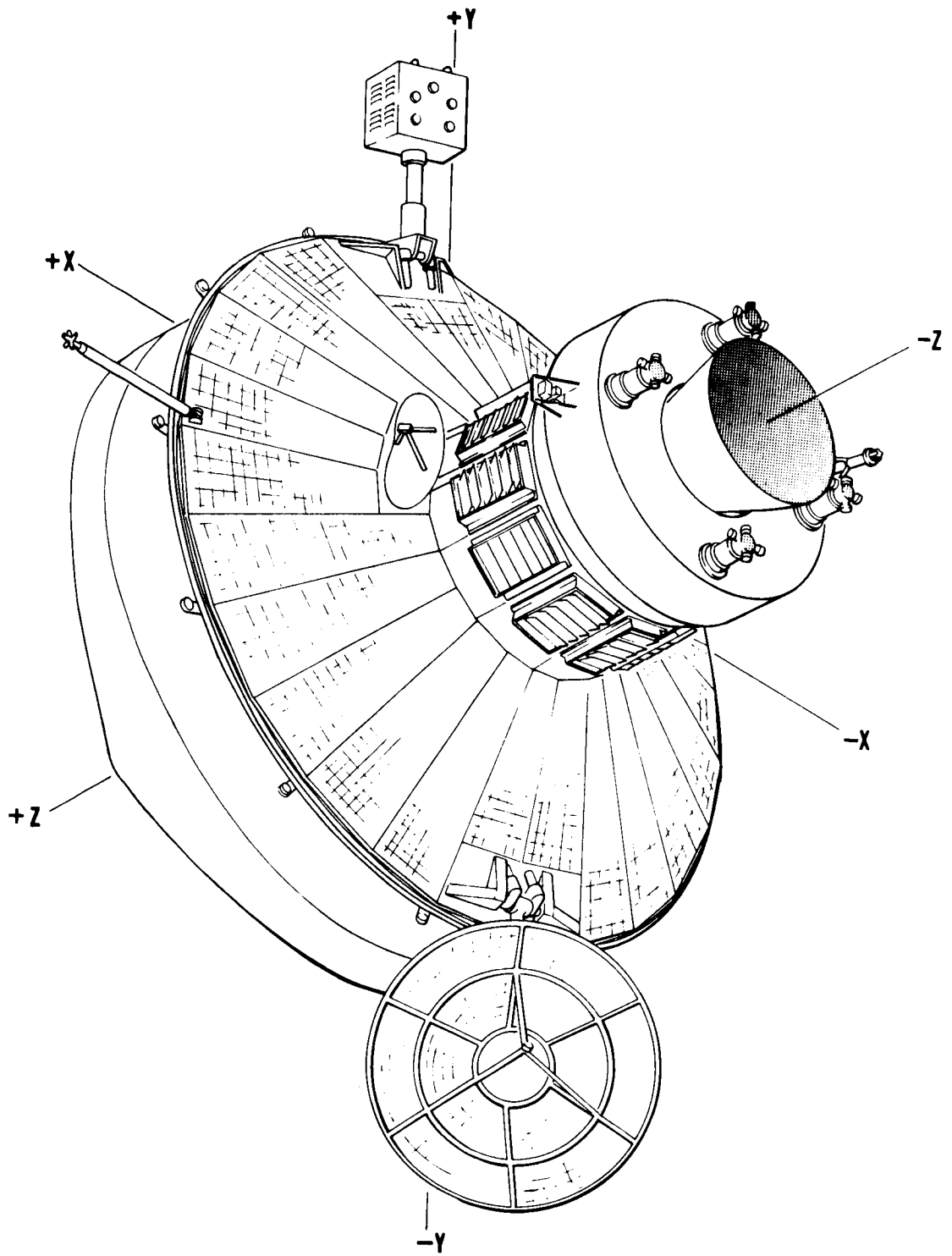


Figure 4-1. Solar-Powered Spacecraft

The spacecraft general arrangement is shown in Figure 4-2. Antenna and sensor locations along with fields of view are shown in Figure 4-3. The principal differences with respect to the RTG-powered spacecraft are as follows:

- a. Solar panels are substituted for the RTG's and associated mounting panels. A fixed projected area of 229 square feet in the minus Z direction (solar direction) is available for solar cell mounting. Solar array output is conservatively estimated to be 720 watts at 1.52 AU (estimated value at planetary encounter for the 1973 opportunity). Output at Mars aphelion (1.66 AU) is estimated to be 605 watts.
- b. The 90 inch high-gain antenna is articulated for Earth-pointing, and is mounted at the periphery of the truss support structure in the region of the minus Y axis.
- c. A backup medium-gain antenna is mounted with its axis fixed at the encounter cone angle and is located at the inner diameter of the support structure in the region of the plus X axis.
- d. A Sun-Canopus attitude reference system is used identical to that of the Task B design. The need for the equipment bay sun shade, shown in the RTG version, is eliminated because of the Sun-pointing of the Z axis during all non-maneuver periods.
- e. Electronic equipment changes are principally those in the power subsystem and are discussed later. Equipment bay locations and volume allocations are practically identical to those of the RTG spacecraft design.

Operation of the spacecraft during the various mission phases is identical to that of the Task B design excepting for possible revision subsequent to planetary encounter. The Task B design was principally based on the 1971 opportunity with encounter at 1.42 AU. The array power capability at encounter was 820 watts. The design described herein assumes application to the 1973 opportunity with an estimated encounter at 1.52 AU and an associated array encounter output of 720 watts. The 100-watt difference is based on similar solar cell rating factors for the two cases, taking array temperature differences into account because of the configuration change. Since power requirements for the missions are typically highest in the post-encounter period prior to the Flight Capsule separation, the difference in array out-

put for the two cases points to a possible revision to the post-encounter events planned for the Task B design. Such a revision must take into account the possibility of solar occultations just after encounter, and the degree to which the available power can be adequately allocated to the needs of the Flight Capsule and Science.

4.3.2 STRUCTURE

The structural design is shown in the general arrangement drawing (Figure 4-2). The primary structure, selection rationale, and supporting analyses are identical to those of the RTG design.

The spacecraft electronic equipment arrangement is shown in Figure 4-4. The arrangement is identical with the RTG design, with the exception that the weight and power levels of bays 1, 2 and 8 differ because of additional batteries and power conditioning equipment.

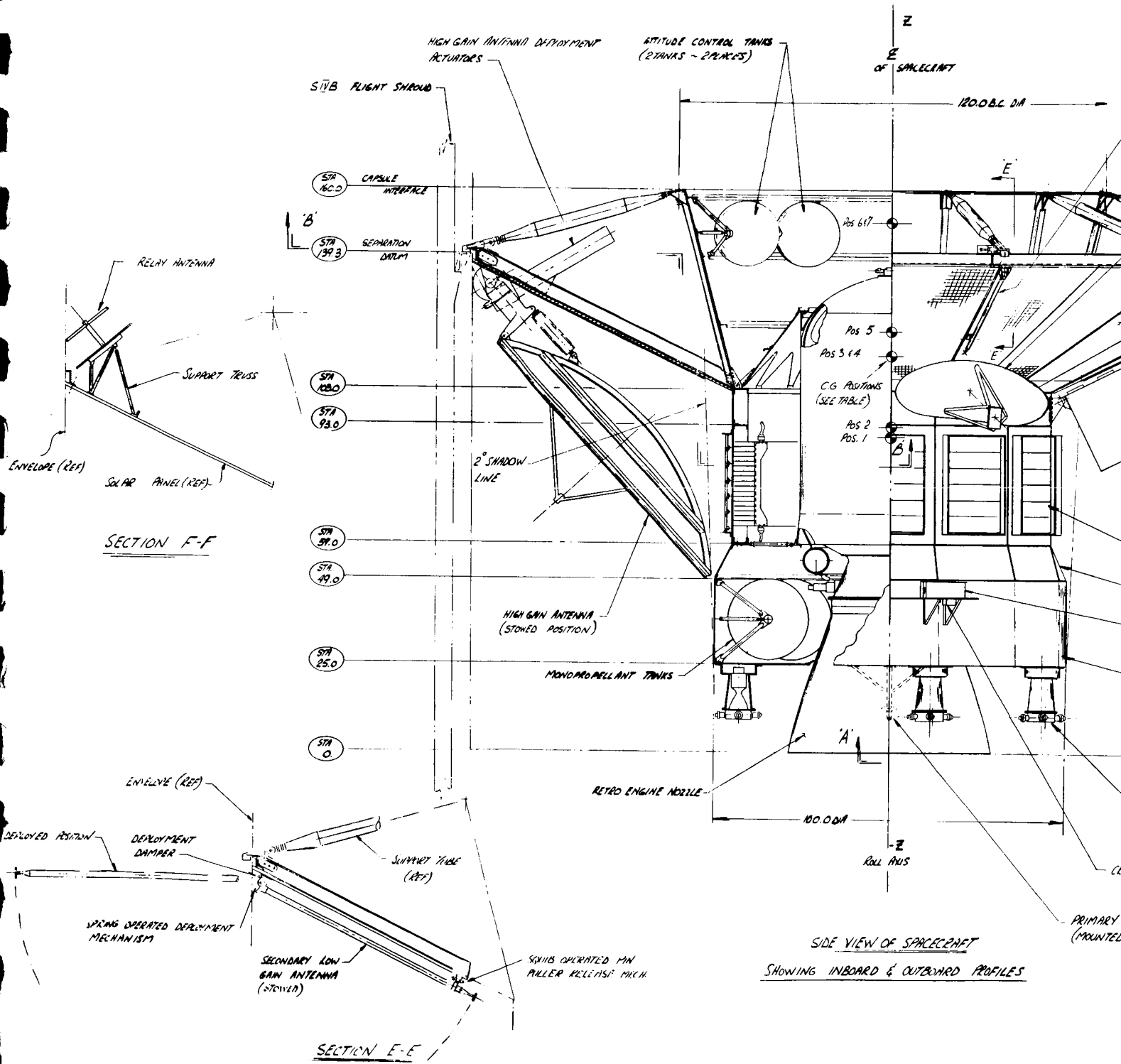
The elliptical Sun shade shelf at STA 37 on the RTG version is not required. The cylinder which encloses the MC&OA engine provides equipment bay shading up to two degrees of Z axis misalignment with the Sun line.

4.3.3 MASS PROPERTIES

A weight summary of the planetary vehicle is presented in Table 4-1. The weight breakdown is by vehicle function with subtotals shown for the spacecraft bus.

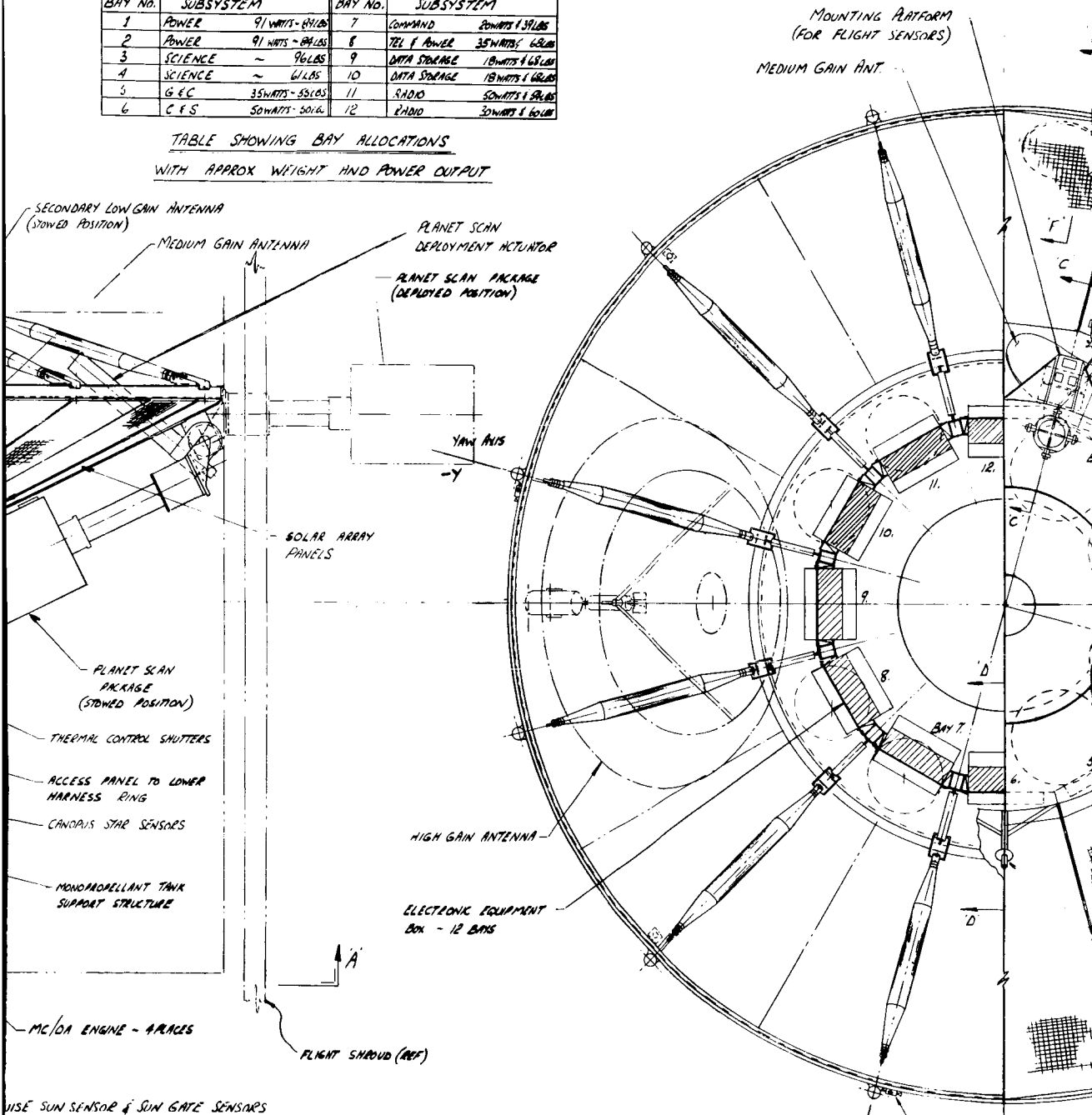
Weight, center of gravity, moments and products of inertia are presented in summary form in Table 4-2 for specific times during the mission. Longitudinal centers of gravity are referenced to Sta.0 shown in Figure 4-2 with positive distances in the direction of +Z. Lateral CG locations are referenced to the roll axis in compliance with the sign convention in Figure 4-1. Each inertia is about the center of gravity.

A detailed weight statement is shown in Table 4-3.



BAY NO.	SUBSYSTEM	BAY NO.	SUBSYSTEM
1	POWER 91 WATS - 89 LBS	7	COMMAND 20 WATS / 37 LBS
2	POWER 91 WATS - 89 LBS	8	TEL. & AUDIO 35 WATS / 62 LBS
3	SCIENCE ~ 96 LBS	9	DATA STORAGE 18 WATS / 63 LBS
4	SCIENCE ~ 61 LBS	10	DATA STORAGE 18 WATS / 63 LBS
5	G.E.C. 35 WATS - 55 LBS	11	RADIO 50 WATS / 50 LBS
6	C.F.S. 50 WATS - 50 LBS	12	RADIO 30 WATS / 50 LBS

TABLE SHOWING BAY ALLOCATIONS
WITH APPROX WEIGHT AND POWER OUTPUT



USE SUN SENSOR & SUN GATE SENSORS

LOW GAIN ANTENNA
(FAR SIDE)

C.G. POSITIONS

POSITION	STATION	FLIGHT SEQUENCE
1	88.9	AFTER CAPSULE SEPARATION
2	92.9	AFTER ORBIT ADJ. ANT. DEPLOYED
3	113.74	TRANSIT
4	113.91	LAUNCH COND. (ON PAD)
5	120.5	AFTER MID COURSE CORRECTION
6	151.7	AFTER RETRO BURN (ORBITING)
7	152.3	P.S.P. DEPLOYED

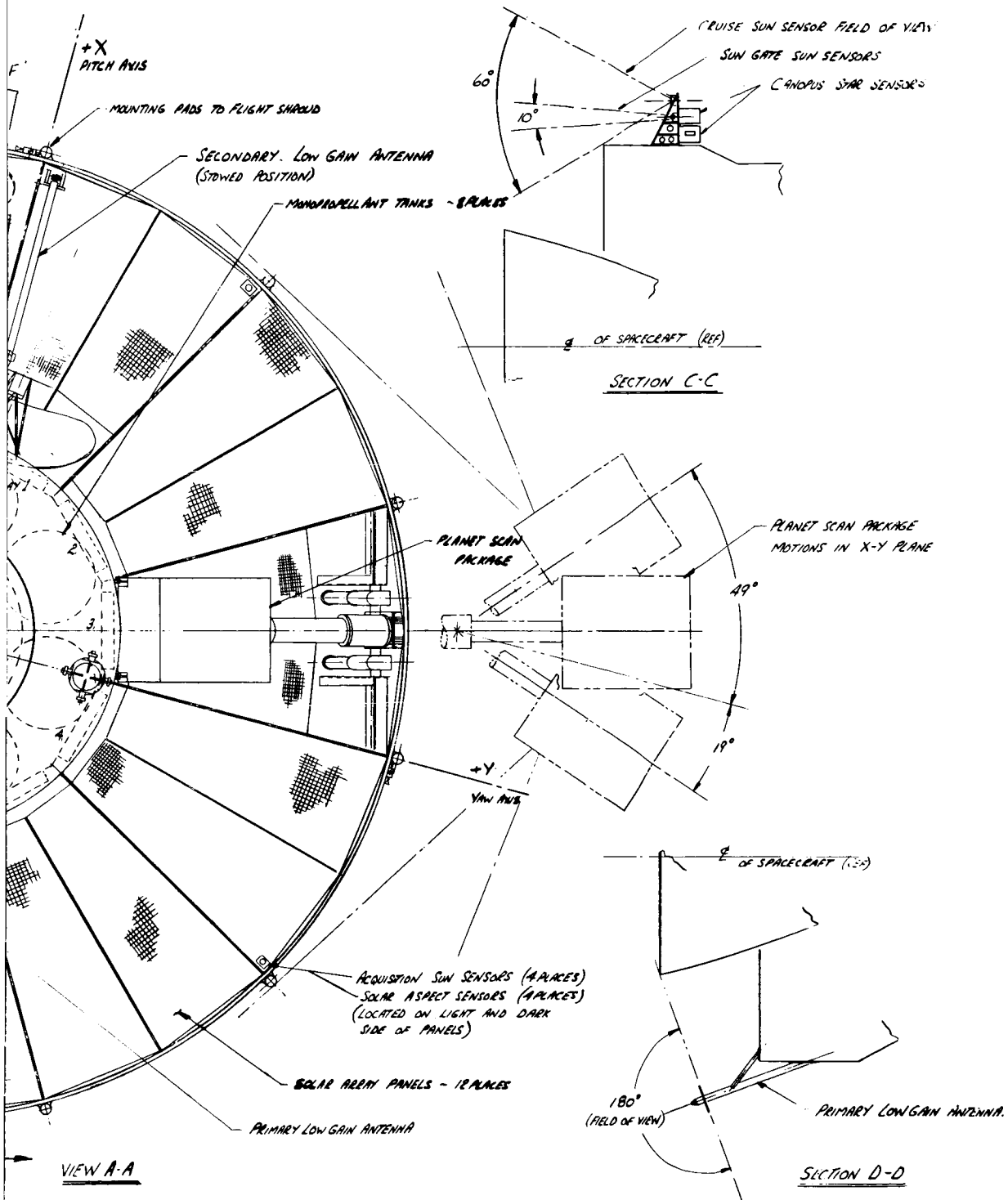
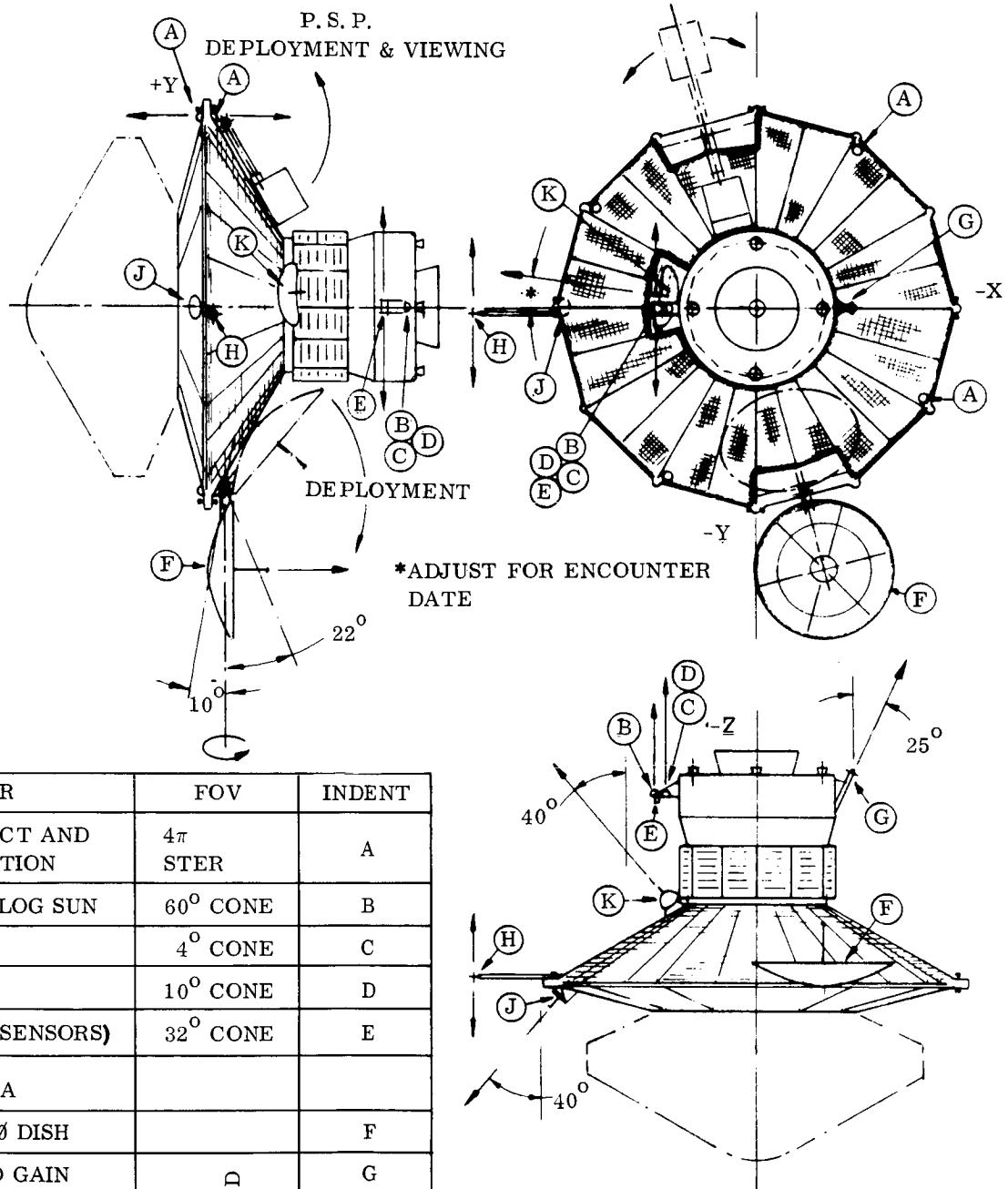


Figure 4-2. Solar Array Spacecraft -- General Arrangement



SENSOR	FOV	INDENT
SOLAR ASPECT AND SUN ACQUISITION	4π STER	A
CRUISE ANALOG SUN	60° CONE	B
SUN GATE 1	4° CONE	C
SUN GATE 2	10° CONE	D
CANOPUS (2 SENSORS)	32° CONE	E
ANTENNA		
HI GAIN 90" ϕ DISH		F
PRIMARY LO GAIN	NOTED	G
SECONDARY LO GAIN		H
RELAY		J
BACKUP (MARINER 4)	*	K

Figure 4-3. Antenna and Sensor Fields of View

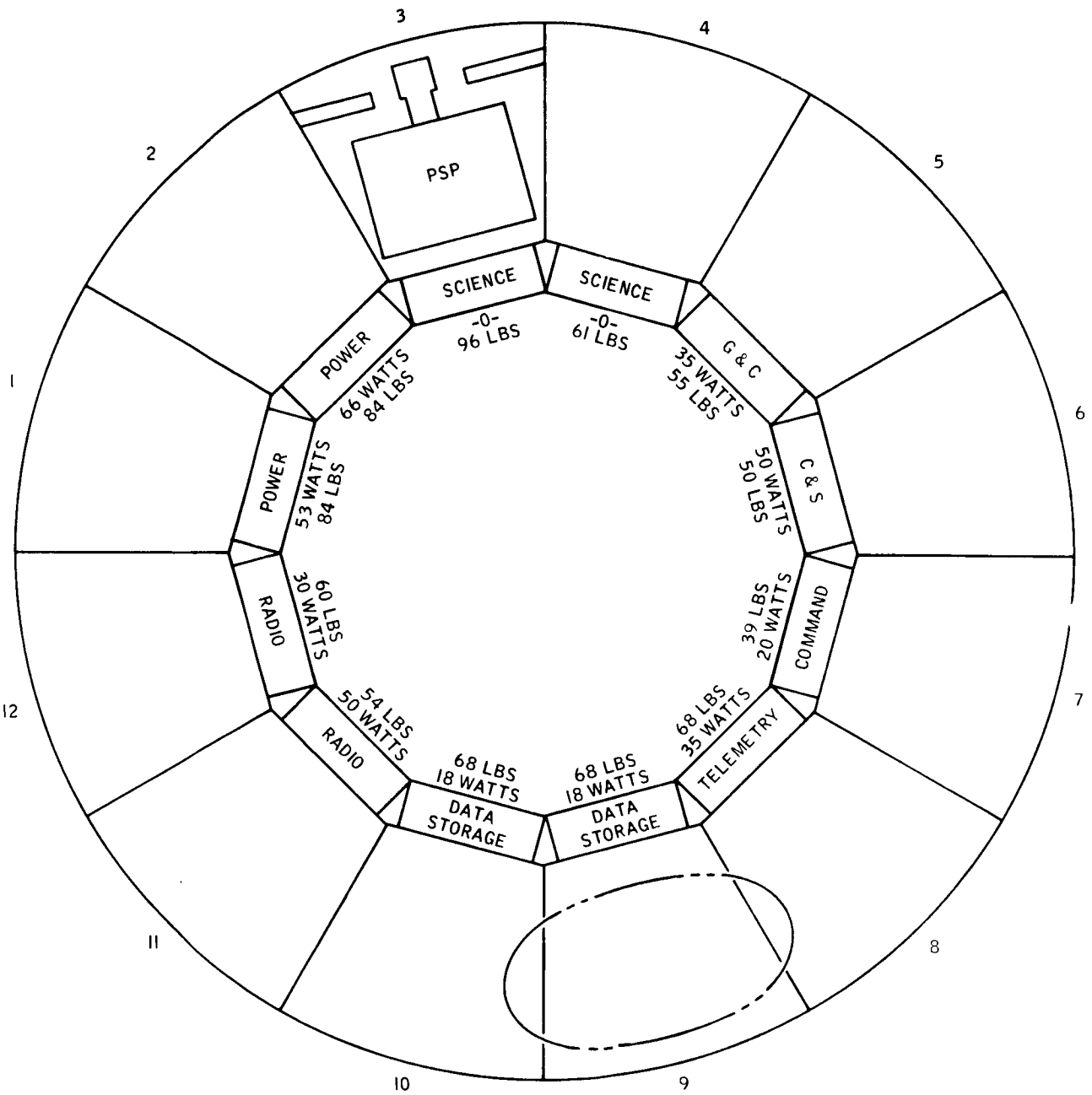


Figure 4-4. Electronic Equipment Bay Arrangement

TABLE 4-1. WEIGHT SUMMARY

Description	Weight (lb)
Bay No. 1 Power System	83.8
Bay No. 2 Power System	84.3
Bay No. 3 Science Electronics	96.0
Bay No. 4 Science Dae	61.0
Bay No. 5 Guidance and Control	55.5
Bay No. 6 Computer and Sequencer	50.1
Bay No. 7 Command System	38.9
Bay No. 8 Telemetry & Power System	67.7
Bay No. 9 Data Storage	68.4
Bay No. 10 Data Storage	68.4
Bay No. 11 Radio System	54.0
Bay No. 12 Radio System	60.4
Primary Structure	395.6
Scan Platform	150.0
Solar Array System	298.0
A.C. Gas System	247.0
A.C. Independently Mounted Sensors	16.6
Science Sensors	105.4
Antenna Assemblies	92.1
Thermal Control	151.4
Pyrotechnic	4.4
Harness	51.5
Total No. 1 Subtotal Bus Weight	2300.5
Retro Propulsion	9285.5
Mid-Course Propulsion	2138.8
Meteoroid Protection	71.1
Total No. 2 Subtotal Propulsion Weight	11495.4
Capsule (includes Biobarrier)	3000.0
Total No. 3 Subtotal Capsule Weight	3000.0
Total No. 1, No. 2 & No. 3 Separated OverAll Planetary Vehicle	16795.9
Adapter	113.3
Planetary Vehicle	16909.2

TABLE 4-2. MASS PROPERTY SUMMARY

Flight Sequence Description	Case No.	Weight (lbs)	\bar{Z} (in.)	\bar{X} (in.)	\bar{Y} (in.)	I_{zx}^2 (slug ft ²)	I_{zy}^2 (slug ft ²)	I_{xz}^2 (slug ft ²)	I_{oz}^2 (slug ft ²)	I_{ox}^2 (slug ft ²)	I_{oy}^2 (slug ft ²)
Launch Cond. (On PAD)	1	16908.9	114.7	0.22	0.32	-26.0	-0.4	26.0	7536	21855	21592
Transit	2	16795.6	114.5	0.17	0.34	-28.2	0.8	6.5	7326	21716	21440
After Mid Course Correction	3	15427.6	121.3	0.19	0.37	-32.5	-7.6	6.5	6925	19569	19343
After Retro Burn (Orbiting)	4	7290.6	151.9	0.40	0.79	-51.6	-45.5	6.2	6344	15718	15492
P. S. P. Deployed	5	7290.6	152.5	0.89	2.50	-52.2	-43.7	159.2	6949	16209	15462
After Capsule Separation	6	4790.6	89.1	1.33	3.80	34.6	205.3	157.4	3411	2950	2207
After Orbit Adjust. Ant. Depid.	7	4484.6	93.1	1.19	3.14	10.9	117.5	215.1	3558	2961	2005

Notes 1 NOM C.G. on 3000 pound capsule

TABLE 4-3. DETAILED WEIGHT STATEMENT

Item	Weight (lb)	Item	Weight (lb)
BAY 1		BAY 5	
POWER SUBSYT		G + C SUBSYTM	
BATTERY	43.00	AC ELECTRONIC	8.60
MAIN REG.	11.50	AUTO PILOT	6.00
CHARGE REG.	1.50	ACCELMO GYRO	14.50
3 PHSE INVERT	3.50	ACCELMO + GYO	14.50
2.4 KC INVERT	4.50	BAY NO 5 WIRE	5.70
1 PHSE INVERT	1.50	EQUIPMENT CHS	5.47
PWR SW + LOGC	5.50	GYRO TEMP SEN	0.10
BAY NO 1 WIRE	6.70	ACCEL TMP SEN	0.10
EQUIPMENT CHS	5.47	BAY TEMP SEN	0.10
BATT TEMP SEN	0.10	SHUTT ANG DET	0.40
BAY TEMP SEN	0.10		
SHUTT ANG DET	0.40	BAY 6	
BAY 2		COMP + SEQCER	
POWER SUBSYS		COMPUTING + SQ	35.00
BATTERY	43.00	SOLAR ASPECT	5.00
MAIN REG.	11.50	EARTH NULLS	2.00
CHARGE REG.	1.50	BAY NO. 6 WIRE	2.10
3 PHSE INVERT	3.50	EQUIPMENT CHS	5.47
2.4 KC INVERT	4.50	BAY TEMP SEN	0.10
1 PHSE INVERT	1.50	SHUTT ANG DET	0.40
SYNCHRO + CLK	6.00	BAY 7	
BAY NO 2 WIRE	6.70	COMMAND SSY	
EQUIPMENT CHS	5.47	COMM DET P C	4.20
BAY TEMP SEN	0.10	COMM DET P C	4.20
BAY TEMP SEN	0.10	COMM DET P C	4.20
SHUTT ANG DET	0.40	COMM DECODER	5.60
BAY 3		COMM DECODER	5.60
SCIENCE ELECT		DEC ACES SWIT	3.00
SCIENCE ELEC	90.00	POWER SUPPLY	3.10
EQUIPMENT CHS	5.47	BAY NO. 7 WIRE	3.00
BAY TEMP SEN	0.10	EQUIPMENT CHS	5.47
SHUTT ANG DET	0.40	BAY TEMP SEN	0.10
BAY 4		SHUTT ANG DET	0.40
SCIENCE DAE			
DATA AUTO EQ	55.00		
EQUIPMENT CHS	5.47		
BAY TEMP SEN	0.10		
SHUTT ANG DET	0.40		

TABLE 4-3. DETAILED WEIGHT STATEMENT (Continued)

Item	Weight (lb)	Item	Weight (lb)
BAY 8		BAY 11	
TELEMETRY & POWER		RADIO SUBSYTM	
PYRO CONTROLER	7.50	PWR AMP TWT	7.50
TELEMETRY ELE	16.60	PWR AMP TWT	7.50
BAY NO. 8 WIRE	1.10	POWER AMP TWT	3.00
EQUIPMENT CHS	5.47	TRANSPONDER	13.30
BAY TEMP SEN	0.10	DIPLEX + SW	13.40
SHUTT ANG DET	0.40	BAY NO. 11 WIRE	3.70
BATTERY	35.00	EQUIPMENT CHS	5.47
CHARGE REG.	1.50	BAY TEMP SEN	0.10
BAY 9		BAY 12	
DATA STORAGE		RADIO SUBSYS	
TAPE RECORDER	18.00	TRANSPONDER	13.30
TAPE RECORDER	18.00	TRANSPONDER	13.30
TAPE RECORDER	18.00	RELAY RADIO	25.00
CONTROL LOGIC	0.40	BAY NO. 12 WIRE	2.80
CONTROL LOGIC	0.40	EQUIPMENT CHS	5.47
CONTROL LOGIC	0.40	BAY TEMP SEN	0.10
PLAYBACK SEQ	0.60	SHUTT ANG DET	0.40
POWER SUPPLY	2.00		
BAY NO. 9 WIRE	4.60	PRIMARY STR	
EQUIPMENT CHS	5.47	SHEAR PANELS	89.10
BAY TEMP SEN	0.10	CAP SEP RING	9.30
SHUTT ANG DET	0.40	TAP LONGERON	35.00
BAY 10		KICK FRAME	38.90
DATA STORAGE		EQUIP CHANNEL	26.40
TAPE RECORDER	18.00	SUPPT ANGLE	1.04
TAPE RECORDER	18.00	SUPPT ANGLE	0.44
TAPE RECORDER	18.00	OUTER CAP	6.90
CONTROL LOGIC	0.40	TAPERED STRUT	94.00
CONTROL LOGIC	0.40	MISC	4.13
CONTROL LOGIC	0.40	FITTINGS STR	31.40
PLAYBACK SEQ	0.60	HARDWARE STR	38.00
POWER SUPPLY	2.00	SEPARATION FG	21.00
BAY NO. 10 WIRE	4.60		
EQUIPMENT CHS	5.47	METEROID PROT	71.10
BAY TEMP SEN	0.10		
SHUTT ANG DET	0.40	PSP STOWED	150.00

TABLE 4-3. DETAILED WEIGHT STATEMENT (Continued)

Item	Weight (lb)	Item	Weight (lb)
SOLAR ARRAY		SCIENCE SENSOR	
BAY 1	11.25	MISC SCIENCE	95.00
1	11.25	MAGNETOMETER	10.00
2	11.58	TEMP SENSORS	0.40
2	11.58	ANT ASSEMBLIES	
3	11.58	RELAY ANTENNA	2.00
3	11.58	ASSOCIATED ST	2.00
4	11.58	HI GAIN ANT S	46.50
4	11.58	ACTU + STR	33.50
5	11.58	LO GAIN ANT P	0.80
5	11.58	LO GAIN ANT S	0.80
6	11.58	MEDIUM GAIN	4.40
6	11.58	MTG STR	2.00
7	11.58	TEMP SENSORS	0.10
7	11.58	THERMAL CONTL	
8	11.58	SHUTTER FACE	10.80
8	10.55	SHUTTER FACE	10.80
9	10.55	SHUTTER FACE	10.80
9	10.55	INSUL + FACE	10.80
10	10.55	SHUTTER FACE	10.80
10	11.58	SHUTTER FACE	10.80
11	11.58	SHUTTER FACE	10.80
11	11.58	SHUTTER FACE	10.80
12	11.58	SHUTTER FACE	10.83
12	11.25	SHUTTER FACE	10.83
PANEL TEMP SN	0.20	SHUTTER FACE	10.80
ARRAY HARNESS	25.00	SHUTTER FACE	10.83
AC GAS SYSTEM		INSUL + FACE	10.83
GAS + TANK	46.40	INSUL AC SYS	2.50
GAS + TANK	46.40	PAINT	4.00
GAS + TANK	46.40	INSUL ORBITER	15.20
GAS + TANK	46.40	PYROTECHNIC	
HARDWARE	47.40	PIN PULLERS	2.20
GAS SYS MTG SEN	14.00	SQUIBS	2.20
AC IND MTG S		HARNESS	
SUN SENSERS	2.60	MAIN HAR RING	35.00
CANOPUS TRACK	6.30	RELAY CABLE	1.00
CANOPUS TRACK	6.30	HI GAIN CABLE	4.00
MISC MTG STR	1.20	LO GAIN CABLE	5.00
TEMP SENSORS	0.20	MEDIUM G CABLE	2.00
		UMBILICAL	4.50

Table 4-3. Detailed Weight Statement (Continued)

Item	Weight (lb)
RETRO PROPULSION	
RETRO ENGINE	9192.00
TAPERED STRUT	60.80
KICK RING	12.50
TUBLAR STRUT	16.40
KICK RING	3.80
MID COURSE	
MONO ENGINE	516.75
TANK SUPPORT	12.95
MONO ENGINE	516.75
TANK SUPPORT	12.95
MONO ENGINE	516.75
TANK SUPPORT	12.95
MONO ENGINE	516.75
TANK SUPPORT	12.95
FRAMES	20.00

4.3.4 THERMAL ANALYSIS

The solar-power spacecraft design will perform thermally as described in the Task B thermal report both on the pad and in parking orbit. The primary difference from a thermal standpoint between the Task B design and the design described herein will occur when the array is subjected to a solar input. For this reason, thermal analysis was performed for phases of the mission after shroud ejection.

Figure 4-5 shows the steady-state solar array temperatures that will result at different locations on the array during various phases of the mission. Figure 4-6 shows the radial temperature distribution along the solar array as a function of sun distance. A comparison of these results with the solar array temperatures calculated in the Task B report reveals an average increase in array temperature of about 20 degrees F, more or less independent of the AU distance. This results from reduced panel backface radiation to space.

Steady-state spacecraft temperature profiles have been calculated both near Earth and near Mars and are shown in Figures 4-7 and 4-8. During the entire cruise phase of the mission, all spacecraft temperatures are tolerable and no thermal problems are anticipated.

During Mars orbit, the spacecraft will perform thermally as described in the Task B thermal report.

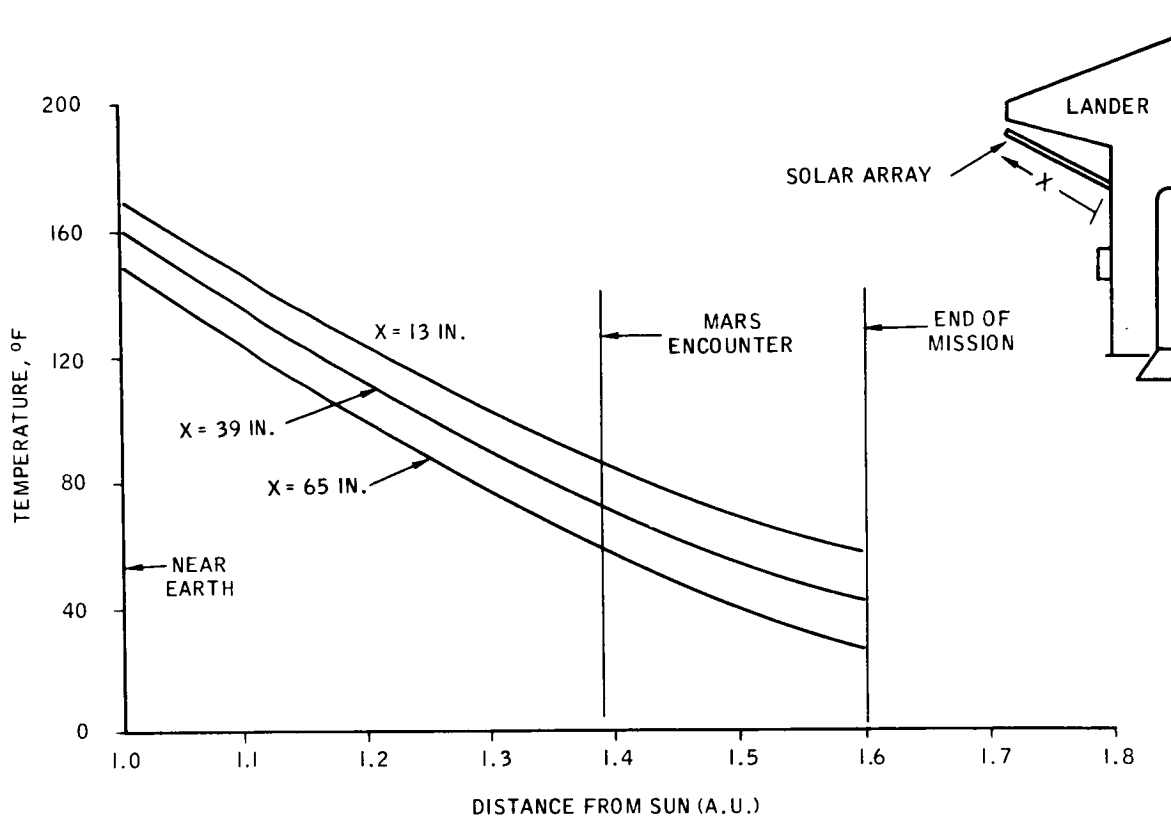


Figure 4-5. Solar Array Temperature Variation versus Distance from Sun

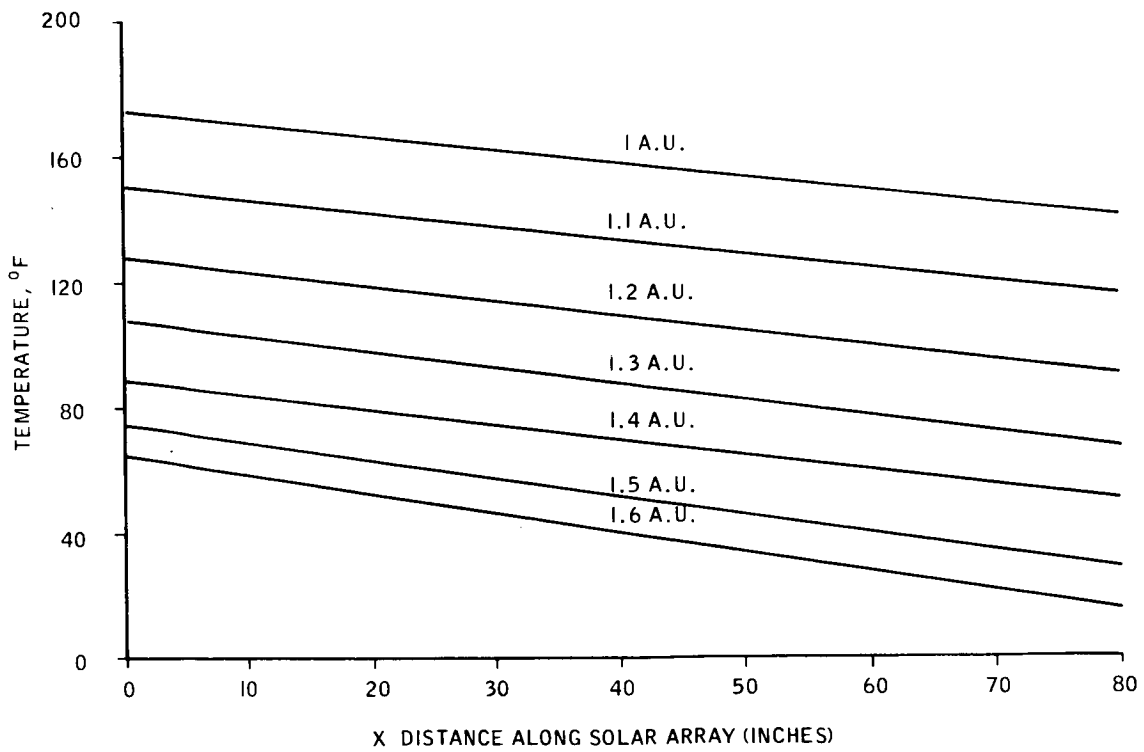


Figure 4-6. Temperature Distribution Along Solar Array

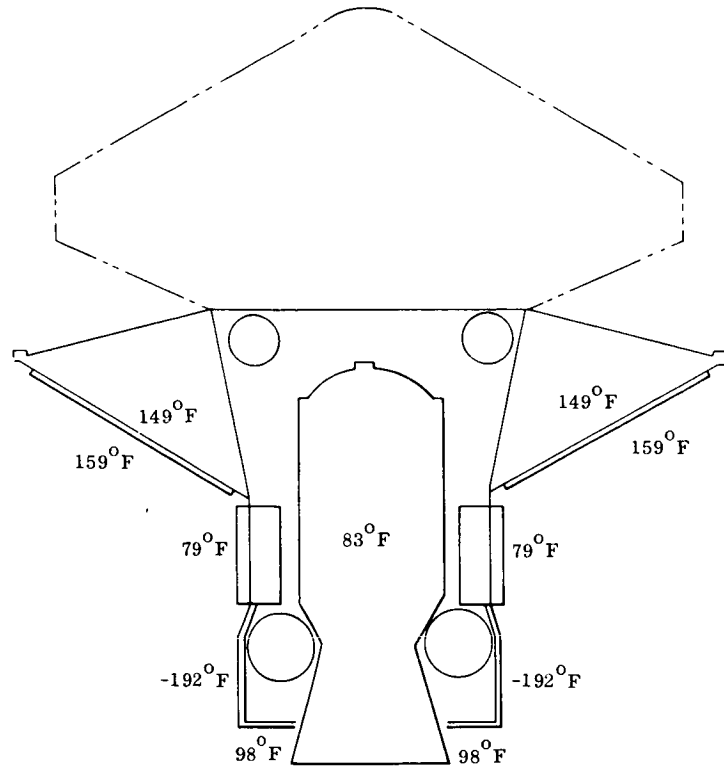


Figure 4-7. Voyager Spacecraft Temperatures near Earth

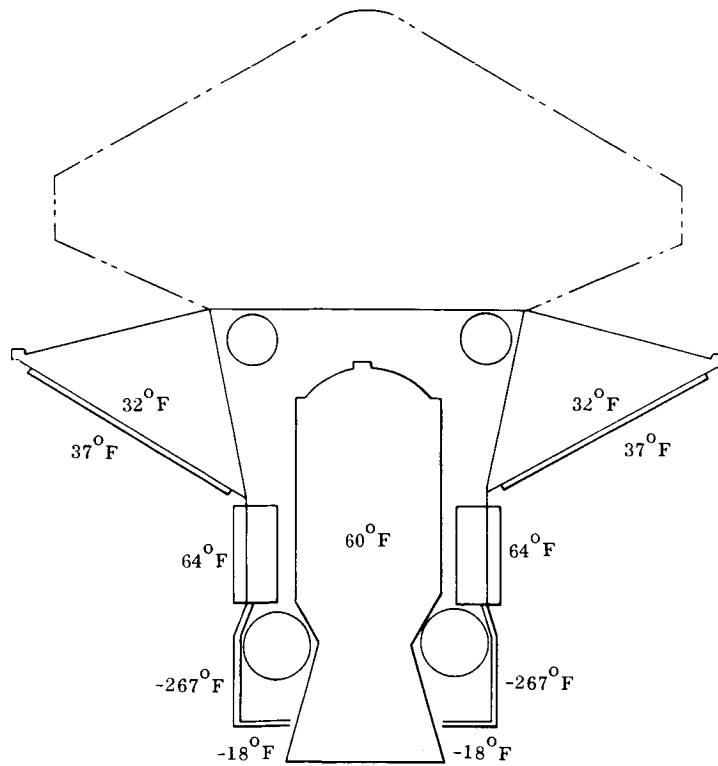


Figure 4-8. Voyager Spacecraft Temperatures near Mars

4.4 SUBSYSTEM DESIGN

This section describes the significant differences in subsystem design required for the solar powered spacecraft version.

4.4.1 POWER SUBSYSTEM

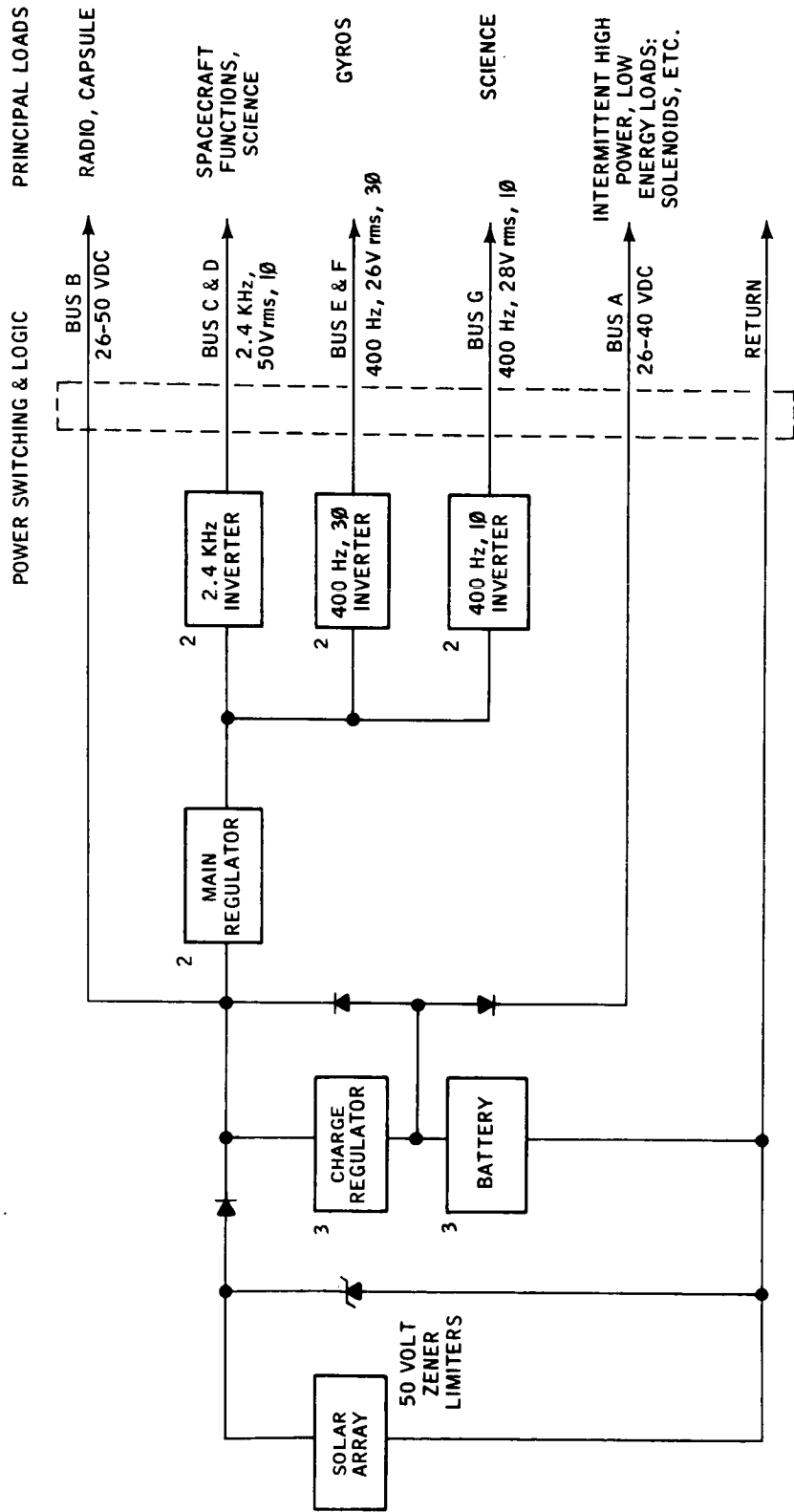
This subsystem is similar to that used in the Task B design. The primary differences occur in the solar array and battery designs. Secondary differences also occur in the detailed design of the power conditioning units. The subsystem arrangement is shown in Figure 4-9 along with revised bus voltage levels reflecting changes discussed below.

4.4.1.1 Solar Array

The solar array for the interchangeable spacecraft has more cells than the Task B array, but approximately the same power output, since the array is mounted at a solar incidence angle of 24 degrees. The predicted power output of the solar array, as a function of Sun-spacecraft distance, is shown in Figure 4-10. Combining this data with trajectory data yields the relationship between array power output and time during the cruise and orbit phases, as shown in Figure 4-11. Detailed voltage-current and voltage-power curves are given for the complete range of Sun-spacecraft distances in Figure 4-12 and 4-13, respectively.

Power is drawn from the solar array at 43 volts or higher for those conditions when the array output is higher than the load demand. This represents a decrease from the 52 volt level used on the Task B design and was selected for two main reasons. First, layout studies of the 24 half-panels produced the most efficient packaging with solar cell strings having a number of series elements which yield optimum power capability at 43 volts. This occurs during late phases of the mission when the power margin is least. Second, the reduced level results in a comparable reduction in the regulated output of the main regulator to 20 volts dc. This is compatible with RTG output and is therefore a desired level from an interchangeability standpoint. This consideration is discussed in greater detail later.

Considering an associated change in the number of battery cells in series, also discussed later, the unregulated bus voltage (array-battery bus) range is reduced from 32-62 volts, for the Task B design, to 26-50 vdc.



NOTE: NUMBER ON UPPER LEFT CORNER OF BLOCKS DESIGNATES NUMBER OF UNITS.

Figure 4-9. Simplified Power Subsystem Schematic

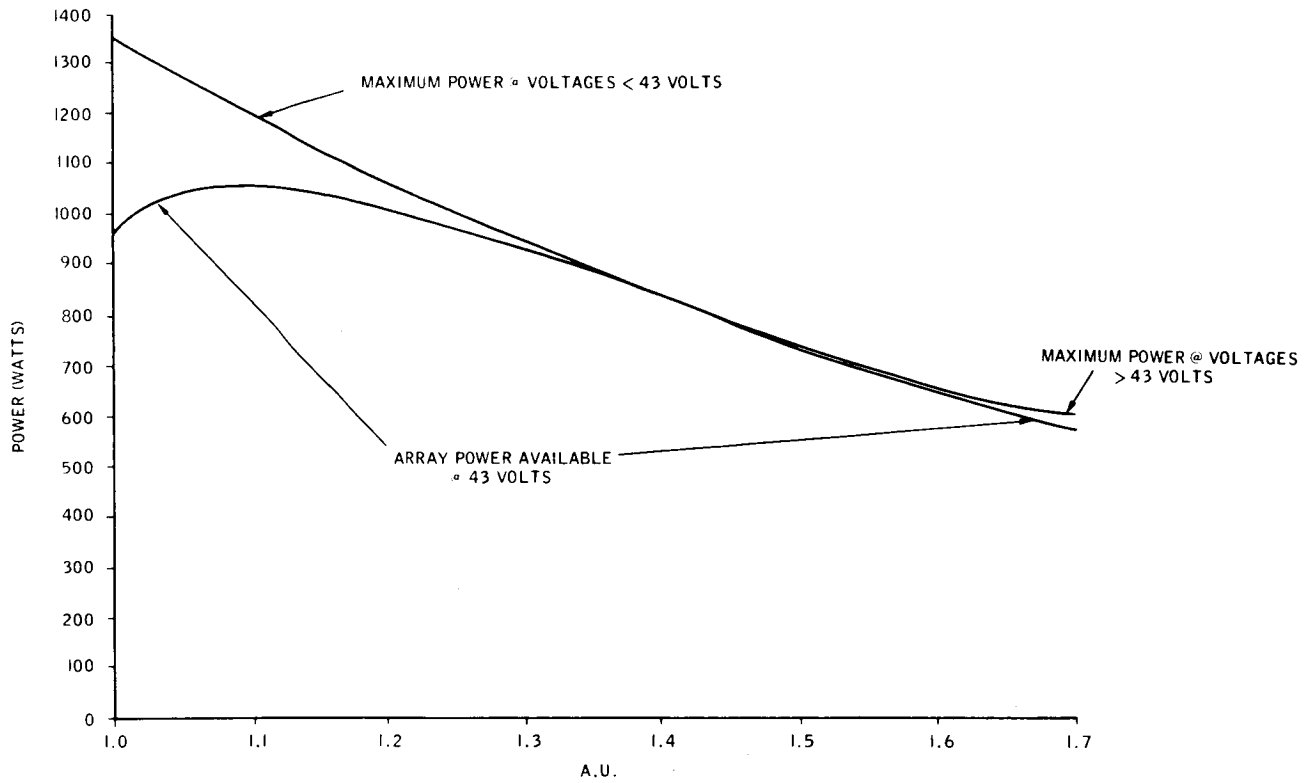


Figure 4-10. Solar Array Power Output vs. Sun Distance

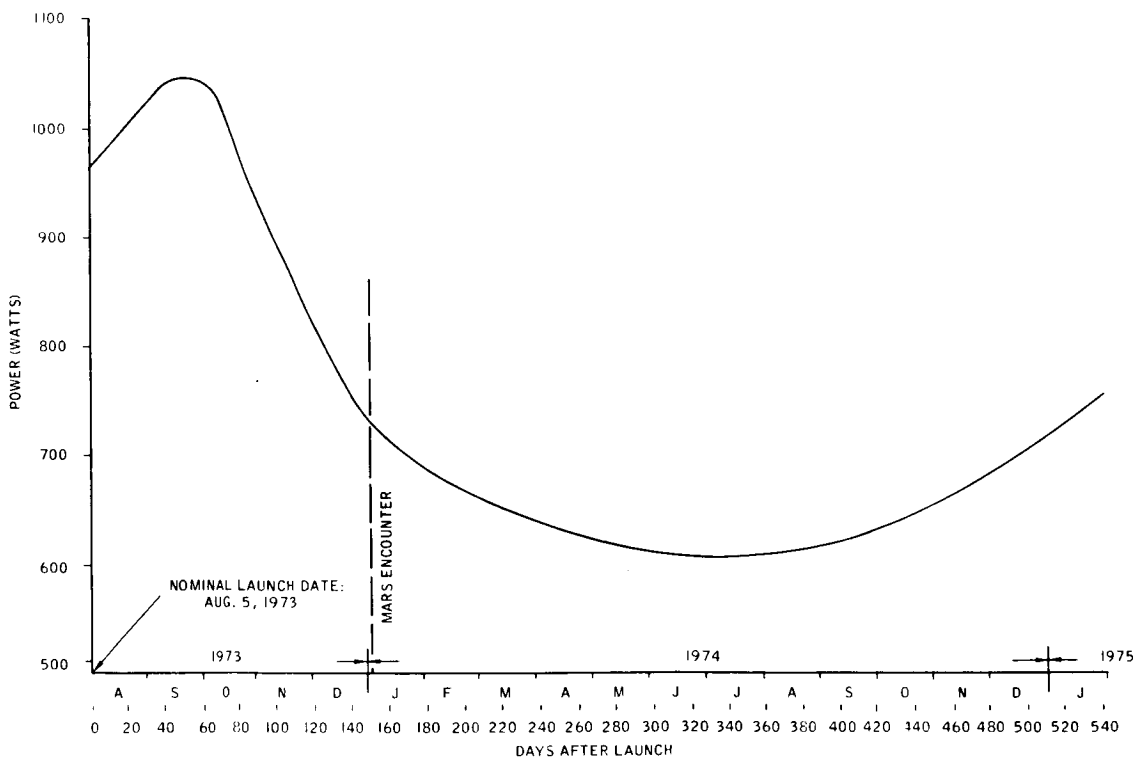


Figure 4-11. Solar Array Output vs. Mission Time

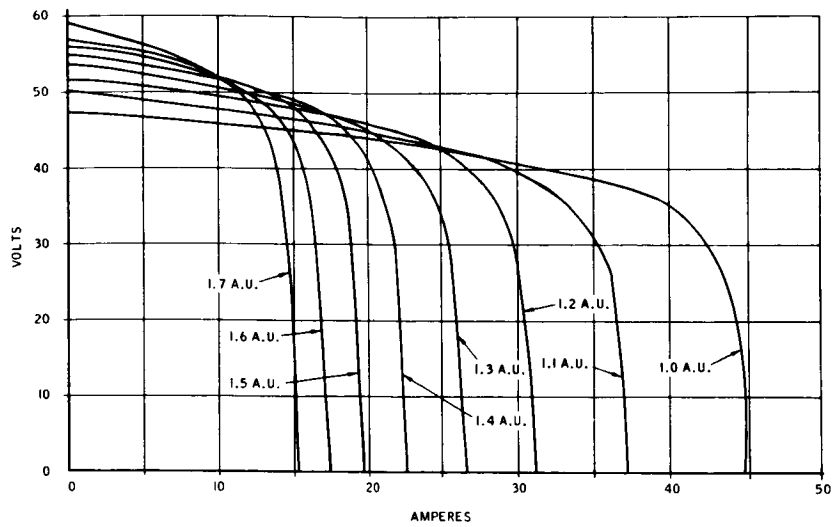


Figure 4-12. Solar Array Voltage-Current Characteristics

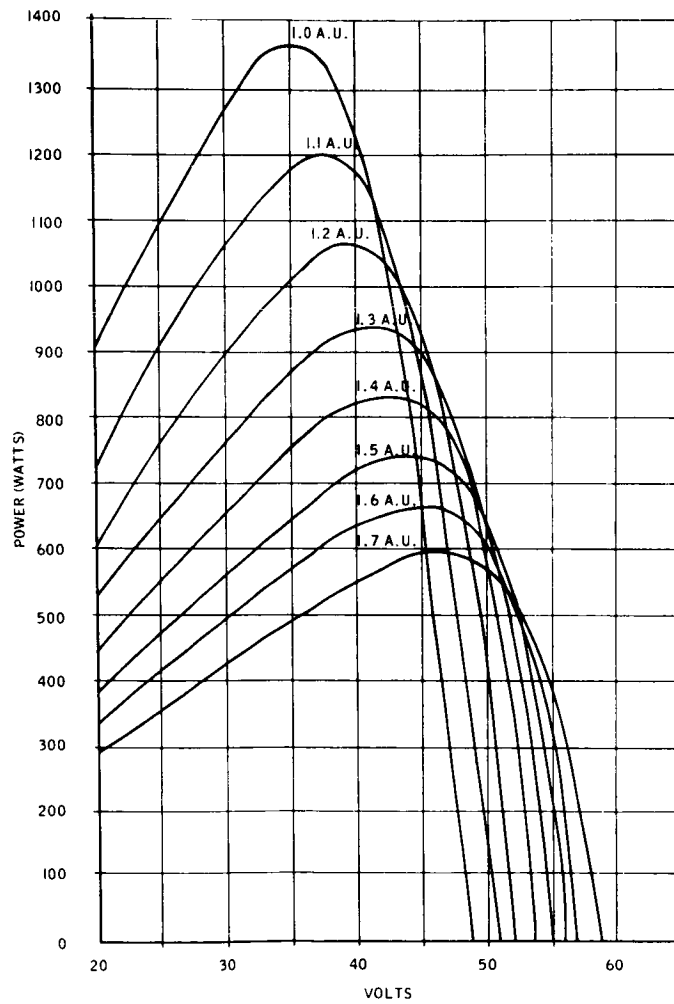


Figure 4-13. Solar Array Power-Voltage Characteristics

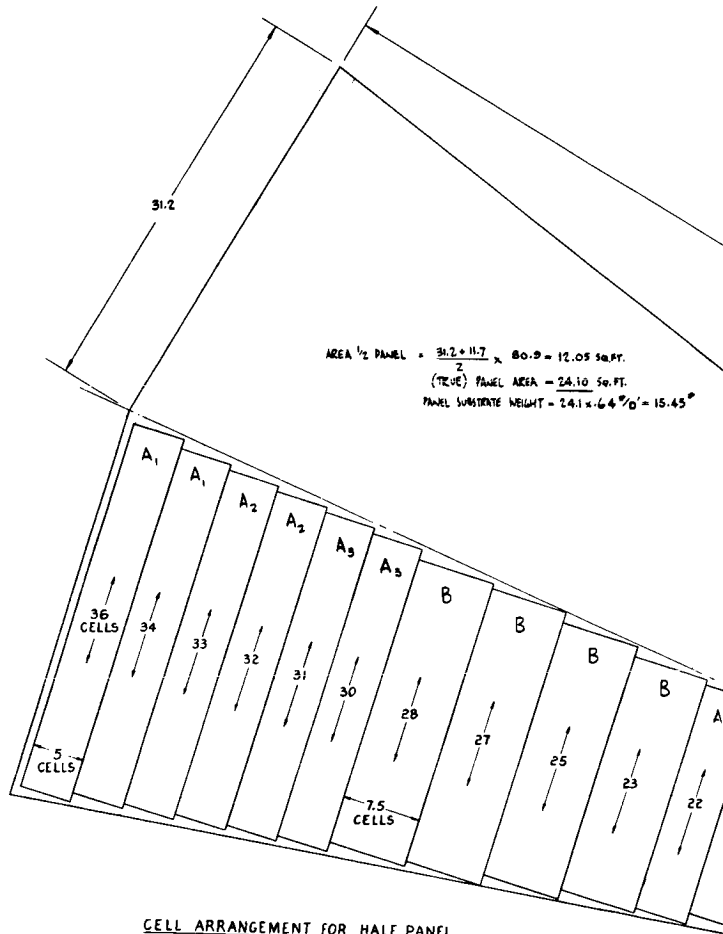
The layout of the solar cells is shown for typical panel sections in Figure 4-14. The solar cell string arrangement is summarized below:

String type:	A	B	C	D	E
Cells in series:	103	103	112	112	115
Cells in parallel:	5	7-1/2	8	9	6
Number of strings:	51	17	3	3	8
Number of cells:	26, 265	13, 132	2688	3024	5520

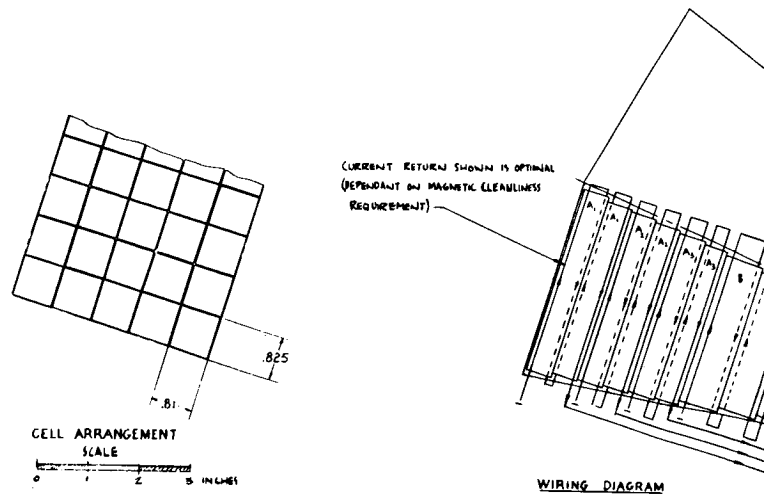
The total number of cells (2 cm x 2 cm) is 50, 629. The net active area of cells is 207.1 ft²; taking into account the angle of solar incidence, the net projected active area of solar cells is 189.1 ft². In spite of the fact that the projected area of the array is greater than the Task B array, its power output is approximately the same because of the higher temperature resulting from the increased thermal radiation blockage caused by locating the array closer to the lander.

The solar array performance characteristics (voltage-current and power-voltage) are based on performance factors used for the Task B design. A computerized technique is used to predict the overall array characteristics and takes into account the series and parallel arrangement of the solar cells, panel temperature distributions plus initial cell efficiency and derating factors. These are listed below for reference purposes:

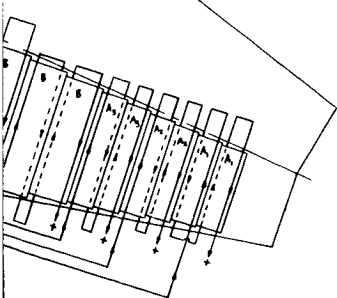
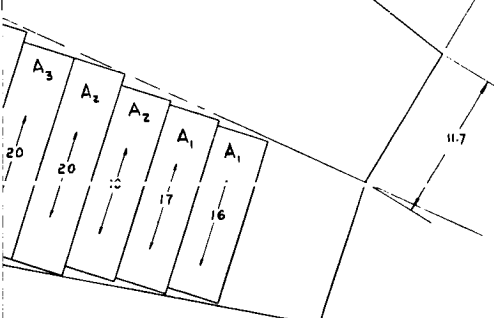
Bare Cell Efficiency (N-P type) @ air mass = zero	
and cell temperature = 25° C	11%
Short Circuit Current Degradation Factors	
Filter transmission loss	.94
Micrometeoroid effects and random failures	.95
Radiation	.879
Uncertainties	.9265
(Computed from rms of:	
mismatch and manufacturing	= 2%
measurement uncertainty	= 5%
UV	= 5%
Variation in solar intensity	= (AU) ⁻²
Voltage Degradation Factor	
Radiation	.981



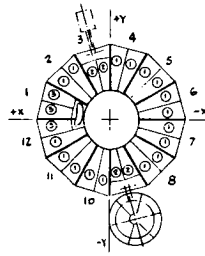
CELL ARRANGEMENT FOR HALF PANEL
 TYPICAL 17 PLACES @



80.9 (12.6)



CELL ARRANGEMENT FOR HALF PANEL
4 PLACES AT H.G.A. AND P.S.P LOCATIONS ①

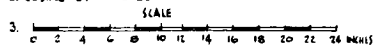


KEY TO TABLE
(NO SCALE)

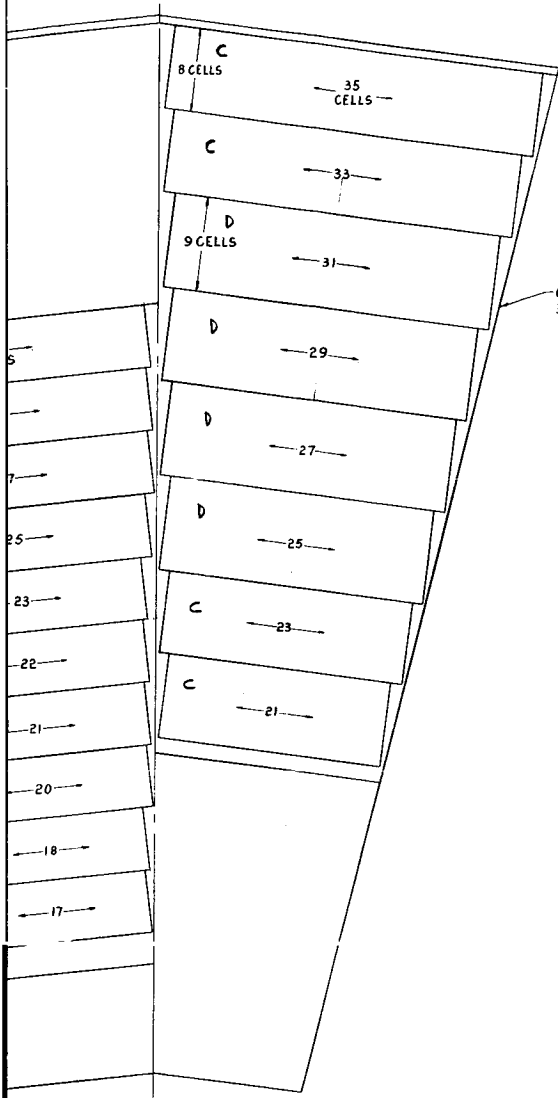
1/2 PANEL CONFIGURATION	CELL ARRANGEMENT	N NUMBER OF CELLS	CELL WT (0.01974) P PER 1/2 PANEL	NUMBER OF 1/2 PANELS	TOTAL No OF CELLS
①	3 'A' STRINGS 105 x 5 = 5	1545	5.64	17	26265
	1 'B' STRING 105 x 7.5 = 1	772.5			13132.5
		2317.5			
②	2 'E' STRINGS 115 x 6 = 2	1380	2.17	4	5520
③	1 'C' STRING 112 x 8 = 1	896	2.99	3	2688
	1 'D' STRING 112 x 9 = 1	1008			3024
		1904			
TOTALS-		79.53	24		50625.5

NOTES. 1. TOTAL PROJECTED ACTIVE CELL AREA, = 180.1 SQ. FT.
(DOES NOT INCLUDE CELL SOLDER CONTACT AREA)

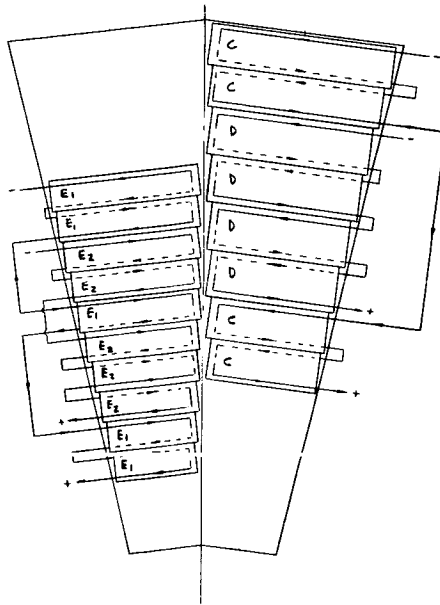
2. COSINE 24° = .9135



4-22-1



CELL ARRANGEMENT FOR HALF PANEL
3 PLACES AT BACK UP ANTENNA LOCATION



WIRING DIAGRAM

Figure 4-14. Solar Panel Layouts

4.4.1.2 Battery

The reduction in unregulated bus voltage requires a reduction in the number of cells in series. For the same power profile as in Task B, the ampere-hour capacity of the cells must be increased. The revised battery size is summarized:

	<u>Task B</u>	<u>This Design</u>
Ag-Cd Batteries	2	2
Cells in Series	33	27
Cell Capacity	20 a-hr	25 a-hr
Charge Voltage Limits	A: 50.4 v B: 48.8 v C: 47.3 v	A : 40.5 v (charge) A': 38.3 v (float) B : 39.0 v (charge) B': 36.9 v (float)
Ag-Zn Batteries	1	1
Cells in Series	24	24
Cell Capacity	50 a-hr	60 a-hr
Charge Voltage Limits	A: 46.5 v B: 44.6 v C: 42.7 v	A : 38.8 v (charge) A': 37.4 v (float) B : 36.9 v (charge) B': 35.5 v (float)
Charge Current Limit (sum)	3.75 amp	4.6 amp

The battery energy capacity, weight, volume, and general description will be approximately the same as the Task B batteries.

4.4.1.3 Battery Charge Regulators

The battery charge regulators will be changed from that for Task B in three areas: (1) the general voltage limit range will be lowered to accommodate the reduced number of cells

in series in both types of batteries; (2) a provision will be included to reduce the charge voltage to the open-circuit voltage after charging is complete; and (3) the charge current limits will be increased as noted previously.

The results of tests made during MSD's Battery Performance Test Program (DA L05-31) have shown that gas evolution in both Ag-Cd and Ag-Zn cells is reduced to negligible levels by lowering the charge voltage imposed on the cells to their open-circuit voltage after the cells are completely charged. The voltage combinations found to be most advantageous for securing full charge with minimum gassing are:

Cell type	Ag-Cd	Ag-Zn
Charge voltage per cell	1.50 v	1.94 v
Float voltage per cell	1.42 v	1.87 v

A two-step charger to perform this function was developed, built, and is being utilized as part of this test program. The charger is still basically a current-limit, voltage-limit charger as described for Task B. Using this type of charger, the battery voltage early in charge is low, while the current is being limited. Later in the charging period, the voltage limit is imposed, and the charge current will taper off as a consequence. The two-step charger senses this current tapering, and when the current has fallen to half of its limit value, the charger will automatically switch to the lower float voltage limit. A subsequent discharge will reset the charger for the next charge cycle through the action of the charge current interruption.

The voltage limits imposed by the charger are indicated in the battery description, A and B being the charge voltage limits, with A' and B' the float voltage limits. A and A' are for the full complement of cells, and B and B' are provisions to allow for the short failure of one cell in series, to be set by ground command.

4.4.1.4 Power Conditioning Equipment

A major parameter in selecting the design of the voltage regulator and inverters is the voltage level chosen for the regulated bus. One solution calls for the use of as high a regulated

voltage as possible, in this case 24 volts, limited by the minimum battery discharge voltage of 26 volts. An alternative is to consider a 20-volt bus, to make the inverters interchangeable between the RTG and PV/ Battery power subsystems. The tradeoff between these two voltages is affected by efficiency considerations.

Lowering the output voltage of the series switching regulator from 24 volts to 20 volts will result in a net loss of regulator efficiency estimated to be slightly less than 2 percent. Lowering the input voltage to the inverters would also result in a loss in efficiency for the same basic design. However, where a 24-volt would be marginally too high, the 20 volt input will permit the use of germanium switching transistors in the output stages of the inverters, instead of the silicon transistors selected for the Task B study. This change would result in a net increase in inverter efficiency of approximately 3 percent in going from a 24-volt regulated bus to a 20-volt regulated bus. Thus, the overall efficiency of the regulator-inverter combination would be slightly higher using a 20-volt bus.

The regulated bus voltage was selected to be 20 volts, since this also allows interchangeability of the inverters between the RTG power subsystem and the PV/ Battery power subsystem. The main (series switching) regulator would be essentially the same as for Task B, with design changes in the voltage reference and output filter to accommodate the lower 20-volt regulated output.

The inverters' transistor output stages would be redesigned from the Task B designs to utilize germanium switching transistors. Design changes would also be required in the transformers to accept the lower input voltage.

It is estimated that the overall regulator - inverter efficiency will be the same as for Task B.

4.4.2 Other Subsystems

Aside from the Power Subsystem, other subsystems are essentially identical to those described in the Task B report.

4.5 INTERCHANGEABILITY SUMMARY

The items described below are those principally affected in converting the spacecraft from a solar powered version to an RTG powered version. No consideration is given to items outside of the spacecraft (e. g., the need for additional ground cooling or modification to OSE).

4.5.1 POWER

- a. Power source - Replace solar panels with RTG's and associated mounting panels.
- b. Bay No. 1 Equipment.
 - 1. Replace 43 lb Ag-Cd battery with 14 lb Ag-Cd battery.
 - 2. Modify battery charge regulator for smaller battery.
 - 3. Replace Main Regulator with battery discharge regulator.
 - 4. Install RTG shunt circuits and partial shunt controls.
- c. Bay No. 2 Equipment
 - 1. Replace 43 lb Ag-Cd battery with 14 lb Ag-Cd battery.
 - 2. Modify battery charge regulator for smaller battery.
 - 3. Replace Main Regulator with battery discharge regulator.
 - 4. Install RTG shunt circuits.
- d. Bay No. 8 Equipment
 - 1. Remove 35 lb Ag-Zn battery.
 - 2. Remove battery charge regulator.
- e. Load Interface

Table 4-4 compares bus voltages for the solar and RTG powered spacecraft and indicates the range for which user equipment must be designed to achieve interchangeability.

TABLE 4-4. LOAD INTERFACE TABLE

Bus	User	RTG Spacecraft	Voltage Solar Powered Spacecraft	User Design Range
B	Radio, Capsule	20 VDC \pm 1%	26-50 VDC	20-50 VDC
A	Intermittent loads: Solenoids, thrust vector control, etc.	26-40 VDC	26-40 VDC	26-40 VDC
C	Spacecraft and Science Loads	2.4 KHz, 1 ϕ 50V rms	→	→
D	Spacecraft and Science Loads	2.4 KHz, 1 ϕ 50V rms	→	→
E	Gyros	400 Hz, 3 ϕ 26V rms	→	→
F	Gyros	400 Hz, 3 ϕ 26V rms	→	→
G	Science	400 Hz, 1 ϕ 28V rms	→	→

4.5.2 GUIDANCE AND CONTROL

- a. Replace null Sun sensors with digital Sun sensors.
- b. Bay No. 5 Equipment - Modify Attitude Control Electronics to accept digital Sun sensor input and C & S Sun-bias input.
- c. Relocate sensor mounting block from +X to -X location.

4.5.3 COMPUTER AND SEQUENCER

- a. Incorporate logic modifications for Sun-bias mode of operation.

4.5.4 COMMUNICATIONS

- a. Bay Equipment (bays 7 to 11) — Logic and circuit modifications to accommodate:
 - 1. Communications modes of operation associated with Sun-biased attitude control system.
 - 2. Revised telemetry format (e.g., RTG inputs replace solar panel and battery inputs).
 - 3. Revised command requirements.
- b. High-gain antenna — Replace articulated HGA with fixed HGA.
- c. Medium-gain antenna — Replace backup antenna used at encounter with mid-course medium-gain antenna.

4.5.5 STRUCTURE

Install shelf to provide equipment bay shading during Sun-biased operational mode.

4.5.6 SCIENCE

Incorporate radiation shielding, extension booms, or thermal shielding as may be required for specific instruments for compatibility with the RTG Radiation environment.

4.5.7 HARNESS

Modification is required for above items.

SECTION 5

SUPPORTING STUDIES

5.1 RTG SIZING RESULTS

RTG performance characteristics have been described in detail in Reference 5-1. The principal sizing results are presented below.

The characteristics are first identified in terms of beginning-of-life (BOL) performance. This is followed by a margin analysis to take account of uncertainties and degradations. A final section illustrates by example how the data should be used in specifying nominal RTG requirements.

5.1.1 BEGINNING-OF-LIFE (BOL) CHARACTERISTICS

Figure 5-1 shows the relationship of weight to power with parameters of overall length and diameter for an RTG employing a lead-telluride thermopile operating at a hot junction of 1100° F. The range of designs represented in this plot is optimized in the sense that for given power and length requirements, a cold junction temperature is selected that results in minimum RTG weight. For other cold junction temperatures, weight is increased either because of decreased thermopile efficiency (as in the case of higher cold junction temperature) or because of increased heat rejection fin size (as in the case of lower cold junction temperatures). Thus the existence of an optimum cold junction temperature is intuitively apparent. Figure 5-2 shows the resultant cold junction temperatures.

Figures 5-3 and 5-4 present similar information for a Pb-Te hot junction temperature at 1050° F. Optimum designs at hot junction temperatures in the range of 1000 to 1200° F may be determined by linear interpolation or extrapolation of the data of Figures 5-1 through 5-4.

Generator efficiency (ratio of electrical power to thermal power) is shown in Figure 5-5 for Pb-Te RTG's as a function of cold junction temperature with parameters of hot junction temperature.

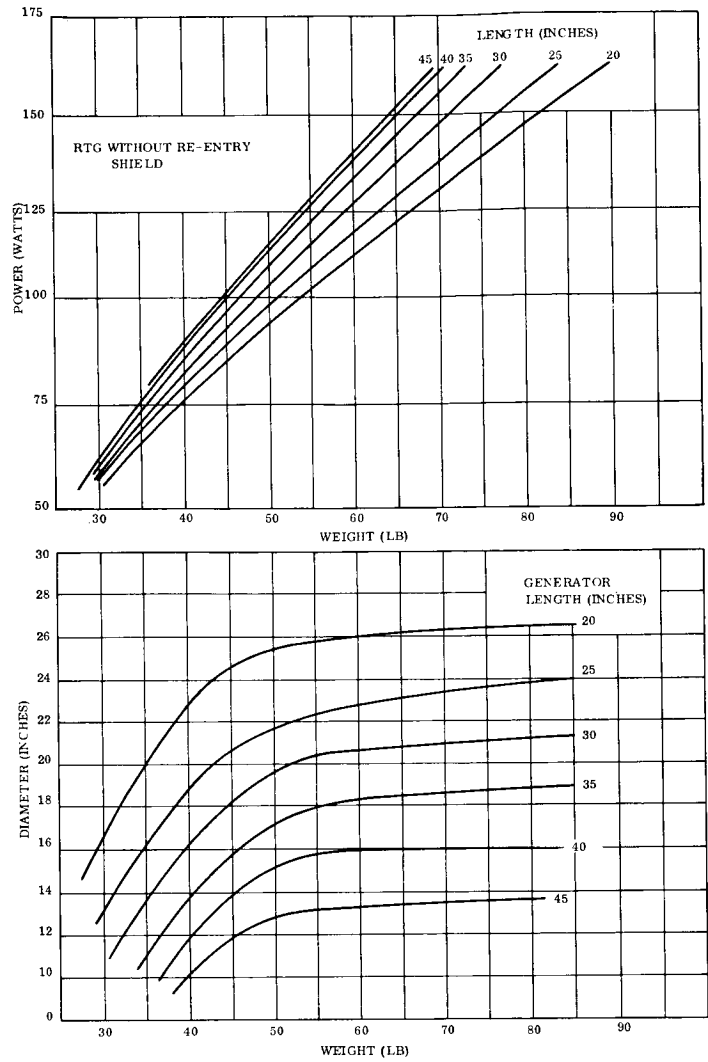


Figure 5-1. Weight, Power, Length and Diameter Relationships for Pb-Te Thermopile RTG's, 1100° F Hot Junction Temperature

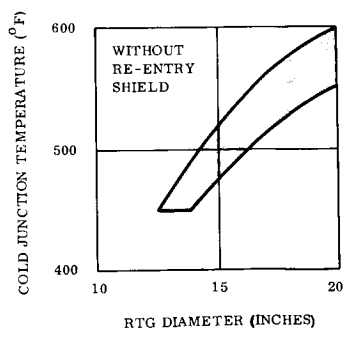


Figure 5-2. Cold Junction Temperature vs RTG Diameter for Pb-Te Thermopile RTG's, 1100° F Hot Junction Temperature

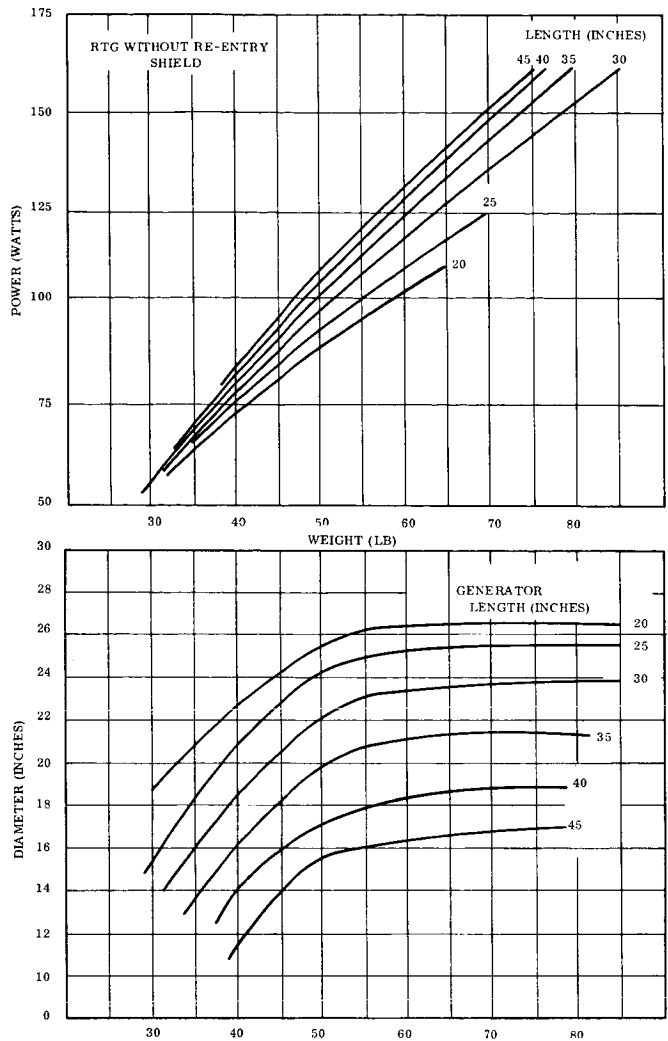


Figure 5-3. Weight, Power, Length and Diameter Relationships for Pb-Te Thermopile RTG's, 1050° F Hot Junction Temperature

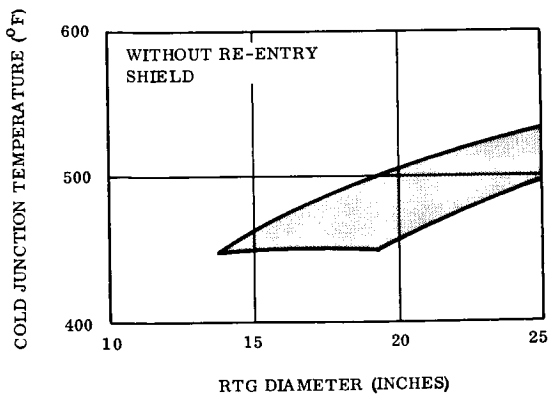


Figure 5-4. Cold Junction Temperature vs RTG Diameter for Pb-Te Thermopile RTG's, 1050° F Hot Junction Temperature

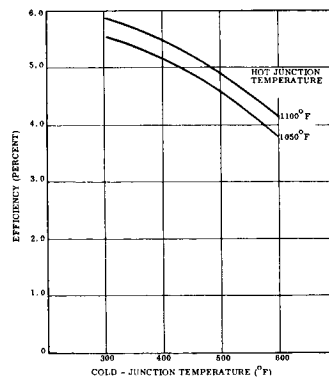


Figure 5-5. Efficiency vs Cold Junction Temperature for Pb-Te Thermopile RTG's, 1050° F Hot Junction Temperature

With the above data, it is possible to determine the range of weight, dimensions, thermal power, and cold junction temperatures for given BOL power requirements. It is emphasized that the data applies to BOL characteristics and does not include allowance for time-dependent degradations. These are treated later in Section 5.1.2.

Corresponding curves for RTG's employing silicon-germanium thermopiles are shown in Figures 5-6 through 5-12.

The RTG's described above are based on heat rejection to a sink temperature of -10°F to the space above the mounting plane of the RTG. This temperature is roughly equivalent to the combined effect of black space at 0°R and solar input at 1 AU. The mounting plane itself is assumed to be adiabatic. The effect of reducing the heat rejection view factor by recessing the RTG below the mounting plane is shown in Figures 5-13 and 5-14, which identify weight and diameter corrections factors. To illustrate their use, assume a 75-watt Pb-Te RTG at an 1100°F hot junction temperature of 30-inch length is required, and is to be installed such that δ/L equals 0.25. Figure 5-1 indicates a weight of 36.5 pounds and a diameter of 16.5 inches. Applying the weight correction factor of 0.05 lb/watt from Figure 5-13 and the diameter correction factor of 28 percent from Figure 5-14 results in modified values of 40.25 lb and 21 inches for the weight and diameter respectively. These correction factors, determined specifically for 75-watt Pb-Te RTG's, are considered to be sufficiently accurate to identify nominal changes for other power ranges for either Pb-Te or Si-Ge thermopiles.

Figure 5-15 provides an estimate of changes in RTG temperature level resulting from heat rejection to sink temperatures higher than -10°F . No first-order changes in thermopile efficiency result when the sink temperature is higher than design. Continued operation at elevated hot junction temperatures results in higher degradation rates.

The weight associated with fuel containment re-entry protection (estimated in Figure 5-16) is to be added to the RTG weight identified earlier.

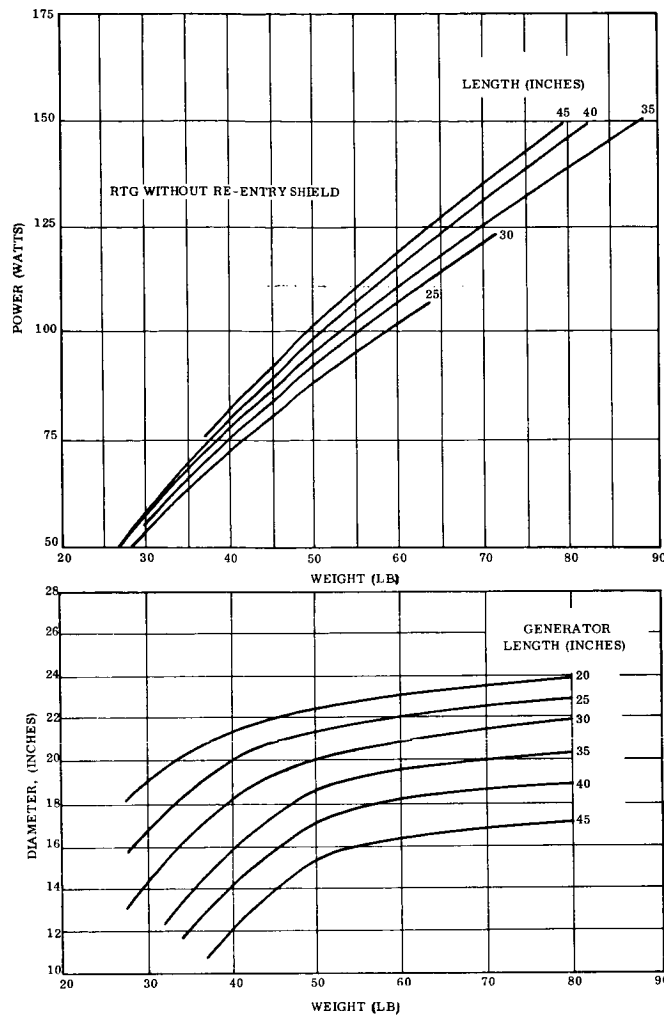


Figure 5-6. Weight, Power, Length and Diameter Relationships for Si-Ge Thermopile RTG's, 1200° F Hot Junction Temperature

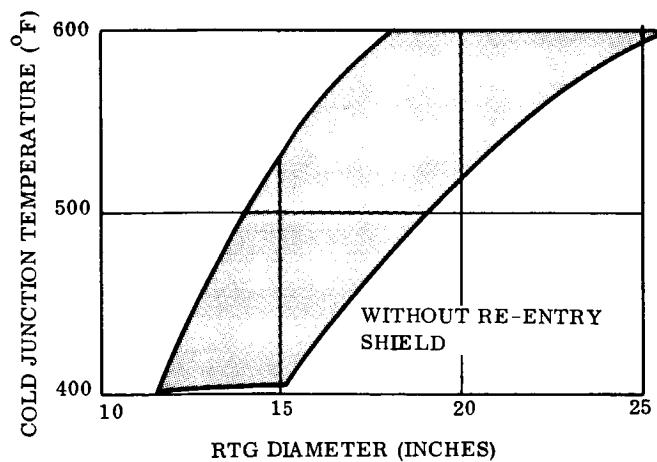


Figure 5-7. Cold Junction Temperature vs RTG Diameter for Si-Ge Thermopile RTG's, 1200° F Hot Junction Temperature

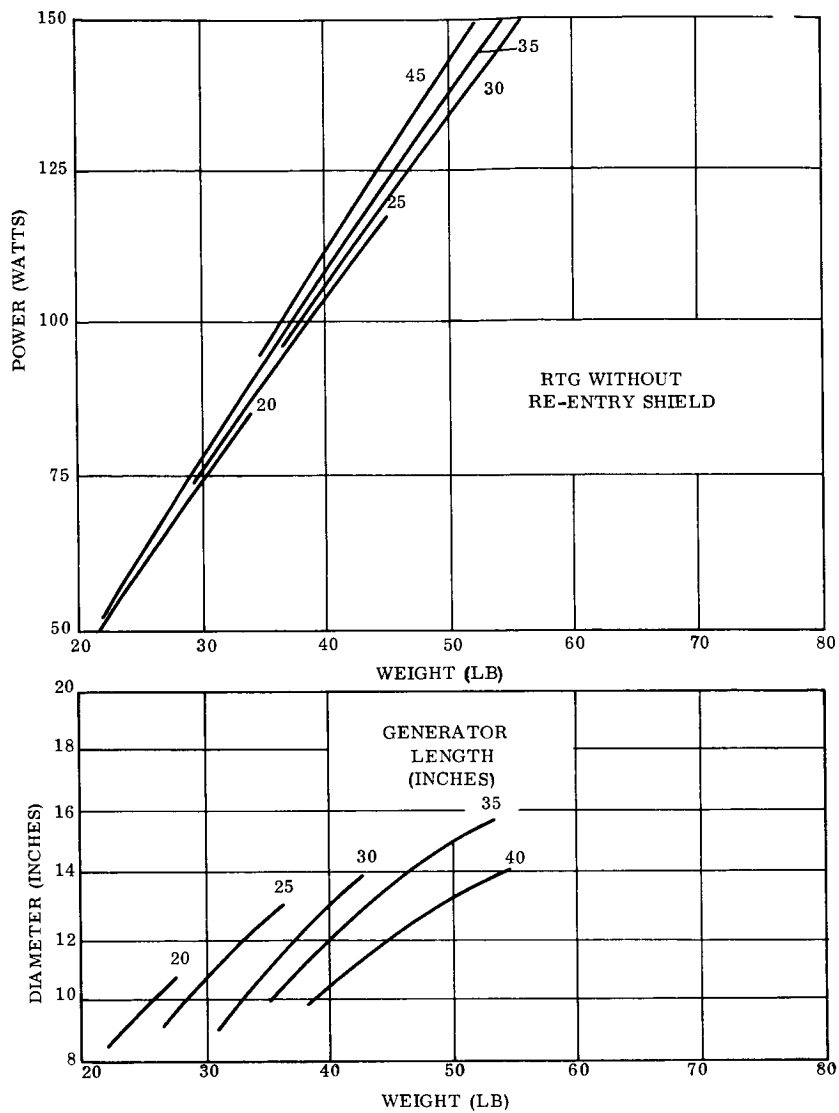


Figure 5-8. Weight, Power, Length and Diameter Relationships for Si-Ge Thermopile RTG's, 1400° F Hot Junction Temperature

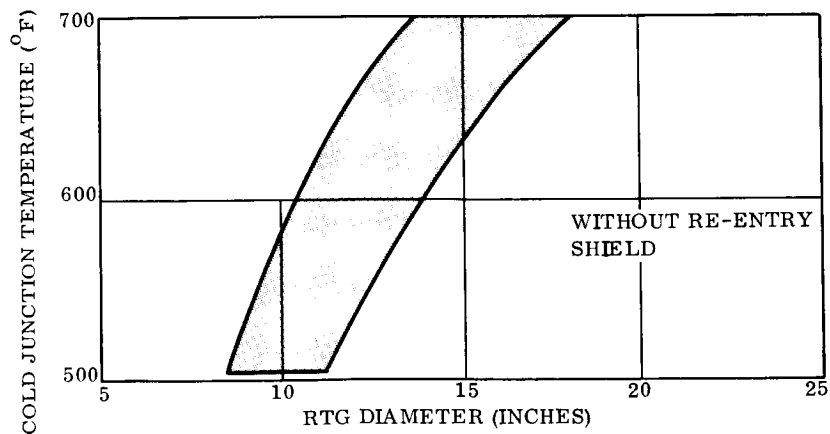


Figure 5-9. Cold Junction Temperature vs RTG Diameter for Si-Ge Thermopile RTG's, 1400° F Hot Junction Temperature

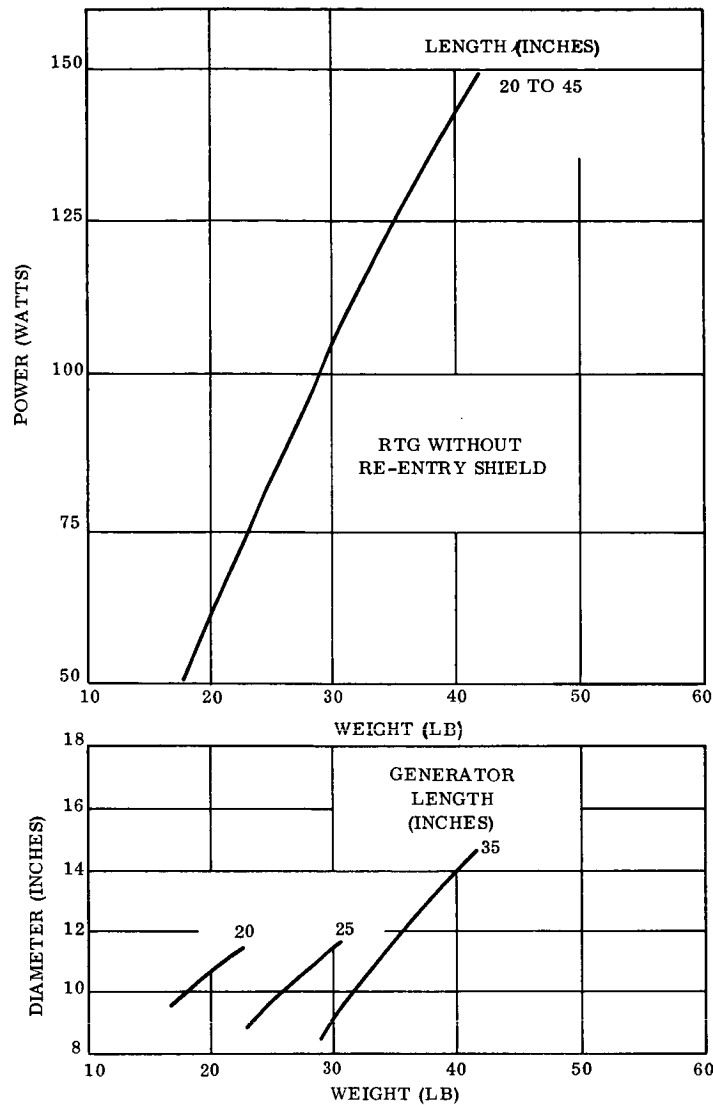


Figure 5-10. Weight, Power, Length and Diameter Relationships for Si-Ge Thermopile RTG's, 1600^oF Hot Junction Temperature

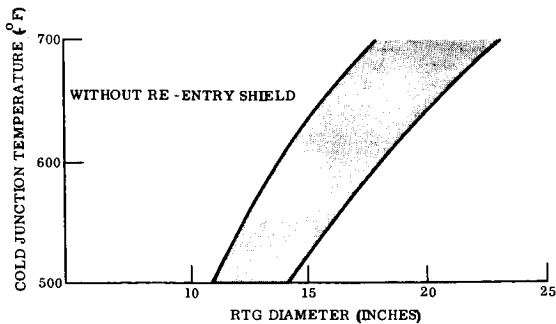


Figure 5-11. Cold Junction Temperature vs RTG Diameter for Si-Ge Thermopile RTG's, 1600^oF Hot Junction Temperature

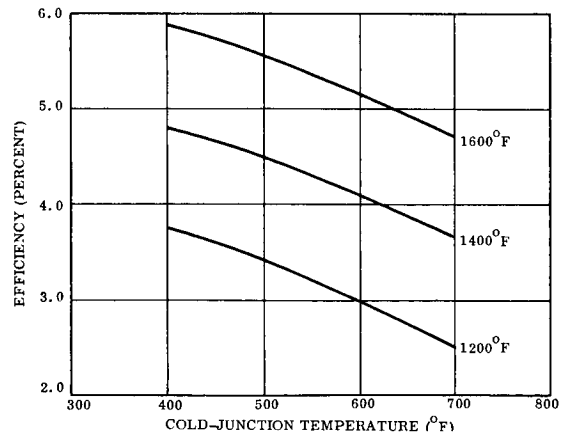


Figure 5-12. Efficiency vs Cold Junction Temperature for Si-Ge Thermopile RTG's

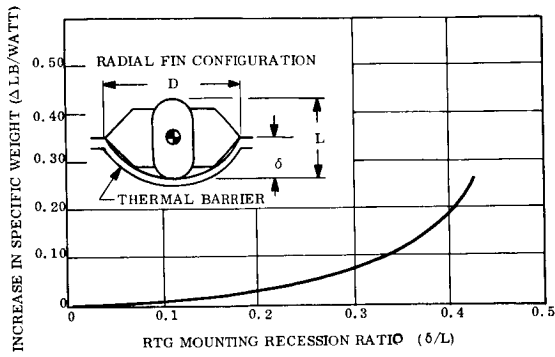


Figure 5-13. Weight Correction for Recessed RTG's

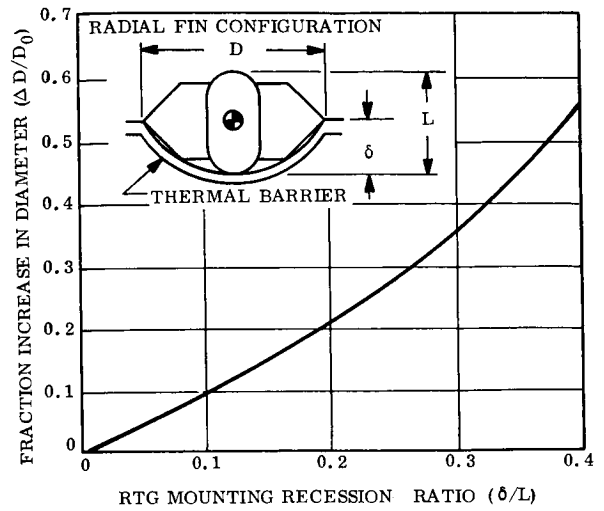


Figure 5-14. Diameter Correction for Recessed RTG's

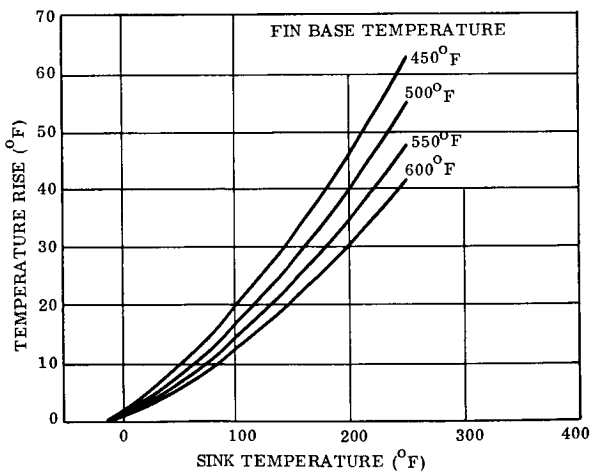


Figure 5-15. RTG Temperature Rise vs Sink Temperature

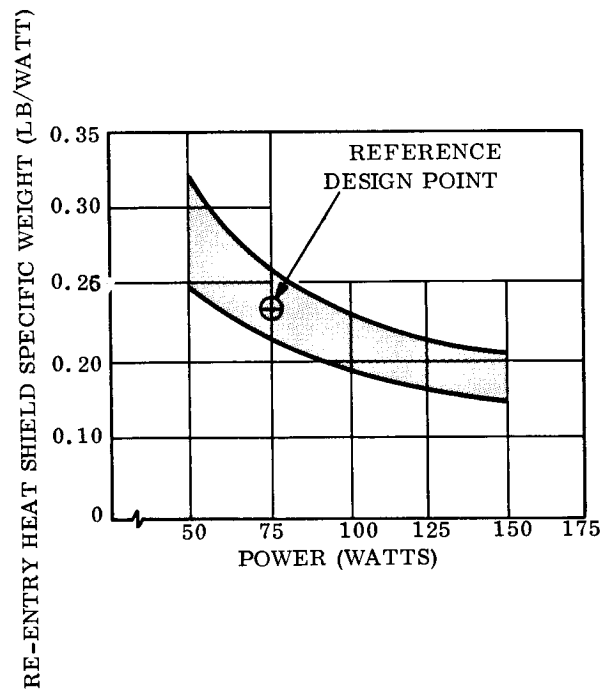


Figure 5-16. RTG Re-entry Protection Weight

5.1.2 MARGIN ANALYSIS

The predicted BOL performance discussed in Section 5.1.1 is largely based on recent experience with the SNAP-27 RTG development. The SNAP-27 RTG originally had an end-of-life (EOL) power design goal of 56 watts after 10,000 hours of operation. Early production models indicate BOL power output in excess of 70 watts with predicted EOL power not less than 64 watts. The generator is currently specified as a 64-watt (EOL) device. The original 16 percent excess EOL power capability may be attributed to initially conservative estimates in the thermal analysis and in the prediction of thermoelectric performance. The BOL data described in Section 5.1.1 has taken this performance gain into account and is still considered to contain some measure of conservatism. From the limited data of operational SNAP-27 generators, this is estimated to be between 0-5 percent.

In the development of a detailed RTG design many uncertainties (such as thermal leaks, contact resistance) must be taken into account. A point is ultimately reached when actual RTG performance can be measured and adjusted. As long as the design uncertainties have been conservatively taken into account it is always possible to adjust the amount of isotope fuel such that the required BOL power is produced at the required voltage level. In this sense these design uncertainties do not fall in the category of design margins, since they can be totally compensated for. Margins are related more to the accuracy of the compensation and to time-dependent degradations. To illustrate the difference, suppose a particular RTG is to be designed at BOL to produce 75 watts at rated voltage at a hot junction of 1100°F. The predicted thermal power input is 1800 watts. In actual test the RTG delivers 85 watts at rated voltage with an 1100°F hot junction temperature and a thermal power of only 1750 watts. A reduction in thermal power permits adjustment to the required 75 watt BOL level with a corresponding drop in the hot junction temperature. This results in a beneficial reduction in fuel inventory and in extended life capability because of reduced temperature operation although of course advantage can be taken of the additional power available. No margins in BOL power are necessary for these uncertainties since their effect has been nullified. Uncertainty of the installed thermal power, on the other hand, cannot be totally compensated for and this identifies one of the margin elements. Only those margin elements falling in this latter category are discussed below.

5.1.2.1 Fuel Loading Uncertainty

In adjusting the thermal power to achieve a required BOL power, electrically heated fuel capsule simulators are used. By current and voltage measurements the thermal power can be determined with high accuracy. In duplicating this thermal power with actual isotope fuel, uncertainties in the power density and in metering the necessary amount of fuel result in an overall thermal power uncertainty of 1 to 3 percent, depending on the fueling technique. This is reflected as a BOL power uncertainty of about 1.5 to 4.5 percent as analyzed below.

The generator output can be expressed by:

$$\text{Power} = \eta_{\text{carnot}} \eta_{\text{material}} Q$$

where

$$\eta_{\text{carnot}} = \frac{\Delta T}{T_{\text{hot}}} = \frac{T_{\text{hot}} - T_{\text{cold}}}{T_{\text{hot}}}$$

η_{material} = the thermoelectric efficiency

Q = thermal power

For a fixed value of the materials efficiency

$$\frac{dP}{P} = \frac{d\eta_c}{\eta_c} + \frac{dQ}{Q} \quad (1)$$

It can be shown that, for a fixed value of T_c ,

$$\frac{d\eta_c}{\eta_c} = (1 - \eta_c) \frac{dQ}{Q} \quad (2)$$

Substituting Equation 2 in Equation 1 gives

$$\begin{aligned} \frac{dP}{P} &= (1 - \eta_c) \frac{dQ}{Q} + \frac{dQ}{Q} \\ &= (2 - \eta_c) \frac{dQ}{Q} \end{aligned}$$

With a hot junction temperature of about 1100° F and a cold junction temperature of 400° F, η_c equals about 0.5. This shows that a 2 percent change in the thermal power, Q , results in about 3 percent change in power.

5.1.2.2 Fuel Decay Margin

Proper adjustment of BOL power must take account of the isotope fuel decay properties. For plutonium-238 fuel (89.6 year half-life), Figure 5-17 shows the additional percentage of thermal loading required as a function of time.

5.1.2.3 Thermoelectric Degradation

Based on estimated extrapolation of laboratory test data, Figure 5-18 shows the ratio of EOL power to BOL power as a function of mission time for various hot junction temperatures. This data pertains to lead-telluride thermopiles of the type used on the SNAP-27 RTG.

Figure 5-19 shows similar data for silicon-germanium thermopiles.

5.1.2.4 Thermocouple Open and Short Circuit Failures

Based on an estimated occurrence of thermocouple open, short circuit, or fault to ground failures the predicted EOL/BOL ratio is shown in Figure 5-20 for several values of reliability.

5.1.2.5 Emissive Coating Degradation

The effect of changes in the properties of the coatings on the RTG heat rejection fins are considered to be included in the BOL data, and therefore no EOL/BOL allowance is used.

5.1.2.6 Net Degradation

The time-dependent degradations identified in Sections 5.1.2.2., 5.1.2.3 and 5.1.2.4 are combined and shown in Figure 5-21 for Pb-Te RTG's and in Figure 5-22 for Si-Ge RTG's (for a 0.990 reliability). This data may be combined with BOL data to indicate the hot junction temperature that results in least RTG weight for given lengths of operation. For example, from Figure 5-21 the EOL/BOL ratio is 0.75 for an 1100° F hot junction temperature after 3 years. Thus the BOL requirement for a 75-watt EOL RTG is 100 watts. The most

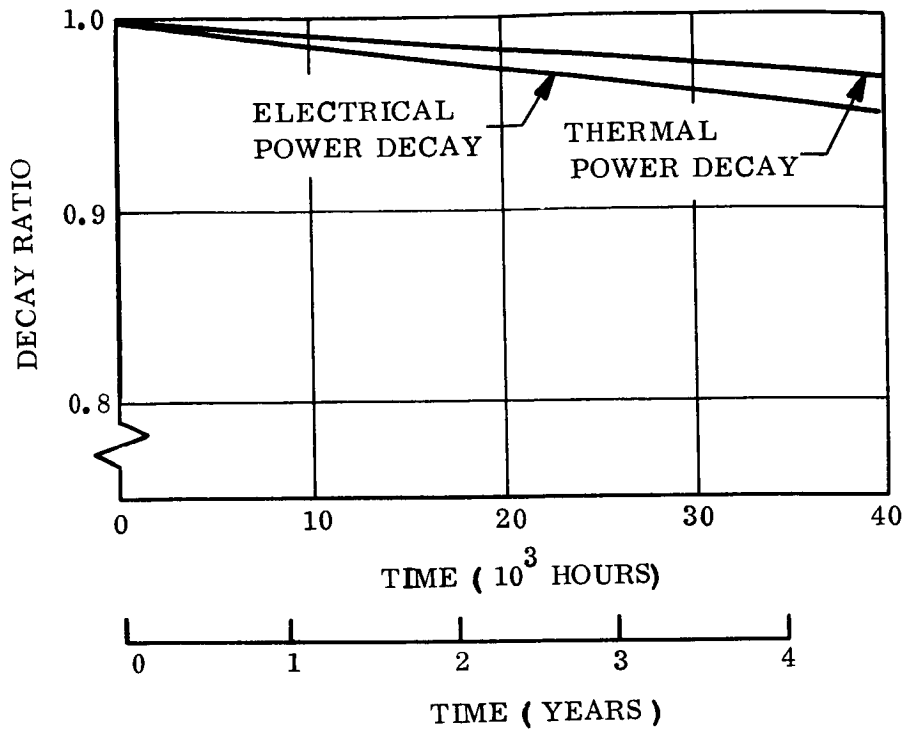


Figure 5-17. Effect of Isotope Fuel Decay

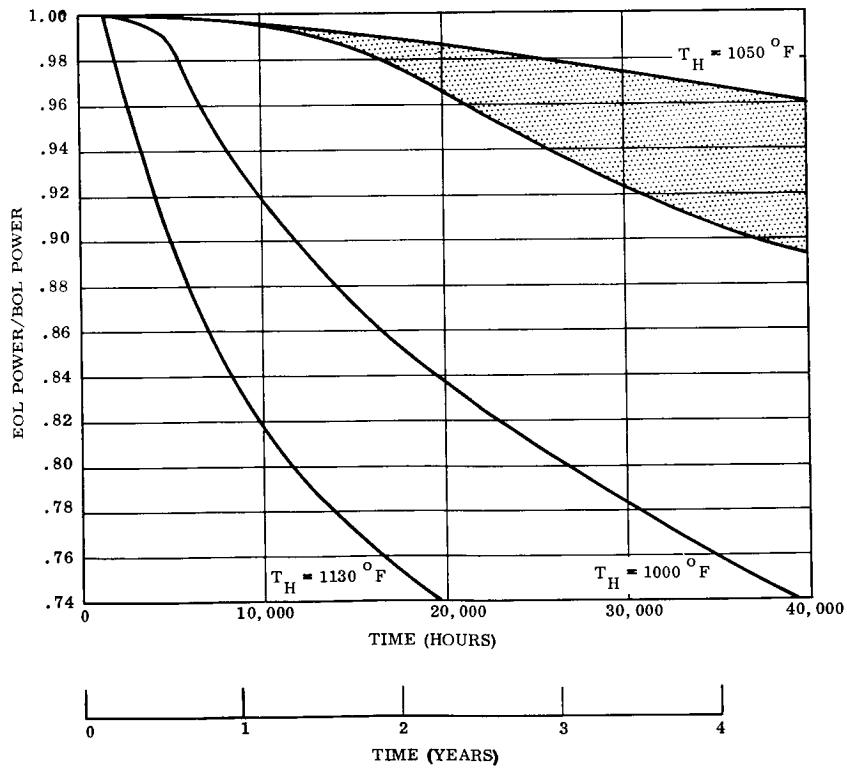


Figure 5-18. Lead-telluride Thermopile Degradation

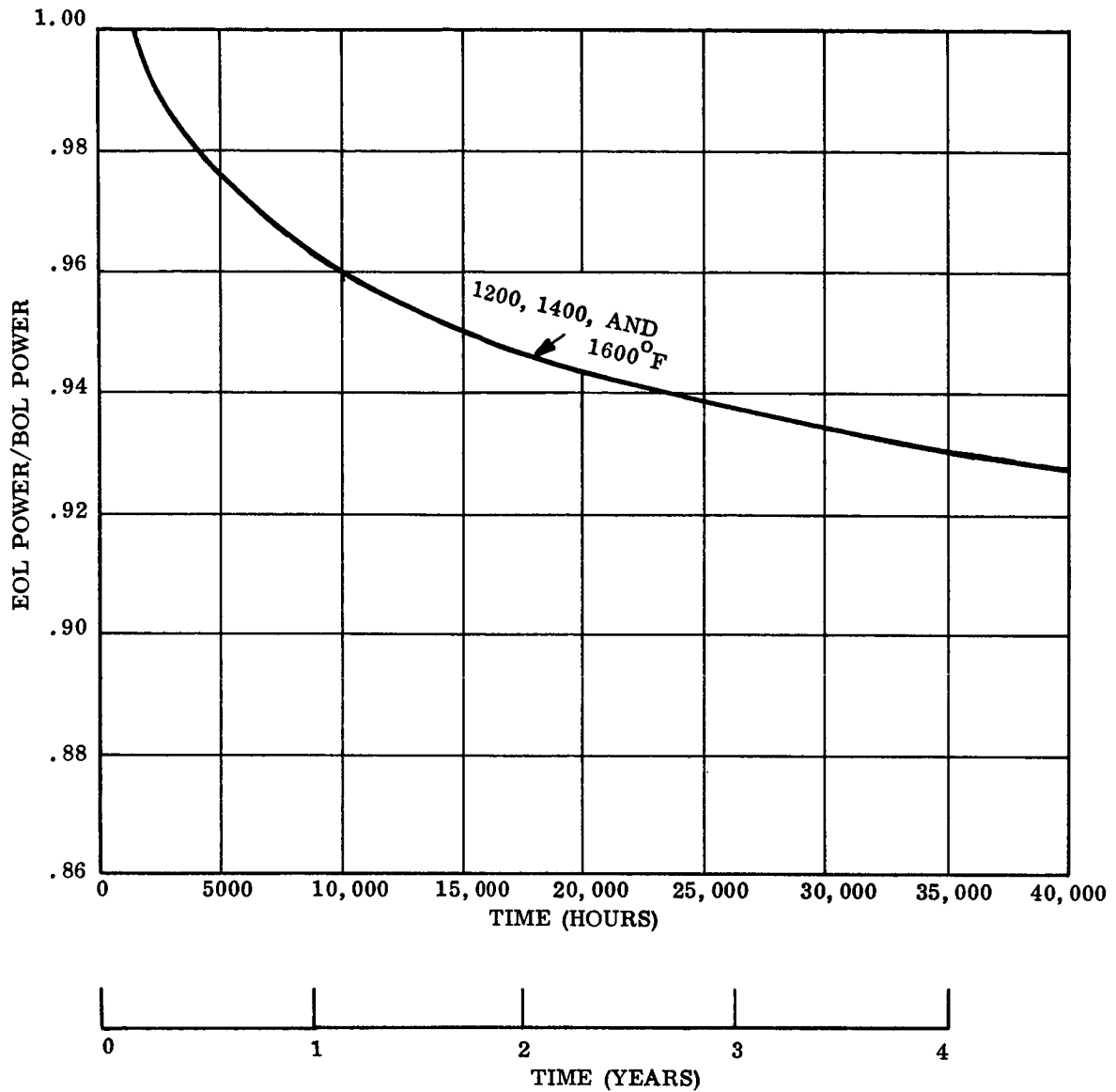


Figure 5-19. Silicon-germanium Thermopile Degradation

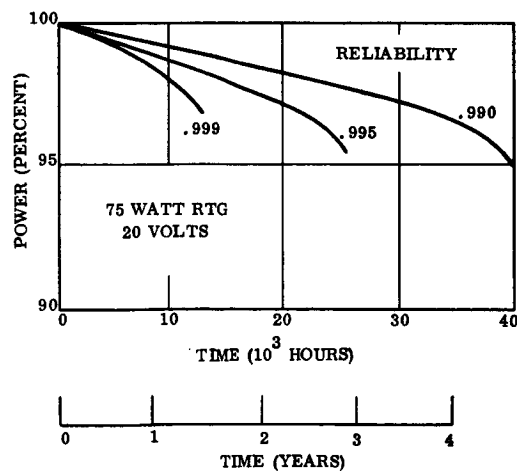


Figure 5-20. RTG Reliability Margin

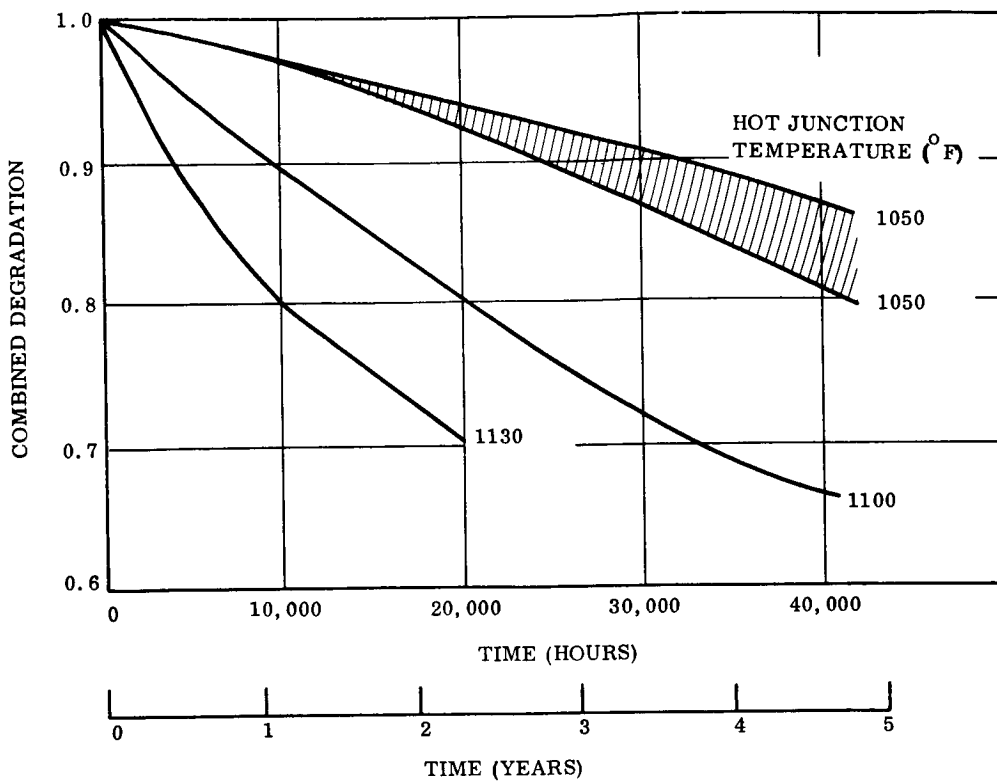


Figure 5-21. Lead-telluride RTG Combined Degradation

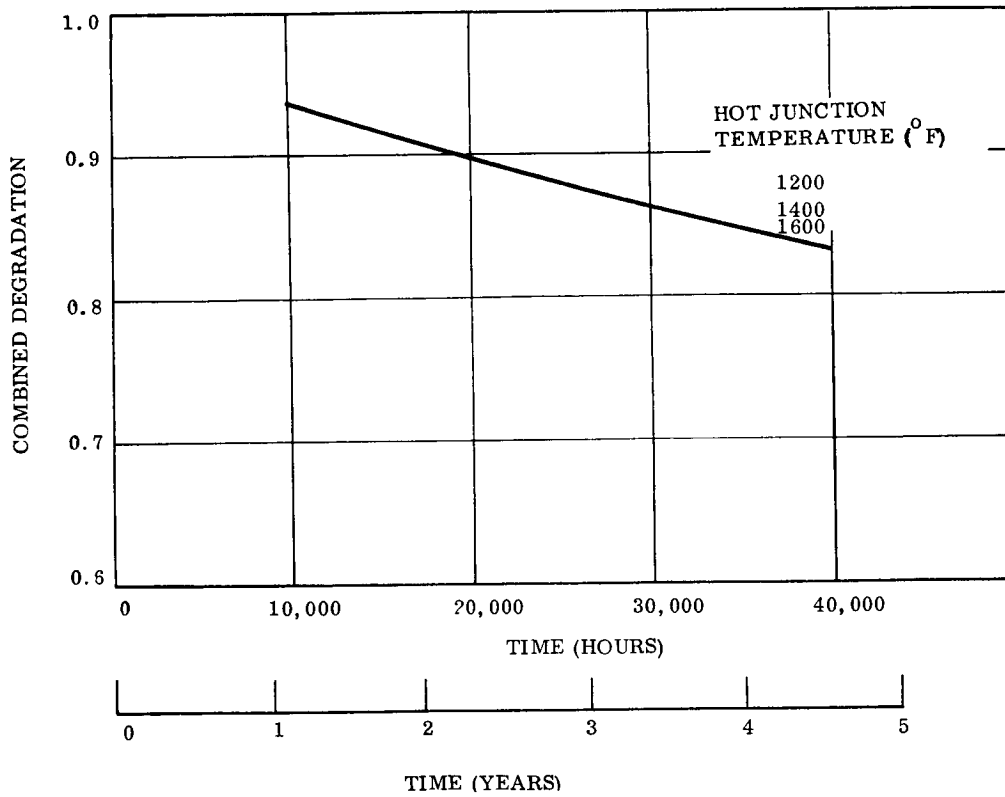


Figure 5-22. Silicon-germanium RTG Combined Degradation

optimistic weight for this is 44 pounds (not including re-entry protection) as shown in Figure 5-1. The specific weight after 3 years is then 44 pounds divided by 75 watts, or 0.585 pounds per watt. In this manner the specific power is determined as a function of operation time; this is shown in Figure 5-23 for several hot junction temperatures for the case of Pb-Te RTG's. In preparing this plot a nominal EOL power requirement of 75 watts was considered with only the most optimistic weights shown on the BOL characteristics. It is apparent that the optimum hot junction temperature selection depends on mission time.

Figure 5-24 shows the corresponding data for Si-Ge RTG's.

5.1.3 NOMINAL RTG SPECIFICATIONS

The example below shows how nominal RTG characteristics may be determined. The particular example reflects the RTG characteristics required for a Voyager Mars mission.

Example:

A lead-telluride RTG is to deliver 75 watts after 14 months of flight operation. PU-238 fuel is to be used with the assumption that fuel capsules are assembled 1 year before launch. A 3-month period is to be allowed for prelaunch RTG testing. The length should be about 25 inches with the base about 6 inches below the mounting plane. The weight, diameter, BOL power, thermal power and cold junction temperature are to be determined for preliminary design purposes.

Solution:

BOL power must be adjusted to take account of time-dependent degradation, fuel decay and fuel loading uncertainty. Each is determined separately below:

- Time-Dependent Degradation — Figure 5-23 indicates an optimum hot junction temperature of 1050 degrees F for a 17 month* period of flight operation. A corresponding EOL/BOL ratio of 0.95 is identified from Figure 5-21.
- Fuel Loading Uncertainty — As discussed in Section 5.1.2.1 the ± 2 percent fuel loading uncertainty can result in ± 3 percent variation in power. The hot junction temperature of the selected RTG design should not exceed 1050° F in order to limit the degradation to the prescribed values. To meet this constraint the BOL capability must be increased an additional 6 percent to span the range of fuel loading uncertainty.

*14 month flight plus 3 month test time

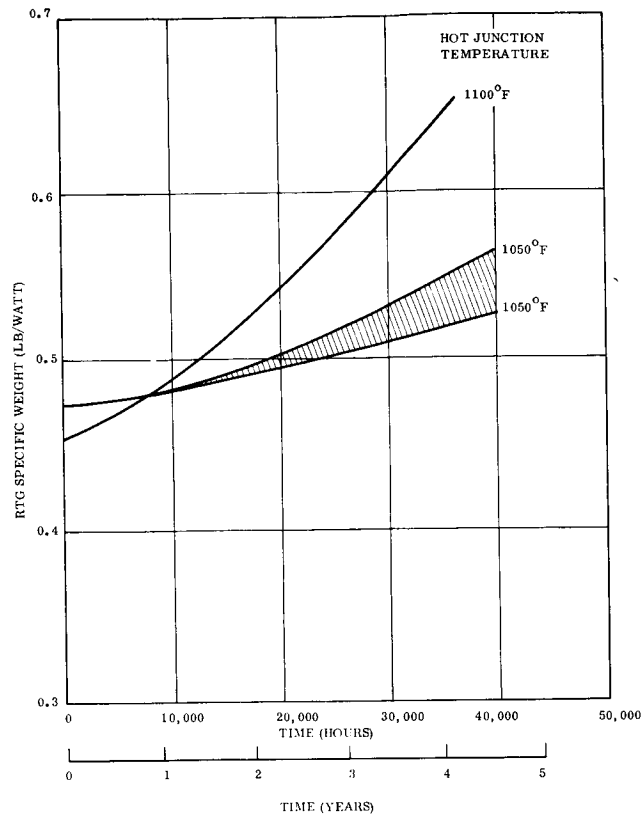


Figure 5-23. Specific Weight vs Time for Lead-telluride RTG's

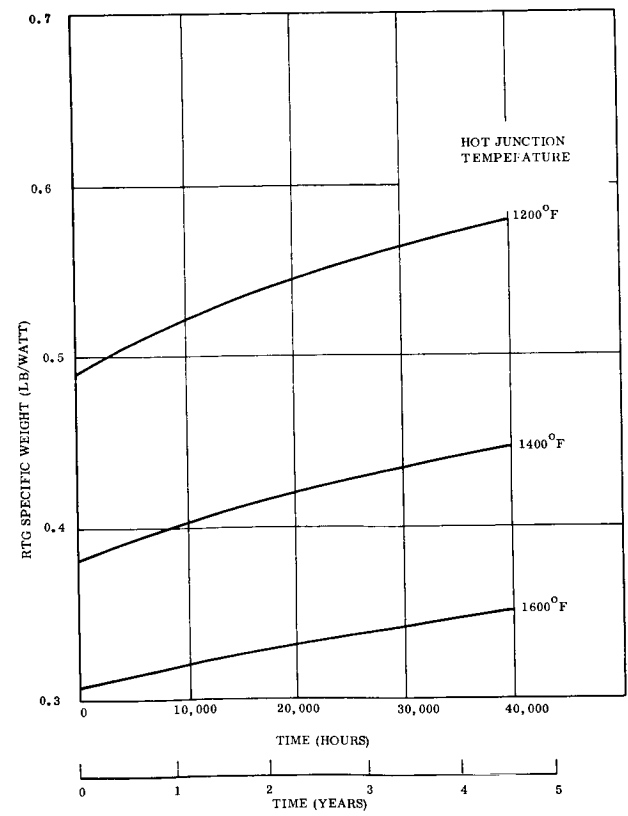


Figure 5-24. Specific Weight vs Time for Silicon-germanium RTG's

Combining these factors the net BOL power is:

$$\begin{aligned} \text{Net BOL Power} &= \frac{1}{0.95} \times 1.06 \times \text{EOL} \\ &= 1.12 \times 75 \\ &= 84 \text{ watts} \end{aligned}$$

Using the BOL characteristics described in Section 5.1.1, the nominal characteristics of the RTG are as follows:

<u>Parameter</u>	<u>Value</u>	<u>Reference</u>
Life	17 months	Given
EOL Power	75 watts	Given
Fuel	Pu-238	Given
Thermopile	Pb-Te	Given
Length	25 inches	Given
BOL Power (electrical)	84 watts	Determined above
Hot Junction Temperature	1050° F	Determined above
RTG Weight	49.2 lb	Fig. 5-3, 5-13
Re-entry Protection Weight	17 to 21 lb	Fig. 5-16
Diameter	28.4 inches	Fig. 5-3, 5-14
Cold Junction Temperature	500 ^o F	Fig. 5-4
BOL Thermal Power	1810 watts*	Fig. 5-5
EOL Thermal Power	1790 watts	Fig. 5-17
Thermal Power at Capsule Assembly	1830 watts**	Fig. 5-17

*Figure 5-5 indicates $\eta = 0.0455$ for $T_c = 500^{\circ}\text{F}$ and $T_H = 1050^{\circ}\text{F}$. This corresponds to a BOL thermal power of 1845 watts. Since this includes the higher uncertainty of fuel loading, the nominal BOL thermal power is reduced by 2 percent to the indicated 1810 watt value.

**The thermal power at the time of capsule assembly is obtained by the thermal power correction factor corresponding to a 26 month period on Figure 5-17 to take account of earlier capsule assembly. It is assumed that the capsule is mated to the RTG shortly before launch.

5.2 RADIATION SENSITIVITY

As a consequence of utilizing RTG's as the primary power source, an additional constraint is imposed upon the spacecraft system due to the effects of the radiation fields created by the isotope fuel.

In general, the effects of this radiation environment will be detrimental to the successful operation of the system, and, therefore, will tend to decrease the probability of mission success unless adequately considered in the spacecraft design. Although similar system effects are also associated with the natural space radiation environment, it is anticipated that for the most part the effects due to the RTG environment will exceed those due to the natural environment.

The detailed analysis of these effects has been divided into the three following broad areas of concern:

- a. Determination of the magnitude and extent of the radiation fields in and around the spacecraft due to the isotope fuel - Shielding calculations which adequately consider the spacecraft geometry and isotope radiation source characteristics have been performed and have resulted in the construction of various radiation field maps which define the levels of neutron and gamma radiation in and around the spacecraft.
- b. Assessment of the generalized radiation effects on the various materials and electronic components which make up the spacecraft bus exclusive of the science payload - For the Pu-238 fuel, these effects are minimal and it is felt that through the use of judicious component design and material selection procedures, the system can be adequately hardened without a significant increase in spacecraft weight or power consumption. The use of Curium-244 fuel, on the other hand, would impose severe weight and power consumption penalties in order to adequately harden the system against the high neutron doses from this fuel. This fuel has therefore not been extensively considered in the present study.
- c. The Science Payload - Since the radiation background due to the RTG's can affect the science payload in unique ways which are strongly dependent upon the specific type of scientific instrument, the assessment of these effects has been treated separately from the effects on the rest of the spacecraft bus. The majority of the scientific instruments likely to be utilized in the science payload will not be affected to any great extent, either through accumulated dose effects or dynamic interference, so that there will not be any significant penalty to the system in terms of increased weight or power, at least for Pu-238 fuel. Several types of instruments can be significantly affected, however, by dynamic interference caused by the RTG background

radiation. These are principally the radiation detection instruments which may be utilized on either Mars or other out-bound missions. The effects on some of these instruments can be serious and would probably require increased shielding, and possibly the utilization of separation booms in order to adequately reduce the RTG background radiation to acceptable levels in these instruments. This would result in a significant weight penalty if such instruments are included as part of the science payload.

Item a is summarized in Section 3.3.6. Items b and c are discussed in more detail below.

5.2.1 RADIATION EFFECTS ON SPACECRAFT BUS ELECTRONICS AND MATERIALS

Each of the spacecraft bus subsystems has been analyzed for its susceptibility to the neutron and gamma ray doses resulting from the on-board RTG's. These results are discussed in detail in References 5-2, 5-3 and 5-4.

The functional description of the Voyager Spacecraft utilized in carrying out this study is that given in the General Electric Company, Phase 1A, Task B, Preliminary Design, Final Report (Ref. 5-5). Since much of the spacecraft design is preliminary in nature, this radiation sensitivity assessment is also preliminary in many respects due to the lack of detailed component design data and piece-part definition for a number of components. The results are none the less quite helpful in determining the overall feasibility of using RTG's as the primary power source for the spacecraft bus.

Where possible, the evaluation has been based upon experimental radiation effects data. For piece parts and materials for which no data is available, either (1) analytical techniques have been utilized to predict the component or material response, or (2) radiation effects data for similar piece parts or materials has been used. Also, where component design was such that the piece parts and materials to be used in the design have not yet been identified, a generic definition of the piece parts or materials usually utilized in such applications has been assumed. Much of the experimental radiation effects data and analytical prediction techniques utilized in determining subsystem and component sensitivity is given in Reference 5-3.

The essential results of the present study are summarized, in general form, in Figures 5-25 and 5-26. Figure 5-25 is a summary of the principal neutron effects in the system,

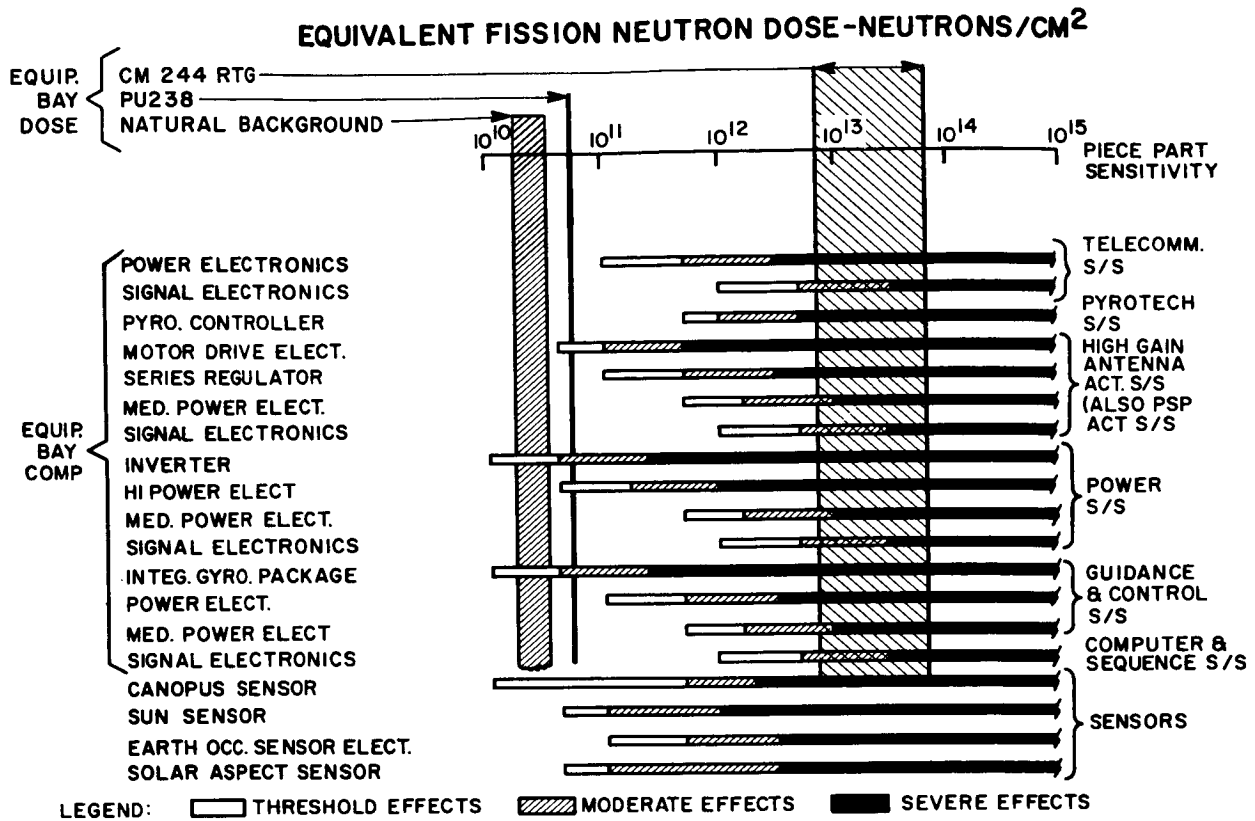


Figure 5-25. Neutron Effects Summary

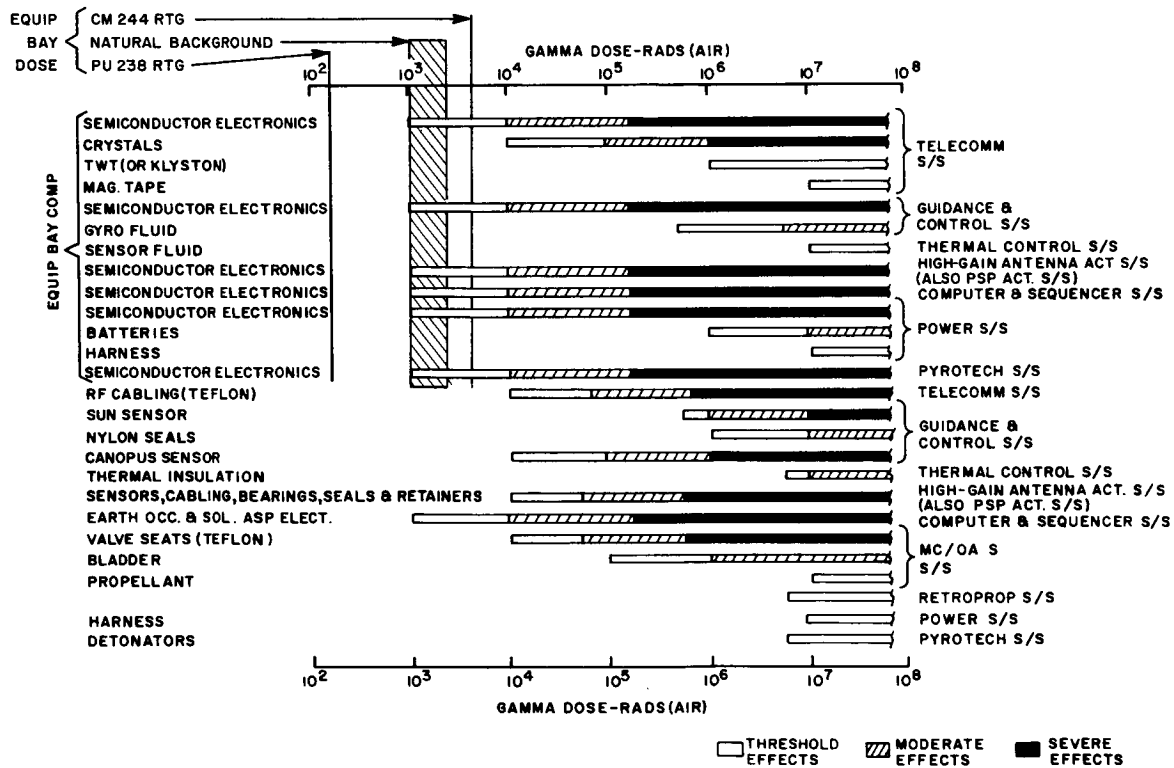


Figure 5-26. Gamma Effects Summary

while Figure 5-26 is a summary of the principal gamma effects in the system. As can be seen, the subsystems in which these effects occur are identified along with either the specific component or the category of piece parts that is affected. Three levels of effects are shown: threshold, moderate, and severe effects. In general, a threshold level denotes that range of radiation dose where specific effects in piece parts begin to occur, although for the most part, component performance would not be seriously impaired. Moderate effects generally denote that range of radiation dose which would significantly affect piece part performance to the point that degradation of component operation results, requiring no special design considerations to permit affected components to operate at this level. The severe effect levels are generally interpreted as those levels which would affect piece part performance to the point where component operation would be significantly impaired and, in many cases, would result in complete component failure. Considerable radiation hardening design effort would be required in order to design components to operate in this severe effects region.

The various subsystem and component radiation sensitivities depicted represent the piece part sensitivities which make up the components rather than the sensitivity of the components themselves. Since, for any given component, a certain amount of design margin is usually included in the design (for reasons other than radiation effects), the component (or circuit) radiation sensitivity will, in general, not be as severe as that indicated. Some discussion on typical circuit radiation sensitivity in relation to the piece part sensitivity is given later.

In order to relate these effects to the RTG power sources of interest, the total accumulated neutron and gamma doses in the area of the bus equipment bay that are anticipated for the entire Voyager mission are also shown for both Pu-238 fueled RTG's and Cm-244 fueled RTG's. These doses are for the 600 watt (e) power system and are obtained from the radiation field mapping studies described in Section 3.3.6. The neutron doses expected from a Cm-244 fueled RTG is a strong function of the amount of Cf-252 contaminant contained in the Cm-244 fuel. Therefore, the expected neutron dose from Cm-244 fueled RTG's is shown as a range. The upper limit of this range corresponds to a Cf-252 contamination level of approximately 100 parts per million, which represents a reasonable estimate of that which

would be anticipated for production grade fuel. The lower limit reflects a contamination level of approximately 10^{-5} parts per million.

The equivalent damage dose expected from the natural radiation environment (principally solar flare protons) is also shown. This equivalent dose is expressed in terms of an equivalent fission neutron dose which can readily be compared to similar doses from the RTG sources. The equivalent fission neutron dose, in this case, represents that dose of fission spectrum neutrons which would cause the same amount of damage as the actual natural radiation environment (which is mostly energetic protons). Similarly, the neutron damage dose for the Pu-238 isotope fuel is also expressed in terms of an equivalent fission neutron dose. The methods for determining these equivalent doses are discussed in Reference 5-3. The neutrons from the Cm-244 isotope fuel are assumed to have a fission energy spectrum, and are therefore expressed directly in terms of fission spectrum neutrons.

5.2.1.1 Summary of Effects

Considering the neutron sensitivities summarized in Figure 5-25, it can be seen that for the Pu-238 fuel the threshold sensitivities of all but a few components are well above the anticipated total neutron dose for the entire Voyager mission. Only a few components appear to be potentially affected by the Pu-238 neutron environment. For the most part, the radiation effects in the power semiconductors utilized in these sensitive components (such as the power inverter) are the primary reasons for their low threshold levels. However, based upon the nominal anticipated neutron dose, these effects appear to be such that they can be readily overcome by appropriate circuit design techniques. Similarly, potential effects in optical sensors, such as the Sun sensors, can be overcome by circuit design and judicious placement on the Planetary Vehicle with respect to the RTG sources. It thus appears that the effects of the neutron dose from the Pu-238 sources will be minimal, and that the system can be adequately hardened without a significant weight or power penalty. Also, the anticipated effects due to this neutron environment are only slightly above those expected from the natural environment considering nominal spacecraft shielding (1 to 2gms/cm^2) of the natural environment.

The use of Cm-244 as the isotope fuel, on the other hand, will create serious effects in almost all spacecraft subsystems. The expected neutron dose from Cm-244 is a factor of 10^2 to 10^3 higher than that anticipated for the Pu-238 fuel, depending upon the Cf-252 contamination level in the Cm-244 fuel. Even for the lower dose level, serious effects would occur for almost all spacecraft subsystems. To harden against these effects would require considerable increased design margins, shielding, and in some cases probably increased separation distances between the more sensitive components and the RTG units. This would result in severe weight and power penalties on the system.

The effect of the accompanying gamma dose, on the other hand, particularly for the Pu-238 source, does not appear to be of any consequence. A possible exception to this is the potential surface effects in the semi-conductor electronics if they are mounted close to the RTG units. This is not expected to be serious, however.

Similarly, the anticipated gamma dose from the Cm-244 source does not appear serious for components in the equipment bay. A possible exception to this may be induced surface effects in any nonpassivated semiconductor devices. Components and materials mounted close to the Cm-244 RTG units, however, may receive a gamma dose that could cause significant degradation. Included here would be RF cables and connectors containing Teflon dielectric, organic valve seats, and semiconductor electronics.

No serious dose rate effects due to the use of either type of RTG unit are anticipated. The most sensitive component to dose rate effects, exclusive of the science payload, is probably the Canopus sensor, where an image disector tube (photomultiplier) is utilized as the sensing element. The threshold dose rate for this type of unit is approximately one rad/hr. In its present location on the spacecraft, the dose rates from either type of RTG unit would be well below this level.

Since radiation effects are for the most part cumulative in nature, the probability of mission success through the initial periods of operation is reasonably high. The risk

beyond initial periods of mission success is principally dependent upon two areas of uncertainty:

- a. The variability of individual response of approved part and material items to given amounts of radiation exposure
- b. The uncertainty relative to the radiation environment to be encountered

For the first area of uncertainty, semiconductor electronic parts presently represent the largest risk because of the large variety of part types used, the wide variety of circuit applications and the variability of device radiation sensitivity. These risks have been identified for the most part, based on accelerated radiation testing of piece parts and materials. A potentially more severe risk is that due to the long-term low-level radiation effects. Very little information presently exists, however, to properly assess this latter risk, particularly for a wide variety of operating conditions.

The second area of uncertainty is primarily governed by the accuracy of the analytical techniques used in the shielding and mapping calculations, an adequate definition of the radiation characteristics of the source itself, and a sufficiently accurate representation of the geometrical model of the spacecraft used in the shielding studies.

The approach to reduce these risks, considering the overall Voyager reliability goals, would be to exercise close control over the selection of materials and parts and over subsystem and component design to ensure proper consideration of the radiation environment. In addition, sufficient radiation testing and analysis should be performed to generate new design data and to verify radiation hardened designs where required. Experimental mapping of the radiation fields in and around an actual model of the spacecraft loaded with live fuel capsules would tend to reduce the second area of uncertainty.

In addition to the utilization of these hardening techniques, it has also been desirable in the past, in many cases, to arbitrarily set the design goal radiation dose a factor of 5 to 10 higher than the expected dose. This would adequately account for the above uncertainties.

With such a radiation safety factor, the effect of as much as 100 percent growth is not considered significant.

A potentially more severe effect would be an extension of mission life requirements. For example, an extension of mission life requirements to, say, 5 years, which may be desirable for certain outbound missions beyond Mars, would begin to significantly alter the vulnerability picture for Pu-238 fuel, particularly if a factor of ten conservatism in design dose is to be maintained.

5.2.2 RADIATION EFFECTS ON SCIENCE INSTRUMENTS

The effect of RTG radiation on science instruments has been described in previous Task C documents (Refs. 5-7, 5-8). These are summarized below in Section 5.2.2.1.

Besides the effect of direct RTG neutron and gamma radiation, several of these instruments respond to secondary radiation resulting from interaction of the primary RTG radiation with surrounding materials. Section 5.2.2.2 provides appropriate information which supplements earlier discussion of the RTG radiation environment presented in Section 3.3.6.

Section 5.2.2.3 presents estimates of shielding weight using a gamma-ray spectrometer as an example. This is treated in more detail in Reference 5-9.

5.2.2.1 Instrument Studies

Table 5-1 lists a variety of science instruments along with estimates of possible RTG interference effects. Instrument numbers 1-7, 9, 10 and 11 were identified by JPL. The others were added as being potential orbiter science instrument candidates.

The instruments in the Fields and Particles Group (Table 5-1) are least compatible with the RTG environment since they are designed to detect natural particles similar to those emanating from the RTG's. Possible solutions may be available through the use of shielding, redesign of low energy channels, use of smaller scintillators to avoid saturation and the use of coincidence circuit techniques.

TABLE 5-1. SUMMARY OF RTG RADIATION EFFECTS ON SCIENCE INSTRUMENTS

<u>Instrument</u>	<u>Scientific Objectives</u>	<u>No Known Sensitivity Problem Exists</u>	<u>Problem Exists</u>	<u>Remarks</u>
<u>Television Group</u>				
1. Stereo-tri color camera	Study topographical features, cloud cover, and general physical and biological characteristics of planetary surfaces.	x		Color and black and white TV remarkably stable in radiation fields. No adverse radiation effects anticipated unless time-integrated neutron and gamma fields are both at least two orders of magnitude higher than computed for Voyager mission.
2. High resolution monoscopic cameras		x		
3. Medium resolution stereo cameras		x		
4. Dual TV cameras		x		
<u>Spectrometer and Radiometer Group</u>				
5. Ultraviolet spectrometer	Abundance and height distribution of atmospheric constituents from 0.11 to 0.45 micron. Spectrum of dayglow and aurora (resonance reradiation, fluorescence, absorption, etc.).		x (1)	Although certain UV detectors are sensitive to low level radiation fluxes, it is possible to select radiation-insensitive detectors. Advanced state-of-the-art detectors sometimes sensitive; Cerenkov radiation in optical system may also be problem. Experimental studies are appropriate for advanced systems. Bolometers not sensitive.
6. High resolution IR spectrometer	Reflectance, emission, and absorption: atmospheric water vapor, CO ₂ , CO, and other gases. Surface geophysical characteristics.	x		
7. Broad Band IR spectrometer		x		
8. High resolution visible spectrometer	Map surface temperatures at several IR wavelengths.	x		
9. High spatial resolution IR radiometer		x		
10. IR radiometer		x		
<u>Fields and Particles Group</u>				
11. Gamma ray spectrometer	Gamma radiation from planet; composition, age, and evolution		x	Very sensitive; detection efficiency of 90% or higher

12. Cosmic ray telescope	studies. Flux and energy of protons, alpha particles, heavier nuclei in interplanetary space. Trapped radiation near Mars.	x	in certain energy ranges. Instrument redesign indicated; must discriminate against RTG gammas or shield against them. Sensitive to RTG radiation. Improved anti-coincidence techniques, pulse-shaping circuitry, and use of shadow shielding will probably permit use in RTG field.
13. Plasma probe	Flux density, energy spectra, arrival direction of solar plasma and trapped particles near Mars. Temporal and spatial variations.	x	Current generation of plasma probes insensitive to RTG radiation. If flux measurement thresholds decreased, probes may become sensitive to RTG radiation.
14. Trapped Radiation Detector	Distribution, energy, and identity of low-energy, magnetically trapped radiation particles near Mars.	x	Three Geiger Muller detectors Will detect electrons and protons efficiently, and gamma rays with less efficiency. However, gamma rays will provide high noise background. This type instrument not believed suitable for redesign. Require shielding or boom mounting for operation in RTG field.
15. Ion Chamber	Average, total, omnidirectional flux of corpuscular radiation in space and near Mars. Relate to solar events.	x	Stainless steel sphere filled with argon. Penetrating electrons and protons detected with efficiency of about 98%. Not suitable for redesign. Require shielding or boom mounting for operation.
16. Mass Spectrometer	Atmospheric studies: chemical composition, diurnal, seasonal, and latitudinal variations of density, isotopic analyses, pressure measurement, molecular vs. atomic abundances.	x	A non-magnetic, time-of-flight unit with no RF field is operational from 10^{-4} to or below 10^{-14} torr. Electron multiplier tube (sensitive to photons and electrons) serves as sensor. System capable of redesign to minimize radiation problem; probably cannot solve problem using known techniques.

<p>techniques.</p> <p>Helium magnetometer, sensitive to $< 2.5 \times 10^{-6}$ gauss. Not sensitive to radiation. May mount on boom to remove from spacecraft magnetic field.</p>			<p>17. Magnetometer</p>
<p>Insensitive to radiation.</p>		<p>Magnitude, direction, multiplicity of planetary magnetic field and its orientation relative to planet axis. Interaction between planetary and interplanetary magnetic fields.</p>	<p>18. Gradiometer</p>
<p>Insensitive to radiation.</p>		<p>Rate of change of acceleration due to gravity. Mass of planetary bodies.</p> <p>Flux as function of direction, distance from sun, particle momentum, and mass distribution.</p>	<p>19. Cosmic Dust Detector</p>
<p>Insensitive to radiation.</p>		<p>Magnitude and time variation of integrated electron density between spacecraft and Earth. Density of ionosphere and atmosphere. Average roughness and dielectric properties of planetary surface.</p>	<p><u>Radio Group</u></p> <p>20. Bistatic Radar</p>
<p>Insensitive to radiation.</p>		<p>Thickness, altitude; longitude and latitude of ionospheric layers in Martian upper atmosphere.</p>	<p>21. Ionospheric Sounder</p>
<p>Insensitive to radiation.</p>		<p>Interplanetary noise due to planetary, solar, and other emissions. Martian spherics.</p>	<p>22. RF Noise Detector</p>
<p>(1) Recent tests at JPL resulted in saturation of a U-V spectrometer photomultiplier tube due to a promethium isotope source.</p>			

5-28-2



UV spectrometers may also present problems as evidenced by recent experience at JPL. Several such instruments were studied. Recently improved photomultipliers can detect dark currents of 10^{-11} to 10^{-13} amperes; 10^{-11} amperes is two to four orders of magnitude too small to operate without radiation interference. Many designs have operated well in moderate radiation fields without signs of sensitivity.

The principal findings of this study are based on literature surveys and numerous contacts made with instrument investigators. Pertinent information is contained in the references summarized below:

<u>Reference</u>	<u>Content</u>
5-10, 5-11	Radiation Effects on the Nimbus B Spacecraft due to presence of the SNAP-19 RTG. No serious effects anticipated, but no fields and particles instruments were included.
5-12	Experimental radiation studies using SNAP-9A RTG in conjunction with IMP-A and OGO instruments.
5-13	Experimental radiation studies using SNAP-13C RTG in conjunction with cosmic ray telescopes and plasma probes for use on Pioneer VI.
5-14	Radiation sensitivity studies of plasma probe, E vs dE/dx telescope, proton analyzer, beta detector, thermal ion analyzer, range vs. dE/dx telescope.

5.2.2.2 Secondary Radiation

In addition to the direct neutron and gamma radiation from the RTG's, secondary radiation may be generated as a result of interactions between the primary particles and spacecraft components.

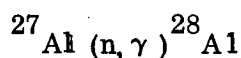
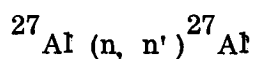
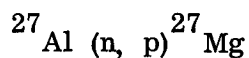
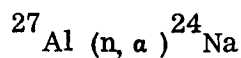
The major secondary sources arise from

- a. Neutron
 1. Radiative capture reactions
 2. Charged particle reactions
 3. Inelastic scattering

- b. Gamma Rays
 1. Compton scattering
 2. Photoelectric effect
 3. Pair production
 4. Fluorescence radiation
 5. Bremsstrahlung
 6. Coherent electron scattering

For the purpose of this study, the reactions of interest are those which enhance the intensity of the primary field, e.g. (n, γ) reactions, and those which create charged particles, e.g. (n, p) reactions; the latter are important because some of the instruments are particularly sensitive to charged particles.

An estimate of the magnitude and effect of secondary radiation may be obtained by studying one representative material. Aluminum serves the purpose because it is the most frequently used and widely distributed element in the spacecraft. ^{27}Al can react with neutrons as follows:



For simplicity the reaction cross sections used (Ref. 5-6) are those associated with the highest probability neutron energy: 2-2.5 Mev according to Figure 3-30. This energy is below the threshold for the (n, α) and (n, p) reactions. The absorption cross section for the (n, γ) reaction is only 0.4 millibarn. The (n, n') inelastic scattering reaction is one

in which neutron capture creates an excited compound nucleus which immediately decays by emitting a lower energy neutron and one or more gamma photons. For aluminum, the characteristic photon energies are 0.842, 1.013, and 2.213 Mev. The cross sections for the first two reactions are 0.1 and 0.4 barn. Because the incident neutron must possess at least the energy of the emitted photon plus the kinetic energy of the target nucleus, the cross section for the 2.213 Mev reaction is taken as zero. Parenthetically, the probability for inelastic scattering increases for most of the heavier nuclides while the emitted gamma energies become smaller; thus, more than one photon is frequently emitted per inelastically scattered neutron.

An upper limit type quantitative estimate of the yield of secondary gammas may be made by assuming an incident neutron flux of 1×10^3 neutrons-cm⁻²-sec⁻¹*, and a mass of 1000 kilograms of aluminum located at one meter from the RTG's and also one meter from a particular receiver point. Assuming no self-shielding of neutrons or gammas in the aluminum and no more than single collisions per neutron, the inelastic scattering produces a gamma photon flux of 18 and 71 photons-cm⁻²-sec⁻¹ of the 0.842 and 1.013 Mev gammas, respectively. The aluminum (n, γ) activations produce a 1.79 Mev photon in the ²⁸Al decay to ²⁸Mg plus a 2.865 Mev (max) beta particle. The photon flux from this reaction at the same one-meter receiver point is 0.07 photon-cm⁻²-sec⁻¹. For comparison, the direct photon flux from the RTG's at one meter is about 10^4 photons-cm⁻²-sec⁻¹. Thus, even in this extreme case the secondary gammas constitute less than one percent of the direct gammas; the aluminum activation gammas are better than five orders of magnitude below the uncollided gamma flux.

The activation of other elements present in the spacecraft will not change the conclusion significantly: fast neutron activation decay products will not materially increase the background radiation coming directly from the RTG's. This rule does not imply that secondary reactions can be neglected, particularly reactions which produce particles similar to those to be detected by nearby instruments. Thus the gamma ray spectrometer discussed in Section 5.2.2.3 is a special case for which even a slight particle flux may be

*The predicted flux in the spacecraft-electronic bays is 800 n-cm⁻²-sec⁻¹ (see Table 3-13.)

of the same order of magnitude as the predicted signal. Similarly, the very small aluminum activation could produce a beta particle signal in the charged particle detector if the reaction occurs within the detector structure; this signal may then be registered in anticoincidence as desired intelligence. To be sure, the reaction cannot occur deep in the structure, because the range of, say, the ^{28}Al decay beta (2.865 Mev) in aluminum is only 0.7 cm.

Neutron cross sections for all spacecraft materials must be studied in a comprehensive analysis. The photon-producing processes include the (n, α) , (n, p) , (n, γ) , and (n, n') reactions. Unstable nuclei often emit electrons as they decay toward a stable state. Some instrument sensors are sensitive to charged particles. For instance, a plasma probe may not be capable of distinguishing an alpha particle produced by the Al (n, α) reaction in the walls of the probe near the charged particle collection plate from a solar wind alpha particle. The lighter elements (H, C, O, Mg, Si, etc.) generally have very small cross sections for the productions of photons at neutron energies of interest. The heavier elements (Fe, Ni, Cr, Cu, Pb, etc.) have relatively small photon-producing cross sections (usually less than one barn) for each reaction but a higher density of levels, resulting in the production of a larger number of photons. Some of these photons have penetrating energies (from 1 to about 10 Mev).

Of the interactions of gamma photons with matter listed above, Compton scattering, pair production, and photoelectron production are the most probable ones.

Compton scattering changes the direction and the energy of the incident gamma photon by elastic collision with an orbital electron. In the process the photon loses a part of its energy to the electron; there is no net change in the number of particles, only in their energy and direction. In thick shields, multiple Compton scattering will eventually lead to photoelectric absorption. The probability for this process varies linearly, roughly as Z/E , where Z is the atomic number and E the photon energy.

The absorption of positrons and electrons from the pair production mechanism will not produce a significant problem in most Voyager instruments because only a small percentage of RTG gamma rays will have energies above 3 or 4 Mev. Pair production cross sections

are relatively small in comparison to the combination of photoelectric and Compton scattering cross sections in all elements at energies below 3 or 4 Mev.

On the other hand, photoelectron production is predominant in the absorption of low energy gamma rays. An incident photon transfers its energy to an atomic electron, causing its ejection from the atom. One-half the total absorption coefficient for aluminum is due to the photoelectric effect at a photon energy of 46,000 electron volts. At lower energies, a larger fraction of the absorption coefficient is due to photoelectron production and at higher (intermediate) energies another mechanism (Compton scattering) becomes increasingly important. When low to moderate energy gamma rays are absorbed in the surface layer of Al or other materials, the relatively low energy photoelectrons (up to several tens of thousands of electron volts) are likely to be produced. Their proximity to and effect on sensors must be studied.

Gamma photons with energies above 1.02 Mev can be annihilated, if they pass near a nucleus, by the strong electrical field there. In the process an electron-positron pair is formed. The energy difference between the incident photon and the energy equivalence of the mass of the electron-positron pair (1.02 Mev) appears mainly as kinetic energy of the pair. The reaction probability is roughly proportional to that energy difference and to the square of Z , the atomic number of the nucleus.

Because of the complexity of the gamma reactions, it requires sophisticated techniques to predict the spatial and energy distribution of the equilibrium gamma field and of the charged particles created in gamma interactions. Monte Carlo programs are available for this purpose; however, experimental determinations would undoubtedly be more reliable.

As charged particles penetrate matter, electromagnetic radiation (bremsstrahlung) is produced due to particle deceleration. This phenomenon is important in some materials. Fluorescent radiation, coherent electron scattering, Cerenkov radiation and others are ordinarily small effects compared with the three principal interactions and are not expected to seriously affect the science payload.

Electrons are created in or released from atoms due to gamma ray absorption or scattering interactions. Due to the small mass of the electron, large angular and energy straggling effects render computation from microscopic cross section data more difficult than for heavy ion penetrations. This is particularly true when the maximum electron range approximately equals the material thickness.

In certain instruments charged particles emanating from materials in or near the sensor can produce false signals. An analysis of the problem must consider what electron fluxes and energies are present.

An inspection of Figure 5-27 reveals that 1 Mev electrons moving perpendicular to the surface are almost completely absorbed after traversing 0.070 inch or 1.8 mm thickness of Al. Minimum typical Al thicknesses around spacecraft electronics are typically 0.1 inch. A sizeable portion of electrons in the Van Allen belts will be shielded by this thickness. However, problems in certain instruments arise when electrons are created or

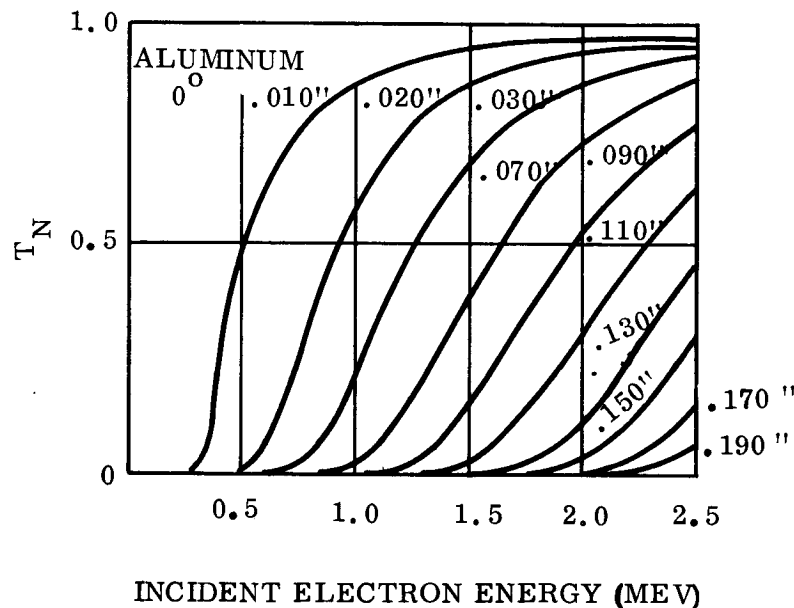


Figure 5-27. Number Transmission Coefficient Incident at 0° on Various Thicknesses of Aluminum

are scattered within a few mils of the surface which borders a sensitive sensor. Electrons are also generated within the detectors. The only way to eliminate this inherent difficulty is to shield, or devise ingenious discrimination techniques.

5.2.2.3 Shielding Calculations

The instrument in the science payload probably least tolerant of RTG radiation is the gamma-ray spectrometer. A preliminary shielding analysis for this instrument was therefore undertaken.

Information from JPL indicated a tolerable background level from sources other than cosmic ray induced activity to be on the order of $0.005 \text{ photon-cm}^{-2}\text{-sec}^{-1}\text{-Mev}^{-1}$ at 1.5 Mev, the energy of the significant ^{40}K line, with allowable contributions at other energies varying roughly as E^{-2} , where E is the photon energy.

Representing this relationship for the tolerable background level as

$$K \int_{E_1}^{E_2} E^{-2} dE = -K E^{-1} \Big]_{E_1}^{E_2}$$

the value of the integral is set to $0.005 \text{ photon-cm}^{-2}\text{-sec}^{-1}$ over the arbitrary range of 1 to 2 Mev, and the equation is solved for K, a proportionality constant. With K thus evaluated at $0.01 \text{ photon-Mev-cm}^{-2}\text{-sec}^{-1}$, the integral is again evaluated for the tolerable background level of photons over the plausible energy range from 0.04 to 10 Mev; the result is $0.25 \text{ photon-cm}^{-2}\text{-sec}^{-1}$. For convenience it was conservatively assumed that every neutron seen by the detector reacts in the detector to release one gamma photon. Shielding is therefore required to reduce the total particle flux to $0.25 \text{ (gammas + neutrons)-cm}^{-2}\text{-sec}^{-1}$.

Lead and LiH shield thicknesses were calculated at 10, 20, 50, and 100 meters from the spacecraft centerline to reduce the gamma plus neutron flux at those locations to 0.1, 1.0, and 10 particles-cm⁻²-sec⁻¹. The calculations used the infinite slab approximation with gamma dose buildup and with the usual fast neutron removal theory approach. Geometric

attenuation was assumed to vary as the inverse square of the distance. The resulting shield thicknesses are shown in Table 5-2.

TABLE 5-2. SHIELD THICKNESSES (IN CENTIMETERS)

Distance (Meters)	Tolerable Particle Flux ($\text{cm}^{-2}\text{-sec}^{-1}$)					
	0.1		1.0		10	
	Pb	LiH	Pb	LiH	Pb	LiH
10	12.4	63.8	9.2	40.8	6.1	18.5
20	10.6	50.0	7.3	27.0	4.0	10.5
50	7.9	31.7	4.9	10.5	1.4	-
100	6.0	17.8	2.5	6.0	-	-

An approach to shield weight optimization is to combine geometric and mass attenuation, i.e., to deploy the sensor on a retractable boom and to add a small shadow shield between the sensor and the spacecraft. Two cases were considered, as illustrated in Figure 5-28. In one the shield shadows the minimum angle which encompasses only the RTGs. In the other case it is conservatively assumed that neutrons and gammas scattered by spacecraft components have the same intensity as the direct beam; the shield was therefore extended to shadow the entire spacecraft. The deployed shield weight for the two cases is shown in Figure 5-29 as a function of boom length.

In order to estimate the total shielding weight, the weight of the boom and deployment mechanism had to be considered. The STEM overlap boom was selected for this application. This boom is formed by a flat strip of thin material which assumes a tubular shape of high strength when extended. For storage the strip is coiled on a drum.

The boom sizes varied from 0.5 inch diameter and 0.003 inch wall thickness to 3 inch diameter and 0.010 inch wall thickness. The material was stainless steel in all cases. The total weight of shield plus boom and boom deployer mechanism is shown in Figure 5-30 as a function of boom length. It is noted that in all cases a weight-optimum boom length exists in the neighborhood of 100-foot boom lengths; this is cross-plotted in Figure 5-31. A shielded and deployed

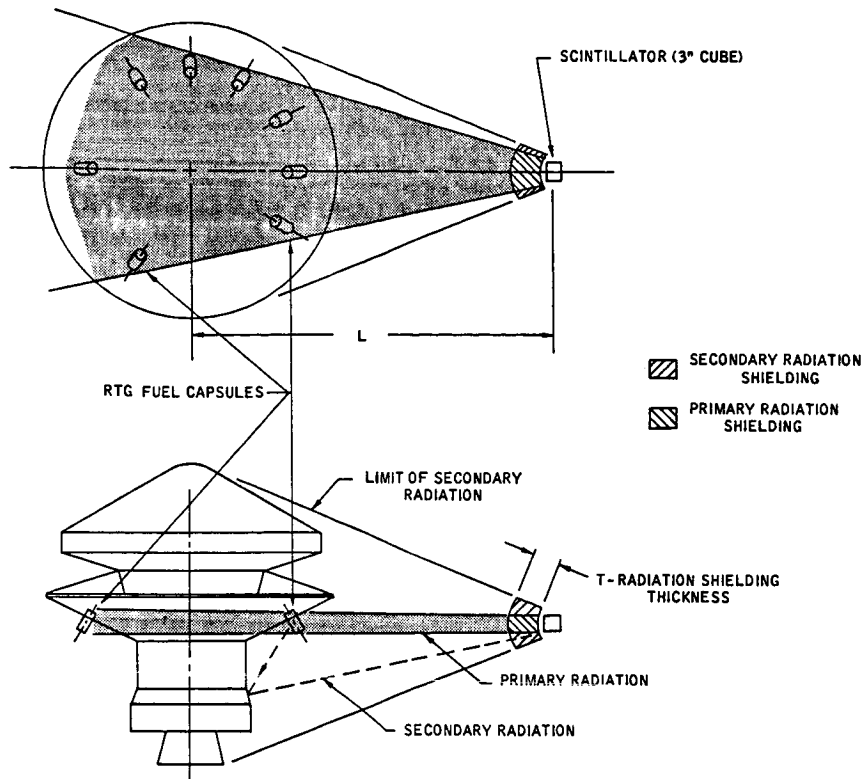


Figure 5-28. Schematic View of the Shadow Shield for the Gamma Ray Spectrometer

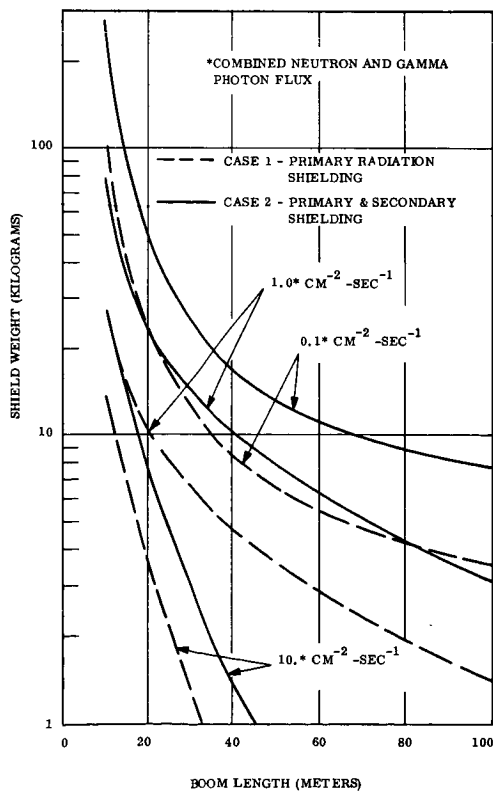


Figure 5-29. Shadow Shield Weight vs Boom Length

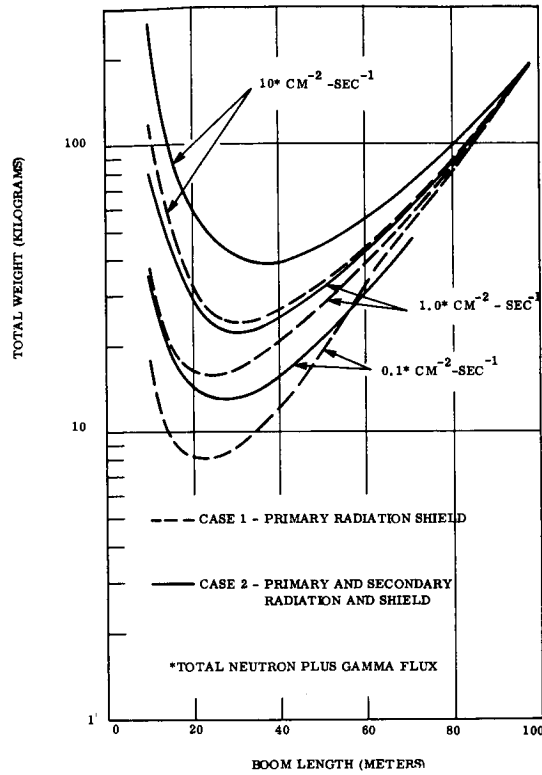


Figure 5-30. Total Weight of the Tip Shield, Boom and Deployment Mechanism vs Boom Length

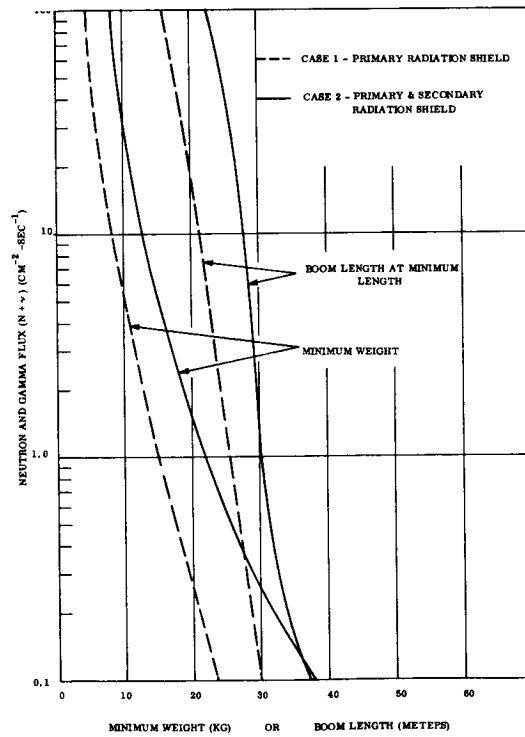


Figure 5-31. Minimum Weight Shield Systems for the Gamma Ray Spectrometer

gamma ray spectrometer detector would thus weigh about 50 to 80 pounds, exclusive of detector and signal cable. This is, of course, only a preliminary estimate, employing consistently conservative assumptions.

5.2.3 RADIATION SENSITIVITY STUDIES BY TEXAS INSTRUMENTS, INC.

5.2.3.1 Summary of the Initial Study

The Apparatus Division of Texas Instruments, Inc., a member of the General Electric Voyager Study Team, analyzed the radiation sensitivities of the following five instruments.

- a. Helium magnetometer
- b. Infrared interferometer spectrometer (IRIS)
- c. Light ion mass spectrometer (LIMS)
- d. Lunar orbiter radiation dosage measurement system (LDMS)
- e. Gamma ray spectrograph

The instruments, all of which are manufactured by TI, were carefully studied in order to evaluate the sensitivity of state-of-the-art techniques utilized in typical space science instruments. Although this selection is not necessarily representative of experiments which may be performed on Voyager missions, valuable contributions were made by defining the more sensitive components. Estimates of the radiation damage thresholds of various electronic networks, materials, and sensors described in Reference 5-8.

The contents and results of this independent study may be briefly summarized as follows:

- a. Tabulation of a baseline radiation environment — The characteristics of the 57 w SNAP-27 RTG were extrapolated to a 600-watt configuration. A worst-case environment was tabulated for a 1-meter separation from the 600-watt Pu-238 system. The integrated exposure for a 15-month period in the baseline environment was assumed to be 6×10^{10} n/cm² and 1.58×10^4 erg/g(c). (This radiation environment is somewhat more intense than that more recently computed and shown in Tables 3-13 and 3-14 of this final report.)
- b. Tabulation of the radiation damage thresholds for components and materials — The damage threshold data was tabulated from literature surveys. Most materials and nonsemiconductor components will not be affected by the radiation exposure on Voyager. Some semiconductor components and Teflon may receive slight to moderate damage.

- c. Tabulation of components and materials lists for the instruments — The components list has been tabulated from design and/or manufacturing data on the instruments. The detailed components list is shown in Reference 5-8.
- d. Identification of the components whose parameter variations would produce the most serious data errors or catastrophic failures — The component classes utilized in each instrument were reviewed to determine the more sensitive components. Next, the sensitivity of the instruments to component parameter variation was reviewed, and the more sensitive circuits and their components were identified. It was discovered that the analog circuitry will usually degrade slowly, producing a proportional degradation in the instrument performance. The digital circuitry components will degrade slowly, but the circuitry will continue to operate within specification, until a given degradation has been reached. At this point, a catastrophic failure occurs. The damage thresholds identified in Figure 5-32 indicate the region where the degradation of components in analog circuitry will begin to degrade instrument performance and/or the regions where the performance of the digital circuitry begins to degrade (not malfunction).

It may be noted, for example, that a 1 percent change induced by radiation effects in an operating characteristic of some specific semiconductor in one part of an instrument (e.g., a logic circuit) would not affect the readout of the instrument. A 1 percent change in the same semiconductor placed in a calibration or preamplifier circuit might alter the readout by an appreciable amount.

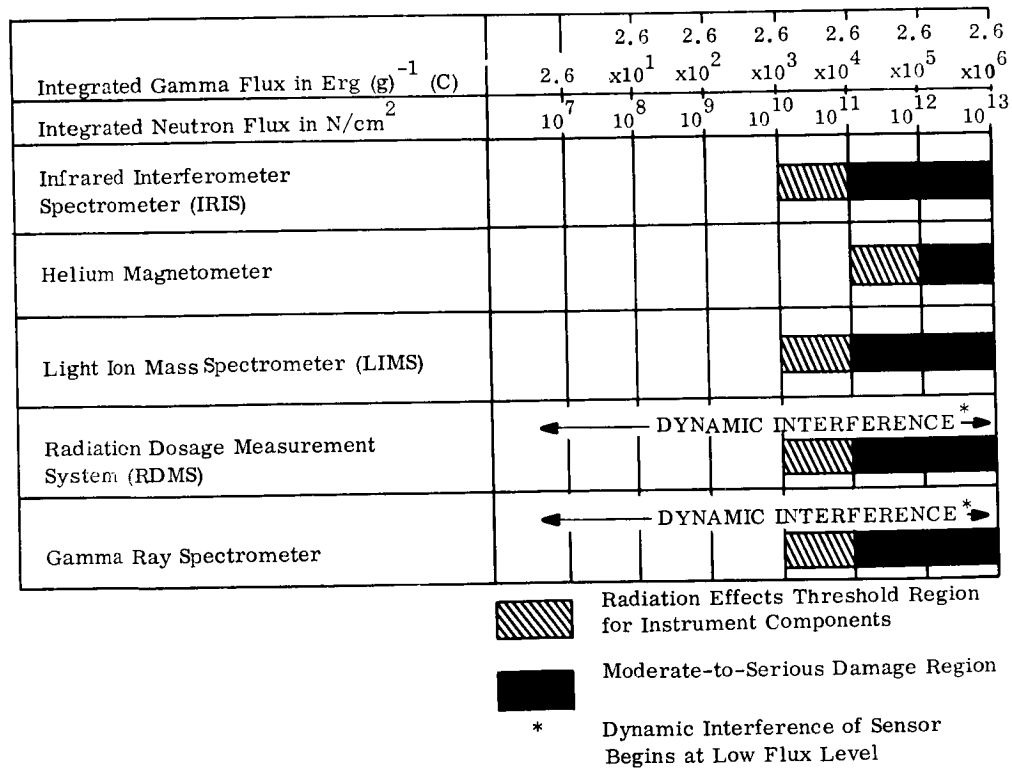


Figure 5-32. Damage Thresholds for Instruments

The semiconductor networks are responsible for low sensitivity thresholds on the IRIS, LIMS, RDMS, and the gamma ray spectrometer. However, the degradation of the networks in the damage threshold region of Figure 5-32 will not produce a measurable effect on the instrument output. This threshold can be increased an order of magnitude by using faster networks and a lower fan-out.

- e. Investigation of the dynamic interference resulting from the radiation flux on the instrument electronics or sensors — Nuclear and molecular mechanisms effective in producing dynamic interference were studied. It was found that the radiation flux from the RTG will be too low to produce dynamic interference in the electronic circuitry. Only the radiation-particle detection instruments and instruments using very sensitive photomultiplier detectors will experience dynamic interference problems. These include the LDMS and gamma ray spectrometer, neither of which was designed to operate in an RTG radiation field.

In LDMS the radiation flux is detected with CsI (Tl) crystals. Typical gamma ray spectrometers utilize NaI (Tl) crystals. Both are highly efficient radiation detectors.

Operation of a gamma ray spectrometer in the RTG environment will be very difficult in view of low signal count rate, which must be detected, and the high background count rate. The effectiveness of several techniques that can be applied to minimize the background or the effects of the background are listed below:

- a. Shielding - See section 5.2.2.3
- b. Mounting on a Boom - See section 5.2.2.3
- c. Anticoincidence Technique — Anticoincidence techniques can be employed to reject RTG-induced signals. These techniques would employ an anticoincidence detector between the RTG and the spectrometer detector. The anticoincidence detector output would be used to disable the spectrometer detector record circuitry for all events detected in the anticoincidence detectors. The primary limitations of the anticoincidence method are: (1) The probability of absorption (signal generation) in the anticoincidence detector is fairly low — about 75 percent for 1-inch thick crystals, and (2) the signal generation rates for the anticoincidence detector will be high and therefore degrade the performance of the spectrometer.

The significance of the first limitation is clarified by the realization that in order to reject a photon it must first be detected by the anticoincidence system. Therefore, it may be more efficient to simply shield the spectrometer. The second limitation, the deadtime buildup due to high background fluxes, is limited fundamentally by the time constant of the crystals. A typical time constant is approximately 1×10^{-6} seconds.

The background count rate must be limited to a level much less than maximum count rate to prevent large errors due to the random arrival of the photons. Simply shielding the spectrometer detector circumvents this difficulty also.

- d. Subtract the RTG Background — Within limits, the background radiation can be separated from the composite data if the background radiation is sufficiently characterized. The separation process consists of subtracting the known background data from the composite signal. The effectiveness of the process is a function of the record period, the time stability of the background, degree of characterization of the background, and the ratio of the background to the signal counts. The errors due to the statistics of the background can be computed for any given record period. The characterization of the background radiation for low ratio background to signal situations will be relatively easy. For the precise characterization of the background needed for high background to signal situation, the problem becomes complex. The measurement environment in the laboratory will be sufficiently different for the space environment to make precise measurement most difficult.

In summary, the operation of a gamma spectrometer in the RTG environment will impose limitations on the spectrometer and the quality of the data. The most effective techniques for reducing the effects of the background are separation between the spectrometer and the RTG, and shielding. The spectrometer measuring the recording circuits can be designed to operate with a given background radiation. The effects of the background can be partially removed from a knowledge of the background characteristic.

The gamma ray spectrometer sensor studied by TI was designed for use in airborne geophysical surveys. The sensor contains a sodium iodide crystal 11 inches in diameter and 4 inches thick to detect the gamma rays. The output of the crystal is optically coupled to the photomultiplier tube array. The outputs of the photomultiplier tubes is connected to a 400 channel analyzer covering the spectral range from about 400 kev to 8 Mev. This sensor was designed for an aircraft installation where size and weight were minor design constraints. The concepts, however, can be applied directly to space applications.

5.2.3.2 Radiation Effects Test

During the study of the components utilized in the various instruments, two components were identified that performed critical functions and for which insufficient data was available. The MOSFET (used in the input stages of the electrometer amplifier) and the circular

polarizer (used in the helium magnetometer) were selected for testing in the second phase of the program. The results are reported here for the first time. The importance of these components reaches beyond these specific instruments because of their application in other instruments.

The MOS field effect transistors are finding applications in mass spectrometers, ion measuring instruments, and plasma probes. MOS microcircuitry is being rapidly developed and appears to have many applications where speed is less important than minimum weight and power. Experimental devices using metal nitride in place of the metal oxide have demonstrated much higher radiation resistance; however, more experimental work on these devices is required.

A circular polarizer is used in all of the optically pumped magnetometers. The polarizers use a long chain-like molecule to polarize the light. Substitutes having reasonable size, weight and efficiency have not been developed.

5.2.3.2.1 Radiation Exposure Facility and Source

The radiation exposure of components was performed in the gamma radiation test facility of Texas Instruments' Central Research and Engineering Laboratory. This facility was constructed for the purpose of calibration of gamma ray spectrometers and has facilities for mounting and exposing components which must be biased during exposure.

The material selected as a radiation source was approximately 0.7 curie of Cs^{137} which as a result of radioactive decay emits monoenergetic 0.66 Mev gamma radiation. The radiation at 10 cm from the source was monitored by film badge exposure which indicated an average exposure of 23.4 rads per hour for four tests. This compares with the calculated value of 22 rads per hour for a source of exactly 0.7 curie. This variation can be attributed to radiation scatter in the exposure chamber.

5.2.3.2.2 Radiation Damage Study: Infrared Polarizer-Filter

A nonresonance optical pumping magnetometer (Ref. 5-15) developed for obtaining vector field information in deep space has been used successfully on the Mariner IV Mars probe to determine the Martian dipole moment (Ref. 5-16). In considering the effects of radiation

exposure on this instrument, the infrared circular polarizer is the component not previously tested for radiation damage effects and was therefore chosen for testing. It had been previously determined that polarization deterioration degrades the performance of the instrument (Ref. 5-17) and the purpose of this test was to determine the contribution by radiation exposure to this deterioration.

The radiation damage study indicates that a gamma radiation dose of 7000 rads produces no significant change in the polarizer. The polarizer was exposed to the gamma radiation of the Cs¹³⁷ source for periods of 93.5 and 219.0 hours for a total dose of greater than 7000 rads as shown in Table 5-3.

TABLE 5-3. POLARIZER GAMMA RADIATION EFFECTS

Exposure Time (Hr.)	Dose (rads)	R _{trans.} X 100 (%)	R _{circ.} X 100 (%)
0	2,187.9	0.9	13
93.5	5,124.6	2.0	15
219	7,312.5	1.7	9

Polarizer evaluation was performed by determining the transmissivity and polarizing ability on the instrument at Texas Instruments designed specifically for the evaluation of these parameters. A matched set of infrared polarizers (described at the end of this section) was used for the test. Polarizer No. 1 was exposed to radiation and Polarizer No. 2 was used as a reference. The parameter chosen to indicate the difference between the two elements is

$$R = \frac{R_1 - R_2}{R_1 + R_2}$$

where R_i is the signal of the i th component. The percent difference (R X 100) is recorded in Table 5-3 for the transmissivity and polarizing ability measurements.

These measurements indicate that the variation in R over the course of the exposure lies within the range of experimental error. It is concluded that for doses up to 7000 rads the radiation effects on the polarizer will not degrade the magnetometer performance.

5.2.3.2.3 Radiation Damage Study: MOS Transistor

The high input impedance of the MOSFET* is most attractive for scientific instruments using solid state dc electrometers. Plasma probes, mass-spectrometers and ionization chambers are examples of this type instrument. The MOSFET was selected for radiation testing because of its radiation susceptibility and the difficulties associated with finding an equivalent substitute. A review of the data in the literature indicates a high V_{GST} (Gate Threshold Voltage) sensitivity to ionization radiation.

A sample of six developmental MOSFET's was obtained for the radiation test. Two units failed during the test sequence; one failure was catastrophic and the other failure resulted from increased leakage. It is believed that screening would have eliminated these units from the sample. The failures were not considered to be a function of the radiation exposure.

The test consisted of subjecting the samples to gamma radiation from a Cs^{137} source when biased as shown in Figure 5-33. The exposure rate was measured as 23.4 rads per hour. The devices were removed from the test chamber for parameter checks at cumulative exposures of approximately 100, 200, 600, 1000, 2000, and 4000 rads. The units were returned to the test chamber following each parameter check and bias power was reapplied. The MOSFET parameters of g_m , I_{DSS} , and V_{GST} were recorded for each parametric check.

The device transconductance g_m in millivolts is measured at $V_D = 20.00$ volts and $V_G = 7.00$ volts. I_{DSS} is the device source leakage in nanoamperes measured at 20 volts drain-source voltage. V_{GST} is the device gate threshold or turn-on voltage in volts measured at $V_{DS} = V_{GS}$, $I_D = 10$ microamp.

The parametric variations as a function of radiation exposure are presented in Figures 5-34, 5-35 and 5-36 for V_{GST} , g_m , and I_{DSS} respectively. V_{GST} variations are less than 50 millivolts for 4000 rads exposure except for device No. 80. This sample exhibited a much higher deviation as a function of radiation exposure than the other devices. The reasons for device No. 80's instability are unknown.

*Metal-Oxide Silicon Field Effect Transistor

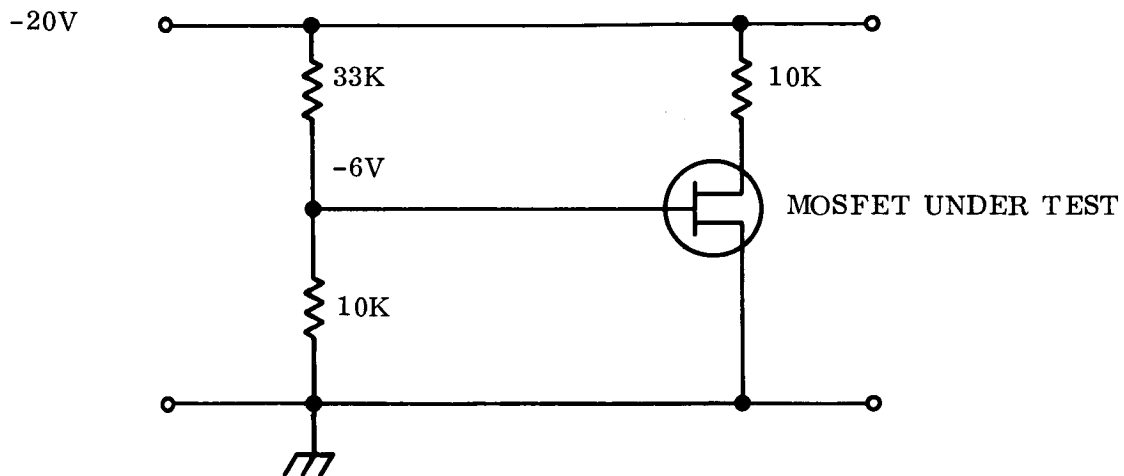


Figure 5-33. MOSFET Test Circuit

For devices 55, 77 and 78, g_m variations were in general less than 10 percent. Device 80, again, exhibited a much higher parameter variation than the other devices.

The I_{DSS} data were much less systematic than g_m and V_{GST} data. The deviations and the nominal values, however, were much less than the device specification of 10 na maximum.

It can be concluded that MOSFET's can be produced that have parametric stability for gamma radiation exposures in excess of 4000 rads sufficient for sensitive electrometer applications. The tests were conducted under low exposure rate more analogous to the RTG environment than most radiation tests.

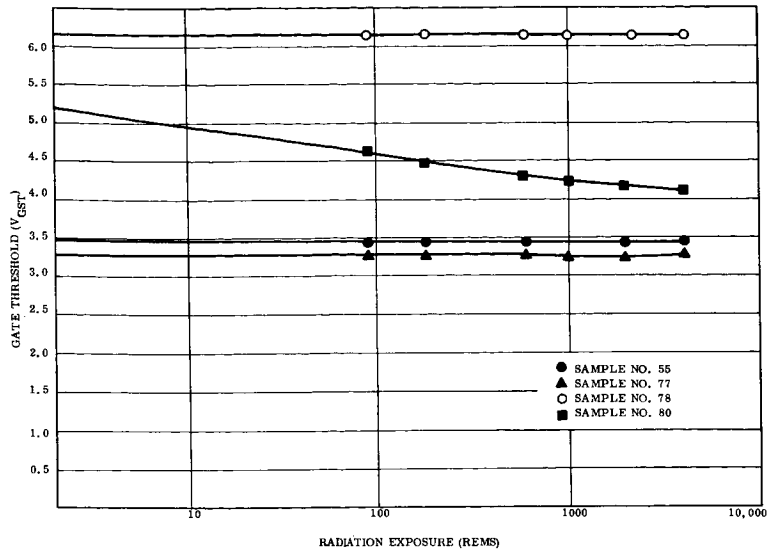


Figure 5-34. MOSFET Device Gate Threshold vs Radiation Exposure

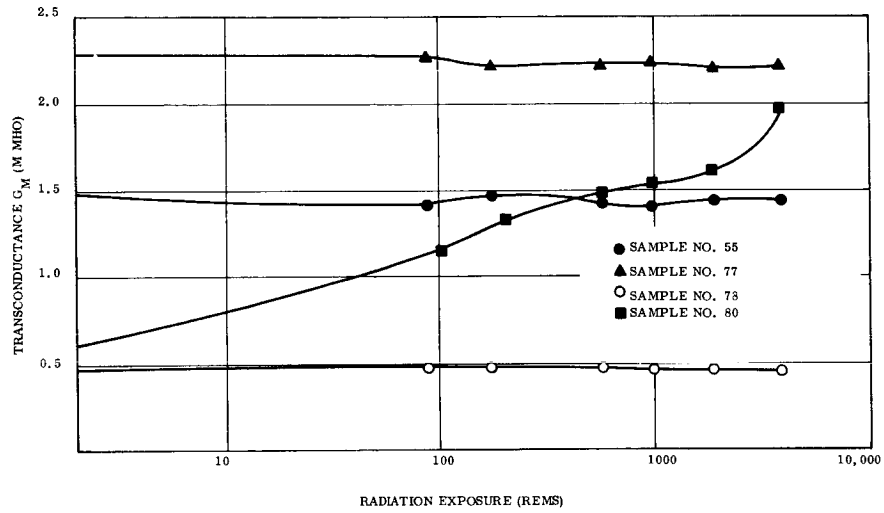


Figure 5-35. MOSFET Device Transconductance vs Radiation Exposure

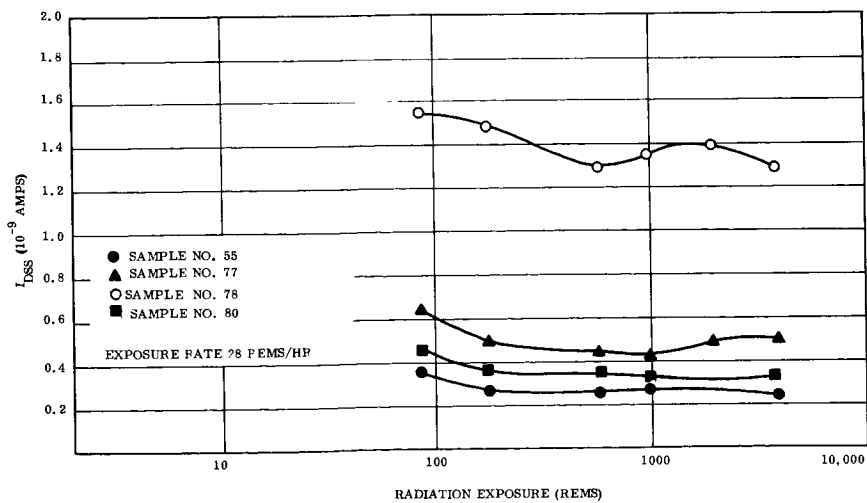


Figure 5-36. MOSFET Device Source Leakage vs Radiation Exposure

5.3 SAFETY

The principal safety criterion regarding the use of RTG's is the assurance that at no time in the life of the generators will the general population be exposed to undue radiological hazards. As noted in the RTG Guidelines, (Section 3.1.1), containment of the RTG isotope fuel under all credible abort environments was assumed to be the approach for meeting the safety criterion.

Two specific studies were conducted relative to the safety problem; these studies are summarized below.

5.3.1 MISSION ABORT STUDY

This study examined the environment to which the RTG's would be subjected in the event of a mission abort, in an attempt to establish suitable protection schemes. The results are reported in Task C Document No. VOY-C1-TR14.

In summary, two methods of assuring fuel containment under re-entry conditions were considered:

- a. Separable re-entry, in which the RTG's are separated from the spacecraft and re-enter with a directed orientation through the use of a stabilizing aerodynamic protection shield.
- b. Integral re-entry, in which no RTG separation is required by virtue of protection material which completely surrounds the vulnerable portion of the RTG.

It was concluded that separable re-entry is difficult to achieve because of numerous active steps that must occur subsequent to the abort event. In general, the separable approach is limited to the class of abort situations in which structural and electrical integrity is still sufficient to permit successful separation.

Integral re-entry, on the other hand, though avoiding system complexities associated with separation, poses weight uncertainty problems because of uncertainties in the re-entry environment. These are associated with the nature of spacecraft breakup during re-entry and the possible effect of onboard propellants in further aggravating the environmental severity.

The re-entry protection weight presently constitutes the largest unknown in the RTG and should be given early priority in the development cycle for a Voyager RTG.

5.3.2 LAUNCH AZIMUTH CONSIDERATIONS

Early in the study, the possibility of launch azimuth restrictions resulting from the use of RTG's was considered. Such restrictions might be desirable to minimize the possibility of impacting the RTG's on populated land masses. Assuming that the RTG's are designed to contain the fuel in the event of a mission abort, then launch azimuth restrictions serve as a backup means to reducing the possibility of nuclear hazard. This is in contrast to the non-containment approach in which the isotope fuel is dispersed at high altitudes subsequent to re-entry burnup. In the latter case launch azimuth restrictions are a more dominant consideration. For either approach, it should be recognized that, subsequent to parking orbit, impact or fuel dispersion can occur over a very large geographical region in the event of failure to inject into a heliocentric orbit.

In the absence of specific hazard probability goals a detailed study of hazard probabilities as a function of launch azimuth was not conducted. Rather, a study of the influence of launch azimuths for different opportunities (1973, 75, 77 and 79 Mars opportunities) was conducted to serve as a possible input to later safety and mission tradeoff studies. This work is contained in Task C Document No. VOY-C1-TR2. The principal results are briefly summarized here.

Figure 5-37 shows the trace of abort landing points for various launch azimuths. Land impact is minimized for launch azimuths of 90 to 115 degrees east of north. The ability to accomplish this with the specific opportunities is summarized below:

- a. The 1973 opportunity appears acceptable via Type I transfers within a 90 to 115 degree launch azimuth.
- b. The 1975, 1977 and 1979 opportunities may be satisfied by Type I transfers if the launch period is less than 45 days. Launch azimuths more northerly than 68 degrees are required for the 1975 and 1977 opportunities.
- c. Type II trajectories would satisfy the 90 to 115 degree launch azimuth and launch periods of 45 days and greater for the 1975, 1977 and 1979 opportunities.

Item b appears to impose the greatest difficulty with respect to the desired launch azimuth range in view of the undesirability of Type II trajectories. As indicated earlier, RTG's designed for fuel containment may minimize the impact of this result.

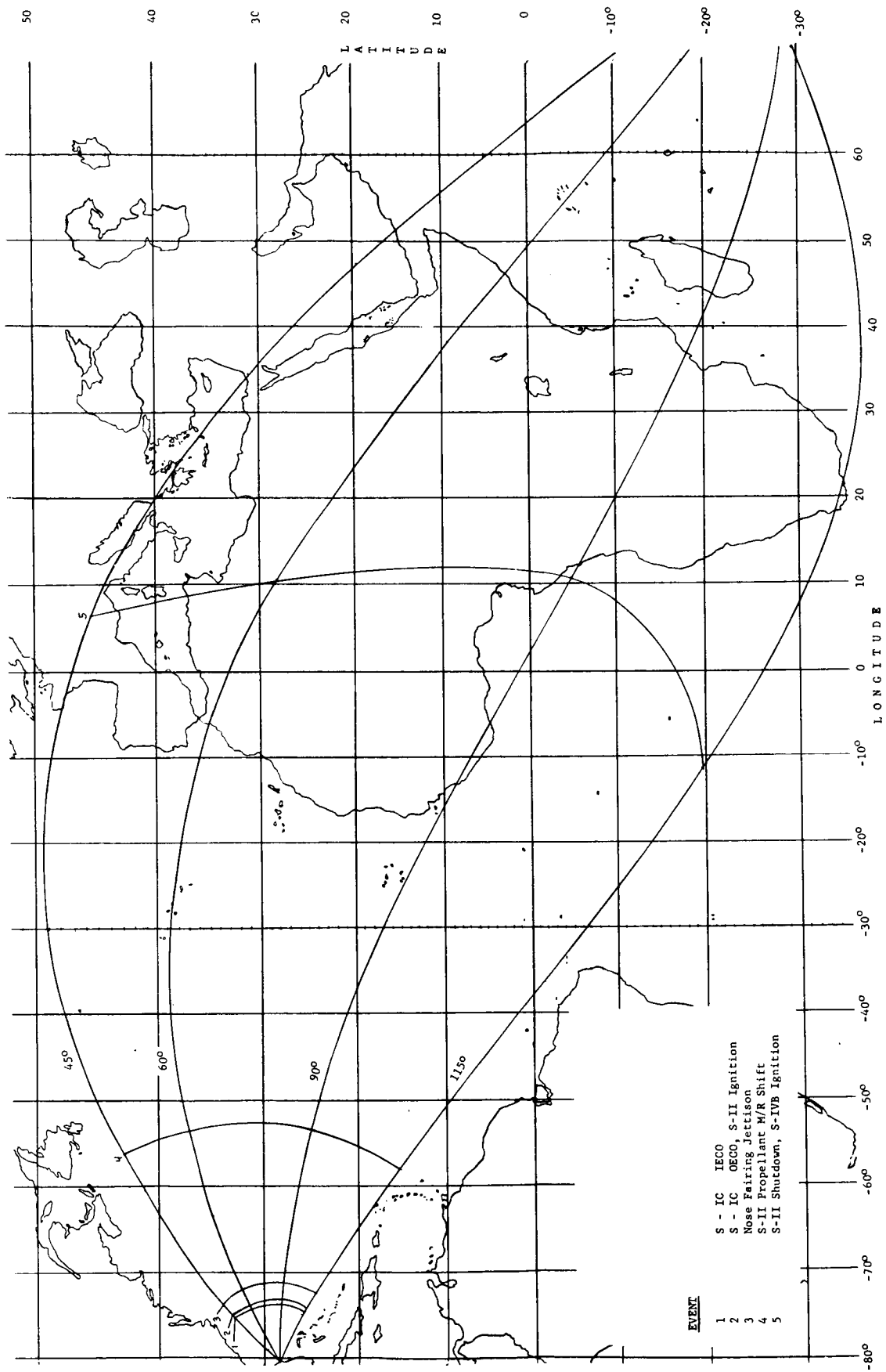


Figure 5-37. Saturn V--Voyager Vacuum Impact Critical Events

REFERENCES

- 5-1 Voyager Task C Document, VOY-C1-TR15, RTG Handbook, S. Freedman.
- 5-2 Voyager Task C Document, VOY-C1-TR3, Spacecraft Electronics and Materials Radiation Sensitivity Study Report, J. Peden, D. Tasca, P. Johnston.
- 5-3 Voyager Task C Document, VOY-C1-TR5, Spacecraft Electronics and Materials Radiation Sensitivity Study Report-Appendices, J. Peden D. Tasca, P. Johnston.
- 5-4 Voyager Task C Document, VOY-C1-TR8, Spacecraft Radiation Mapping Study, J. Peden, H. Bermanis.
- 5-5 Voyager Spacecraft System Phase 1A, Task B, Preliminary Design-Spacecraft Functional Description, DIN-5SD4514, January 31, 1966.
- 5-6 "Neutron Cross Sections," Hughes, D.J. and Harvey, J.A., USAEC Report BNL-325, Brookhave National Lab., July 1955.
- 5-7 Voyager Task C Document, VOY-C1-TR4, Scientific Instrument Radiation Sensitivity Report I, T.D. Roberts.
- 5-8 Voyager Task C Document, VOY-C1-TR11, Scientific Instrument Radiation Sensitivity Report II, F.N. Reilly.
- 5-9 Voyager Task C Document, VOY-C1-TR4A, Supplement to Radiation Sensitivity Report I, T.D. Roberts, J. Peden, D. Matteo.
- 5-10 "Preliminary Assessment of the Effects of Nuclear Radiation on the Nimbus B Spacecraft", HIT-190, (HA-3404-2004), Hittman Associates, Inc., Baltimore, Md., November, 1965. GFSC Contract NAS5-9548.
- 5-11 Fihally, A., NASA/Goddard, monitor for the Hittman Associates Contract, Private Communication, September 9, 1966.
- 5-12 Epstein, J., NASA/Goddard, Private Communications, July 26, 1966 and August 24, 1966.
- 5-13 Wilbur, A.C., NASA/Ames, Private Communication, July and October, 1966.
- 5-14 Space Research V: Proceedings of the Fifth International Space Science Symposium, Florence, May 12-16, 1964, ed. D.C. King-Hele et al, North-Holland Publishing Company, 1965.

- 5-15 R. E. Slocum and F.N. Reilly, in Proceedings of the International Symposium on Space Phenomena and Measurements, Detroit, 1962, IEEE Transactions on Nuclear Science, NS-10, 165 (1963).
- 5-16 E.J. Smith, L. Davis, Jr., J. P. Coleman, Jr., D.E. Jones, "Science", 149, 1241 (1965).
- 5-17 Final Engineering Report: Prototype Low-Field Magnetometer, Texas Instruments Incorporated, 25 June 1962, prepared under JPL Contract No. 950152-1.

SECTION 6
COMPARISON OF RTG-POWERED
AND SOLAR-POWERED SPACECRAFT

A detailed comparison of the two spacecraft types was presented in Task C Document No. VOY-C1-TR17. The more significant results are extracted and presented below.

In order to extend comparisons beyond the RTG-powered and solar-powered baseline designs (described in Sections 3 and 4), growth versions are first considered in Section 6.1. This permits a broader interpretation of the comparison results which follow. A final section discusses RTG spacecraft program implementation.

6.1 SPACECRAFT GROWTH VERSIONS

6.1.1 RTG-POWERED SPACECRAFT

The RTG sizing data contained in Section 5.1 indicate that RTG's of 125 watt rating may be conveniently mounted on the spacecraft in place of the 75 watt RTG's. There appears to be more than sufficient mounting area available for this purpose. In addition it appears feasible to mount four additional RTG's around the cylinder enclosing the MC and OA engine, as shown in Figure 6-1. This possibility was only examined on a preliminary basis to verify that required fields of view of the spacecraft were not severely comprised and that overall integration factors could be reasonably satisfied. Some of these factors are discussed briefly below.

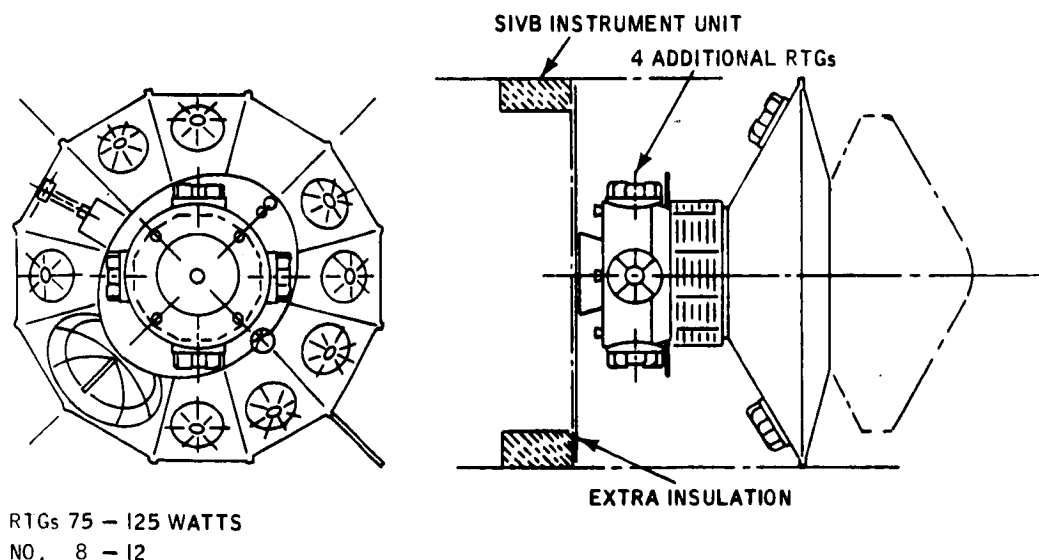


Figure 6-1. RTG Spacecraft Growth Version

6.1.1.1 Thermal Effect

The principal thermal effect will concern the need for additional cooling during prelaunch operations. The information contained in Section 3.3.5 permits an estimation of this additional cooling which will result from two principal factors: (1) cooling to maintain acceptable spacecraft temperatures during prelaunch operations; and (2) further cooling just prior to launch to depress temperatures such that excessive temperatures are not reached at the time of shroud separation. During other mission phases, (such as cruise, etc.) it is considered that proper thermal insulation can be incorporated to avoid thermal problems. This will of course depend on the extent of growth considered and proposed RTG mounting locations.

6.1.1.2 Radiation Effect

Fundamentally, the magnitude of the number flux of radiation from the RTG's is linearly proportional to the amount of the radioisotope fuel present; it is thus also linearly proportional to the thermal power level of the devices. In practice this clean relationship is perturbed by effects of RTG geometry and by self-shielding of the radiation within the RTG. At one meter or more from the RTG, an increase in the power by 50 percent will produce an increase in dose rate by just about 50 percent. The increase will be less at shorter distances. Increasing the RTG diameter might increase the thickness of the various materials surrounding the fuel and also the fuel itself. As a result, neutron and gamma absorptions inside the RTG may be slightly increased. This self-shielding effect is not significant and will not noticeably affect the direct proportionality between radiation and power within the 50 percent growth range. It is believed that the most significant effect of increasing the radiation level could well be on the prelaunch ground handling activities where it will be reflected in proportionately reduced residence times for personnel in certain exposed locations. The effect of RTG growth, of say up to 100 percent, on spacecraft equipment will be negligible from a radiation sensitivity standpoint, since the equipment is exponentially rather than linearly sensitive to the radiation dose (see Figures 5-25 and 5-26).

6.1.2 SOLAR-POWERED SPACECRAFT

Growth for the solar powered spacecraft is provided by the deployment of auxiliary panels. The placement and size of these panels is influenced by the following factors:

- a. Antennae viewing requirements
- b. Planet scan platform viewing requirements
- c. Sun sensor viewing requirements
- d. Packaging volume requirements for storage of array panels in the launch configuration
- e. Bending moment limitation of the deployed panel configuration

Figure 6-2 shows two growth versions for the basic spacecraft configuration described in Section 4. The first growth version, Figure 6 (b), uses a simple single panel deployment scheme similar to that employed on Mariner. Existing hardware such as hinges, springs, latches and deployment dampers would be utilized with minimum modifications required. The panels are attached by hinges to the closure ring bounding the fixed portion of the solar array and are folded back to their stowed launch position behind it. The length of the panel is restricted during deployment by the capsule interface boundary.

It is possible that a panel area exceeding the 3.9 square feet shown is obtainable by increasing this length. This depends on further definition of the adjacent portion of the capsule.

The second growth version, Figure 6-2 (c), requires a compound deployment. Some of the fixed array panels are required for support of various spacecraft components, and to provide torsional shear capability for the spacecraft support structure. These fixed panels are located in the vicinity of the high gain antenna and the planet scanner. The remaining panels are hinged at the ends adjacent to the spacecraft body and are deployed to a position about 10 degrees past the plane normal to the sun line, allowing deployment of secondary panels stowed underneath and hinged at the outboard edges of the primary panels. The primary panels employ a bracing strut with an over dead center locking device to stiffen them against maneuver loads. A sequencing device must be used to prevent premature deployment of the secondary panels.

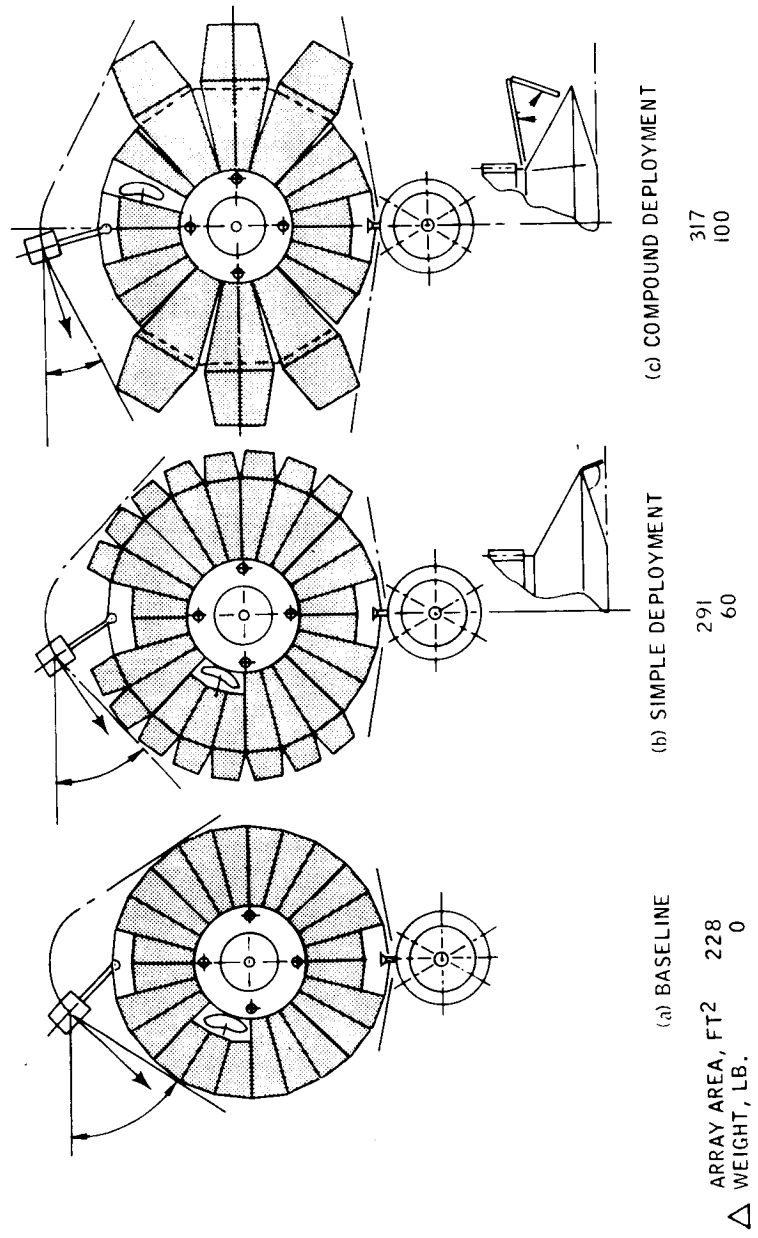


Figure 6-2. Solar Spacecraft Growth Version

6.2 WEIGHT AND POWER COMPARISONS

A power comparison of the baseline RTG and solar powered design is shown in Figure 6-3 for that portion of the mission beyond planetary encounter. Because power source regulation equipment differs for the two spacecraft types, power output has been referenced to the main regulated bus from which most of the spacecraft loads draw power. Thus, the RTG's, with an installed capability of 600 watts, can produce 512 watts at the regulated bus. This output reflects end-of-life (EOL) capability. In actuality, the RTG power will be slightly higher just after encounter because of degradation allowance, as discussed in Section 5.1. The solar power capability is based on the arrival times listed below for each of the Mars opportunities:

<u>Opportunity</u>	<u>Nominal Arrival Date</u>
1973	24 January 1974
1975	16 April 1976
1977	15 June 1978
1979	26 July 1980

The solar power curves do not include any allowance for solar occultations. Figure 6-4 provides appropriate occultation correction factors. If, for example, a 0.10 fractional eclipse time is encountered, then the effective array power is 82 percent of that indicated for any condition on Figure 6-3, including such power availability from batteries during the occultation itself.

If load demands are reduced concurrently with the occultation then of course more array power is available during the non-occulted periods up to the limits shown on Figure 6-3. The ratio of loads during occulted periods to those during non-occulted periods, expressed in terms of energy, will modify the result of Figure 6-4 to some extent, since battery efficiency factors are taken into account. However, the curve provides a good estimation for comparison purposes.

Figure 6-5 provides another interpretation of power availability after encounter and applies only to the 1973 mission. Using a conditioned baseload demand of 326 watts, based on the Task B design requirements, this figure shows the additional power that would be available.

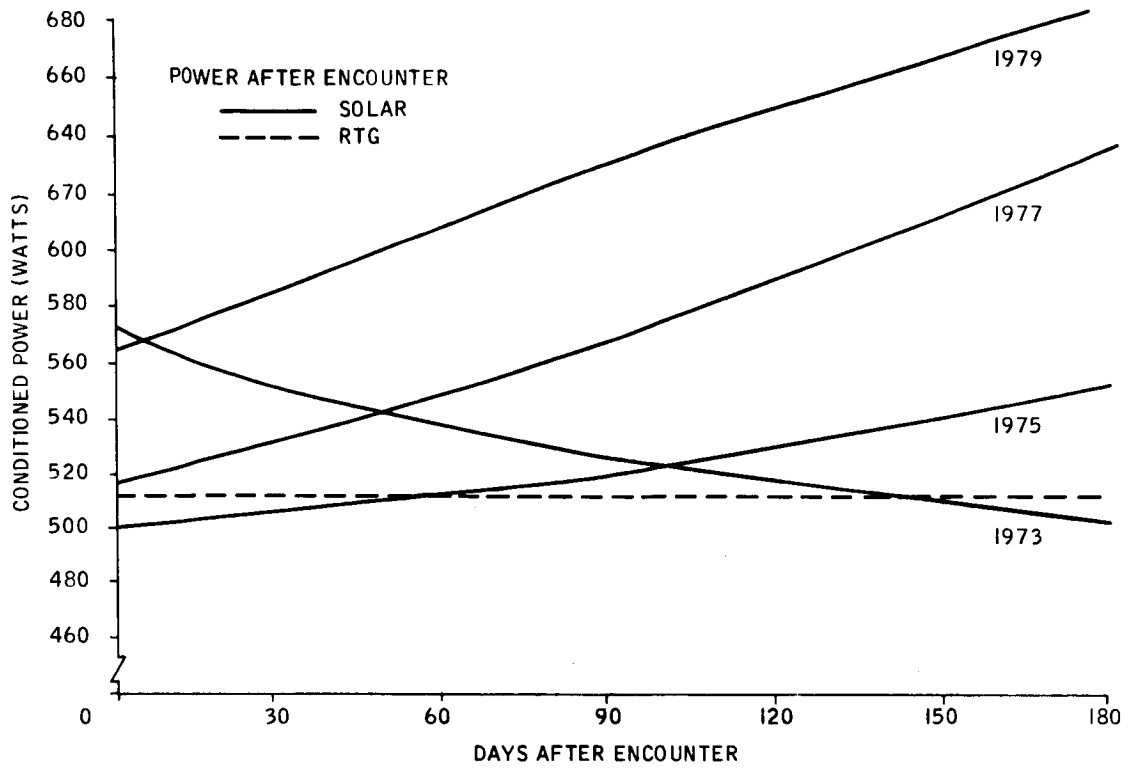


Figure 6-3. Power After Encounter

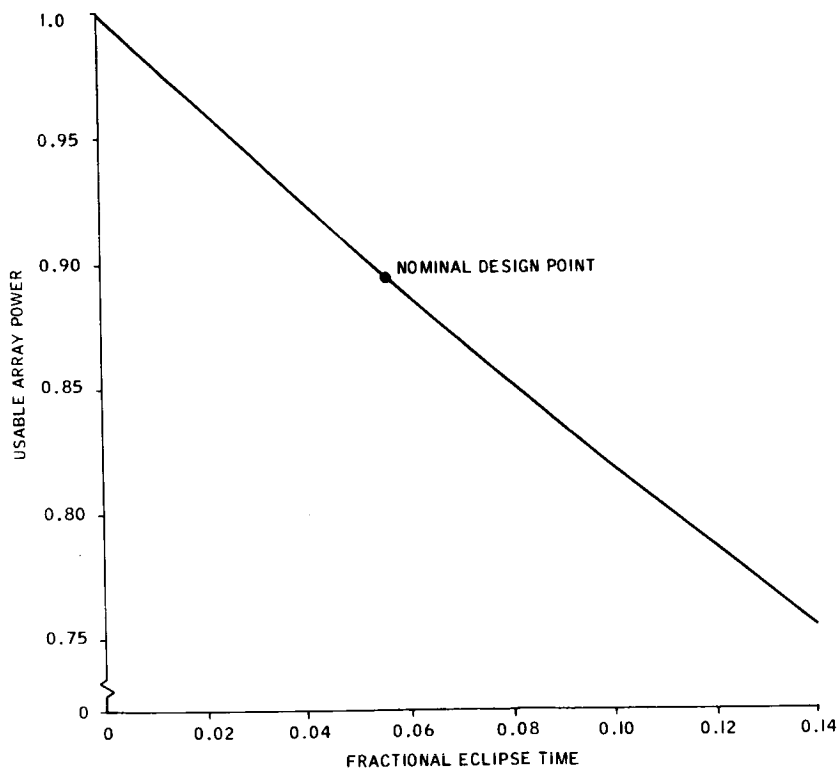
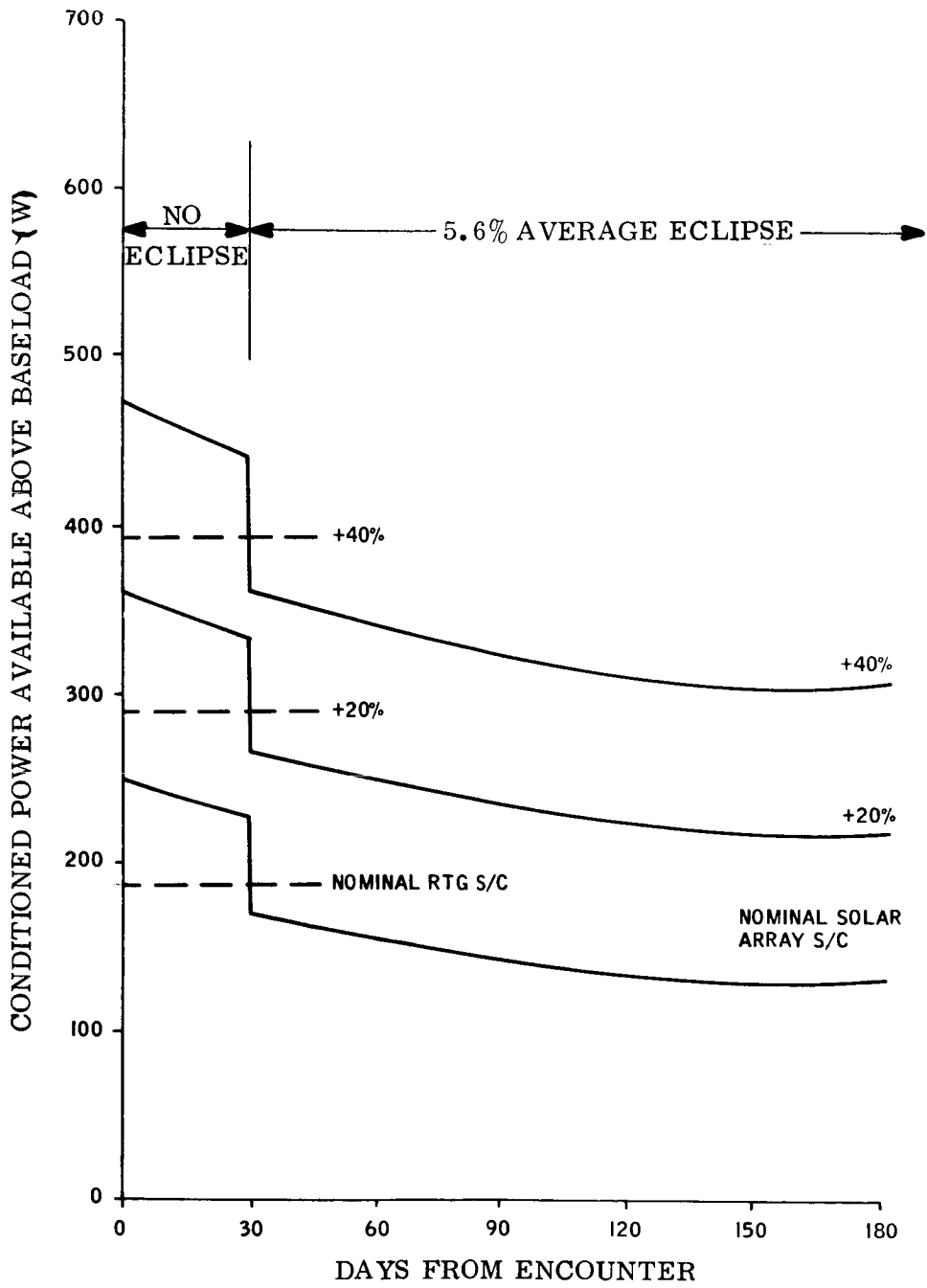
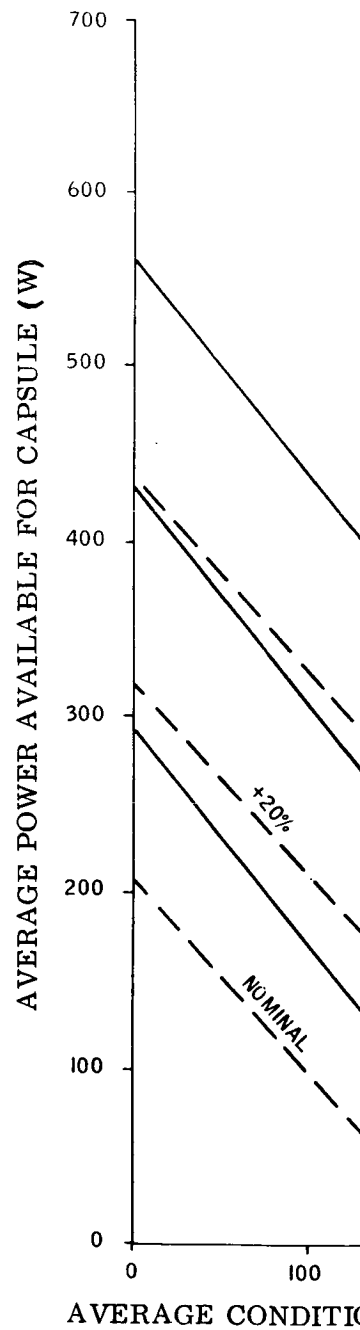


Figure 6-4. Usable Array Power Versus Fractional Eclipse Time



(a)



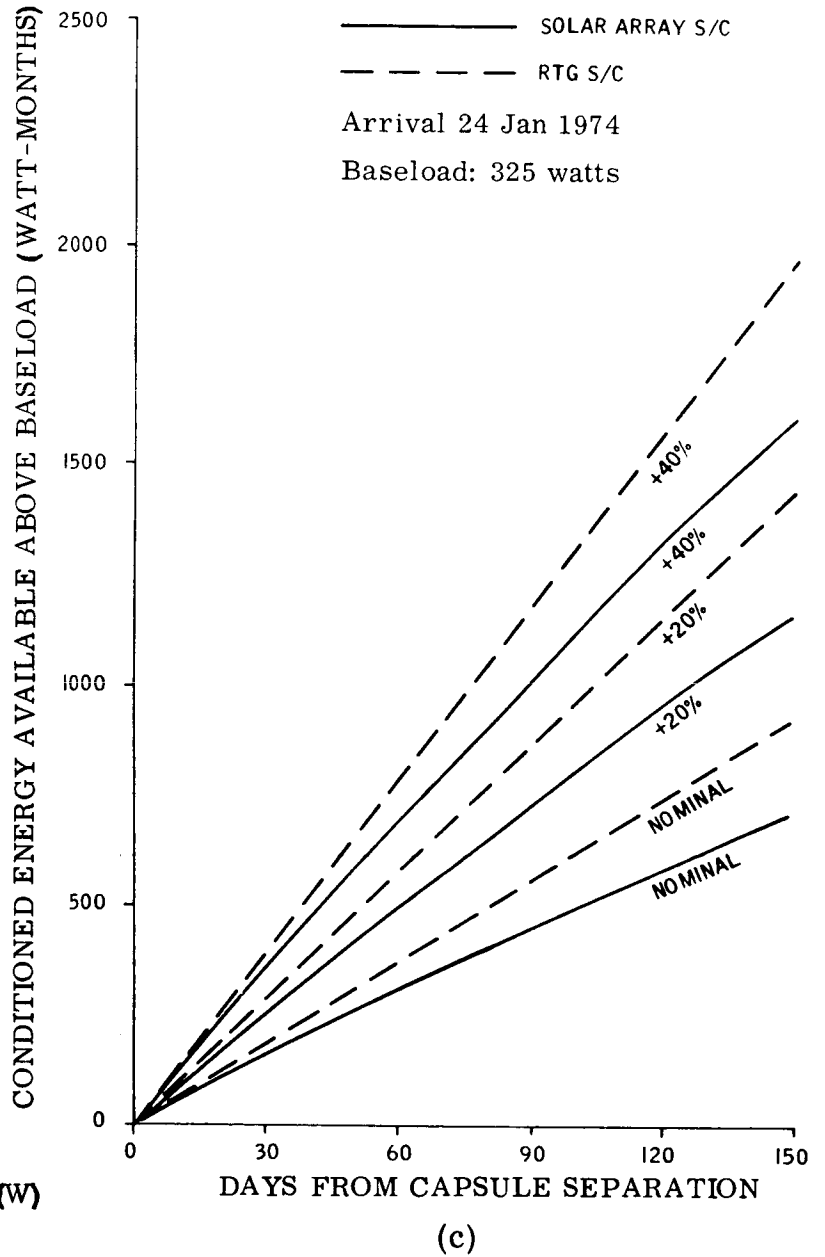
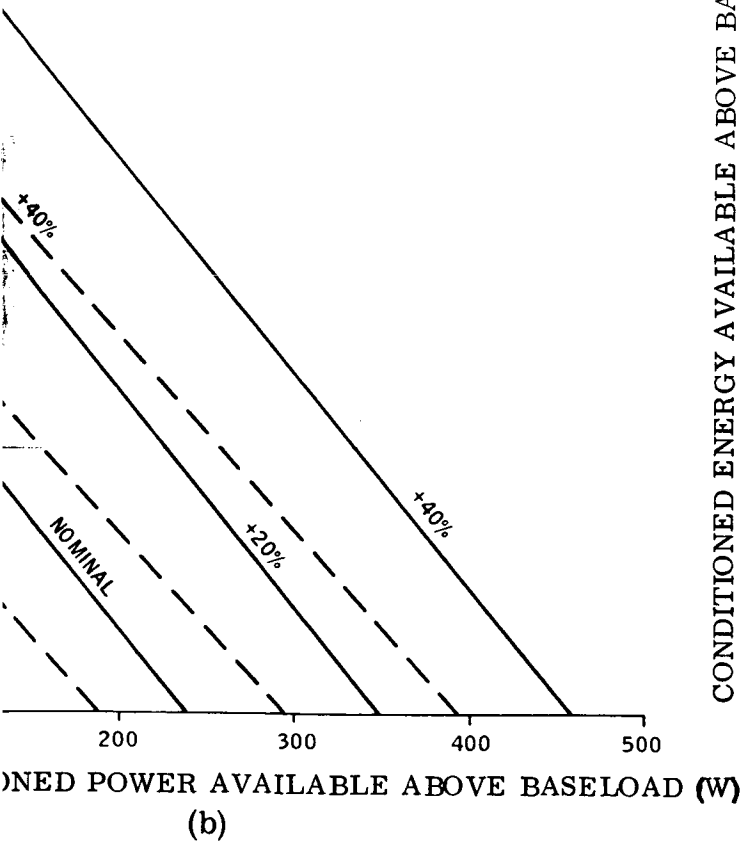


Figure 6-5. RTG and PV/B Power Performance—1973 Mission

The 20 and 40 percent growth curves refer to such increases in area for solar arrays and power output for RTG's. For the first 30 days after encounter it is assumed that no occultations occur; thereafter an average occultation period of 5.6 percent is assumed. This is shown in Figure 6-5(a). Figure 6-5(b) shows the tradeoff between science and capsule power up to the time of capsule separation assumed to occur no later than 30 days after encounter. For either the solar or RTG systems this is a particularly crucial period because of the combined power demands of the science payload and the capsule. The nominal 200 watt capsule load defined for the Task B design is presumably used for thermal reasons and cannot be interrupted for long periods. On the other hand, the science payload demands just after encounter may be high to establish suitable landing zones for the capsule and to accumulate a maximum of scientific data as early as possible in the orbital phase. The division of available power to these principal demands has not been established in this study since many extraneous factors enter into the consideration, such as orbit selection and the nature of the science instruments themselves. Figure 6-5(b) only provides one element entering into this consideration. Figure 6-5(c) integrates the power available above the baseload over the time of the orbital phase and provides a measure of overall science data return capability assuming the additional power is devoted to Science.

Curves similar to Figure 6-5 have been prepared for the 1975, 1977 and 1979 missions and have been presented in VOY-C1-TR17.

Based on the growth versions described in Section 6.1, Figure 6-6 summarizes power capability as a function of spacecraft bus weight. RTG weight increase is based on the results given in Section 5.1; solar array weight is based on 1 pound per square foot for deployed panels. The spacecraft weight increases shown in Figure 6-6 do not include increases due to other factors, and should therefore be used only on a relative basis for comparing RTG and solar power.

Figure 6-7 shows a final weight comparison curve and shows the integrated energy above the baseload equivalent to a 150 day orbital mission, beyond the time of capsule separation, as a function of spacecraft bus weight.

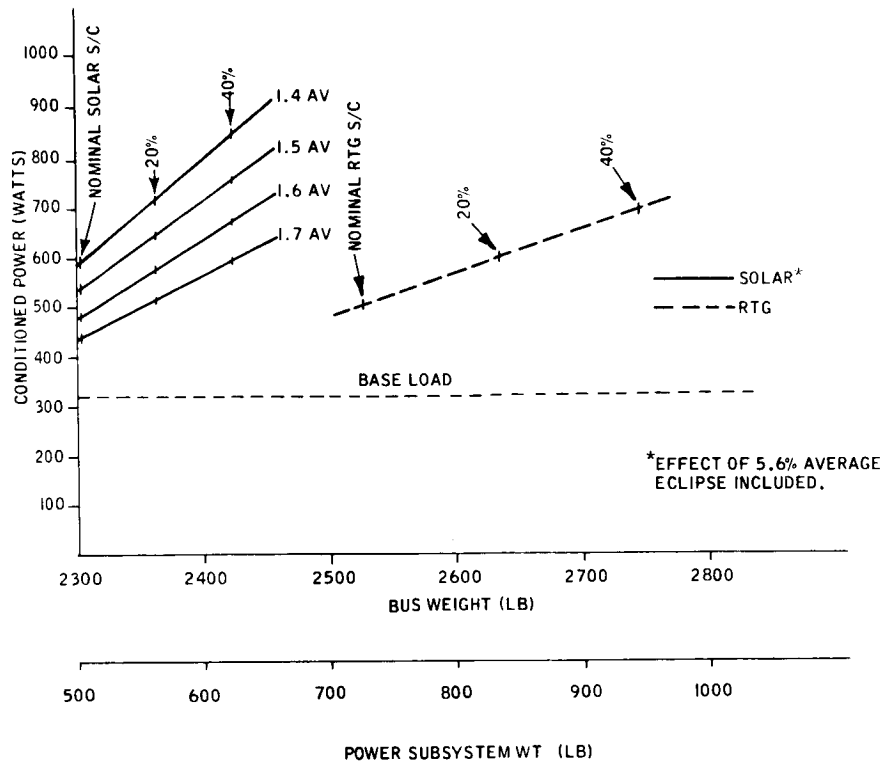


Figure 6-6. Conditioned Power Versus Weight

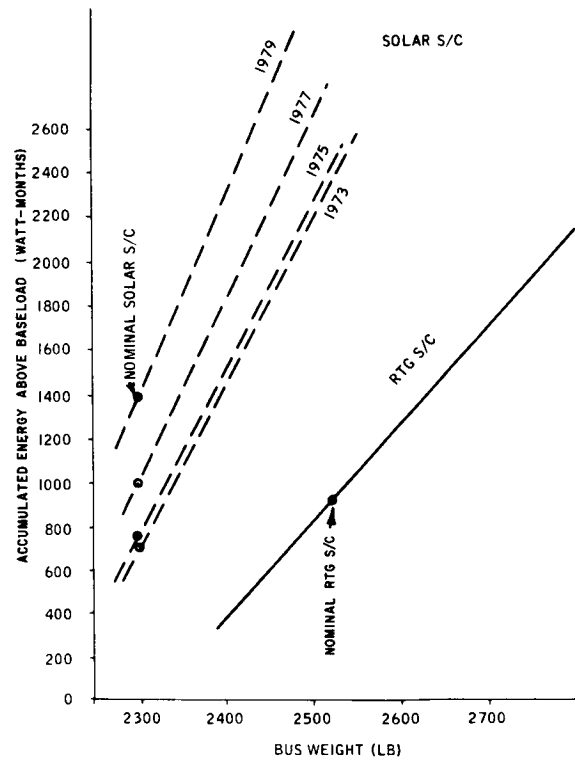


Figure 6-7. Accumulated Energy Comparison

6.3 RELIABILITY

The relative reliabilites of the RTG-powered and solar-powered spacecraft are compared below on a qualitative basis. Insufficient design definition and failure rate data ruled out a quantitative approach originally considered. The qualitative data is sufficiently strong to identify the RTG spacecraft as the more reliable system for the following reasons.

6.3.1 INDEPENDENCE OF SOLAR ORIENTATION

Because of the removal of battery energy limitations, RTG power results in benefit to several aspects of spacecraft operation:

- a. Midcourse Maneuvers - Under abnormal conditions, such as failure to verify the proper vehicle attitude before engine firing, it may be necessary to reacquire the sun, recharge the batteries (in the case of a solar powered vehicle), and re-attempt the midcourse correction sequence. RTG's would not require the reacquisition sequence (at least not for battery recharging) and would permit longer periods for troubleshooting and corrective action. Reliability is enchanced by the potential avoidance of additional maneuvers, and the associated saving of attitude control gas.
- b. Orbit Insertion Maneuver - As differentiated from midcourse correction maneuvers, there is a very limited period during which the orbit insertion maneuver can be executed. It is estimated that with solar power a maximum of 5 hours is available for this maneuver because of battery energy limitations. About two attempts of achieving the proper spacecraft attitude can be made. An analysis has indicated that the solar panels are typically pointed 150 to 175 degrees from the sun so that no battery charging is possible. With RTG power this period can be increased to permit additional attitude attempts. The exact number depends on gyro drift and errors in orbit insertion parameters that would not result in violation of the planetary quarantine constraint. A gross estimate indicates that a 10 hour period might be acceptable. Thus the RTG's provide the potential for increased mission reliability by permitting greater flexibility with respect to this critical maneuver.
- c. Loss of Solar Reference - As in the solar powered spacecraft, the RTG powered spacecraft uses a Sun-Canopus attitude reference system. In the case of the solar powered spacecraft, failure of the fine Sun sensors or acquisition Sun sensors could result in a variety of failure modes ranging from minor effects to total mission failure. The question of failure effects is complex and depends on the nature of the failure and conditions at the time of failure. The use of redundant sensors potentially relieves this problem and the question is then one of how to implement such redundancy. Logic to distinguish between good and bad sensors is not always straightforward, and majority vote techniques employing additional sensors may be required. RTG's, through their ability to sustain power, may permit reductions in such complexity by permitting ground control switchover to redundant sensors by interpretation of telemetry information.

6.3.2 ELIMINATION OF HIGH DUTY CYCLE BATTERIES

As mentioned earlier, spacecraft reliability increases with the removal of battery energy limitations. In addition, batteries themselves, unless properly accommodated, can provide further sources of unreliability. Both silver-cadmium and silver-zinc batteries (the types considered thus far for Voyager) require careful charge and thermal control. The sensitivity of these control parameters is such that failure may occur if their limits are slightly exceeded. Thus very conservative design approaches are used, backed up by extensive testing under simulated flight conditions. Even so, there is usually some doubt that all possible conditions have been sufficiently simulated. Both silver-cadmium and silver-zinc batteries exhibit limited cycle life capability. This, along with the above reasons, indicates improved reliability with RTG's. Total elimination of batteries is not feasible because of high power momentary loads. However, such batteries experience very few charge/discharge cycles and would therefore be more reliable.

6.3.3 CONSTANT OPERATING CONDITION

RTG's operate under constant temperature conditions throughout their life. Elements of the solar power system on the other hand experience varying temperature conditions. The solar array temperature decreases gradually from 160°F to 50°F in going from Earth to Mars. During maneuvers or occultations its temperature may drop to minus 200°F. During eclipse seasons in Mars orbit such temperature cycles (50°F to -200°F) will occur for many successive orbits. The batteries similarly experience variations in dissipated heat. The batteries require close temperature control and therefore the dissipated heat variations will be reflected in cyclic operation of the thermal controllers.

6.3.4 FIXED HIGH-GAIN ANTENNA

The independence of RTG's for solar orientation permits the use of a fixed high-gain antenna. The method for achieving this is described in Section 3.4.2. In effect, digital Sun sensors are substituted for a 2-motion antenna gimbal and this is considered to increase spacecraft reliability. This could be achieved with solar power but would require deployed solar panels to provide sufficient power during Sun-bias operation.

6.4 MISSION FLEXIBILITY

RTG-powered and solar-powered spacecraft are compared below as they relate to several mission flexibility criteria:

6.4.1 EFFECT OF SOLAR DISTANCE

The ability of RTG's to operate independently of the sun distance provides a very significant advantage over solar power. For a mission to Jupiter using solar power, it would be necessary to deploy an area of about 1500 square feet to provide 600 watts of raw power. This is about six times the fixed area for current Voyager solar-powered designs. Solar array designs are presently being developed for weight of 0.35 to 0.5 pound per square foot and would result in a total array weight of 500 to 750 pounds. Assuming that about 120 pounds of batteries would be required, the solar-powered system would weigh at least several hundred pounds more than an RTG-powered version. Complexity in the solar array design would result from the large variation in generated power in going from Earth to Jupiter and in the need to withstand midcourse correction thrust loads.

In missions toward the sun, solar arrays would ultimately encounter problems of excessive temperature operation. At Venus the problem can probably be adequately handled. In orbital eclipse operation array temperature excursions might be rather severe and would degrade array reliability.

6.4.2 ORBIT SELECTION

Constraints on planetary orbit selections may be related to avoiding or reducing the extent of battery discharge during solar occultations. Such constraints pertain to solar powered spacecraft and are removed with the use of RTG power.

6.4.3 LAUNCH AZIMUTHS

Safety questions relating to mission aborts and the possible need to confine the RTG isotope fuel within certain geographical zones may restrict the range of launch azimuths. The implications of such restrictions can only be assessed in terms of a specific mission and associated hazards analysis.

6.5 DESIGN IMPLEMENTATION

The items discussed below are those principally affected by RTG integration in the general area of spacecraft design implementation. Comparisons are made relative to solar spacecraft design implementation in the specific areas identified.

6.5.1 THERMAL INTEGRATION

The principal thermal problem identified for the RTG's concerns the need to provide under-shroud cooling during prelaunch phases. Such cooling will have to be provided continuously, with only short interruptions, from the time that the spacecraft is encapsulated in its shroud and end diaphragm dirt barriers. Although the solar-powered spacecraft may also require cooling to remove ambient heat loads, the problem is much less severe since the RTG's dissipate about 15 kw (t) per spacecraft and the solar-powered spacecraft will dissipate from 0 to 300 watts, depending on particular checkout sequences.

Assuming that the spacecraft electronics and propulsion unit temperatures are about 80 to 90°F at launch, no thermal problem has been identified for either spacecraft (solar or RTG) until they are separated and on a heliocentric transfer trajectory. This is based on a maximum 90-minute period from launch until separation.

Similarly, no thermal problem was identified for either spacecraft during free space flight.

Some advantage is seen for the RTG spacecraft with respect to thermal integration of the lander. Previous guidelines indicate that 200 watts of electrical power are needed by the lander more or less continuously during the cruise phase. Short interruptions are permissible during maneuver or occultation periods. Assuming that this power is used principally to maintain temperatures within the lander, it is conceivable that with the design of particular thermal paths in the lander, the RTG's can supply this power thermally rather than electrically. Figure 6-8 is used to illustrate this ability of the RTG's in comparison with a solar-powered spacecraft. The left-hand sketch shows a cross section of the baseline solar-powered spacecraft and the right-hand sketch shows the baseline RTG-powered spacecraft. In near-Earth space the solar array temperature is around 160°F. It is possible to imagine that the lander biocarrier is designed to intercept radiated heat from the back

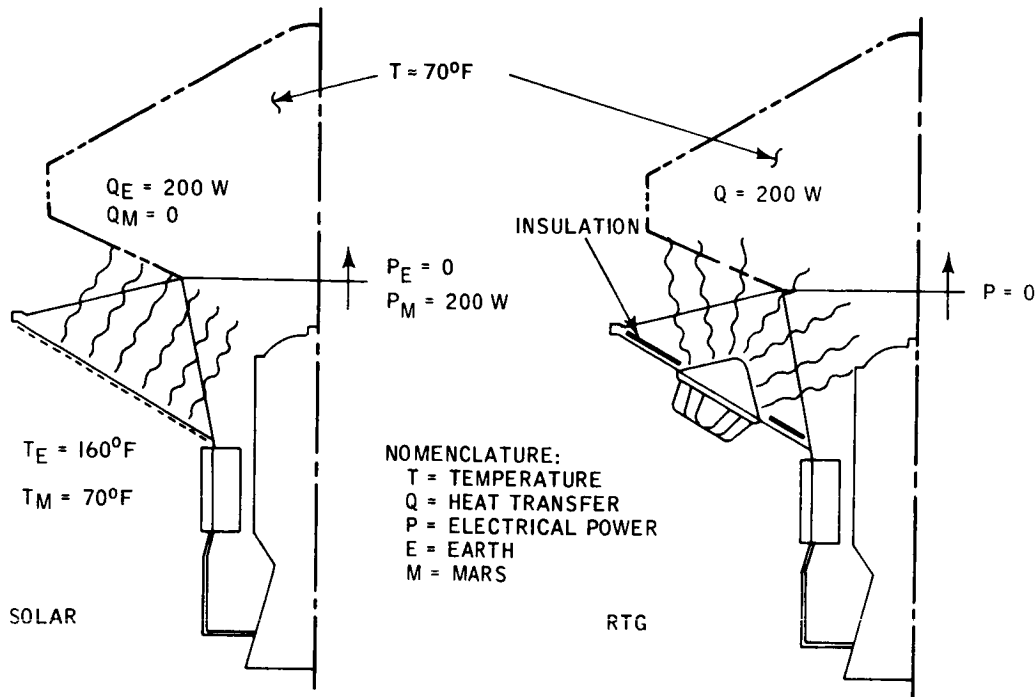


Figure 6-8. Lander Thermal Integration

solar array surface such that 200 watts of power, Q_E , is introduced into and distributed within the lander. Both the interception and distribution of this power require intricate but conceptually feasible thermal design. No electrical power, P , from the spacecraft would be required during this period. In near-Mars space the solar array temperature is around 70°F . Assuming the lander biobarrier temperature is similar, no radiative heat transfer is possible and the 200 watts must be supplied electrically.

With the RTG's, on the other hand, the amount of heat intercepted by the lander can be varied by adjusting the thermal impedance of the RTG thermal barrier as shown in the right-hand sketch. Once established, this heat input is constant, assuming the effects of the varying solar input are removed by properly insulating the back surface of the RTG mounting panels.

To summarize the above: With solar power, the transfer of power to the lander by thermal means is not attractive because of the varying solar constant. Since solar electrical power

would be required anyway in near-Mars space and is in excess of that required in near-Earth space, it is probably the best means of supplying the lander power as far as a solar-powered spacecraft is concerned. Alternately, the constancy of the RTG thermal environment makes the thermal transfer of power to the lander more attractive. The alleviation of a 200 watt electrical requirement for the RTG's during the post-injection period with the lander still on-board would permit more power to be devoted to planetary science.

6.5.2 RADIATION

Nuclear radiation from the RTG's influences the following areas of spacecraft design.

6.5.2.1 Spacecraft Equipment

Threshold damage effects are predicted to occur in several types of electronic equipment. The extent of effects is documented in detail in Task C Document Nos. VOY-C1-TR3 and TR5. It is expected that component and circuit derating will adequately solve this problem. Testing of some of the components and circuits predicted to be more sensitive will establish the need for imposing the radiation environment as a general design requirement for spacecraft equipment. Similar though less severe requirements may be necessary for the solar powered spacecraft from two possible sources: (1) the use of RTG's in the lander; (2) solar flare protons. With the occurrence of solar storms, the equivalent neutron effect of the solar flare protons has been estimated to be about one-fourth to one-half as damaging as the RTG neutrons.

6.5.2.2 Science Integration

Twenty-two possible instruments for use on the orbiting spacecraft have been examined with respect to interaction with an RTG power source. Of these, seven would experience dynamic interference from the RTG radiation and are listed below:

- a. Gamma Ray Spectrometer
- b. Cosmic Ray Telescope
- c. Plasma Probe
- d. Mars Spectroscope

- e. Trapped Radiation Detector
- f. Ion Chamber
- g. UV Spectrometer

All of these instruments are radiation detection devices, so that solutions aimed at permitting their use must in some way discriminate between the natural radiation of interest and those emanating from the RTG's. Solutions will in general combine the effects of shielding, distance and possible instrument redesign. If instruments in this category are considered for use on an RTG-powered spacecraft, extensive analysis and testing will be required to solve the indicated incompatibility.

The possible use of magnetometers was examined in Document No. VOY-C1-TR7. The results indicated that background fluxes were sufficiently low for magnetometers mounted about 5 to 10 feet from the maximum diameter of the spacecraft. Of particular note is the fact that the magnetic field remains relatively stable throughout the mission, independent of solar distance and occultations. Contrasted with this, the solar array contribution to the flux might be expected to vary to a greater extent since higher array current is required in near-Earth space because of lower array voltages (and vice-versa in near-Mars space).

6.5.2.3 Personnel Radiation Exposure

Data contained in the RTG Spacecraft Design Definition Report, VOY-C1-TR16, indicate that unshielded fueled RTG's on the spacecraft will limit the amount of time that personnel can work around the spacecraft during prelaunch ground operations. By delaying fuel loading until the latest possible time and placing protective shielding near the RTG's the problem can be minimized. It does nevertheless necessitate additional procedures that will require careful control and monitoring.

6.5.3 DEVELOPMENT

The principal development requirement for the RTG-powered spacecraft concerns re-entry protection to assure fuel containment in the event of a near-Earth mission abort. The problems relating to this have been discussed in the Mission Abort Profile Report, VOY-C1-TR14.

Since the re-entry protection intimately influences the overall RTG designs, both would undoubtedly be developed concurrently. However, the basic operating elements of the RTG could depend heavily on well-developed designs, such as SNAP-27, and in this sense these elements are within the category of available technology. All non-similar elements of the solar-powered spacecraft (those principally associated with the power subsystem) also fall within the category of available technology.

6.5.4 TEST

The principal items of comparison identified in this area are discussed below.

6.5.4.1 Power Subsystem

Since the heat output of the RTG fuel capsules can be simulated within several percent by electrical heater simulators, the overall power system performance can be accurately measured in ground tests. Of course, these tests could be performed with actual fuel capsules, but the simulators permit unlimited testing without radiation exposure to personnel. Contrasted with this, test of the total solar power system requires a source of solar simulation. This is complicated by the need for a varying solar input simulating the actual flight condition and the need to duplicate predicted panel temperature conditions. These considerations can lead to very sophisticated test equipment. The practice has been to predict solar array output on the basis of terrestrial measurements and careful extrapolation of solar intensity and panel temperatures. Limited power subsystem testing with full solar arrays may be conducted to verify interface compatibility but overall performance mapping is difficult and usually avoided. Solar array simulators are used to duplicate the solar array electrical characteristics for system testing, but here too the simulation is only as good as predicted analysis will permit. In an overall sense ground testing of an RTG power system provides a more accurate appraisal of space performance and therefore increased confidence in its operation.

6.5.4.2 Radiation Test

With respect to the use of radiation detecting instruments as part of the science payload, verification of their compatibility with the RTG-powered spacecraft may result in the need for complicated test arrangements. Of particular concern are the possibilities of secondary

radiations from surrounding materials not necessarily a part of the spacecraft - walls, test equipment, etc. The complexity of the problem will depend largely on the nature of the particular instruments being used.

6.5.4.3 Magnetic Tests

As in the case of power subsystem test, light stimulation of the solar array would be required to induce currents to permit magnetic mapping of the spacecraft. A number of such tests might be required to determine the effects of varying sun distances and occultations. With the RTG's these complexities are reduced, since the RTG contribution to the magnetic flux remains constant independent of solar intensity. With actual fuel capsules and proper compensation for the Earth magnetic flux contribution, ground test mapping should closely duplicate the spacecraft magnetic fields in space flight. Some additional compensation might be required if electrically simulated fuel capsules are used because of power leads. With careful attention to minimizing the areas of the enclosed current loops, this problem can be adequately handled.

6.6 PROGRAM IMPLEMENTATION

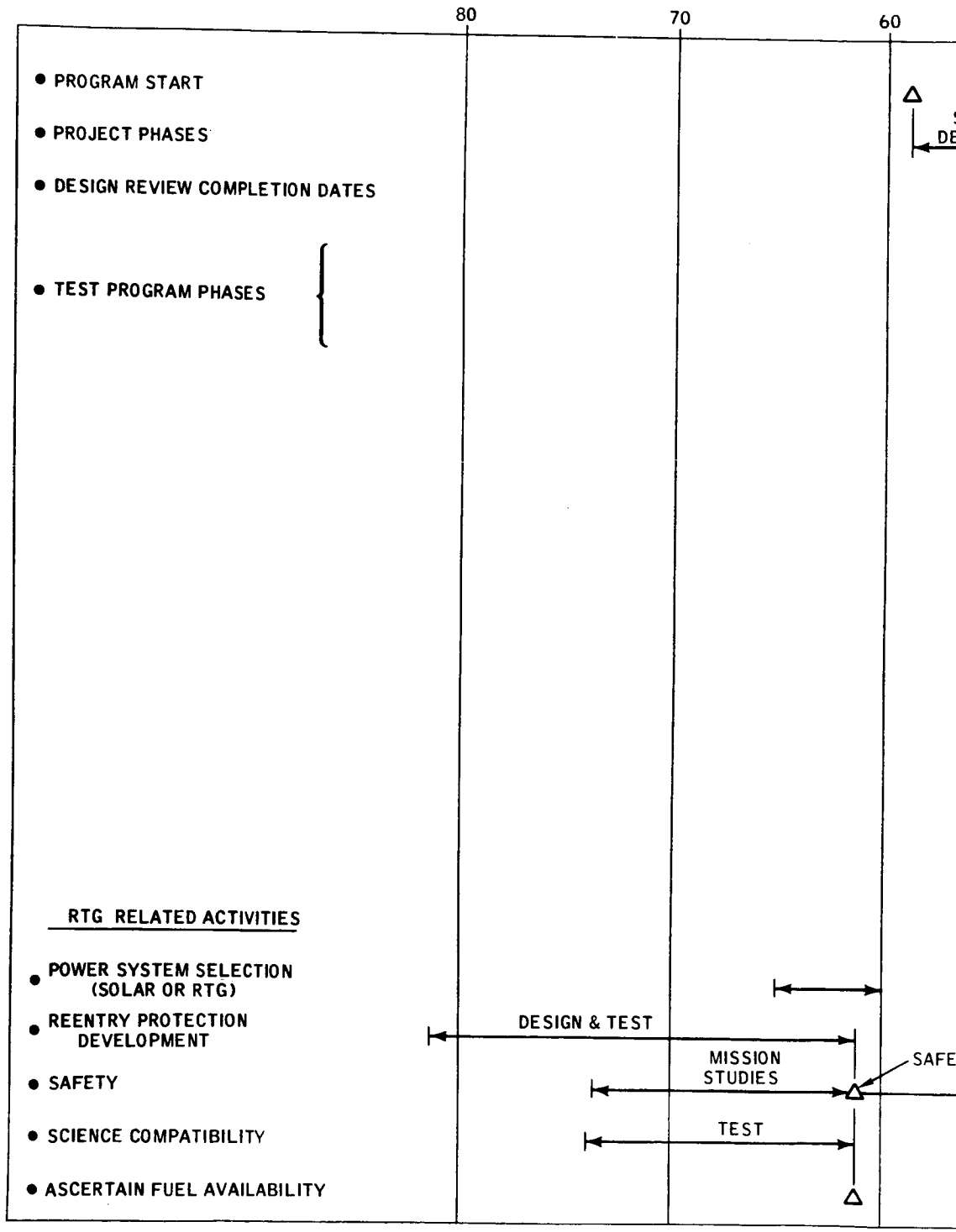
This portion of the report identifies RTG hardware requirements in relation to the principal project activities. The project schedule was assumed to be identical to that established in the Task B report. It is also assumed that a power system selection (either RTG or solar power) has been made at the time that the program associated with a particular mission opportunity is underway. Such a selection in favor of RTG's is contingent on the following:

- a. Proof of RTG isotope fuel containment which meets safety criteria objectives. It is estimated that development efforts to prove this capability would take approximately 24 months.
- b. Safety concept approval, and acceptability of possible compromises on mission flexibility, e. g. , restrictions on launch azimuths. It is estimated that 12 months would be required for these studies.
- c. Assurance of sufficient isotope fuel availability.
- d. Program acceptance of possible compromises in science instrument selection resulting from the RTG radiation environment. Substantiation of these possible compromises should be based on experimental investigations of science instrument interactions with actual or simulated RTG's.

6.6.1 PROJECT SCHEDULE

The project schedule developed during the Task B study has been taken as representative of the development cycle for the Voyager system using a conventional solar power source. This schedule is illustrated on the upper portion of Figure 6-9. Calendar times have been removed and only months prior to launch have been shown. It is recognized that specific dates in the schedule were based upon an assumed starting date and a 1971 launch opportunity, but the general time periods apply for purposes of this study.

The lower part of Figure 6-9 indicates the probable activities related to the RTG's which would precede the overall spacecraft project activity. These earlier RTG activities are considered to be necessary based on the present evaluation of RTG applicability to a Voyager spacecraft. The results of other R & D programs, particularly related to the re-entry protection problem, could reduce and possibly eliminate the earlier activities shown.



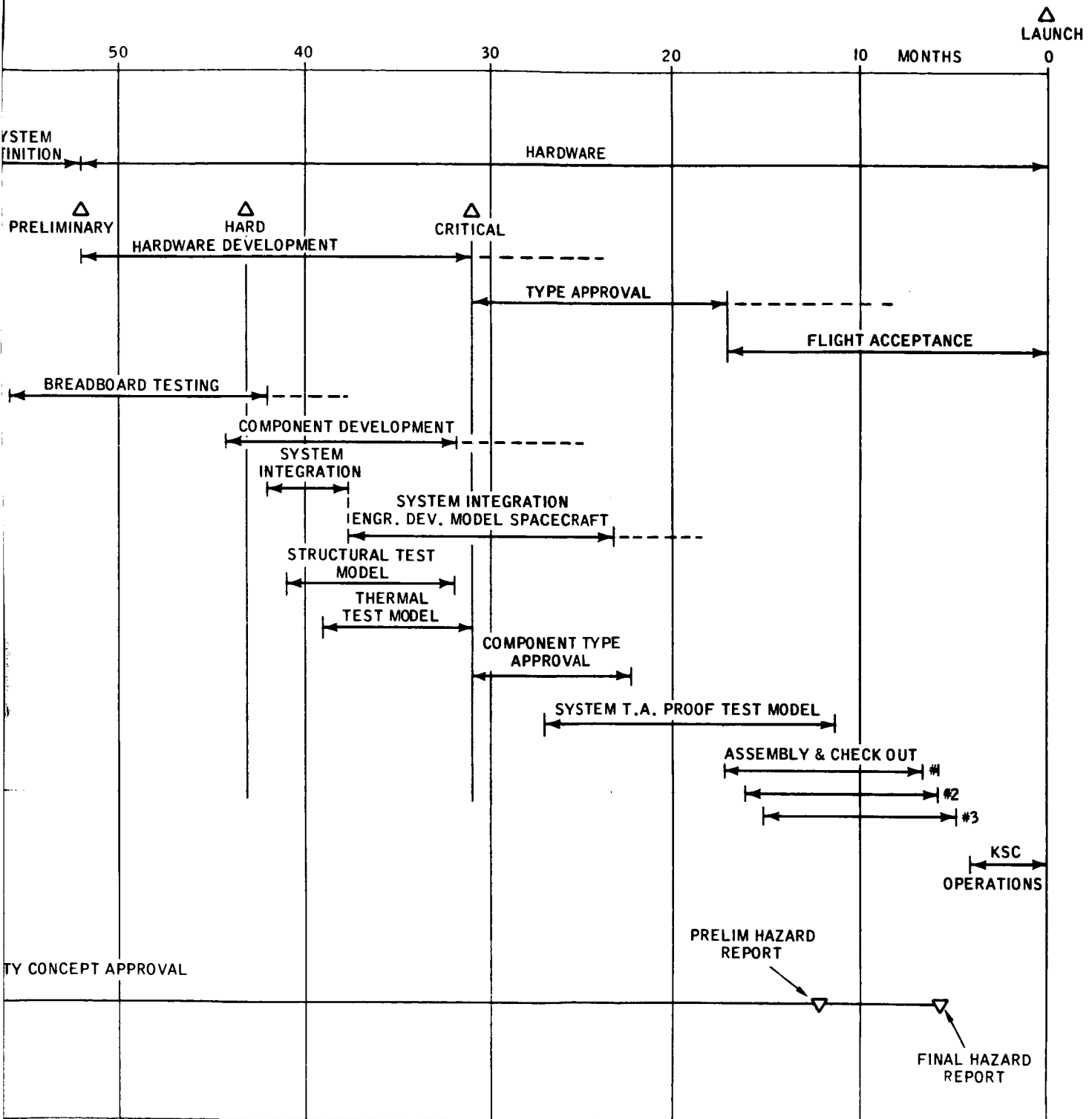


Figure 6-9. Spacecraft Project Cycle



6.6.2 SPACECRAFT DEVELOPMENT

6.6.2.1 Development Phase

For spacecraft development, the key point in the program is the Critical Design Review (CDR) which occurs about 30 to 32 months before launch. In order to reduce risk, it is necessary to make a comprehensive system evaluation before the CDR. In the program shown in Figure 6-9, three system models are used. The Structural Test Model is used to evaluate the structure and the dynamic response of it to such expected inputs as vibration, shock, acoustics, etc. Particular emphasis will be placed upon evaluation of the dynamic environment at various locations on the structure. The Thermal Test Model will be tested to validate the thermal control devices and to determine the thermal environment throughout the system. The Engineering Development Model spacecraft will be used for spacecraft system integration and performance evaluation excluding mechanical and thermal environments. Integration of the RTG into the system has been considered within this general framework.

Because of the necessity of designing the RTG for entry conditions, it is felt that the mechanical integration of the RTG into the system will be straightforward. The RTG assembly will be relatively stiff and it is felt that there is a minimum probability that the spacecraft system will induce loads in the assembly beyond the specified design requirements which will be derived analytically.

Preliminary thermal analysis has shown that no major problems exist for the thermal interactions of the RTG with the spacecraft; however, due to the relatively high operating temperature of the RTG, its influence on the spacecraft may be significant. A relatively sophisticated thermal model and test program will be required to validate the analysis.

The requirements for development hardware are summarized in Figure 6-10 and discussed below:

- a. Development Components The most critical development component will be the RTG re-entry protection, and therefore earlier efforts should be initiated for this element. The extent to which flight testing is required would be determined in the initial phases of such a development effort. Other components of the RTG, such as the

thermopile and heat rejection system will be based largely on the SNAP-27 technology and earlier development efforts need not be devoted to these.

- b. Subsystem and System Integration Eight electrically operated RTG's are required to evaluate subsystem and system performance in all modes of operation. It is also expected that two or three fuel capsules will be required to determine the radiation levels at specific spacecraft hardware locations. This will be done by making measurements with the RTG's in various locations and summing the totals. The RTG's must be representative of the design from the electrical performance point of view and in the sense that the proper mass, cg location, etc., is present; however, materials can be substituted to reduce cost if desirable.
- c. Thermal Models Eight thermally representative models will be required for use in Thermal Test Model testing. These models will be thermal masses with heaters.
- d. Structural Models Eight structurally representative models will be required for use in tests of the Structural Test Model. These models would be representative in terms of mass properties, center of gravity, and attachment hardware.

6.6.2.2 Type Approval Phase

Hardware identified for the Type Approval phase in Figure 6-10 is that principally associated with the thermopile and heat rejection system. Fuel capsules are also required insofar as they would affect the thermopile and heat rejection system during Type Approval tests. It is assumed that qualification of the fuel capsules will have been carried out in conjunction with earlier proof of fuel containment re-entry capability. The validity of this assumption depends largely on the method of re-entry protection finally selected. If the re-entry protection is principally in the form of fuel capsule cladding, the assumption is reasonable. If the thermopile and heat rejection system provide a major part of this protection, additional Type Approval models may be required for specific re-entry protection proof tests.

Proof Test Model (PTM) testing for system type approval will require eight RTG's of the flight design which are electrically operated.

6.6.2.3 Acceptance Testing

The schedule in Figure 6-9 shows that acceptance tested RTG assemblies are required for assembly and checkout of the Flight Spacecraft about 15 to 18 months before launch. It is expected that electrical heaters will be used in the assembly and checkout tests and that the

FUEL CAPSULES	ELECTRICAL FUEL CAPSULE SIMULATORS	THERMOELECTRIC & FIN ASSEMBLY	RE-ENTRY PROTECTION UNITS	SIMULATED RTGS	O.S.E.	
					TEST CONSOLES	HANDLING TOOLS & FUEL CASKS
- FUELED NON FUELED	4	4	10	—	✓	✓
—	—	—	—	8	—	—
—	—	—	—	8 (ELECTRICAL)	—	—
—	—	—	—	8 (MASS, C.G.)	—	—
—	—	—	—	8 (THERMAL)	—	—
2	2	2	2	—	✓	✓
INCLUDING 2 ABOVE)	8	8	8	—	✓	✓
26	24	26	26	—	✓	✓

Figure 6-10. RTG Development Schedule
and Hardware Requirements

actual fuel capsules will be assembled into the RTG during the launch preparations at KSC. Twenty-four RTG's plus two spares are required for the flight spacecraft. Only 16 fuel capsules are launched; therefore, the remaining 10 are available for subsequent opportunities subject to possible fuel reconditioning.

6.6.3 FUEL DELIVERY SCHEDULE

With the use of eight 75 watt (e) RTG's for each spacecraft bus (not including lander RTG's), Figure 6-11 shows the required isotope fuel delivery schedule in terms of thermal watts for the hardware requirements as defined previously. Thermal power is based on 1820 thermal watts per RTG, as described in Section 3.3.2.2. It is assumed that fuel used in development fuel capsules can be reinvested into flight capsules.

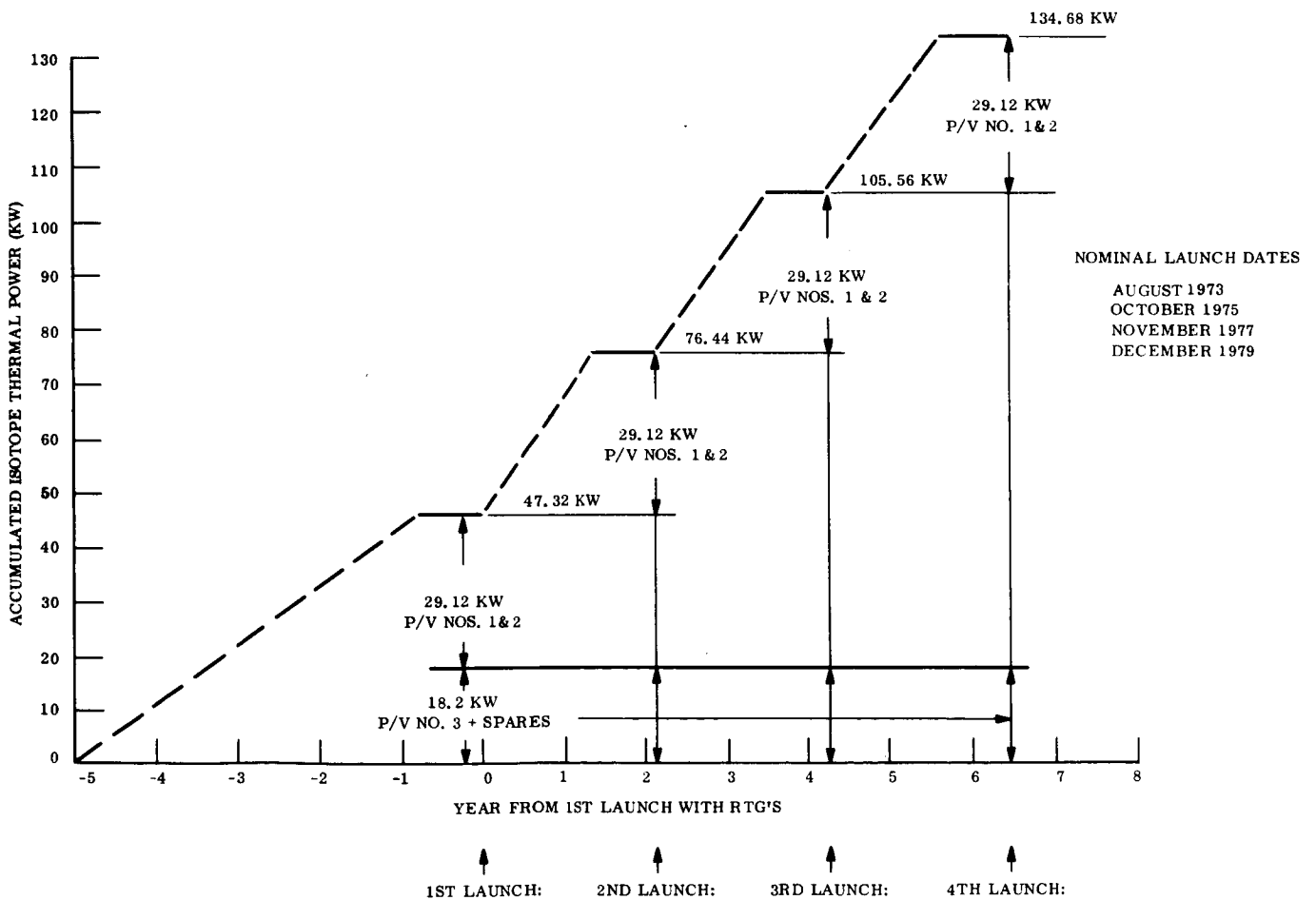


Figure 6-11. Isotope Fuel Inventory Requirements

SECTION 7

CONCLUSIONS

This study has examined the practicality of RTG power for Voyager spacecraft. In the process an RTG-powered spacecraft design was developed along with a convertible solar-powered version. In support of this RTG integration activity basic data were generated concerning RTG design, radiation sensitivity, and nuclear safety considerations. The principal conclusions are presented below in three sections: (1) a summary of the dominant factors and problems encountered in the spacecraft design process; (2) a review of the advantages and disadvantages of RTG power relative to solar power; and (3) recommendations for future activity.

7.1 SPACECRAFT DESIGN EFFECTS

On an overall basis RTG's do not result in the need for drastic revisions in Voyager spacecraft functional concepts. The spacecraft design resulting from this study is quite similar to that of the Task B effort. In fact, the differences are more associated with the desire to accommodate features not always directly related to RTG's, e. g. , the use of either over-the-nose or clamshell shrouds. Although one particular spacecraft configuration was selected and developed in this study to permit a detailed examination, it appears that numerous other configuration candidates could have been equally satisfied. The methods of accommodating the dominant interaction factors encountered in this study are summarized in the following sections and may serve as a guide for future studies.

7.1.1 THERMAL INTERACTION

It was initially thought that this would constitute a major integration difficulty. These fears have not been substantiated. In particular it is not necessary to precool the RTG's for their own self-protection while the spacecraft is enshrouded. As long as the RTG thermal dissipation is reasonably distributed, through the use of multiple RTG units and their relative mounting locations, the thermal effect on other spacecraft equipment is also minimized. It does appear necessary to continuously provide internal cooling once the spacecraft is enshrouded up to the time of launch.

7.1.2 RADIATION SENSITIVITY

For RTG's fueled with Pu-238, radiation damage to spacecraft electronics and materials is virtually non-existent. For some of the subsystems as defined by the Task B spacecraft design, performance parameters may be slightly affected. It is believed that with proper component and circuit derating these effects can be adequately handled. Dynamic interference, on the other hand, is a problem with certain sensitive instruments and sensors. Solutions will lie in the proper application of shielding and remote mounting from the RTG's and the probable need for instrument redesign in certain cases.

7.1.3 RTG TYPE

The spacecraft design was developed using currently available RTG designs, of which the SNAP-27 generator is representative. Although the specific RTG for Voyager may differ in detail from the available designs, there is no strong motivation to consider designs that are grossly different in power and weight characteristics. This results from the fact that specific power (watts per pound) is fairly constant over a broad range of size. Further, RTG designs which are, for example, twice as large as those presently available might require significant development due to unforeseen problems. For instance, these might be related to thermal distributions and their effect on performance and structural integrity. In general, very little if any compromise is incurred by using available designs; in fact, there are gains provided in the form of more equitable thermal distributions and higher reliability as compared to using fewer and larger units.

7.1.4 STRUCTURAL INTEGRATION

No problems of any significance were encountered in this area. Sufficient space is available to permit adequate overall mass distribution, and at the same time the field of view requirements of various sensors and antennae are satisfied. The available mounting locations permit sufficient growth margin.

7.1.5 SOLAR/RTG CONVERSION

As long as this intended goal is borne in mind, there are no overriding constraints that prevent its implementation. The extent to which it is accomplished is a matter of degree. In a gross sense the two spacecraft versions (RTG and solar) can be made interchangeable in terms

of shroud mechanical support. At a higher level of interpretation the spacecraft structural framework and the relative location of various equipment bays can remain identical. Finally, at the subsystem detail level, numerous changes become necessary (power source regulation equipment must be drastically modified, antenna location will change, C & S formats will be modified, etc.). However, it would be expected that even with the consideration of a single power system type, such changes would normally be incorporated from opportunity to opportunity. In this sense it is believed that a high degree of convertibility is possible.

7.1.6 PRELAUNCH OPERATIONS

The most significant item uncovered in this area is the requirement for continuous cooling once the spacecraft is enshrouded. There are potential interactions of this requirement with the possibility of under-the-shroud ETO decontamination, and this must be studied in greater detail.

7.1.7 SAFETY

Safety considerations are particularly dominant because of the RTG isotope fuel. In terms of spacecraft integration, safety becomes a matter of concern from the time of fuel capsule delivery until the spacecraft is on a transfer trajectory to Mars (and perhaps even beyond for the remote possibility of ultimate super-orbital re-entry with failure to inject onto a Mars orbit - a question not considered in this study).

During prelaunch operations, the principal safety concern is one of minimizing personnel radiation exposure. The best means for assuring this is to delay RTG fueling until shortly before shroud encapsulation. The use of local radiation shields may be necessary along with appropriate radiation monitoring and control procedures. There is sufficient experience available in the field of nuclear technology to permit solution of this problem.

Once in flight the safety concern turns to the problem of assuring isotope fuel containment in the event of a mission abort. In this case the safety burden must be borne by proper design of the RTG itself. From the evaluation of this study, this capability does not wholly exist in terms of available RTG designs. The SNAP-27 RTG for the ALSEP program fulfills this need in part, since the fuel capsule will be transported through the Earth's atmosphere in a

specially design re-entry fuel cask; the RTG per se will be fueled on the lunar surface and is not specifically designed for earth re-entry. Thus this need identifies the principal development requirement for Voyager RTG's, since these will be launched in the fueled condition. The possibility of separating the RTG's from the spacecraft as a means of more accurately predicting the subsequent re-enty behavior was considered and found to be too complicated. There are simply too many combinations and possibilities for which this approach would not work. The best approach is rather to surround the vulnerable portion of the RTG in all directions thus avoiding separation complexities. Initial estimates indicating promise for this approach must be more firmly established by appropriate test programs.

7.2 RTG POWER RELATIVE TO SOLAR POWER

The advantages and disadvantages of RTG power relative to solar power are summarized below:

a. Advantages

1. RTG's are believed to provide higher overall reliability for a number of reasons:
 - (a) RTG's operate at relatively constant conditions throughout their life. This is contrasted with temperature cycling experienced by both solar arrays and batteries.
 - (b) RTG's are relatively immune to environmental degradations such as that resulting from ionizing radiation on solar arrays.
 - (c) RTG's permit significant reductions in battery requirements and associated problems of reliable cycle charge/discharge operation. Batteries that are required with RTG's to provide peak load capability are only used intermittently with correspondingly decreased cyclic stress.
 - (d) With respect to failure mode operation, particularly those associated with the loss of solar reference, RTG's provide many additional options for corrective action.
 - (e) Due to removal of the Sun-pointing constraint RTG's permit the use of a fixed high-gain antenna with gains in reliability because of removal of 2 gimbal motions.
2. RTG's provide greater mission flexibility because of their independence of solar energy.
3. RTG's permit improved ground test verification with respect to predicted space output. In fact, ground power performance is identical to flight power performance. They also permit under-the-shroud power system verification just prior to launch.

b. Disadvantages

1. RTG's are heavier; an improvement of about 20 to 25 percent in specific power (watts per pound) is needed to make them comparable with solar power. This disadvantage must be viewed in the context of present technology. On the basis of developments presently under way, particularly those related to higher thermoelectric efficiency, there is a high expectation that the weight differential will be appreciably narrowed.

2. As mentioned earlier, development is required relative to isotope fuel containment re-entry protection. This constitutes the largest source of RTG weight uncertainty and should receive early priority in Voyager RTG developments.
3. Also as mentioned earlier, certain radiation detection instruments are incompatible with the RTG environment.
4. Sufficient quantities of Pu-238 isotope may not be available to fill the needs for RTG-powered Voyager spacecraft. This may be considered as a temporary disadvantage until it is ascertained that sufficient production facilities have been committed for this purpose.

7.3 RECOMMENDATIONS

The advantage of RTG power for Mars missions must be weighed against the flight proven adequacy of solar power as demonstrated in Venus and Mars flyby programs. The scope of this study was not sufficient to provide the basis for firm recommendations, however, since it has been restricted to the spacecraft. The decision (and timing) regarding RTG spacecraft power will certainly be influenced by the capsule program. Employment of RTG's in the capsule will of necessity solve many of the problems and resolve many of the uncertainties common to both spacecraft and capsule.

Thus, it seems prudent to provide for the possibility of eventual incorporation of RTG power in the Voyager spacecraft. By designing a "convertible" spacecraft, later modifications may be minimized. Specific examples of this general recommendation are:

- a. Design the shroud to be consistent with the incorporation of shroud wall cooling.
- b. Design spacecraft subsystems for operation in an RTG radiation environment. Table 7-1 tentatively defines the environment and considers an integrated dose that is 10 times larger than predicted equipment bay values. The dose is integrated for a mission time of 14 months.
- c. Design solar power subsystem output characteristics so that user subsystems are relatively unaffected by the substitution of an RTG power subsystem.
- d. Where possible, design science instruments for operation in an RTG radiation environment.

TABLE 7-1. RTG NUCLEAR RADIATION DESIGN ENVIRONMENT

TOTAL MISSION DESIGN DOSE		
Neutrons:	4 X 10 ¹¹ Neutrons per cm ²	
Gammas:	2 X 10 ³ RADS (C)	
ENERGY SPECTRA		
Energy Group	Limits (Mev)	Percent of Total Integrated Dose
Neutrons:	0 - 1	27
	1 - 3	51
	3 - 5	16.5
	5 - 8	5
	8 - 13	0.5
Gammas:	0 - 0.07	~ 0
	0.07 - 0.13	~ 0
	0.13 - 0.18	~ 0
	0.18 - 0.5	~ 0.002
	0.5 - 0.8	48
	0.8 - 0.9	28
	0.9 - 1.3	4.6
	1.3 - 1.9	4.9
	1.9 - 2.7	9.9
2.7 - 4.0	2.7	
4.0 - 7.0	1.8	